

**On the applicability of imaging spectrometry for the
detection and investigation of contaminated sites with
particular consideration given to the detection of fuel
hydrocarbon contaminants in soil**

Von der Fakultät für Umweltwissenschaften und Verfahrenstechnik der
Brandenburgischen Technischen Universität Cottbus zur Erlangung des
akademischen Grades eines Doktor-Ingenieurs genehmigte Dissertation

vorgelegt von

Diplom-Ingenieur

Kay Hasko Winkelmann

geboren am 16. August 1973 in Berlin

Gutachter: Prof. Dr.-Ing. Wolfgang Spyra (BTU Cottbus)

Gutachter: Prof. Dr. rer. nat. habil. Dr. h.c. Reinhard F. Hüttl (BTU Cottbus)

Gutachter: Colonel Prof. Dr. Wendell C. King (USMA West Point, USA)

Tag der mündlichen Prüfung: 30. Juni 2005

Preface

This dissertation on the applicability of imaging spectrometry for contaminated site detection and investigation is based on an idea of my advisor, Prof. Dr.-Ing. Wolfgang Spyra, who considered imaging spectrometry as a tool for contaminated site detection and investigation as early as 1998. I am grateful that he entrusted this interesting topic to me and gave me the freedom to work largely independent on it. Also, I am grateful for his advice and discussions on the directions to take.

Due to the complexity and huge variety of “contaminated sites” that will be outlined in this thesis, it was found necessary to confine the work to the detection and investigation of one ubiquitous type of contamination: fuel hydrocarbon contaminations of soils. However, the general applicability of imaging spectrometry with respect to other important types of contaminated sites is considered and briefly discussed herein.

Because this dissertation is likely to be the basis for application projects of imaging spectrometry for contaminated site detection and investigation, and also the starting point for additional research work, it is written to provide a comprehensive basis and contain all necessary information for these purposes. Therefore, some information, in particular in the introductory part on optical spectrometry and remote sensing imaging spectrometry, might be well-known to some readers and can be skipped when reading this work. All relevant data acquired during this work are found on the enclosed CD-ROM in different data formats ready for use in spectral libraries or for additional research. Therefore, it does not contain an extensive appendix with spectra and other data.

This dissertation describes work done between May 2000 and March 2005 at the Chair of Chemical Engineering and Hazardous Wastes of Brandenburg University of Technology at Cottbus, under the supervision of Prof. Dr.-Ing. Wolfgang Spyra.

Except where stated otherwise, this dissertation is the result of my own work and contains nothing which is the outcome of work done in collaboration. This dissertation has not been submitted in whole or in part for any degree or diploma at this or any other university. Also, no parts of this dissertation have been published previously.

I would like to thank my colleagues, friends and family for their support during the time that I spent working on this dissertation, in particular for taking over parts of my tasks and duties during the final months of its realization.

Kay Winkelmann
April 2005

Abstract

Based on laboratory investigations and data interpretation experiments, this study investigates the applicability of remote sensing in general and imaging spectrometry in particular, for contaminated site detection and investigation with a focus on fuel hydrocarbon soil contaminations.

Laboratory experiments were conducted to obtain reflectance spectra of organic and inorganic chemicals, natural and man-made materials, and twelve selected organic contaminants at three different concentrations in seven different soil types (sands, clays, organic soils) at three different moisture levels in a range of wavelengths from 0.38 μm to 2.5 μm . Based on the results, characteristic absorption features of different organic chemicals as well as natural and man-made materials are described, detection limits for fuel hydrocarbon contaminants in different soil types at different moisture levels are defined, and the separability of hydrocarbon soil contaminations from other hydrocarbon-bearing materials is described.

Data interpretation experiments using an imaging spectrometry dataset were conducted to assess the applicability of established data interpretation algorithms for imaging spectrometry data and to develop a method of detecting and separating different classes of hydrocarbons in imaging spectrometry datasets. A detection method based on characteristic band differences with respect to aliphatic and aromatic hydrocarbon absorption features is proposed.

Zusammenfassung

Gegenstand dieser Arbeit ist die Untersuchung der Anwendbarkeit von Methoden der Fernerkundung, insbesondere der Anwendung der abbildenden Spektrometrie zur Detektion und Untersuchung von Mineralölkohlenwasserstoff-Kontaminationen von Böden.

Laboruntersuchungen zur Gewinnung von Spektren von organischen und anorganischen Stoffen, natürlichen und anthropogenen Materialien sowie zwölf ausgewählten Kontaminanten in drei Konzentrationsstufen in sieben unterschiedlichen Bodentypen (Sande, Tone, organische Böden) mit unterschiedlichen Bodenfeuchtegehalten im Bereich von 0,38 μm bis 2,5 μm wurden durchgeführt. Aufgrund der Ergebnisse dieser Versuche werden charakteristische Absorptionsmerkmale von verschiedenen Gruppen organischer Stoffe und Materialien anthropogenen und natürlichen Ursprungs beschrieben, Detektionsgrenzen von organischen Schadstoffen in kontaminierten Böden definiert und die Unterscheidbarkeit von Mineralölkohlenwasserstoff-Bodenkontaminationen von anderen organischen Materialien untersucht.

Versuche zur Datenauswertung von abbildenden Spektrometerdaten wurden durchgeführt, um die Anwendbarkeit von bestehenden Interpretationsmethoden von abbildenden Spektrometerdaten für die Detektion und Separierung von unterschiedlichen Kohlenwasserstoffmaterialien zu untersuchen. Eine Methode zur differenzierten Detektion von aliphatischen und aromatischen Kohlenwasserstoffmaterialien in abbildenden Spektrometerdaten basierend auf charakteristischen Absorptionsmerkmalen wurde entwickelt.

Table of Contents

Preface	II
Abstract	III
Zusammenfassung (German Abstract)	III
Table of Contents	IV
1 Introduction	1
2 The problem of contaminated site investigation	5
2.1 Types and characteristics of contaminated sites	7
<i>Oilfields, Absheron peninsula, Azerbaijan</i>	10
<i>Industrial site "Schwarze Pumpe", Brandenburg/Saxony, Germany</i>	12
<i>Former military training area Döberitzer Heide near Berlin, Germany</i>	14
<i>Uncontrolled waste dump near Puerto La Cruz, Venezuela</i>	17
<i>Mingecevir rocket fuel depot, western Azerbaijan</i>	18
<i>Crude oil spill on marshland soil, Abadan, Iran</i>	20
<i>Illegal waste dump Groß Pinnow, northern Brandenburg, Germany</i>	21
<i>Abandoned glassworks Haidemühl, southern Brandenburg, Germany</i>	23
<i>Ordchonikidse manganese mining district, Ukraine</i>	25
<i>Small diesel filling station, Rio Unare Basin, Venezuela</i>	26
2.2 Site registration and site investigation	30
2.3 Contaminants	31
2.4 Fuel hydrocarbons as environmental contaminants	32
3 Principles and technology of imaging spectrometry	37
3.1 Spectrometry basics	42
<i>Energy-matter interactions</i>	43
<i>Interaction mechanisms</i>	44
<i>Absorption features of organic compounds</i>	47
<i>NIR spectroscopy of organic chemicals</i>	50
<i>NIR analysis of petrochemicals</i>	54
<i>Absorption features of inorganics</i>	57
<i>Summary: Capabilities of NIR spectroscopy</i>	58
3.2 Remote sensing imaging spectrometry	59
<i>Data acquisition and processing</i>	63
3.3 Imaging spectrometry systems	64
<i>Imaging spectrometry system designs</i>	65
<i>Important system parameters</i>	66

3.4	Imaging spectrometry data interpretation	70
	<i>Spectra</i>	72
	<i>Characteristics of imaging spectrometry datasets</i>	73
	<i>Data interpretation preprocessing</i>	75
	<i>Analytical data interpretation</i>	77
	<i>Spectral library comparison techniques</i>	78
	<i>Target detection techniques</i>	81
	<i>Anomaly detection</i>	81
	<i>Spectral mixture analysis</i>	82
	<i>Other analysis tools</i>	83
4	Environmental applications of imaging spectrometry	84
4.1	Applications of imaging spectrometry	84
4.2	Environmental applications	87
	<i>Fuel hydrocarbon soil contaminations</i>	88
	<i>Heavy metal soil contaminations</i>	93
	<i>Soil salinization</i>	95
	<i>Mine tailing characterization (ore mining)</i>	96
	<i>Overburden dump and residual lake characterization (lignite mining)</i>	98
	<i>Water contamination monitoring</i>	99
	<i>Other applications</i>	100
	<i>Summary, conclusions, and critique on recent applications</i>	100
5	Applicability of imaging spectrometry for contaminated site detection and investigation	102
5.1	Soils and soil spectral properties	102
	<i>Soils</i>	102
	<i>Water (soil moisture)</i>	104
	<i>Spectral properties of soils</i>	105
5.2	Fuel hydrocarbons and their spectral characteristics	109
	<i>Spectral response of fuel hydrocarbons</i>	111
5.3	Fuel hydrocarbon soil contaminations and spectral properties	112
	<i>Fuel hydrocarbon soil contaminations</i>	112
	<i>Expected spectral behavior of soil contaminated with fuel hydrocarbons</i>	114
5.4	Research objectives	115
	<i>Fuel hydrocarbon spectra</i>	115
	<i>Spectral response of fuel hydrocarbon soil contaminations</i>	115
	<i>Instrumentation and remote sensing parameters</i>	115
	<i>Possibilities & restrictions: remote sensing contaminated site investigation</i>	116
	<i>Data interpretation approaches</i>	116

6	Spectrometry experiments	118
6.1	Sample materials	119
	<i>Organic and inorganic chemicals</i>	119
	<i>Anthropogenic materials</i>	119
	<i>Soil samples</i>	121
6.2	Experiment design – fuel hydrocarbon contaminated soils	127
	<i>Soil moisture level selection</i>	127
	<i>Contaminant selection</i>	128
	<i>Contaminant concentrations selection</i>	128
6.3	Sample preparation	130
	<i>Sample description system</i>	130
	<i>Preparation of moist soil samples</i>	130
	<i>Preparation of soil samples with liquid contaminants</i>	131
	<i>Preparation of soil samples with solid contaminants</i>	132
6.4	Instrumentation and measurement set-up	134
6.5	Results and discussion	137
	<i>Spectral characteristics of major groups of organic chemicals</i>	137
	<i>Spectral uniqueness of organic chemicals and other materials</i>	142
	<i>Spectral characteristics of selected soil contaminants</i>	145
	<i>Spectral characteristics of selected soils</i>	150
	<i>Dry soil spectra</i>	150
	<i>Moist soil spectra</i>	152
	<i>Contaminated soil experiments</i>	154
	<i>General observations</i>	154
	<i>Spectral mixing behavior of soil / moisture / organic contaminant spectra</i>	159
	<i>Detection limits</i>	166
	<i>Quantitative analysis</i>	172
6.6	Field samples of contaminated soils and related materials	173
7	Data interpretation	178
7.1	HyMap dataset military training area Döberitzer Heide	180
7.2	Data interpretation standard procedures	181
	<i>Detection of hydrocarbons</i>	181
7.3	Data interpretation for the detection of fuel hydrocarbon soil contaminations	184

8	Synopsis, conclusion and vision	199
	<i>General applicability of remote sensing for contaminated site investigation</i>	199
	<i>Spectral characteristics of fuel hydrocarbons</i>	201
	<i>Ability to differentiate between different hydrocarbon classes</i>	201
	<i>Detectability and detection limits of fuel hydrocarbon soil contaminations</i>	201
	<i>Imaging spectrometry quantitative analysis of soil contaminations</i>	202
	<i>Remote sensing implications</i>	203
	<i>Data interpretation for hydrocarbon detection, mapping and separation</i>	204
	<i>Applicability to contaminated site types</i>	205
	<i>Vision</i>	206
	<i>Future research topics</i>	207
	References	208
	List of Abbreviations	231
	List of tables	232
	List of figures	235

1 - Introduction

Contaminated areas on industrial and military brownfields, soil contaminated by accidental or deliberate release of organic or inorganic chemicals, and salinized soils pose severe problems worldwide. Basic natural resources such as groundwater and soil that are the basis for human life and intact ecosystems are endangered in many regions of the world due to increasing anthropogenic contamination.

The main areas affected are metropolitan and industrial centers and their surroundings in both industrialized and developing countries worldwide. The causes of contaminations, however, are different in industrialized and developing countries.

In industrialized countries, both the economic structural changes from industrial production towards service-oriented societies, and the end of the Cold War in the early 1990s left large industrial facilities and military installations abandoned. These sites – several thousand square kilometers in Germany alone – typically lie fallow after closure. Although environmental legislation requires investigation and remediation of such sites in order to make them available for reuse often nothing happens for decades. In most cases, the sites fall into a state of hibernation. This state of hibernation often is due to legal uncertainties for former owners and potential investors concerning responsibilities and costs for site investigation and site clean-up.

In developing countries, the reasons for the contamination of natural resources are different. A lack of environmental legislation or poor enforcement of existing environmental legislation, poor access to (expensive) environmental technology, overexploitation or uncontrolled exploitation of natural resources, requirements of the economic catching-up process, the price regime at international commodity markets, and basic needs of a growing population are some of the reasons for pollution and overexploitation of the environment in urban and rural areas.

Despite differing reasons for the remediation and redevelopment of brownfields and soil contaminations in developing and industrialized countries, these are quite similar from a scientific point of view taking into account chemistry, pedology, geology, hydrogeology and toxicology. They all represent a distribution of typically low but varying amounts of organic or inorganic contaminants of anthropogenic origin in environmental abiotic media, in particular soil and water. The contaminated media may be hidden in the subsurface or exposed at the surface – thus soils may or may not be open to direct access. Depending on climate, soil properties and the intensity of a contamination, soils may or not be covered by vegetation.

Contaminated sites may include any of the following: large industrial areas (steel production, coal conversion, energy production, chemical and pharmaceutical industry, glass production, galvanization, etc.), mining areas (salts, ores, coal, tar sands – surface and subsurface mining), crude oil production and petroleum refining facilities, controlled waste dumps or uncontrolled burials containing liquid and solid

wastes (municipal wastes, industrial wastes, overburden), and post-war areas (battlefields, military training areas, armament factories, etc.). In some cases, rural agricultural areas might also be considered contaminated. This may be due to salinization from inappropriate irrigation or fertilization, excessive use of pesticides, or airborne contaminants released from nearby industrial areas. Depending on the region considered, one or more of these typical contaminated sites may occur or predominate.

With the above considerations, it becomes clear that contaminated sites are a globally relevant problem, endangering many vital environmental resources such as drinking water and arable land. This problem affects industrialized countries as well as developing countries with varying regional patterns.

Contaminants are as diverse as the variety of chemical substances invented and used. A substance's significance as an environmental contaminant is determined by the amount used and/or its human or environmental toxicity. Its physical and chemical properties determine its behavior once released into the environment. It follows that that fuel hydrocarbons (crude oil and its refinery products), which are the group of chemicals most widely used worldwide as fuels, lubricants, solvents and basic substances in chemical industry, are also the most important contaminants worldwide. Besides fuel hydrocarbons, there are other organic and inorganic chemicals that are of importance as contaminants. These will be considered later in more detail.

In many countries, a methodological approach for the treatment of contaminated sites has been developed. It traditionally consists of several steps including site registration, historic investigation, sampling and non-sampling site investigation, risk assessment, remediation planning, site clean-up and remediation, and finally, monitoring the success of the remediation. While this approach has proven successful for tens of thousands of sites worldwide, problems remain in particular with respect to the investigation of large industrial or military brownfields. These sites, which typically comprise from one or two square kilometers to sometimes more than two hundred square kilometers, are difficult to deal with using the traditional site investigation and clean-up approach outlined above. Historic investigations may still be possible for these sites and provide useful results, depending on secrecy of the facility and the availability of historic files, maps and aerial photographs. However, the costs of field sampling and chemical analysis often are economically impossible if applied comprehensively on the site.

The costs for sampling and analysis could be substantially reduced if an alternative means of detection could be used to locate "hot spots" with high contaminant concentrations on these sites. By using non-contact technologies for overview investigation, the area that requires sampling and analysis could be dramatically reduced, thus reducing the investigation costs to a similar extent.

The Chair of Chemical Engineering and Hazardous Wastes of the Brandenburg University of Technology at Cottbus considers remote sensing techniques one

possible approach to achieve this objective. During recent years, the work of the site investigation group of the Chair has focused on different remote sensing techniques, investigating them for their suitability for the investigation of large industrial and military brownfield with respect to land use analysis and contamination (“hot spot”) detection and mapping. Among the methods and systems tested were airborne laser scanning, thermal remote sensing, color infrared aerial photographs, multispectral imaging and imaging spectrometry (also known as hyperspectral imaging).

Imaging spectrometry means the “acquisition of images in hundreds of registered, contiguous spectral bands such that for each picture element of an image it is possible to derive a complete reflectance spectrum” [Goetz 1992]. Typically, between 100 and 300 spectral bands with a bandwidth of two to ten nanometers are sampled in the 400 nm to 2,500 nm wavelength region. Recent applications of imaging spectrometry include, among others, mineralogical exploration, geologic mapping, vegetation analysis for precision agriculture, military target detection and terrain analysis, soil mapping, vegetation mapping, monitoring of inland, coastal and marine water bodies, and other environmental applications [e.g., Curran 1994, Clevers 2001, Messinger 2004, Pavlin 1996, Ben-Dor 2001a, Curran 2000, van der Meer 2001c, Gallagher 2003b].

The objective of this study is to investigate the fundamentals of optical spectrometry in the visible to mid-infrared wavelength regions for the detection of soil contaminations. In doing this, I will assess the applicability of imaging spectrometry for overview site investigations and the detection and mapping of hot spots. The study focuses on investigations of brownfields or other possibly contaminated sites with particular consideration of fuel hydrocarbon soil contaminations.

The problem addressed in this thesis can be summarized as follows: Detection of low contaminant concentrations in a soil matrix with varying background parameters such as soil constituents, soil moisture and vegetation cover by means of environmental remote sensing, in particular imaging spectrometry.

The subsequent sections of this thesis will:

- Consider different types of common contaminated sites and the spatial distribution of contaminants and indicators of contamination in three-dimensional space with a focus on fuel hydrocarbon contaminations as the most abundant contamination type world-wide (section 2)
- Outline the principles of imaging spectrometry and describe the absorption features of contaminants as target materials to be detected in the 0.4 μm – 2.5 μm wavelength region with a focus on fuel hydrocarbons and data interpretation techniques available for the interpretation of complex imaging spectrometry datasets (section 3)
- Give a summary of state-of-the-art applications of imaging spectrometry to environmental problems (section 4)

- Discuss the general applicability and instrument requirements (spatial, spectral or radiometric resolution) of imaging spectrometry for contaminated site detection and investigation, considering the organic contaminants, their concentration, the composition and moisture of the contaminated materials (soils), the type of surface cover, and the separability of fuel hydrocarbons from other hydrocarbon-bearing materials (in particular plastics, vegetation and wood) (section 5)
- Describe and discuss results from laboratory and field experiments carried out to determine the detection threshold of different contaminants of the fuel hydrocarbon group in different soil types with varying soil moisture content (section 6)
- Investigate the detectability of fuel hydrocarbons and related materials in an imaging spectrometer dataset of the former military training area Döberitzer Heide using different data interpretation approaches described in section 3, and develop a method for the improved detection and separation of hydrocarbon classes in imaging spectrometry data (section 7)
- Based on the description of typical contaminated sites and spatial distribution patterns of soil contaminations (section 2), the results obtained in the laboratory and field experiments (section 6) and the interpretation of the imaging spectrometer dataset (section 7) conclude on the possibilities and limitations of imaging spectrometry for contaminated site detection and investigation (section 8)
- Give recommendations for applications of imaging spectrometry in the field of contaminated site detection and investigation, outline fields for future research with respect to the application of imaging spectrometry for contaminated site detection and investigation and develop visions for the application of imaging spectrometry and its integration with other data and tools for real-time environmental monitoring (section 8)

2 – The problem of contaminated site investigation

According to recently published data, in Germany alone there are more than 360,000 civilian sites that are considered possibly contaminated sites. This number comprises approximately 260,000 industrial brownfields and 100,000 old waste deposits. It does not include armament facilities and military installations such as barracks, airfields and military training areas [SRU 2004]. The number of contaminated sites that resulted from armament production was estimated at 5,000 – 5,500 in 1993 [Thieme 1993]. However, for the federal state of Brandenburg (Germany) with a total number of 21,300 potentially contaminated sites alone, about 42 % of these sites (almost 9,000 sites) are listed as former military sites or sites of armament production [MLUR 1998].

For the United States, it is not possible to derive a total number of potentially contaminated sites due to a diversified allocation of responsibilities to different national, federal, regional and private institutions. However, two numbers may illustrate that the situation in the US can be considered similar to that in Germany. The United States Environmental Protection Agency reports nearly 440,000 confirmed underground storage tank releases between 1988 and 2003, 303,000 of which have since been cleaned up. Every year between 6,000 and 14,000 new leakages from underground storage tanks are reported in the United States. Most of the underground storage tank leakages include a release of fuel hydrocarbons into both soil and groundwater [US EPA 2004a]. Also for the United States, more than 90,000 sites of improper hazardous waste disposal are reported. These sites include the disposal of hazardous organic and inorganic chemicals as well as the improper disposal of radioactive wastes. The total cleanup costs for these sites are estimated at a minimum of \$195 billion [Watts 1997]. For the period 2004 – 2033, the US Environmental Protection Agency estimates a total number of 235,000 – 355,000 (average 294,000) hazardous wastes sites that will need to be remediated in the United States, assuming current regulations and practice. This number includes 77,000 sites that have already been discovered plus a projected (average) 217,000 sites that will be discovered in the future based on the rate of discoveries in the late 1990s and early 2000s. The total cost for the site investigation and cleanup efforts in the 2004 – 2033 period is estimated at 170 – 250 billion US-\$ [US EPA 2004b].

One must note that the numbers given for Germany and the United States are not comparable. While the German statistics on contaminated sites take only those sites into account that have already been registered as potential contaminated sites, the numbers of the US Environmental Protection Agency are estimates of future clean-up needs based on the experience of the past decade. For the given number of potential contaminated sites in Germany, it is expected from experience that only 10 – 15 % of the recent 360,000 potential contaminated sites will undergo detailed site investigation, risk assessment and remediation (i.e. 36,000 – 54,000 potential sites) [SRU 2004].

In most cases, armament factories and military installations comprising severe contamination of soil and groundwater are omitted from the statistical data or site clean-up measures given to civilian sites for two reasons. First, these sites often include the additional hazard of explosives, warfare agents, unexploded ordnance and abandoned ammunitions. Due to the risks involved with these hazards, they must be addressed separately and have a priority over the investigation and remediation of conventional contamination of environmental media. Second, the conventional approach for site-investigation, based on technologies developed to deal with common contaminants, sources and contamination patterns, is usually non-transferable to armament factories, military installations and facilities. A historical investigation of a non-military brownfield typically includes resources such as site inspections, analysis of company files, maps, aerial photographs etc., which often yield useful results upon which further testing can be based. These resources, however, are often unavailable for military installations due to secrecy reasons. Furthermore, the pattern and intensity of land use, as well as the hazardous materials handled at armament factories and military installations were often subject to fluctuations influenced by the onset of wars or expansions in military and warfare technology. Military and armament facilities are included in this investigation for two important reasons. First, the purpose of this thesis is to investigate the applicability of a remote sensing, i.e. a non-contact investigation technique to contaminated site investigation. Therefore, contaminations of soil can be addressed separately from explosives, ammunition, and warfare agents, since the use of remote sensing techniques prevents human contact with these hazards. Second, new approaches are needed to take into account the historical significance of contaminated sites resulting from armament and military use in the pasts. The dimension of this problem becomes clear when considering the federal state of Brandenburg (Germany). A total of 2,000 square kilometers (approximately 10 % of the state area) have been used for armament and military facilities in the past, former military training areas making up the largest part of this portion [MLUR 1998]. Not included in this number are the major battlefields of the final stages of World War II, which still pose severe hazards in some areas of the state.

2.1 – Types and characteristics of contaminated sites

In the United States and Germany alone, the huge number of contaminated sites of different origins indicate the dimension of the problem and the fact that contaminated sites may originate from every stage or sector of modern industrial economy:

- Raw material production (mining, crude oil production, industrial agriculture)
- Energy production (electricity generation, conversion of fuels, etc.)
- Production of intermediate products (chemical industry, steel production, etc.)
- Construction
- Production of industrial, military and consuming goods
- Crafts and service industry (transport, cleaning, building, painting, etc.)
- Waste disposal

Important industrial brownfields, contaminated sites and hazardous wastes sites subject to site investigation, site assessment and remediation efforts are, among others

- Landfills and uncontrolled burials of household wastes
- Landfills and uncontrolled burials of industrial wastes
- Oil fields
- Underground and open-cast mines (metals, coal, tar sands, etc.), in particular when associated overburden dumps and technical facilities
- Industrial production facilities where hazardous materials have been used for production or hazardous wastes were usually generated during the production (e.g. refineries, coking plants, glassworks, electroplating plants, pharmaceutical and chemical industry, etc.)
- Military training areas
- Armament factories, in particular plants for the production of explosives, chemical warfare agents and nuclear weapons
- Accidental spills during the transport and intermediate storage of hazardous materials

With respect to the objective of this thesis, the investigation of imaging spectrometry and its applicability for contaminated site investigation, the terms “industrial brownfields”, “hazardous wastes”, and “potentially contaminated sites” are subsumed under the term “contaminated sites”. The term “contaminated sites” as used in this thesis refers to suspected or existing contamination of soil and/or groundwater with organic or inorganic contaminants regardless of their sources or development.

The investigation and remediation of contaminated sites is typically divided into several stages. A typical approach that may vary to some extent from country to country and case to case includes (1) a registration of suspicious sites based on formal evidence, (2) a historical investigation to assess the potential of contamination, (3) an overview (sampling and analysis) investigation to confirm or preclude the contamination of soil or groundwater, (4) a detailed investigation applying non-sampling, sampling and analysis techniques to develop a detailed description a confirmed contamination, (5) a risk assessment based on the results of the detailed investigation, (6) an assessment of applicable remediation technologies, the determination of remediation targets and remediation planning, (7) remediation, and (8) a post-remediation monitoring. (1) – (5) are sometimes referred to with the more general term “site characterization”.

Site registration, site investigation and characterization, and risk assessment are usually based on historic investigations, sampling, and analysis investigations. Historic investigations typically include historical maps, aerial photographs, company and administration files, and other written information such as classified directories. Based on the information retrieved, suspicious areas on a potential contaminated site may be identified and in the next step, the overview investigation, samples from potentially affected media such as soil and groundwater might be taken. These samples are then analyzed using state-of-the-art instrumental analytical methods. If a suspected contamination is verified, detailed site investigation with systematic sampling of affected media (usually soil and groundwater) and comprehensive chemical analyses are part of the next step: detailed site investigation and risk assessment. The objective of this step is to derive a comprehensive and detailed description of the contamination at a site in order to enable a precise risk assessment. Apart from sampling and analysis techniques, non-sampling investigation methods such as geophysics and remote sensing might also be applied for detailed site investigation. Based on experiences from site investigations carried out by the Chair of Chemical Engineering and Hazardous Wastes of the Brandenburg University of Technology, costs for conventional overview and detailed site investigation of a contaminated site using non-sampling, sampling and analysis techniques may, depending on the type and depth of the contamination, exceed \$50,000 per hectare, i.e. \$5,000,000 US per square kilometer in case of heavily contaminated areas such as the industrial facility Schwarze Pumpe in Brandenburg / Northern Saxony (Germany).

Based on its origin and development, contaminated soil and groundwater must to be distinguished into three main classes. These three classes are (1) unsecured deposits or deliberate releases of hazardous wastes or materials into the environment, in particular onto or into the soil, (2) minimal, usually unintentional leaching of hazardous materials into the soil or subsurface water resources over a long period of time which, over years, added up to a substantial contamination (e.g. at production facilities, where minimal losses can be considered normal and are usually not detected), and (3) accidental spills of larger quantities of hazardous materials over a

short period of time. In any case, the result is the anthropogenic contamination of soil and, through migration of the contaminants through the vadose zone into the saturated zone, also the contamination of groundwater with one or more organic or inorganic contaminants.

Although we define “contaminated sites” generally as areas where hazardous materials have spilled into soil and/or groundwater or have been deposited improperly, it should be stressed that every contaminated site is unique, even if the environmental media affected and the contaminants involved are identical. Apart from the contaminant type, their concentration and mixture, contaminations occur in varying geological conditions (varying combinations of solid rock or sedimentary layers), in different soil types with differing quantities of basic compounds such as silica sand, clay minerals, organic matter, iron, and soil moisture, and in different hydrogeological environments. External conditions such as climate (e.g., temperatures, precipitation), aside from the principal chemical and physical properties of the involved contaminants and matrices, may determine the environmental fate of the contaminants.

Contaminated sites may be covered by vegetation or by built structures such as roads, technological installations, and buildings. If a contaminated site is covered by vegetation, the rhizosphere of the vegetation may or may not reach into contaminated soil or groundwater. Vegetation covering contaminated sites may be different from the vegetation in a nearby uncontaminated area, and may exhibit vegetation stress or even enhanced growth if the anthropogenic contaminant is a nutrient to a specific vegetation species. Contamination may also inhibit normal plant growth, leaving open voids in an otherwise closed canopy, or supporting specialized species different from the native vegetation. If the plant cover of a contaminated site or soil is different from that of the uncontaminated area, it can be regarded as a vegetation anomaly.

The size of a contaminated site can vary from a few square meters to several hundred square kilometers. It may comprise a single source or multiple sources with similar or different contaminants. A contamination may affect soil, groundwater or both. The surface structure or macro scale “texture” of a contaminated site may be homogeneous over large areas or heterogeneous with many different, small and diversified structures. The following examples will illustrate typical contaminated sites and their characteristics as these are important for subsequent considerations on the applicability of imaging spectrometry for contaminated site investigation. The sites described have been subject to projects of the Chair of Chemical Engineering and Hazardous Wastes of the Brandenburg University of Technology Cottbus during the years 2000 – 2004.

Oilfields, Absheron peninsula, Azerbaijan

Industrial Sector:	Crude oil production
Location:	Absheron Peninsula / Caspian Sea, larger Baku area, Azerbaijan
Plants:	Oil production facilities, pipelines, storage facilities, refineries
Contaminants:	Crude oil, fuel hydrocarbons
Operation time:	ca. 1850 – today (industrial crude oil production)
Area:	ca. 200 sq. km
Site description:	Onshore oil production from shallow wells since the medieval ages. Industrial production of crude oil since the middle of the 19 th century. In the late 19 th century, the oilfields around Baku on the Absheron Peninsula produced more than 11 million tons of light crude oil, nearly 50 % of the annual world production at that time [Mir-Babayev 2002, Narimanov 1995, Jacobson 1999].

Today, light crude oil is produced from onshore fields on the Absheron Peninsula together with salty ground water from wells and separated by density separation in staple tanks. Significant leakage of both crude oil and salt water occurs from wells, tanks and pipelines. Drilling mud containing crude oil is usually deposited near the production wells. Carbonate and sand soils on the oilfields are usually highly contaminated with light crude oil. Fuel hydrocarbon concentrations in soil is typically between 20 g/kg and 50 g/kg but may also exceed 100 g/kg. Often, liquid crude oil is found at the surface in combination with salt water and salt crystallizations. Plant cover is absent on the oil fields [Winkelmann 2003a]. Contamination of this type and genesis has occurred ever since the start of oil production in the mid-1850s [Mir-Babayev 2002]. Widespread and intense contamination can be found over extremely large areas on the whole Absheron peninsula.

The oil fields are located in and around the Baku area on the Absheron peninsula which extends from the lower Caucasus into the Caspian Sea. The oil fields reach well into urban areas. However, the oil fields themselves are usually large and relatively homogeneous areas that are separated from settlements and other industrial or commercial facilities [Winkelmann 2003a].

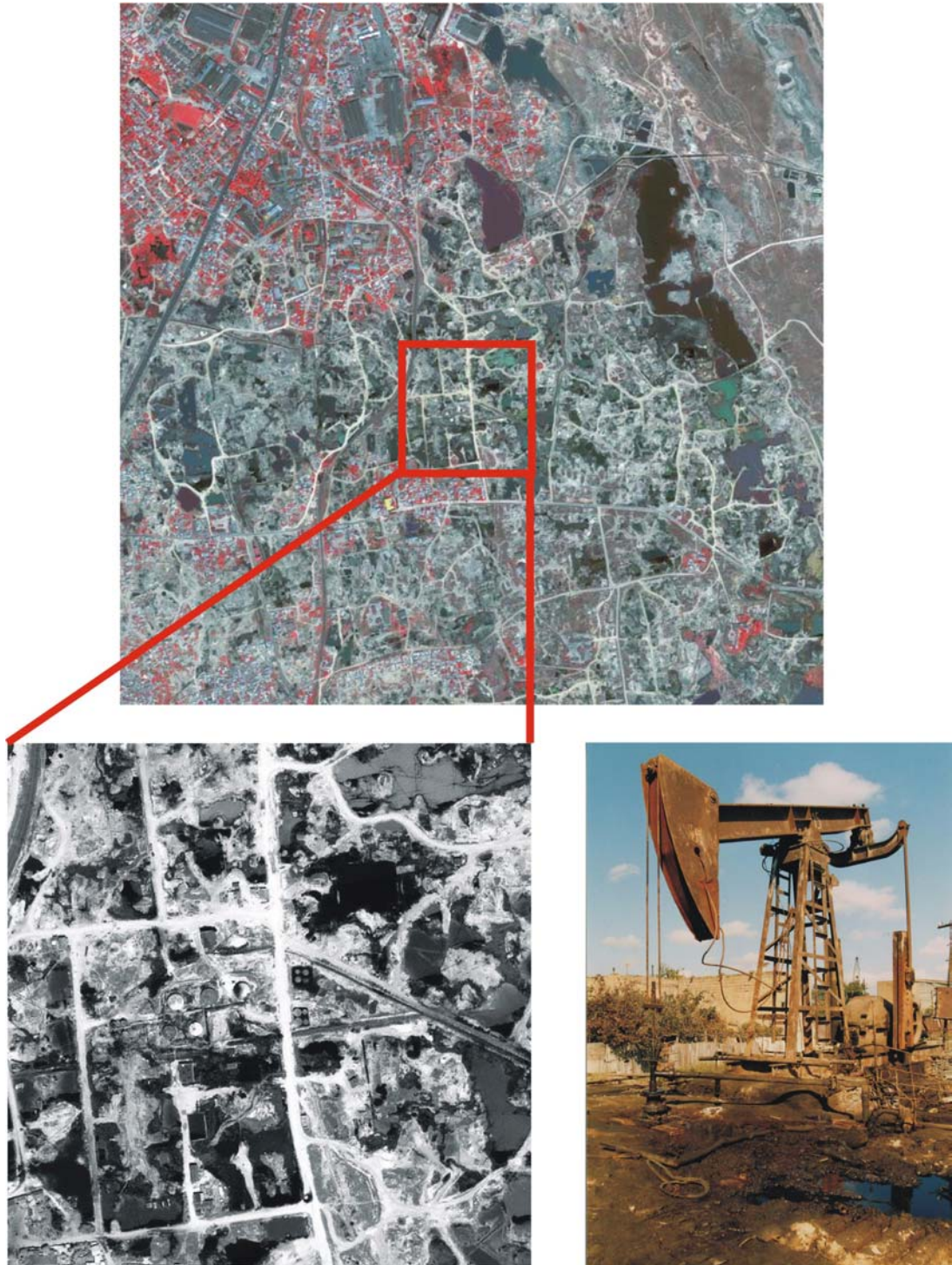


Figure 2-1: Oilfields on the Absheron Peninsula in Azerbaijan. Top: Subset of an IKONOS satellite image (false-color-infrared) of the northern suburbs of Baku, the capital of Azerbaijan with a spatial resolution of four meters. The belt of oilfields is clearly visible in this satellite image, appearing grayish to black without any vegetation. Bottom left: Enlargement of a part of the oilfields (IKONOS PAN, 1 meter spatial resolution). Storage tanks and crude oil spills and basins are clearly visible, intersected by a network of unpaved roads. Bottom right: Oil pump in the area with typical surrounding soil contaminations.

Industrial site “Schwarze Pumpe”, Brandenburg/Saxony, Germany

Industrial Sector:	Conversion of lignitic coal (brown / soft coal)
Location:	30 km south of Cottbus, Brandenburg, Germany
Plants:	Briquetting plants, power plants, coking plant, gasworks, workshops, wastewater treatment plants
Contaminants:	Polynuclear aromatic hydrocarbons (PAH), phenols, benzene, fuel hydrocarbons
Operation time:	ca. 1950 – today
Area:	ca. 6 sq. km
Site description:	<p>Conversion of lignitic coal into electricity, lignite coke, town gas, and briquettes. Conversion plants for electricity generation, briquetting, coking and gasification plus auxiliary installations are part of the industrial site. Workshops and fuel storage for nearby open cast lignite mines located on-site. Water treatment plants and landfill sites for residual and waste products from gasworks and coking plant (in particular tar, water containing phenols and benzene) have been erected on-site and nearby. Gravel pits that were exploited during the erection of the industrial facilities in the 1950s were used as landfills for tar and other waste products without top or bottom sealing. Extensive road and railway networks connect the facilities onsite with external landfills and open cast lignite mines. Due to lowering for mining, the groundwater table has been reduced to an average fifteen metres below ground surface. Huge quantities of contaminants have leaked over more than 40 years into the subsurface, in particular from a relatively small source areas at the gasworks’ gas purification installations and the wastewater treatment plant. A large groundwater plume of circa four by two kilometers has developed with benzene and phenols as the major contaminants. Surface contaminations of soils and anthropogenic surfaces (roads, ballast road and track beds, concrete surfaces) are limited to major transportation pathways of waste products. Large areas are sealed with anthropogenic materials (concrete, asphalt, pavement, buildings). Several smaller groundwater plumes including contaminants such as fuel hydrocarbons and chlorinated hydrocarbons originate from other installations on the site [Spyra 2001-2004, Winkelmann 2001a].</p>

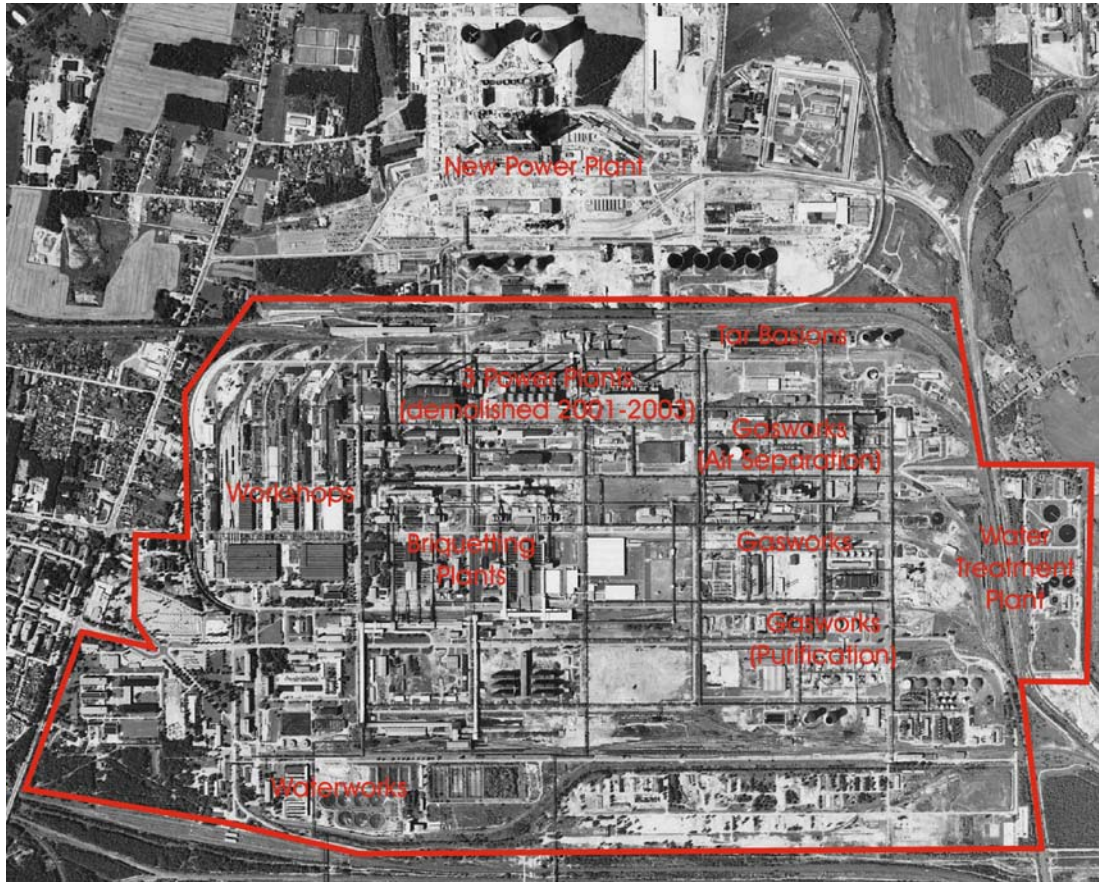


Figure 2-2: Industrial facility Schwarze Pumpe in a panchromatic aerial photograph from 1996. As of 2004, many of the old facilities have been demolished, in particular the three old power plants, the tar basins, a briquetting plant and parts of the gasworks. A huge groundwater plume with high concentrations of benzene and phenols extends from the gasworks purification plant to the western border of the facility [Courtesy aerial photograph: Landesvermessung Sachsen 1996].

Former military training area Döberitzer Heide near Berlin, Germany

Industrial Sector:	Military training area
Location:	10 km west of Berlin-Spandau
Plants:	Barracks, workshops, fuel storage facilities, airfield, and firing ranges for small arms, artillery and tanks
Contaminants:	Uncontrolled waste and scrap deposits, explosives and unexploded ordnance, chemical warfare agents (burials), fuel hydrocarbons
Operation time:	ca. 1890 - 1994
Area:	ca. 50 sq. km
Description:	The former military training area Döberitzer Heide was used by German forces since approximately 1890 until the end of World War II. From the 1950s until 1994 it was used by Soviet forces. Since the withdrawal of Soviet forces, a small portion of the former military training area (ca. 20 %) serves as a training area for the German Bundeswehr. The parts that are no longer used for military purposes have become a natural reserve in 1994.

Due to its proximity to Berlin, the Döberitzer Heide was not only used for standard military training (in particular artillery, tanks and infantry), but also for the development and testing of new warfare technologies. During World War I, the Kaiser Wilhelm Institute of Physical Chemistry and Electrochemistry used parts of the Döberitzer Heide for testing of newly developed chemical warfare agents. During World War II and the interwar years, the site was used for the development and testing of new infantry weaponry and equipment.

Due to long-term military use, land use structures of the Döberitzer Heide must be viewed as highly heterogeneous, if not chaotic. Intensive shooting exercises with artillery and tanks, driving exercises with heavy equipment, blasting of old structures and expired ammunition, exercises with vehicles in the field including maintenance and digging of emplacements and infantry trenches, and the uncontrolled dumping of household, commercial and ammunition wastes from three major barracks in the neighborhood have created a highly diversified landscape. Furthermore, like other military training areas, the Döberitzer Heide was regularly restructured to meet new the requirements of military strategy and tactics, equipment and weaponry. Restructuring included: changes to

road systems, the installation of new shooting ranges and the closure of old ones, dismantling of old installations and buildings and extensive earthworks in order to form the training facilities to meet requirements.

Therefore, the land use patterns are highly diversified. Typical structures, such as unpaved and concrete roads, heather landscapes, open soil, moors, succession woodlands of oak, alder, birch, poplar and (rarely) pine, old forests, shooting ranges, waste deposits, vehicle emplacements etc., change from one to another within several meters over the whole site.

Based on information gathered in previous investigations, uncontrolled waste dumps are usually found in the vicinity of one of three barracks on the outskirts of the Döberitzer Heide. Unexploded ordnance is found everywhere on the site with accumulations on shooting ranges and in the vicinity of barracks. However, due to unconventional disposal or unknown historical activities, larger amounts of ammunition could be found everywhere on the site. Chemical warfare ammunition was buried near two known proving grounds used during World War I. Soil contaminated with fuel hydrocarbons is typically found near filling stations at the barracks or on the site and, randomly distributed, over the whole site. However, the latter have to be considered as small-scale contaminations resulting from field refueling or maintenance exercises [Winkelmann 2001d, Spyra 2004].

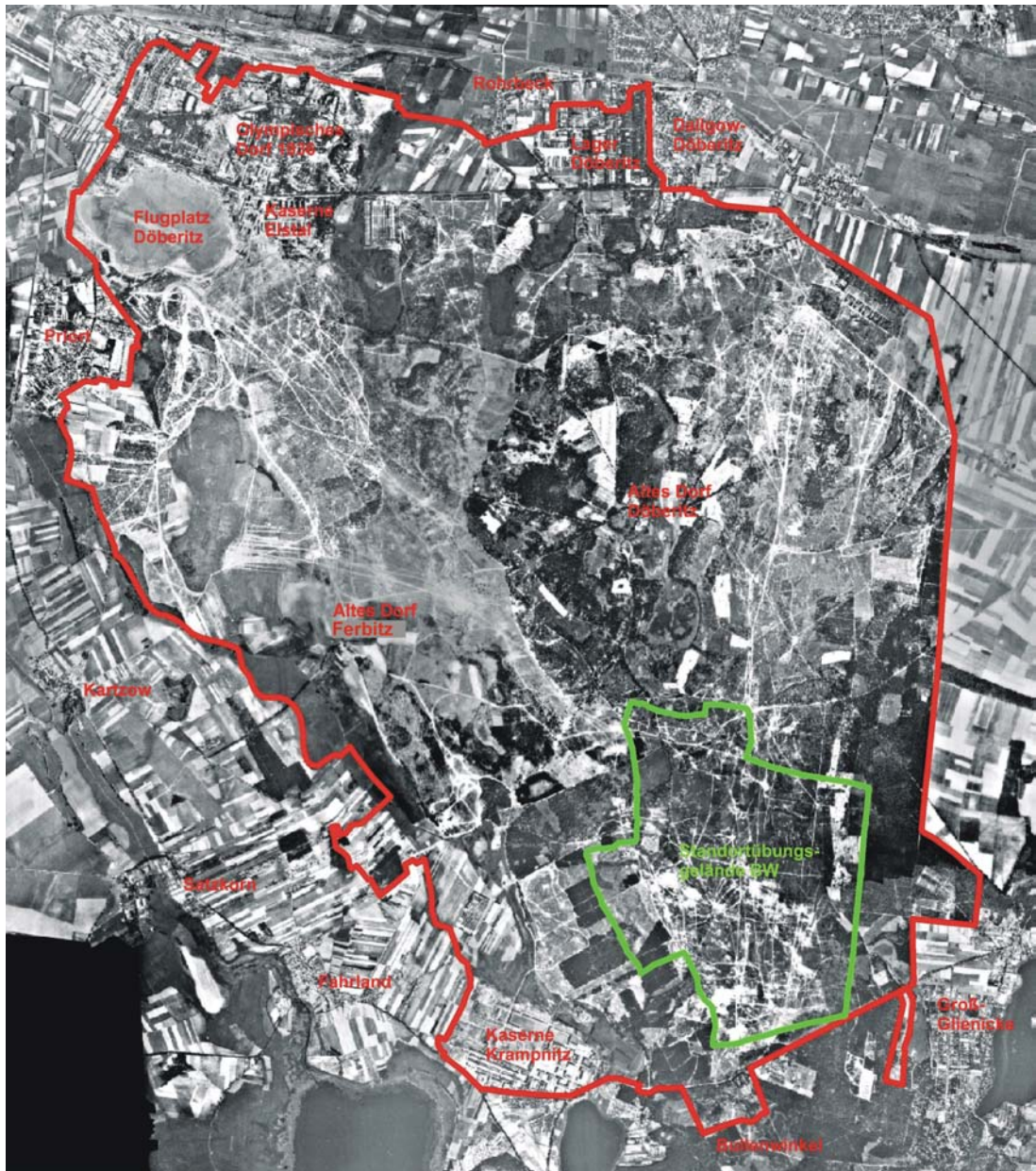


Figure 2-3: Panchromatic aerial photograph of 1953 of the former military training area *Döberitzer Heide* west of Berlin illustrating the highly diversified and heterogeneous land use structures. Today, only the small area in green borders is still used for military training. The largest part of the site is now a natural reserve. Today, the open spaces are in large part covered by heather and succession forests [Courtesy aerial photograph: Landesvermessung Brandenburg].

Uncontrolled waste dump, Rio Unare Basin near Puerto La Cruz, Venezuela

Industrial Sector:	Waste disposal
Location:	ca. 50 km southwest of Puerto La Cruz, Venezuela in the River Unare catchment area
Plants:	None
Contaminants:	Uncontrolled deposit of household and commercial wastes
Operation time:	ca. 1990 - today
Area:	ca. 100 meters by 300 meters
Description:	Household and commercial wastes of all kinds are being deposited on an area of circa 100 meters by 300 meters of open soil with some minor areas covered by vegetation. According to visual inspection, the wastes deposited consist of the following major fractions: plastics, metal, organic material, wood, paper, and containers containing artificial and natural waste materials. Accumulations of wastes are burning or smoldering. The maximum age of the waste deposit was estimated at ten years. However, as people are obviously sorting, re-using and burning parts of the wastes, the age of the deposit can not be dated exactly. The groundwater level at the site is estimated at two to four meters below ground surface. Groundwater contamination is likely [Winkelmann 2001b].



Figure 2-4: Photograph of the uncontrolled wastes dump in the Rio Unare Basin in Venezuela with a variety of household and commercial wastes on open soil, in parts burning and smoldering.

Mingecevir rocket fuel depot, western Azerbaijan

Industrial Sector:	Military fuel depot
Location:	Western Azerbaijan, 20 km west of Mingecevir, southern shoreline of Mingecevir reservoir
Plants:	Storage tanks for several fuels, lubricants and propellants used by the military
Contaminants:	Triethylamine, xylidines, isopropyl nitrate, red fuming nitric acid
Operation time:	ca. 1960 - today
Area:	ca. 200 meters by 400 meters
Description:	Different fuels (diesel, kerosene, gasoline, lubricants, liquid missile propellants, etc.), and liquid missile propellants are stored in large storage tanks above surface. An inventory of the liquid rocket fuels stored (as of January 2003) stated that 380 metric tons of oxidizers (red fuming nitric acid), 290 metric tons of samine (50 % triethylamine + 50 % xylidines) and 24 metric tons of isonite (isopropyl nitrate) are stored at the Mingecevir depot. The oxidizers are stored in about 15 large storage tanks (20 – 40 m ³), most of which are lying on the bear ground. Leaks and traces of spills (rusty-brown, open soil) are visible, usually covering an area of about 100 – 200 square meters around a tank.

Samine is stored in similar storage tanks that are lying in an open pit two meters deep in contact with groundwater together with other tanks containing a mixture of kerosene and gasoline. Due to contact with water, the steel tanks show severe corrosion. A characteristic smell and floatings on the water in the open pit are evidence for leakage of samine and fuel hydrocarbons (kerosene, gasoline) from the storage tanks in the pit. Because of the high groundwater level of about one to two meters below ground surface and the long term storage in this condition, groundwater contamination is expected. Dark red coloring of the soil surrounding the storage pit point to larger spills of samine as the constituents of samine typically form dark red complexes with soil constituents. However, the dark red colored soil is covered by wind-deposited fine sediments, and it becomes only visible if the covering layer (about 2 – 5 millimeters thick) is removed [Spyra 2003, Winkelmann 2004].



Figure 2-5: Steel storage tanks containing liquid rocket fuels (samine, kerosene, gasoline), stored in an open pit in contact with the groundwater. Fuels that leaked from the tanks are floating on the water.



Figure 2-6: Red complexes in the soil indicating leakages of samine. At the Mingecevir depot, this indicator of soil contamination with samine is largely covered by wind deposited fine sediments.



Figure 2-7: Leaking oxidizer (red fuming nitric acid) tank. Due to the leakage of the acid, soil iron has been oxidized – visible through red-brown coloring of the soil.

Crude oil spill on marshland soil, Abadan, Iran

Industrial Sector: Crude oil spill (pipeline spill)
Location: Southern Iran on the Iran-Iraq border in the Shatt al-Arab
Plants: Pipeline crossing the spill area
Contaminants: Crude oil
Operation time: NA
Area: Several square kilometers
Description: During the Iran-Iraq war in the 1980s, a crude oil pipeline on Iranian territory in the Shatt al-Arab was destroyed by Iraqi armed forces. Crude oil spilled from the pipeline into a protected marshland near the town of Abadan on the shores of the Persian Gulf.

Large parts of the contamination remain visible at the surface (heavy crude oil that solidifies at low temperatures and liquefies at high temperatures). In some parts, the contaminated marshland soil has been covered by atmospheric and maritime deposition of fine sediments. Some parts of the contaminated area are sparsely covered by salt marsh plants, in particular halophytic grass species [Spyra 2002].



Figure 2-8: Heavy crude oil leaked from a pipeline, destroyed in the Iran-Iraq wars, into protected maritime wetlands in the Shatt al-Arab in southern Iran.

Illegal waste dump Groß Pinnow, northern Brandenburg, Germany

Industrial Sector:	Illegal gravel/sand pit and waste dump (waste burials)
Location:	20 km north of Schwedt, northern Brandenburg
Plants:	None
Contaminants:	Fuel hydrocarbons, asbestos, sewage sludge containing increased heavy metal concentrations
Operation time:	ca. 1990 - 1998
Area:	ca. 100 meters by 200 meters
Description:	In the boundary area of a German national park, a building contractor established an illegal sand and gravel pit and used the pit for the illegal disposal of construction and demolition wastes as well as sewage sludge and scrap metal. The site is located about 50 meters south of an old, abandoned landfill within farmland used for agriculture (2001: rapeseed). The site is characterized by topography and vegetation anomalies. The prevailing species found on the site are typical to fallow lands. Contaminated soil is mainly found at depths between one and four meters. The surface is covered with local sediments and inert construction wastes similar to sandy soils. Groundwater contamination is unlikely considering the low groundwater level (> 20 meters below the surface) and the contaminants involved [Spyra 2001b].



Figure 2-9: Photograph of the illegal waste burial site within an agricultural field (rapeseed) in 2001. The burial is characterized by a vegetation anomaly with species typical of fallow land. The picture was taken from the old landfill that lies on a natural cliff northwest of the burial site.

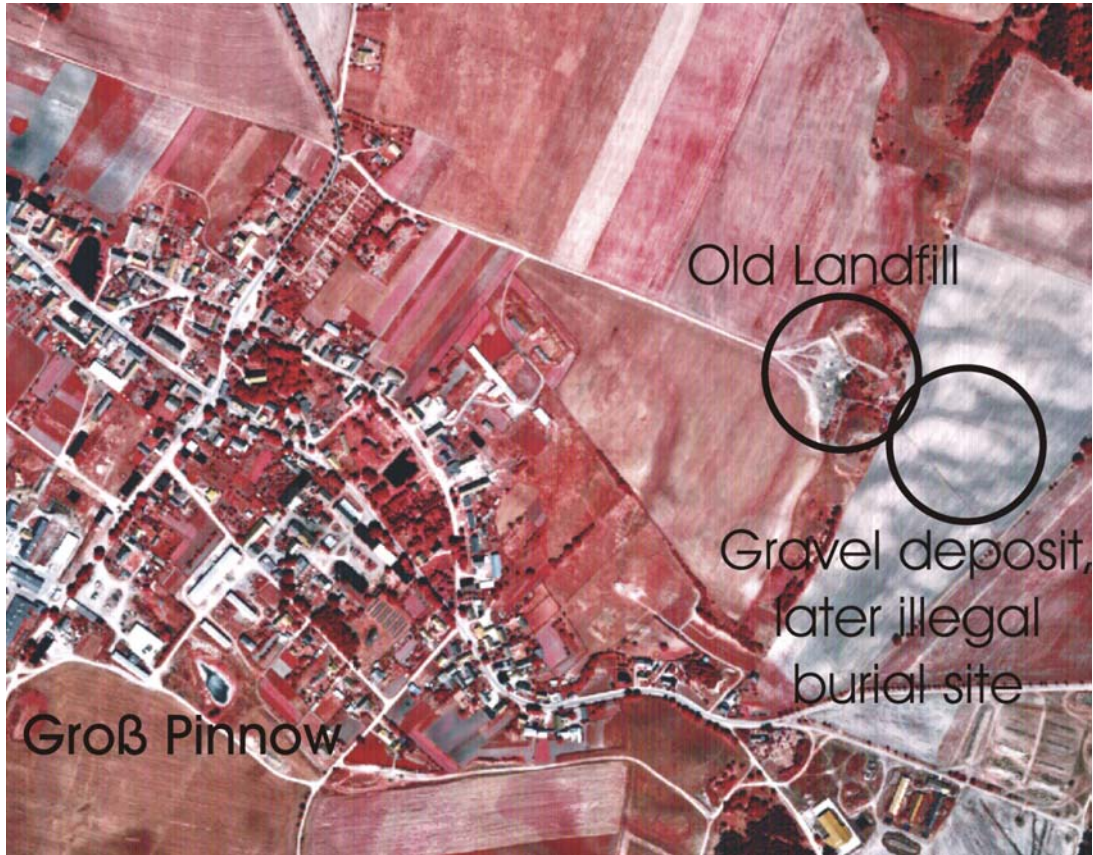


Figure 2-10: False-color infrared aerial photograph of the village of Groß Pinnow, the old landfill and the gravel deposit on an agricultural field was illegally exploited and later backfilled with wastes [Courtesy aerial photograph: Landesvermessung Brandenburg 1992].

Abandoned glassworks Haidemühl, southern Brandenburg, Germany

Industrial Sector:	Glassworks
Location:	ca. 30 km southwest of Cottbus, southern Brandenburg, Germany
Plants:	Gasworks for gas production (furnace heating), fuel oil tanks, industrial waste dump, two large tank furnaces for glass melting, maintenance workshops, storage and processing facilities for raw materials
Contaminants:	Tar / polynuclear aromatic hydrocarbons (PAH), heavy metals (in particular arsenic, cobalt, chromium, copper), fuel hydrocarbons
Operation time:	1837 - 1996
Area:	ca. 200 meters by 400 meters
Description:	<p>The former glassworks Haidemühl have been producing household glassware for more than two centuries with a focus on clear, milk, blue and green glass. While in the early days wood was used for heating the glass melting furnaces, from the 1870ies on, gas produced in two on-site gasworks and later heavy fuel oil and gas produced off-site were used as fuels. Raw materials used for glass production apart from the major inert constituents such as silica sand like arsenic oxide, chromium oxide, and cobalt oxide were stored in processed in a glass batch house.</p> <p>Most parts of the glassworks facility except the on-site landfill are covered by concrete pavements, railroad tracks, and buildings.</p> <p>Wastes generated in the production process, such as cullet, residues of raw materials and in particular huge quantities of ashes and tars from the two on-site gasworks were disposed off on two on-site landfills that were continuously enlarged. While the smaller landfill has been built over with auxiliary facilities, the larger landfill lies fallow and is largely covered by grass and similar vegetation with few exceptions where deposited glass cullet prevents vegetation growth.</p> <p>Two heavy fuel oil contaminations are located under the tank furnace buildings, with both contaminations reaching at least eight meters below the basement of the buildings. A third fuel oil contamination is expected at the site of surface fuel oil tanks that were removed during the 1980s. Groundwater contamination is not expected because the groundwater level</p>

has been lowered to more than 20 meters below ground for decades because of lignite mining in the vicinity.

Because of the area of the Haidemühl village was utilized for open cast lignite mining, the abandoned facility will be demolished in 2006 [Spyra 2001a].



Figure 2-11: Aerial photograph (panchromatic, 1996) of the former Haidemühl glassworks. While housing several severe soil contaminations and waste deposits with contaminants like fuel hydrocarbons, tars (PAH), and heavy metals, none of these contaminations are directly evident at the surface [Courtesy aerial photograph: Landesvermessung Brandenburg].

Ordchodnikidse manganese mining district, Ukraine

Industrial Sector:	Manganese metallurgy industrial waste dumps
Location:	130 km southwest of Dnepropetrovsk, central Ukraine
Plants:	Metallurgical plant for extraction of manganese from manganese oxide and carbonate ores from nearby open cast mines
Contaminants:	Manganese metallurgy wastes, probably heavy metals
Operation time:	ca. 1930 - today
Area:	ca. 500 meters by 1500 meters
Description:	Large quantities of manganese ores (manganese carbonates and manganese oxides) are produced from open cast mines in the Ordchodnikidse region in central Ukraine. The manganese ores are processed in a local metallurgical plant in order to extract the manganese. Large quantities of metallurgical wastes, both liquid and solid, are produced during the manganese extraction. Although floating liquid wastes are disposed of in large embankments, solid wastes are disposed of in a large dump at the factory.

An elution of heavy metals associated with the manganese ores is reported from the dump. The dump extends over an area of approximately 500 meters by 1,500 meters. The make-shift dump of residuals, resulting from the extraction of manganese from its ores, is not covered by any vegetation, while the surrounding landscape is dominated by grasslands [Winkelmann 2001c].

Small diesel filling station, Rio Unare Basin, Venezuela

Industrial Sector:	Diesel filling station on unpaved ground with underground storage tank
Location:	circa 60 km southwest of Puerto La Cruz, Venezuela
Plants:	Underground storage tank and petrol pump
Contaminants:	Diesel fuel
Operation time:	ca. 1970 – today (estimated)
Area:	ca. 10 meters by 10 meters
Description:	A diesel filling station consisting of an underground storage tank and a petrol pump is situated on a country road in the Rio Unare catchment area. The filling station, probably used for more than 30 years, is erected on unpaved soil. Dark coloring and a characteristic smell indicate heavy diesel fuel contamination of the soil surrounding the petrol pump on an area of approximately 10 by 10 meters.

Based on the water level of the nearby river, the groundwater level is estimated at three to five meters below ground surface. Based on the age of the pump and the degree of the surface contamination, a groundwater contamination is likely – regardless of unknown leakages from the underground storage tank [Winkelmann 2001b].



Figure 2-12: Photo of the small diesel filling station in the Rio Unare Basin in Venezuela, with clearly evident heavy diesel fuel contamination.

From the above descriptions of some typical contaminated sites it becomes clear that contaminated sites are not objects with a homogenous appearance or contamination pattern but rather individual, and in some cases even unique situations that occur in the anthropogenic environment. However, most contaminations can be categorized in one of the following classes by their overall description, outer appearance, and size:

- Large, homogeneous areas with repeated contamination patterns with surface expression (examples: oilfields Absheron Peninsula, Azerbaijan; metallurgy industrial waste dump near Ordchonikidse, Ukraine)
- Large, heterogeneous, almost “chaotic” sites with many small contaminations that do not necessarily exhibit surface expressions (example: military training area *Döberitzer Heide*)
- Industrial facilities (built-up areas) with surface sealing of large areas, severe contamination but only few surface expressions (example: industrial facility *Schwarze Pumpe*)
- Areas of covered contamination such as burials or covered landfills (example: illegal waste dump / burial *Groß Pinnow*)
- Relatively small contaminated areas (hot spots) in larger, uncontaminated areas of similar appearances (example: refined product pipeline leakage into permeable soil)
- Relatively small contaminated areas (hot spots) in larger, uncontaminated areas of different appearances (examples: diesel filling station and uncontrolled waste dump in Venezuela)
- Relatively low contaminant concentrations (percentage) over large areas (example: downwind areas of large industrial facilities)
- Large contaminated areas of homogeneous surface but with no or only partial expressions of the contamination at the surface (example: Abadan marshland oil spill, Iran)

When comparing different contaminated sites it also becomes obvious that soil contaminations and their surface expression also occur in different geometric patterns. Contaminations and/or their surface expressions typically occur as point, linear or area (polygon) contaminations.

Point soil contaminations occur, for example, at the sites of accidental liquid contaminant spills. Liquid contaminants infiltrate quickly into the soil and do not spread on the surface (soil). This is due to chemical and physical properties of both soil and contaminant. A typical example for this case is the leakage of low-viscosity fuel hydrocarbons into coarse sand soil on even surfaces.

Linear contaminations typically occur along the major axis of infrastructure facilities such as roads, railways or pipelines that are used for the transport of hazardous goods. Small quantities of contaminants continuously lost during transport add up to substantial contamination over time. Examples include, among others: the main railroad line from Baku (Azerbaijan) to Georgia, which is used for crude oil exports and where obviously leaky tank cars are used for transport; the railway tracks of the Schwarze Pumpe facility in Germany that were used for the transport of waste products such as tar sludge in open rail cars or leaky pipelines; and the border region of Iran and Iraq, which were affected by wartime events.

Polygon contaminations involve larger areas that are more or less homogeneously affected by a contamination of one type or origin. Typical examples include oilfields, landfills, overburdened dumps, and areas of salinized soils.

However, depending on the scale applied to the considerations concerning one or more contaminated sites or regions, no clear dividing line can be defined between point, linear and polygon contaminations. Depending on the scale, point or linear contamination could be considered as a polygon (area) contaminations and vice versa.

Furthermore, the contaminations described above also indicate that, according to their genesis, contaminations can be class into the following groups:

- Burials of wastes (landfills and uncontrolled/illegal burials containing household, commercial, industrial or hazardous wastes)
- Industrial facilities where relatively small quantities of contaminants leaked over a long time of operation, thus resulting in a considerable contamination of soil and/or groundwater
- Mining areas (in particular for metal mining), where acid-generating and heavy-metal-containing minerals are disposed on unsecured overburdened dumps that are subject to leaching processes resulting in soil and/or surface water and groundwater contaminations
- Spill sites where large quantities of (usually liquid) contaminants leaked over a short period of time into the environment accidentally, and depending on local conditions and environmental media affected, result in minor or major contaminations of soil and/or surface water and groundwater

Contamination of soil and groundwater can result from short-term, singular events as well as long-term exposure to contaminants. The latter case applies to many sites that have been subject to long-term use for industrial production and experience changes in land use or production technology, or change due to the development of new products and the erection of new facilities at the site. In such long-term use

situations, multi-layer, superimposed contaminations appear where only parts of a contamination or contaminations might show surface expressions.

The above considerations are summarized in figure 2-13. A soil contamination that is largely covered in the subsurface might:

- Show no surface expression if it is covered by uncontaminated soil or anthropogenic surfaces (pavements etc.)
- Exhibit contaminated soil or waste at the surface
- Be covered by unstressed native vegetation if the species are insensitive to the contaminants or concentrations levels found in the rhizosphere of the plants
- Be covered by stressed native vegetation if contaminants or concentrations in the rhizosphere of the plants are above the specific sensitivity and below the maximum specific tolerance level of the vegetation species affected
- Be covered by vegetation species that are adapted to the site conditions (contaminants / contaminant concentrations) and that are different from the normal, “native” vegetation

In addition, depending on physicochemical soil and contaminant properties, a groundwater contamination could develop due to percolation and leaching processes from the soil contamination and extend over large areas without exhibiting any surface expression.

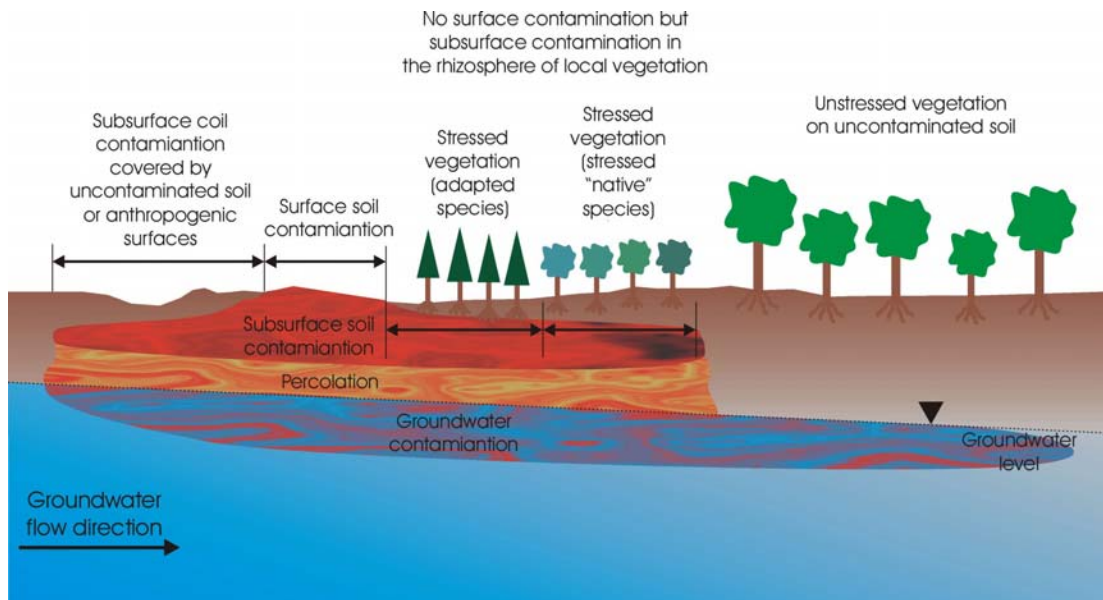


Figure 2-13: Illustration of different cases of soil and groundwater contaminations exhibiting different or no surface expressions.

2.2 - Site registration and site investigation

In most industrialized countries, in particular in the G8-countries (except Russia), and countries of the European Union, Australia and New Zealand, the problem of contaminated sites has been addressed for more than two or three decades. The problem is still being ignored, however, in most developing countries, newly industrialized countries and oil-exporting countries. Examples are Eastern and Southeastern European countries, countries of the former Soviet Union, oil-producing countries in the Middle East, the Southeast-Asian “Tiger” countries, China and South America with their booming industry and developing countries in Africa, South and Central America. Typically, the importance of environmental protection is acknowledged by the wider public in these countries. However, legislation and enforcement are usually of minor overall interest compared to the prioritized issues of economic growth. In most cases, legislation and enforcement are directed at preventive measures for environmental protection in the economic catching-up process that often takes a considerable toll on natural resources. Therefore, contaminated sites that require considerable technological efforts and expenses for investigation and clean-up are typically not an important issue on the environmental agenda of these countries.

This might change as the effects of improper waste disposal, industrial waste water discharge into streams and rivers, and site contaminations due to “dirty” industrial production become obvious because basic natural resources become heavily affected in particular in fast-growing metropolitan areas and centers of industry. In particular the contamination of drinking water resources and agricultural soils might prove to be a critical issue in these areas and raise the awareness for contaminated sites.

While the problem of contaminated sites is being addressed with time-consuming and highly expensive methodologies and technologies for site registration, site investigation, risk assessment and site clean-up in the industrialized countries, it is obvious that these methodologies and technologies could not be applied in developing and newly industrialized countries. Therefore it will be necessary to develop new methods and technologies that are adapted to the problems arising and the possibilities of these countries. Because usually no inventory of potential contaminated sites is maintained, it will be necessary to start with the systematic registration of potential contaminated sites once the problem is acknowledged. For contaminated site registration it will be necessary to develop technologies to reliably detect unknown contaminations and to map larger, known contaminations. In order to improve the process of contaminated site investigation it would be desirable to enable a preliminary site characterization with the data acquired for site registration. A further step that could be derived from the preliminary site characterization could be the development of a priority list for subsequent measures with respect to contaminated site characterization and clean-up.

A technology developed for this purpose could also prove useful in industrialized countries. Even though the problem of contaminated sites is has been addressed in

most industrialized countries for more than two decades, many sites have only been registered as potential contaminated sites without subsequent investigation, risk assessment or clean-up. Many sites, in particular larger sites in remote areas, lie fallow because of lacking economic interest and a lack of public resources for the characterization and clean-up of these sites. Here also, the development of cost-effective new methods and technologies for site investigation is desirable.

2.3 - Contaminants

Chemical substances are usually considered as relevant contaminants of important natural resources such as soil, surface water and groundwater because of their toxicity, their overall abundance or their physicochemical properties that enable fast and widespread distribution and therefore fast and widespread contamination of natural resources. Among the contaminants that are of special interest in contaminated site investigation and clean-up because of their acute or chronic toxicity or their proven or presumed cancerogenicity are, among others:

- Chemicals of the group of persistent organic pollutants (POPs) such as dioxins, DDT, polychlorinated biphenyls, and hexachlorobenzene that have served for different purposes such as pesticides, transformer oil, flameproofing agents in the past or that are byproducts in incomplete combustion processes
- Volatile organic compounds, many of which are halogenated hydrocarbons such as trichloroethylene (TCE) and perchloroethylene (PCE) that have been used extensively as dry-cleaners, solvents and degreasing agents
- Polynuclear aromatic hydrocarbons (PAH) that are the important components of tars and heavy crude oils and are generated in incomplete combustion processes
- Petroleum or fuel hydrocarbons with their subgroups aliphatic (alkanes, alkenes, alkynes, cycloalkanes) and aromatic (monoaromatics and PAH) hydrocarbons as the most important fuels and basic compounds of industrialized societies
- Heavy metals such as arsenic, chromium, lead and mercury that are relevant in metal mining areas, but also as contaminants at electroplating facilities, metallurgical plants and paint production facilities
- Radionuclides and nuclear wastes containing uranium, plutonium, and radioactive isotopes of other elements (although in some countries dealt with separately from hazardous wastes and contaminated sites, e.g., in Germany)

The environmental behavior and fate of contaminants in the environmental media soil, water and atmosphere is determined by their physicochemical properties,

namely water solubility, melting and boiling point temperature, specific gravity, vapor pressure, viscosity, reactivity / half-life and partition coefficients. Depending on their physicochemical properties and the actual environment in which they are released, contaminants can be mobile or immobile and therefore spread or not spread in the environmental media. They may undergo biotic or abiotic transformation or be persistent, and might have to be considered toxic or non-persistent and considered non-toxic. Depending on their human and environmental toxicity and the exposure pathways that are to be considered, the concentration from which a chemical is considered a contaminant in a given matrix (soil, surface water, groundwater, air) might vary considerably.

2.4 - Fuel hydrocarbons as environmental contaminants

Among the chemicals that are relevant as environmental contaminants, fuel hydrocarbons are of particular significance. In 2003, more than four billion cubic meters of crude oil were produced in more than 50 countries worldwide [OPEC 2004, EIA 2004a]. Crude oil and refined crude oil products are utilized in all countries of the world for heating, as feedstock for the chemical industry, as a fuel for power plants and as fuels for all means of transportation vehicles and machinery. In most countries, crude oil and refined crude oil products are the primary fuel and therefore the basis of the economy. In more than 16 countries worldwide, more than one million barrels ($\approx 159,000 \text{ m}^3/\text{d}$) of crude oil are produced every day [OPEC 2004].

Crude oil and refined crude oil products therefore occur at almost every location on earth at the different stages of crude oil production, handling, transportation, refining and consumption:

- Crude oil production
- Transport and intermediate storage of crude oil
- Refining
- Transport and intermediate storage of refined products
- Distribution of refined products (filling stations)
- Use of refined products as fuels
- Use of refined products as base materials in the chemical industry (e.g., intermediate products, solvents, plasticizers, etc.)

The historical development of total world crude oil production in million cubic meters per day and billion cubic meters per year is illustrated in table 2-1.

Table 2-1: Annual world production of crude oil in cubic meters per day and per year for selected years between 1960 and 2003.

Year	Million m ³ /day	Billion m ³ /year
1960	3.34	1.22
1970	7.30	2.66
1980	9.48	3.46
1990	9.63	3.51
2000	10.87	3.97
2003*	11.05	4.03

*The International Energy Agency reports a daily production of 12.65 million m³/day for 2003, equivalent to 4.62 billion m³/year.
 [Based on EIA 2004a, IEA 2004a]

The historical development of world crude oil production is illustrated in figure 2-14. Apart from two relatively short periods that became known as the oil crises in the mid-1970s and the early 1980s, the production of crude oil has continuously increased from 1.22 billion cubic meters per year in 1960 to 4.03 billion cubic meters in 2003.

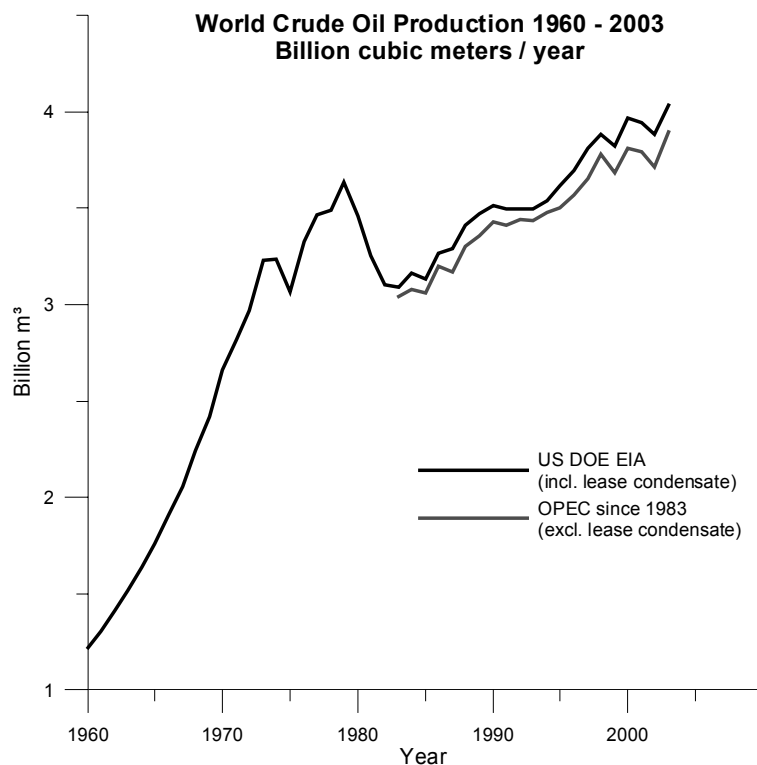


Figure 2-14: Graph of the development of crude oil production since 1960 [Based on data of OPEC 2004, EIA 2004a].

With the continuing and accelerated growth of economies in Asia (in particular China, India and Southeast-Asian countries), Eastern Europe and South America, a continuing growth of the world population from 6.3 billions in 2003 to 7.4 – 10.6 billions in 2050, and proven world oil reserves of more than 180 billion cubic meters (as of 2003), it is expected that the annual production of crude oil will continue to rise until at least 2025 [UNWPP 2003, OPEC 2004, EIA 2004a]. In contrast to this prognosis, some analysts also predict that after a short-term increase in world oil production, oil production will sharply decrease until 2050. They argue that because fewer new oil reserves are discovered, production costs will increase sharply as new reserves are more difficult to exploit and therefore crude oil prices raise further [Heinberg 2003].

However, with a total of more than 134 billion cubic meters of crude oil produced between 1960 and 2003 alone and recent world production rates of 13.26 million cubic meters of crude oil per day, the significance of crude oil and refined crude oil products as a potential contaminant is apparent [EIA 2004a, EIA 2004b, BGR 2002].

Because of the huge quantities involved, it is also evident that fuel hydrocarbon contaminations are to be expected almost everywhere due to accidents or improper handling during production, processing or distribution. For example, leakages or losses during the production of crude oil from wells, offshore oil spills, pipeline leakages, leakage from underground storage tanks, accidents of vehicles transporting fuel hydrocarbons, and drop losses at filling stations occur daily in uncounted locations worldwide.

Some examples have been described above: the filling station in Venezuela, the oil fields on the Absheron peninsula in Azerbaijan and the Abadan pipeline spill in Iran. At each of the sites described, the fuel hydrocarbon contamination is detectable by simple organoleptic examination at the surface. Fuel hydrocarbon concentrations are known or expected to exceed 5 % of dry soil weight at each of these sites. Fuel hydrocarbon contamination may affect the surface as well as the subsurface. Due to the production from many wells over a large area and the high viscosity of crude oil, onshore crude oil contamination typically remain at the surface and spread over larger areas. In contrast to this, refined product contaminations typically affect only small surface areas but spread in the subsurface due to a relatively low viscosity and a specific gravity lower than that of water. Therefore, floating product is often observed on the groundwater table at sites where refined fuel hydrocarbon byproduct has been spilled.

Some realistic scenarios for fuel hydrocarbon spills into or onto soil and groundwater at the sites of pipelines, filling stations and oilfields are illustrated in figure 2-15. It stresses that the largest parts of fuel hydrocarbon contamination of soil and groundwater are usually hidden in the subsurface and that only the contamination source areas (hot spots) might be evident at the surface. Oilfields, where large quantities of crude oil are produced from many wells over a large area, can be

considered an exception in this respect because crude oil usually does not infiltrate into the subsurface due to its physicochemical properties.

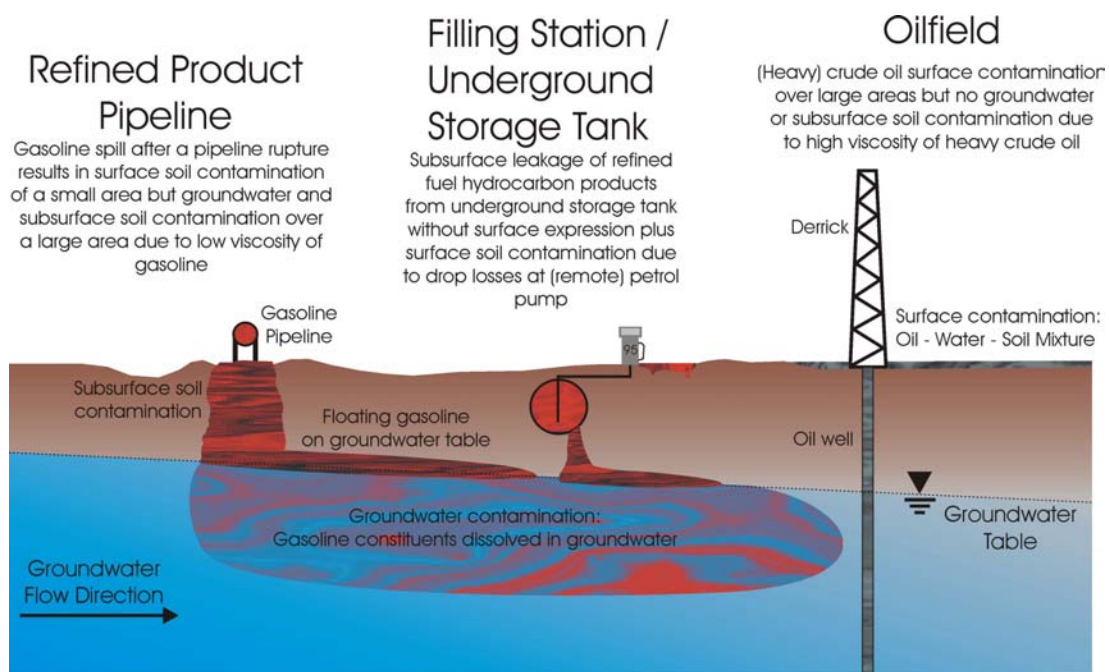


Figure 2-15: Sources and distribution pattern of typical fuel hydrocarbon contaminations of soil and groundwater.

Fuel hydrocarbons have been selected as the model contaminant for the investigation of this thesis because of their overall relevance as environmental contaminants. Fuel hydrocarbons are ubiquitously used in vast quantities almost everywhere in the world. Fuel hydrocarbon spills are common everywhere worldwide and therefore occur in every climactic, geologic, vegetation and topographic region. From a chemical point of view, fuel hydrocarbons are relatively homogeneous with six main subgroups (alkanes, alkenes, alkynes, cycloalkanes, monoaromatics, polynuclear aromatics). However, fuel hydrocarbons for commercial bulk use (fuels) are usually mixtures consisting of chemical compounds of all subgroups. Due to their physicochemical properties, fuel hydrocarbons biodegrade relatively slowly in soil and groundwater and occur as surface contaminants as well as subsurface contaminants.

The considerations of this chapter can be summarized as follows.

Contaminated sites, i.e. contaminations of soil and groundwater and the improper disposal of hazardous wastes, pose severe problems worldwide. Contaminations of soil and groundwater are endangering important natural resources such as drinking water and arable land in both industrialized and developing countries.

Soil and groundwater contaminations cover varying areas from several square meters up to hundreds of square kilometers. They occur in complex structures of built areas as well as in relatively homogeneous rural areas. Sites of industrial facilities or military installations may host several independent contaminations of different origin and genesis. Soil contaminations may be exhibited at the surface level, or may be covered by soil, anthropogenic surfaces or by stressed or unstressed vegetation. Typically, the majority of a contamination is hidden in the subsurface, and only parts of the contamination are revealed at the surface, either as affected soil or stressed covering vegetation.

Among all contaminants that are of interest because of their toxicological potential, their physicochemical properties that enable fast spreading in the environmental media soil and groundwater, and their overall abundance, fuel hydrocarbons must be considered the most important contaminants. Every year, more than four billion cubic meters of fuel hydrocarbons are produced and consumed worldwide.

The methods and technologies that have been developed for contaminated site investigation and clean-up in the industrialized countries require considerable technological efforts, resources, and expenses. While in most industrialized countries the problem of contaminated site investigation is already being addressed, the problem is still being ignored in most developing and newly industrialized countries. At the same time, a considerable backlog with respect to the investigation and clean-up of contaminated sites is not likely to be overcome in most industrialized countries when applying conventional methods and technologies that require considerable resources. Therefore, the development of new methods and techniques for contaminated site investigation and clean-up is necessary.

3 - Principles and technology of imaging spectrometry

The roots of remote sensing go back to the 1860s, when panchromatic photographs were first taken from balloons. In 1908, the first panchromatic photograph was taken from one of the motor-powered aircrafts of the Wright brothers in Italy. Soon after that, remote sensing in the form of panchromatic aerial photographs was extensively used for mapping purposes, and, during the First and Second World War, for military photo-reconnaissance purposes [Jensen 2000]. After the Second World War the development of new remote sensing technologies led to many new applications for environmental remote sensing. Simple electro-optical and thermal remote sensing systems were developed and applied for meteorological remote sensing of cloud cover in the 1960s. Color and false-color near infrared photographic films were used for cartography, habitat mapping, forest inventory, urban planning, archaeology and many other applications. The first electro-optical, multispectral satellites for land remote sensing, the Landsat series, were launched during the 1970s and continue to map the Earth's surface today. Multi-spectral satellite systems provide relatively low-resolution digital image data for large areas in a range of typically four to ten broad wavelength bands, thus enabling land cover classifications using digital image interpretation techniques. With magnified computing capacities during the 1980s and 1990s, the spatial, spectral and radiometric resolution of remote sensing systems was improved, enabling more and more applications and complex interpretation of digital remote sensing data. Radar imaging applying microwave radiation was also developed during the 1970s and 1980s, enabling remote sensing of clouded areas and the derivation of low-resolution surface elevation models. Recent developments in remote sensing that were made possible by the developments in the computing and electronics sectors include airborne laser scanning of surfaces for the derivation of high-resolution digital elevation models, digital cameras for aerial photography with improved spatial and radiometric resolution, and high spectral resolution imaging spectrometry for qualitative and quantitative analysis of surface materials [Lillesand 1999, Jensen 2000].

The subject of this study is the applicability of imaging spectrometry, a high spectral resolution remote sensing method, for the detection and investigation of contaminated sites.

Imaging spectrometry means the “acquisition of images in hundreds of registered, contiguous spectral bands such that for each picture element of an image it is possible to derive a complete reflectance spectrum” [Goetz 1992]. Typically, between 100 and 300 spectral bands with a bandwidth of two to ten nanometers are acquired in the 400 nm to 2,500 nm wavelength region. The spatial (ground) resolution of airborne imaging spectrometry systems typically ranges from 1 to 30 meters. The concept of imaging spectrometry is illustrated in figure 3-1.

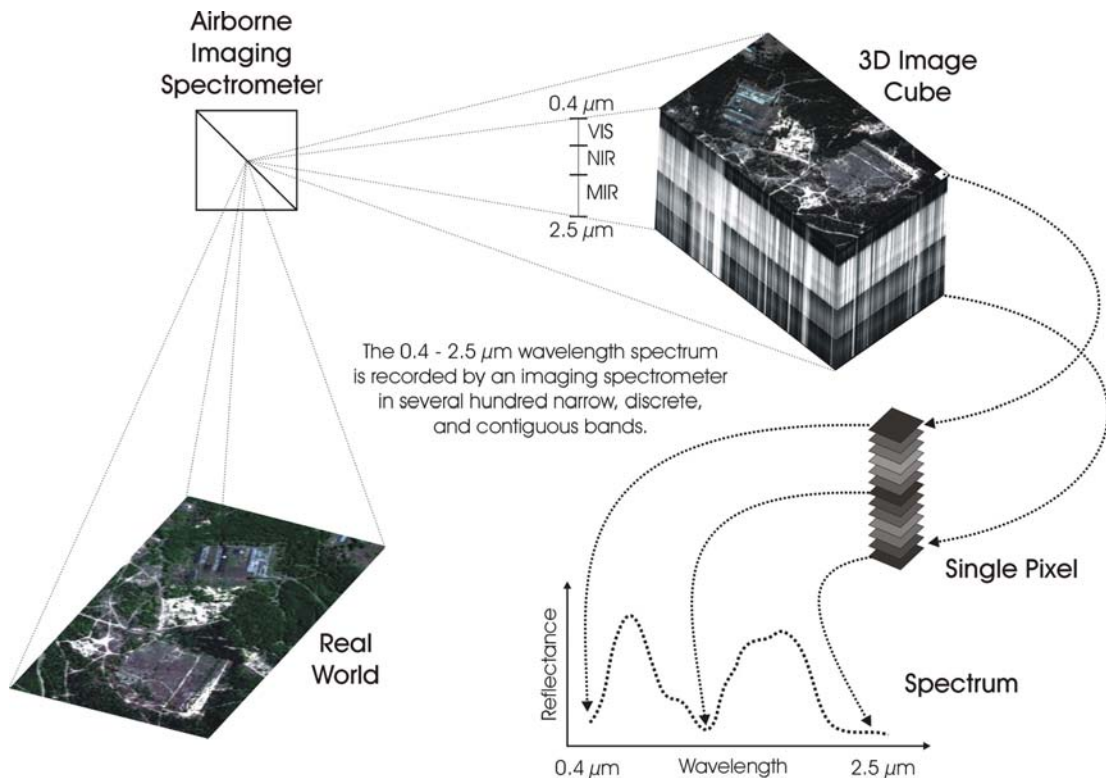


Figure 3-1: Concept of imaging spectrometry (alias hyperspectral imaging): an image of the surface under investigation is acquired in hundreds of small bands typically covering the wavelength region between 0.4 μm and 2.5 μm. Thus, every pixel of the dataset acquired is represented by an individual spectrum containing information about the surface materials and fractions covering the pixel surface.

Imaging spectrometry is sometimes also referred to as “hyperspectral imaging” or “imaging spectroscopy” which are used as synonyms in the remote sensing terminology, even though the meaning is different (spectrometry – “measuring”, spectroscopy – “seeing”, hyperspectral – “too many bands”) [van der Meer 2001e]. However, the term imaging spectroscopy is, in most cases, applied to extraterrestrial applications in astronomy and the terms “imaging spectrometry” and “hyperspectral imaging” are mainly used in terrestrial remote sensing.

Many surface materials of the Earth have diagnostic absorption features in the 400 nm to 2,500 nm wavelength spectrum that are 20 nm to 40 nm wide at half the band depth [Hunt 1980]. This means that solar radiation that interacts with the Earth’s surface is reflected as a function of wavelength and surface material absorption and reflectance characteristics. Depending on the absorption and reflection properties of the surface material and the wavelength of the incident radiation, the reflected radiation over the wavelengths shows characteristic absorption features.

Hyperspectral imaging systems sampling this wavelength region with a spectral resolution of two to ten nanometers in hundreds of contiguous bands therefore produce digital data sets that are sufficient for qualitative material detection or

identification and quantitative material mapping. Multispectral imaging systems that sample selected wavelength regions over a spectral range (bandwidth) of 100 nm to 300 nm do not resolve these characteristic absorption features [Goetz 1985, Vane 1988a]. With its capabilities for high-resolution material identification and quantification, imaging spectrometry can be considered a remote sensing analytical chemistry method that is applied in an uncontrolled environment [Goetz 1996a]. However, it must be stated that not all surface materials exhibit characteristic absorption features and that therefore not all surface materials can be identified unambiguously. Furthermore, if a material has diagnostic absorption features, it must be present at a minimum concentration or coverage in a pixel to be detected.

The datasets that are produced by imaging spectrometers are huge and highly complex, containing large amounts of information. Due to often similar spectral characteristics in neighboring bands, as well as and similar materials over large image scenes, datasets also contain much redundant information. Besides data compression and data processing with appropriate software tools, the reduction of redundancy in the data while at the same time conserving the unique information in the scenes and the interpretation of the datasets pose considerable challenges [Boardman 1995b]. Furthermore, depending on the spatial resolution and the structure of the surface investigated, spectra for individual image pixels may not represent a pure spectrum of one singular material, but a mixed spectrum consisting of spectral responses of the various materials that cover the area sampled on the ground. Various data interpretation software tools have been developed for a variety of applications and have the ability to perform supervised and unsupervised classification and mapping, detection of targets, detection of subpixel targets, and spectral unmixing of “mixed” pixels [Chang 2003b].

Another issue is the derivation of surface reflectance from imaging spectrometer data. Imaging spectrometers covering the 0.4 μm to 2.5 μm region of the electromagnetic spectrum record radiance spectra that depend on both solar illumination and atmospheric absorption. The process of deriving surface reflectance data from imaging spectrometer data is referred to as atmospheric correction based on sophisticated correction algorithms [Goetz 1997].

Recent applications of imaging spectrometry include, among others, mineralogical exploration, geologic mapping, vegetation analysis for precision agriculture, military target detection and terrain analysis, soil mapping, vegetation mapping, monitoring of inland, coastal and marine water bodies, and other environmental applications [e.g., Curran 1994, Clevers 2001, Messinger 2004, Pavlin 1996, Ben-Dor 2001a, Curran 2000, van der Meer 2001c, Gallagher 2003b].

The subsequent sections will provide an overview on the basics of imaging spectrometry, its application in remote sensing, recent imaging spectrometry systems, data processing and data interpretation approaches and methods.

For the subsequent considerations of laboratory spectroscopy and remote sensing imaging spectrometry it must be noted that the definition of wavelength regions used

in the field of remote sensing is different from that used in the field of analytical chemistry. While the definition used in analytical chemistry is based on classes of energy-matter interactions and physical properties of the wavelengths involved, the remote sensing classification takes into account additional properties such as radiation sources and atmospheric windows that prohibit the use of certain wavelength regions for remote sensing. Figure 3-2 depicts the two wavelength region definitions and the background for the definitions used in the field of remote sensing.

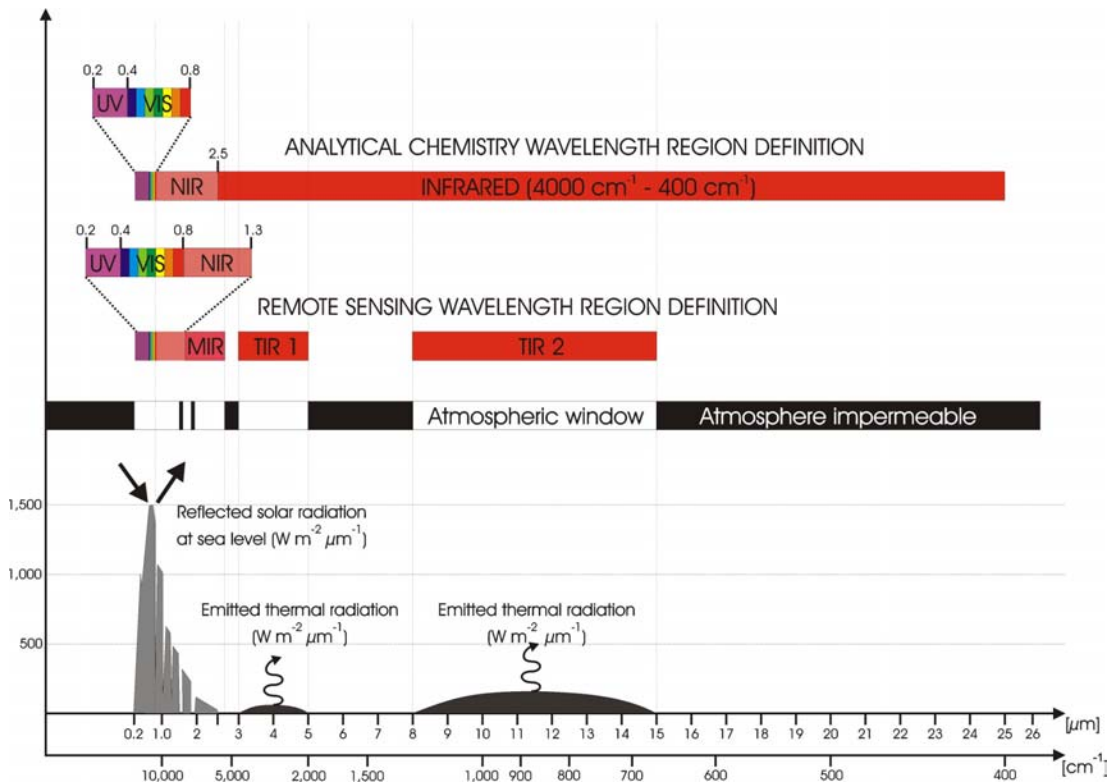


Figure 3-2: Wavelength region definitions for analytical chemistry and remote sensing compared, with atmospheric windows and radiation sources used for passive remote sensing. The comparison shows important differences concerning the “availability” of radiation for sensing and atmospheric interferences in remote sensing.

The wavelength regions and applications in remote sensing are mainly determined by the permeability of the atmosphere for electromagnetic radiation. Because of absorption by atmospheric gases and vapors, in particular water vapor, carbon dioxide, oxygen, and ozone, the atmosphere is impermeable for electromagnetic radiation in most parts of the spectrum between 0.1 μm and 25 μm . The wavelength regions in which the atmosphere is (at least partially) permeable for electromagnetic radiation are referred to as atmospheric windows. Another factor influencing the nomenclature of wavelength regions in the field of remote sensing are the energy sources. In the ultraviolet (0.18-0.4 μm), visible (0.4-0.8 μm), near infrared (0.8-1.3 μm) and mid or shortwave infrared (1.3-2.5 μm) wavelength regions, incident solar radiation is transmitted through the atmosphere and reflected by the

Earth's surface. In the thermal infrared I (3 – 5 μm) and thermal infrared II (8 – 15 μm) wavelength regions, energy in the form of long-wave infrared radiation is emitted by objects on the Earth's surface, objects of around 800 Kelvin ($\sim 520^\circ\text{C}$) and around 300 Kelvin ($\sim 20^\circ\text{C}$), respectively [Lillesand 1999, Jensen 2000]. The energy sources in the ultraviolet through mid infrared, thermal infrared I and thermal infrared II wavelength regions are depicted in figure 3-2 with their approximate intensities.

Table 3-1 summarizes the wavelength according to the remote sensing definition regions and remote sensing applications in these wavelength regions.

Table 3-1: Remote sensing definitions and applications of wavelength regions between 0.18 μm and 1,000 μm wavelength.

Wavelength Region	Remote Sensing Nomenclature	Remote Sensing Applications
0.18 – 0.4 μm	Ultraviolet Light	Imaging spectrometry, multispectral imaging
0.4 – 0.8 μm	Visible Light	Panchromatic and color aerial photography, multispectral imaging, imaging spectrometry (cartography, mapping)
0.8 – 1.3 μm	Near Infrared	False color near infrared aerial photography, imaging spectrometry (vegetation studies)
1.3 – 2.5 μm	Mid Infrared (Shortwave Infrared)	Multispectral imaging & imaging spectrometry (geology studies)
3.0 – 5.0 μm	Thermal Infrared I	Thermal remote sensing (emission temperature range of red-hot objects, e.g. fire monitoring, volcanism, etc.)
8.0 – 14 μm	Thermal Infrared II	Thermal remote sensing (emission temperature range of earth-temperature objects, e.g., moisture, heat leakages, geologic mapping, etc.)
14 – 1,000 μm	Far Infrared	No remote sensing applications (atmosphere impermeable for electromagnetic radiation)

3.1 – Spectrometry basics

The remote sensing technique of imaging spectrometry has its roots in infrared and near infrared laboratory spectroscopy that have been used for qualitative analysis of organic molecules and quantitative analysis in process monitoring respectively for several decades. Both are based on characteristic vibrations of chemical bounds in molecules.

Near infrared and infrared spectroscopy are absorption spectroscopy methods. Infrared radiation is absorbed by the chemical bonds of molecules which, depending on atoms and type of chemical bond involved, are excited to exhibit characteristic vibrations. The wavelength and amount of infrared radiation absorbed in this process can be measured and is referred to as absorption bands.

Electromagnetic radiation

According to the wave-particle duality, electromagnetic radiation and light as a form of electromagnetic radiation can be considered a wave of characteristic frequency ν [s^{-1}] and wavelength λ [m] that propagates by the velocity of light, c [$m s^{-1}$] and at the same time as small, discrete light quanta (photons). The velocity of light is a universal constant in vacuum, that is 2.9979×10^8 m/s. Wavelength and frequency are related to the speed of light by the equation [Atkins 2001, Ball 2003]:

$$c = \lambda \times \nu [m s^{-1}] \Leftrightarrow \lambda = \frac{c}{\nu} [m] \Leftrightarrow \nu = \frac{c}{\lambda} [s^{-1}]$$

In the ultraviolet and visible wavelength regions, the wavelength is typically given in nanometers [10^{-9} m = 1 nm], and in the near infrared and infrared region, in micrometers [10^{-6} m = 1 μ m].

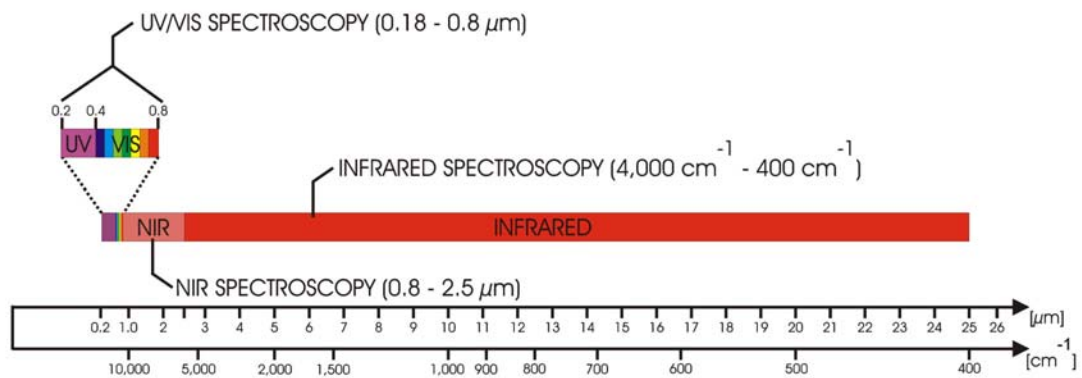


Figure 3-3: Wavelength definitions and analytical methods according to [Otto 1995].

The electromagnetic spectrum is divided into various regions according to the properties of the electromagnetic radiation. Figure 3-3 illustrates the subdivision of

the electromagnetic spectrum in the 0.18 μm to 25 μm region for purposes of laboratory spectroscopy. It comprises the ultraviolet (UV), visible (VIS), near infrared (NIR), and infrared (IR) wavelength regions. However, it should be noted that depending on the application, the definitions of wavelength regions vary considerably.

For practical purposes of spectrum interpretation, the wavenumber [cm^{-1}] denotation is used in infrared spectroscopy in the 4000 cm^{-1} (2.5 μm) to 400 cm^{-1} (25 μm) range instead of the wavelength [μm] denotation. In UV, VIS and NIR spectroscopy, the wavelength denotation (nm or μm respectively) is used. The wavenumber $\tilde{\nu}$ [cm^{-1}] describes the number of electromagnetic waves of a certain wavelength λ that fits into one centimeter according to the following equation:

$$\tilde{\nu} = \frac{10^4}{\lambda} [\text{cm}^{-1}] \quad \Leftrightarrow \quad \lambda = \frac{10^4}{\tilde{\nu}} [\mu\text{m}]$$

Energy – matter interactions

Most, if not all matter interacts with electromagnetic radiation in one way or another. Electromagnetic radiation that is incident onto any kind of matter may be reflected, absorbed or transmitted. For many wavelength regions, specific light interactions of a certain wavelength with specific matter can be observed. While at one wavelength electromagnetic radiation incident onto a specific matter may be reflected almost completely, it might be absorbed at another wavelength or partially absorbed while the rest is reflected at a third wavelength.

The energy-matter interactions in the ultraviolet, visible, near infrared and infrared wavelength regions can be used for qualitative and quantitative chemical analysis of chemical compounds and mixtures. However, it must be noted that only organic molecules, water and most gases exist in energy states that are able to absorb UV, VIS, NIR and IR wavelengths. Metals and most inorganics are incapable of absorbing electromagnetic radiation at these wavelengths. Therefore, metals and most inorganics exhibit no characteristic absorption features in these wavelength regions [ASD 2003].

The methods that were developed for chemical analysis utilizing UV, VIS, NIR and IR light are referred to as optical spectroscopy. According to the wavelength region used for analysis, they are differentiated into UV, VIS, NIR and IR spectroscopy. UV and VIS spectroscopy utilize the absorption of short-wave ultraviolet and visible light in the 0.18 μm to 0.4 μm and 0.4 μm to 0.8 μm wavelength region, respectively. UV and VIS spectroscopy are typically applied for quantitative laboratory analysis based on the extinction of light of a certain wavelength passing through a sample. To some extent, UV and VIS spectroscopy are also applied in qualitative analysis, in particular purity tests and structure elucidation [Otto 1995]. NIR and IR spectroscopy are referred to as vibrational spectroscopy. Both are based on the absorption of near

infrared and infrared radiation by molecular vibrations. While infrared spectroscopy is mainly used for qualitative laboratory analysis, near infrared spectroscopy is mainly used for quantitative laboratory and industrial process analysis. Advantages of NIR spectroscopy over IR spectroscopy are that it requires no sample preparation, that measurements are non-destructive and non-contact, and that it allows real-time measurements and is therefore suitable for on-line, in-situ monitoring and analysis of many kinds of compounds, mixtures and materials. In contrast, IR spectroscopy is a laboratory analysis method that requires considerable sample preparation. While IR spectra can be interpreted directly, NIR spectra must be compared to calibration data sets. Usually, complex chemometrics software packages are used for the interpretation of NIR spectra [Otto 1995, Günzler 2002].

Interaction mechanisms

In the ultraviolet and visible wavelength regions, energy-matter interactions are based on the absorption of electromagnetic radiation by the valence electrons of σ -, π -, and n-bonds of organic molecules or the *d*- or *f*-electrons of metal ions, respectively. Furthermore, the valence electrons of atoms can be excited by incident ultraviolet and visible electromagnetic radiation. The so-called electronic absorption bands of compounds in the UV and VIS wavelength regions are typically very broad and consist of several superimposed bands merged together [Otto 1995, Atkins 2001].

In the near infrared and infrared wavelength regions, the interactions of electromagnetic radiation and matter are based on the absorption of infrared radiation by specific vibrations of (organic) molecules. Molecules, i.e. combinations of different atoms linked together by chemical bonds, are not rigid but can vibrate in different modes. The atoms of molecules can, for example, shift their positions relative to one another, thus moving closer together or drifting apart. Furthermore, a whole molecule can rotate. The total number of vibrational modes of molecules (Z) consisting of a given number of atoms (N) is described by the following equations [Günzler 2002]:

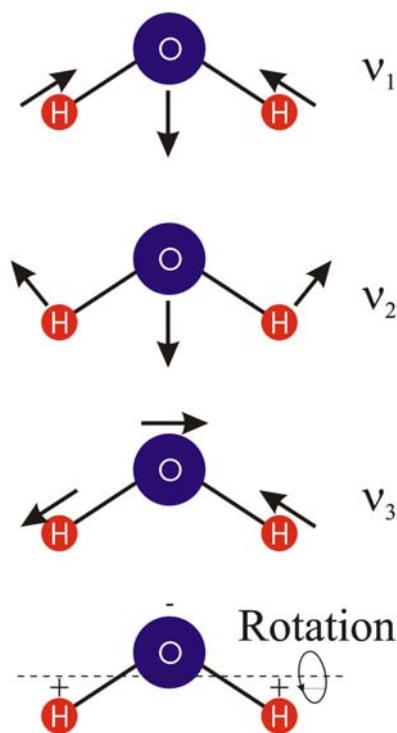
$$Z = 3N - 6 \text{ for non-linear molecules}$$

and

$$Z = 3N - 5 \text{ for linear molecules}$$

The vibration modes of a molecule can be excited independently from one another. Each vibration has a characteristic vibrational frequency. It must be noted that only those vibrations that result in a change of the dipole moment of a molecule can be

excited by infrared radiation and are therefore visible in infrared spectra. Usually, only asymmetric stretch vibrations and deformation vibrations fulfill this requirement; these are referred to as “IR-active” [Günzler 2002, Atkins 2003].



The vibrational modes can be illustrated with the water molecule (gaseous state) as an example. The water molecule as a non-linear molecule has three normal modes of vibration plus a rotation of the whole molecule.

The vibration ν_1 is a symmetric stretching vibration (denotation ν_s) that does not induce a change in the dipole moment of the water molecule and is therefore not detectable in infrared spectra. The vibrations ν_2 (deformation vibration with changed in bond angles, denotation δ) and ν_3 (antisymmetric stretching vibration, denotation ν_s) both result in a change of the dipole moment of the water molecule. Therefore they are both detectable in infrared spectra. They can be observed in the infrared spectrum at wavenumbers of 1595 cm^{-1} and 3756 cm^{-1} , respectively [Günzler 2002, Otto 1995, Atkins 2003, Banwell 1999].

Figure 3-4: H₂O molecular vibrations.

Apart from the so-called fundamental vibrations that typically occur in the 4000 cm^{-1} to 400 cm^{-1} ($4\text{ }\mu\text{m}$ – $25\text{ }\mu\text{m}$ infrared) spectral region, overtones and combination bands can be observed at higher wavenumbers (smaller wavelengths) in the near infrared. As the absorptions (fundamentals and overtones) are quantum mechanical in nature, only discrete energy amounts can be absorbed [ASD 2003]. Because of this, overtones are always observed at approximately multiple wavenumber values of the fundamental vibrations, although generally at somewhat lower values than the exact multiple values due to the so-called anharmonicity effect. Overtones result from transitions into higher energy levels and thus higher vibration modes. Because of their lower probability compared to fundamental vibrations, their intensities are much lower than those of the fundamental vibrations. Taking into account the anharmonicity effect that can be described by a shift of one to five percent towards lower wavenumbers, the overtone absorption bands can be calculated using the following equation [Otto 1995]:

$$\tilde{\nu}_n = (n + 1) \times \tilde{\nu}_0 \times (1 - n\kappa)$$

with

$\tilde{\nu}_n$ - nth overtone vibration

n – Overtone number

$\tilde{\nu}_0$ – Fundamental vibration

κ – Anharmonicity constant (1% – 5% = 0.01 – 0.05)

Combination bands occur when two or more different fundamental vibrations are excited simultaneously and their frequencies are combined. As for the overtone bands, combination bands occur at somewhat lower wavenumbers (higher wavelengths) due to the anharmonicity effect. The position of combination bands can be calculated using the following equation [Otto 1995, Günzler 2002]:

$$\tilde{\nu}_c = a \times (1 - a\kappa) \times \tilde{\nu}_i \pm b \times (1 - b\kappa) \times \tilde{\nu}_j \pm c \times (1 - c\kappa) \times \tilde{\nu}_k \pm \dots$$

with

$\tilde{\nu}_c$ - Combination band wavenumber [cm⁻¹]

a, b, c – Integer multiplier (1, 2, 3, ...)

$\tilde{\nu}_{i,j,k}$ – Fundamental vibration wavenumbers [cm⁻¹]

κ - Anharmonicity constant (1% - 5% = 0.01 - 0.05)

Using the above equations and the fundamental vibrations of the gaseous water molecule ν_2 and ν_3 , cited before, the overtones and combination bands listed in table 3-2 can be calculated.

Table 3-2: Overtone and combination bands of the water molecule in gaseous state.

Gaseous H ₂ O Molecule Vibration	Fundamental [cm ⁻¹]	1 st Overtone [cm ⁻¹]	2 nd Overtone [cm ⁻¹]	3 rd Overtone [cm ⁻¹]
ν_2	1,595 (6.3μm)	3,158 (3.2 μm)	4,689 (2.1 μm)	6,189 (1.6 μm)
ν_3	3,765 (2.7 μm)	7,455 (1.4 μm)	11,069 (0.9 μm)	14,608 (0.7 μm)
+ Binary combination band $\nu_2 + \nu_3$ @ 5306 cm⁻¹ (1.9 μm)				

The overtone absorption band at 1.4 μm and the combination band at 1.9 μm are well-known water absorption bands in the field of remote sensing as atmospheric water denies the transmission of infrared radiation in these wavelength regions.

Absorption features of organic compounds

Carbon-hydrogen-bonds (C-H, C-H₂, C-H₃), hydroxy groups (O-H), double and triple bonds of aliphatics and aromatics, carboxyl groups (C=O), ester groups (C-O-C), amino groups (N-H) and other structural groups of organic chemicals exhibit characteristic fundamental vibrations that are evident in the 4,000 cm⁻¹ (2.5 μm) to 1,500 cm⁻¹ (6.67 μm) wavelength region of the infrared spectrum. Furthermore, they exhibit overtone and combination bands in the infrared and near infrared spectrum between 20,000 cm⁻¹ (0.5 μm) and 1,500 cm⁻¹ (6.67 μm) [Otto 1995, Atkins 2003, Günzler 2002, Hesse 1991, Gauglitz 2004a, Banwell 1999, ASD 2003, Nyquist 2001a, Nyquist 2001b].

Table 3-3 lists some important fundamental vibrations of typical organic molecules and compounds, their wavenumbers and their calculated first, second, and third overtones. From the table it becomes clear that the fundamental and thus most intense absorption bands are limited to the infrared wavelength region beyond 2.5 μm (4000 cm⁻¹) and are thus limited to observation by infrared spectroscopy. Most 1st overtone bands and almost all 2nd and 3rd overtone bands, however, occur in the near infrared wavelength region of the electromagnetic spectrum (0.8 μm – 2.5 μm according to the wavelength region definitions for analytical chemistry). As the intensity of overtone bands is generally much less intense than that of fundamental vibration bands, not all overtone bands are observable in near infrared spectra.

Table 3-3: Important fundamental and resulting overtone vibrations of organic molecules. Overtone and combination bands are calculated based on literature values for the fundamental vibrations. Calculated based on values from [Cloutis 1989, Atkins 2003, and Nyquist 2001a].

Vibration Type	Fundamental Wavenumbers [cm⁻¹]	Fundamental Wavelengths [μm]	1st Overtone Wavelengths [μm]	2nd Overtone Wavelengths [μm]	3rd Overtone Wavelengths [μm]
Aromatic C-H stretch	3000-3100	3.22-3.33	<i>1.61-1.67</i>	<i>1.08-1.11</i>	<i>0.81-0.83</i>
Alkane C-H stretch	2960-2850	3.38-3.51	<i>1.69-1.75</i>	<i>1.13-1.17</i>	<i>0.84-0.88</i>
C-H bend	1465-1340	6.83-7.46	3.41-3.73	<i>2.28-2.49</i>	<i>1.71-1.87</i>
C-C stretch	1250-700	8.00-14.29	4.00-7.14	2.67-4.76	<i>2.00-3.57</i>
C=C stretch	1680-1620	5.95-6.17	2.98-3.09	<i>1.98-2.06</i>	<i>1.49-1.54</i>
C≡C stretch	2,260-2,100	4.42-4.76	<i>2.21-2.38</i>	<i>1.47-1.59</i>	<i>1.11-1.19</i>
O-H stretch	3,650-3,590	2.74-2.79	<i>1.37-1.39</i>	<i>0.91-0.93</i>	<i>0.68-0.70</i>
C=O stretch	1,780-1,640	5.62-6.10	2.81-3.05	<i>1.87-2.03</i>	<i>1.40-1.52</i>
C≡N stretch	2,275-2,215	4.40-4.51	<i>2.20-2.26</i>	<i>1.47-1.50</i>	<i>1.10-1.13</i>
N-H stretch	3,500-3,200	2.86-3.13	<i>1.43-1.56</i>	<i>0.95-1.04</i>	<i>0.71-0.78</i>
Hydrogen bonds	3,570-3,200	2.80-3.13	<i>1.40-1.56</i>	<i>0.93-1.04</i>	<i>0.70-0.78</i>

Figure 3-5 illustrates fundamental and overtone absorption bands of several important functional groups of organic compounds in the near infrared and infrared wavelength regions. From the illustration it becomes clear that in the 4,000 cm⁻¹ (2.5 μm) to 1,500 cm⁻¹ (6.7 μm) wavelength region (infrared) absorption features are clearly distinguishable from one another, while in the 12,500 cm⁻¹ (0.8 μm) to 4,000 cm⁻¹ (2.5 μm) wavelength region (near infrared) highly complex spectra of many overlapping overtone bands are to be expected. Furthermore, figure 3-5 does not take into account combination bands that typically also occur in the near infrared wavelength region. The wavelength region beyond 1,500 cm⁻¹ (6.7 μm) to 900 cm⁻¹ (11.1 μm) is referred to as the “spectral fingerprint region” in infrared spectroscopy because in this wavelength region also highly complex combinations of spectral bands are observed that are characteristic for every single chemical compound. In infrared spectroscopy, visual interpretation of the 4,000 cm⁻¹ to 1,500 cm⁻¹ wavelength region alone allows conclusions on the structural elements of a compound under investigation, while matching the fingerprint region to a library of

known spectra allows the reliable identification of a substance [Günzler 2002, Hesse 1991, Gauglitz 2004a, Otto 1995].

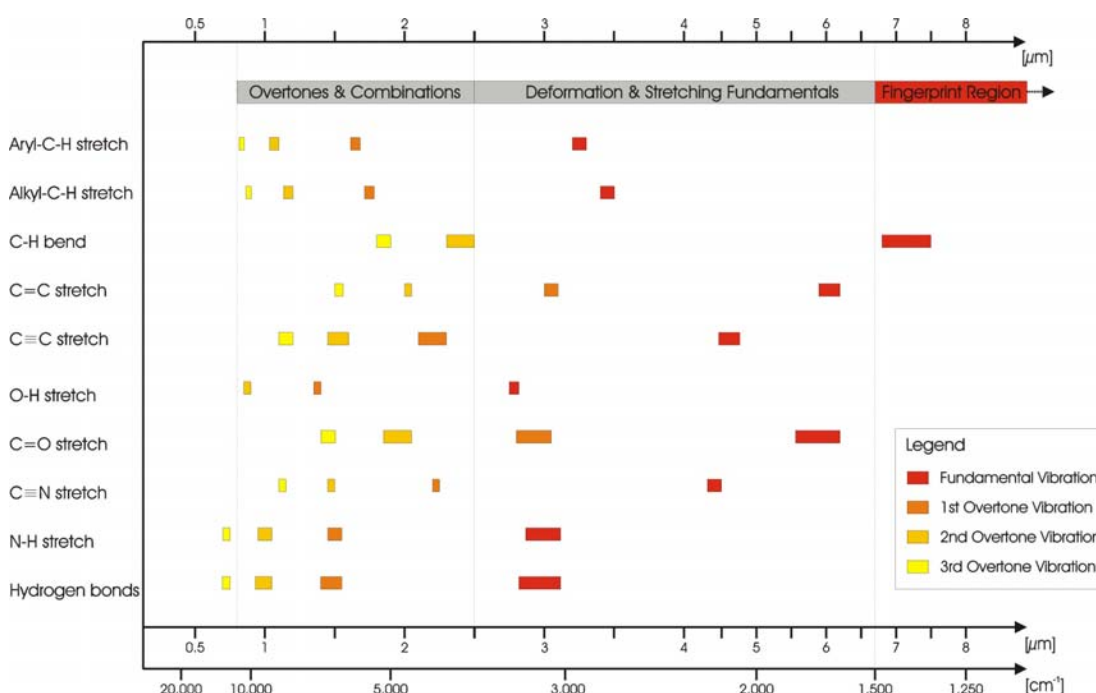


Figure 3-5: Location and intensity of important vibrations of organic molecules and compounds. Calculated based on values from [Cloutis 1989, Atkins 2003, Nyquist 2001a].

In summary, the wavelength regions of infrared and near infrared spectra can be characterized as follows (table 3-4):

Table 3-4: Relevant wavelength regions with respect to the identification of organic molecules in infrared and near infrared spectroscopy. Based on [Günzler 2002, Hesse 1991, Gauglitz 2004a, Otto 1995].

Wavelength Region	Absorption Features
900 – 400 cm ⁻¹ (11.1 – 25.0 μm)	Fundamental bands of aromatic structures and bonds of heavy atoms (> 20 g/mol), e.g. carbon-halogen vibrations
1,500 – 900 cm ⁻¹ (6.7 – 11.1 μm)	Spectral fingerprint region, complex interacting vibrations, no identification of structural or functional groups possible
2,500 – 1,500 cm ⁻¹ (4.0 – 6.7 μm)	Fundamental bands, stretching vibrations of double and triple bonds, e.g. C=O, C=C, C=N, C≡C, C≡N, etc.
4,000 – 2,500 cm ⁻¹ (2.5 – 4.0 μm)	Fundamental bands, stretching vibrations involving movements of light atoms (< 20 g/mol), e.g., C-H, O-H, N-H, etc.
12,500 – 4,000 cm ⁻¹ (0.8 – 2.5 μm)	Overtone and combination bands of fundamental bands in the 4,000 cm ⁻¹ – 2,500 cm ⁻¹ wavelength region, i.e. C-H, O-H, N-H

NIR Spectroscopy of organic chemicals

From the above considerations it is obvious why NIR spectroscopy is primarily applied for quantitative analysis (“chemometrics”) and not for qualitative analysis, for which IR spectroscopy is the better choice. However, despite the fact that NIR spectra of organic chemicals are often highly complex due to many overlapping overtone and combination absorption features, they still contain information on functional and structural groups of the chemicals under investigation.

Figure 3-7 shows spectra of four basic organic compounds: n-Octane (alkane, C_8H_{18}), 1-Octene (alkene, C_8H_{16}), benzene (monoaromatic, C_6H_6), and 2-Octanol (alcohol, $C_8H_{18}O$). Figure 3-6 illustrates the structural formulas of the compounds.

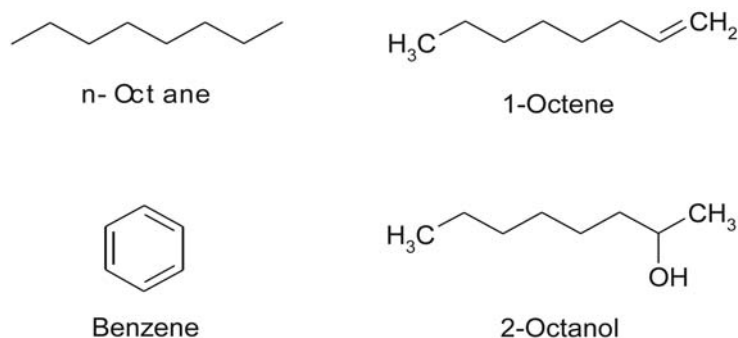


Figure 3-6: Structural formulas of four basic organic compounds. See figure 3-7 for the according near infrared spectra.

The spectra shown in figure 3-7 were acquired using an Analytical Spectral Devices Field Spec Pro FR® instrument. The spectra represent a dual pass through one millimeter of the respective liquid compound. The spectra were acquired over the whole 0.38 μm to 2.5 μm wavelength region.

In the spectra, important absorption bands that represent certain structural or functional groups of the compounds are annotated. Characteristic bands for alkanes, alkenes, aromatic rings and alcohols are clearly distinguishable in the near infrared spectra.

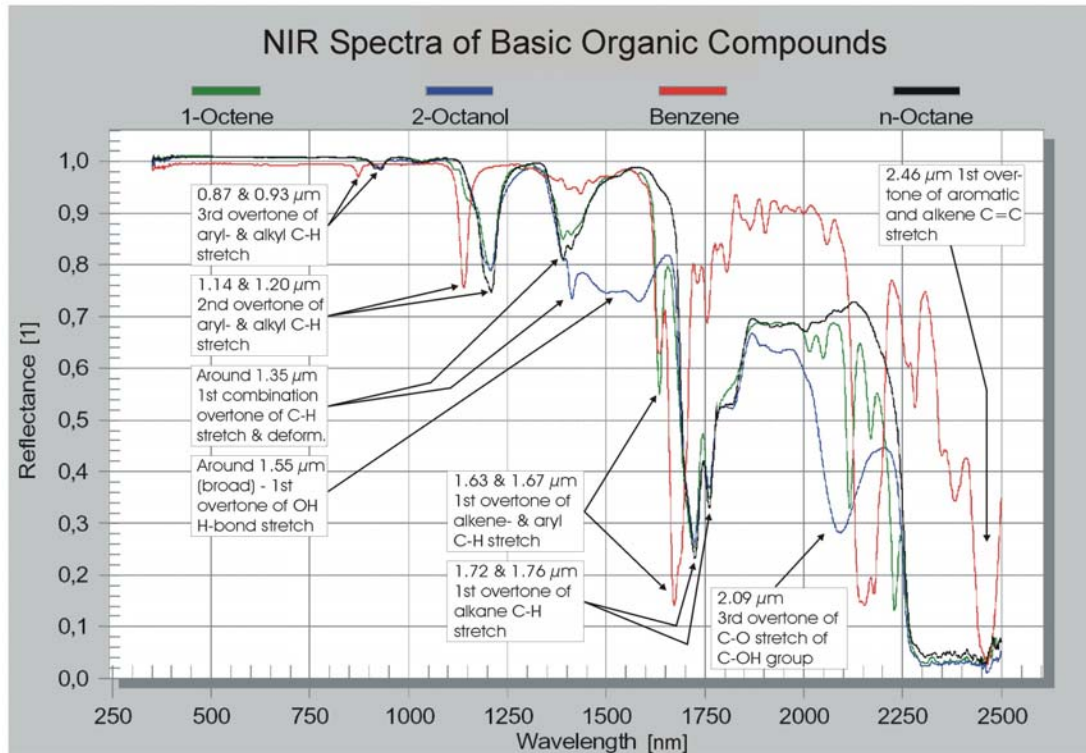


Figure 3-7: Sample near infrared spectra of important organic compounds and functional groups.

The spectra show that several important groups of chemicals are clearly distinguishable in near infrared spectra. Table 3-5 summarizes the possibilities and restrictions of the identification of pure organic compounds in the 0.25 μm to 2.5 μm wavelength region.

All organic substances show intense absorption bands in the 2.35 μm , 1.75 μm , and 1.35 μm wavelength region and, often, in the 1.2 μm wavelength region. Generally, the intensity of absorption bands decreases with decreasing wavelengths. While the 2.35 μm and 1.75 μm absorptions bands can be considered strong, the 1.2 μm and 1.35 μm absorption bands must be considered medium in intensity. Below 1.2 μm , only weak absorption bands appear.

Table 3-5: Assessment of possibilities and restrictions with respect to the identification of organic chemicals in near infrared spectra.

Substance Group	Possibilities	Restrictions
Aliphatics (Alkyl-C-H group)	Alkanes, alkenes, alkynes can be clearly distinguished	All alkanes show similar spectra. For alkenes and alkynes it might be possible to estimate the relation of saturated and unsaturated bonds.
Monoaromatics (Aryl-C-H group)	Benzene and monoaromatics with alkyl groups are clearly distinguishable – depth of neighboring absorption doublets also allows to determine the presence of substituted alkyl groups on the aromatic rings	Liquid monoaromatics and solid polynuclear compounds can be easily distinguished while similar liquid compounds (e.g., toluene and methylnaphthalene) are hard to distinguish.
Explosives (NO₂ group)	Spectra of explosives (consisting usually of C-N, C-C, C-H, N-O, and N-H structural compounds) appear relatively complex and unique.	Nitro groups of explosives are generally hard to distinguish from substituted mono-aromatics and polynuclear compounds.
Alcohols (OH group)	Alcohols generally show strong, broad absorption features that allow for the identification of the O-H group.	The strong, broad absorption features often interfere with the identification of other structural or functional groups of alcohols.
Phenols (Aryl-OH group)	Like alcohols, phenols show strong and broad absorption features that allow the identification of the O-H group. For phenols, the aryl-C-H-stretch is usually still detectable in these overlapping features.	The strong, broad absorption features often interfere with the identification of other structural or functional groups of phenols.
Fuels & Crude Oil	As complex mixtures of many different hydrocarbon classes, fuels and crude oils usually exhibit only three or four major absorption features that mainly represent C-H-stretches (2.35, 1.75, 1.35 1.2 & 0.93 μm). Only an identification as fuel hydrocarbons and estimation of the ratio of aliphatics and aromatics seem feasible.	The determination of functional or structural groups of single compounds is to be considered impossible
Ketones, Aldehydes & Carboxylic Acids (C=O group)	Minor common absorption features occur in the 1.9 μm – 2.2 μm wavelength region.	Although all compound groups contain a C=O group, no common, strong, and specific absorption feature can be identified.
Chlorinated Organics (C-Cl group)	Chlorinated organics generally show sharper and deeper absorption features than unchlorinated organics. The absorption features are often shifted towards shorter wavelengths by 50 nm to 150 nm in comparison to C-H-stretch absorption features.	No clear, unambiguous identification of C-Cl absorption features seems possible in the 0.25 μm – 2.5 μm wavelength region, even though sharp absorption features at 1.1 μm and 2.15 – 2.25 μm often hint at C-Cl groups.

The absorption features of important constituents of basic organic compounds in the visible and near infrared wavelength regions between 0.5 μm and 2.5 μm wavelength are summarized and illustrated in figure 3-8, based on own laboratory measurements of circa 70 organic compounds using an ASD Field Spec Pro FR® instrument. The width of the observed absorption features is represented by the width of the bars, and the intensity of their color, with red representing strong absorption features (> 50 % of the 100 % reflection), orange representing medium absorption features (min. 20 % of the 100 % reflection), and yellow weak absorption features.

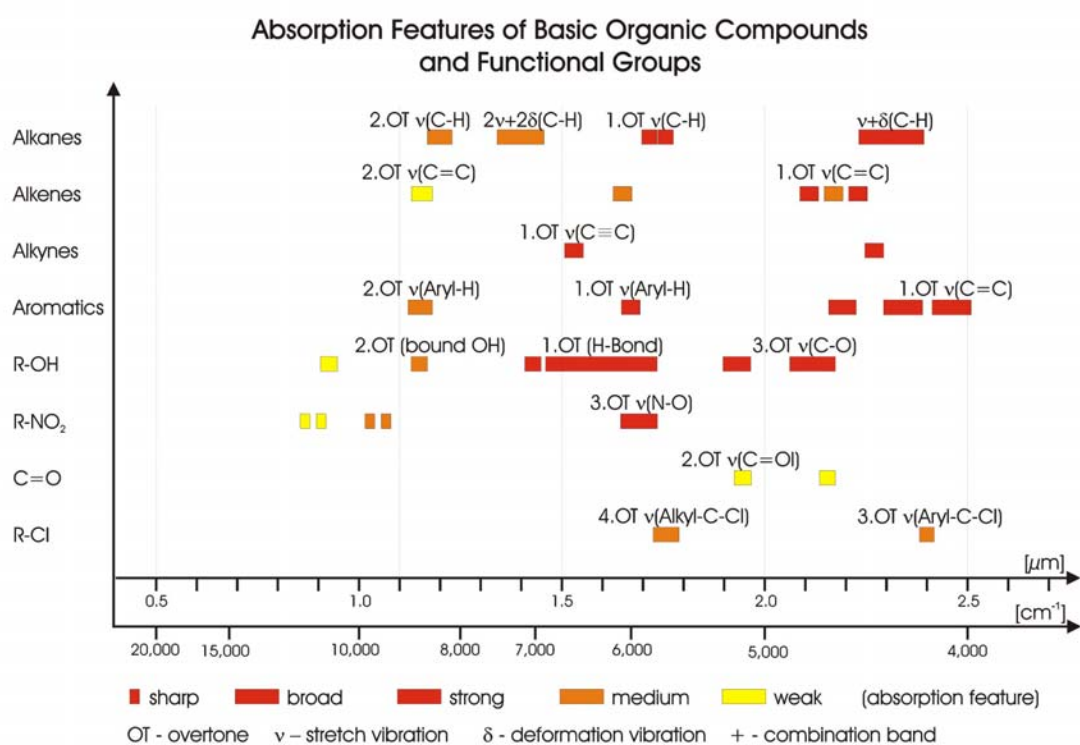


Figure 3-8: Important absorption features of important basic organic compounds and functional groups in the near visible through shortwave infrared wavelength regions.

Although it is not a subject of this investigation, it should to be noted that the data acquired in laboratory measurements of more than 70 organic compounds suggest that spectra in the 0.25 μm to 2.5 μm wavelength region represent a spectral fingerprint of individual organic chemical compounds or at least groups of skeletal isomers. This would allow the identification of at least the substance group if not the exact chemical compound or isomer group of relatively simple chemical compounds if the spectrum of an analyte is compared to a comprehensive spectral library.

NIR analysis of petrochemicals

The analysis of fuel hydrocarbons by means of near infrared spectroscopy dates back from the 1920s to 1940s, when the first publications described the analysis of structural groups of hydrocarbons (methyl, methylene, methine, aromatic C-H groups). The 1.2 μm absorption feature was used to determine the average number of various C-H-groups. In 1989, NIR spectroscopy in the 700 nm to 2500 nm wavelength region was reported useful for the simultaneous estimation of the major classes of hydrocarbon constituents (aliphatics, aromatics, olefinics). Furthermore, the determination of octane number, MTBE (tert-butyl methyl ether) and methanol content was shown to be possible with NIR spectroscopy [Workman 1996, Buchanan 1992, Stark 1992].

Since the early 1990s, NIR spectroscopy has gained an important role in the analysis of hydrocarbon production processes and products because it is an analytical method that can be applied in automated, on-line mode, requiring no sample preparation (in situ measurement) and returning reliable and repeatable results. It is also highly cost-effective. In the petrochemistry industry, NIR spectroscopy is used, among others, for the monitoring of feedstock composition, the polymerization of isobutene, ethylene, etc. in polymerization plants, the determination of the octane number, and the composition with respect to major hydrocarbon classes [Cermelli 1992, Workman 1996, Buchanan 1992].

However, it must be noted that before their continuous application in production processes, all applications require comprehensive and often difficult calibration using other analytical methods (IR, NMR, GC, MS) [Cermelli 1992].

Figure 3-9 illustrates the capabilities of NIR spectroscopy in the field of petrochemical analysis and process control, depicting the spectra of the four compounds of the BTEX group isomers (benzene, ethylbenzene, toluene, and a mixture of xylene). Based on the comparison of the spectra it can be stated that NIR spectroscopy allows the differentiation of the four basic BTEX compounds. The 1.14 μm and 1.19 μm absorption features of a dual-pass measurement through 1 mm of medium (using an ASD Field Spec Pro FR instrument) represent the abundance of aromatic and aliphatic C-H-stretches (2nd overtone), respectively.

The 1.14 – 1.15 μm absorption feature (center) represents the number of aromatic C-H-stretches (2nd overtone of the 3.25 μm fundamental). As summarized in table 3-6, the absorption increases with the number of aryl-C-H stretches, from 85 % relative reflectance for xylene with four aryl-C-H stretches to 76 % relative reflectance for benzene with six aryl-C-H stretches. Simultaneously, a small shift towards longer wavelengths is found with an increase in the number of substituted alkyl-C-H groups: from 1.140 μm for benzene (n alkyl-C-H stretches) to 1.148 μm for xylene (6 alkyl-C-H stretches).

Similar behavior is found for the 1.19 μm absorption feature representing the number of aliphatic C-H- stretches (2nd overtone of the 3.45 μm fundamental). The

absorption increases with the number of alkyl-C-H stretches from 90 % relative reflectance for toluene with three alkyl-C-H stretches to 84 % relative reflectance for xylene with six alkyl-C-H stretches.

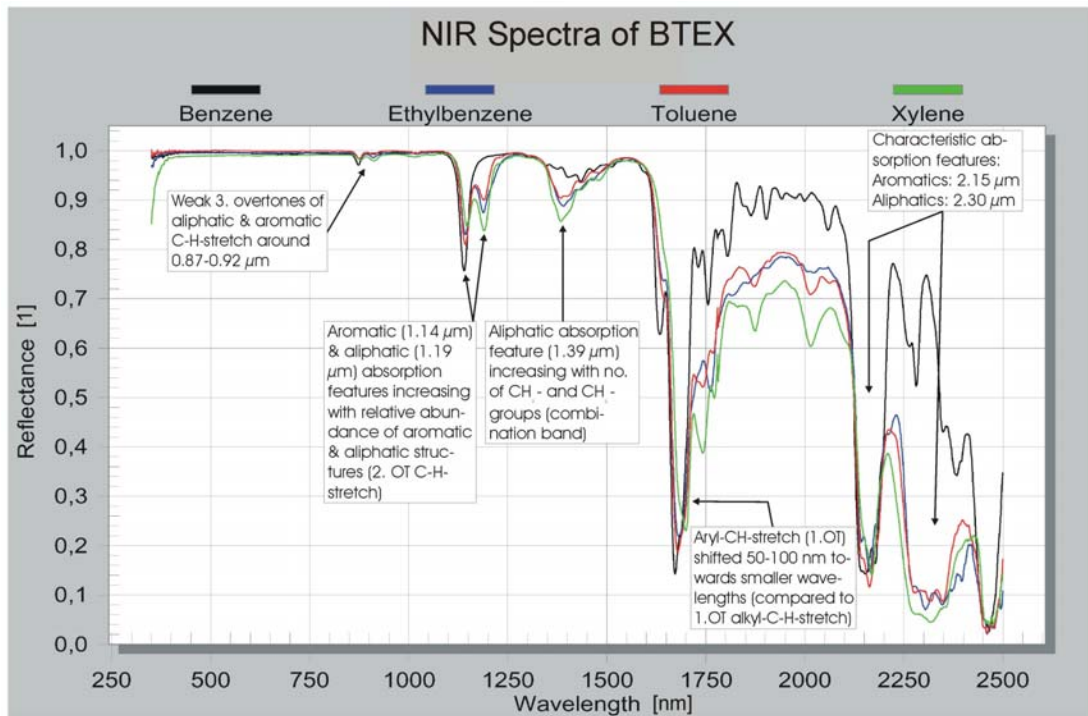
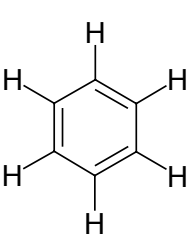
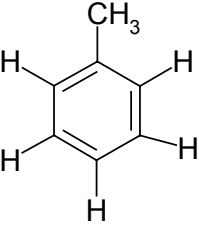
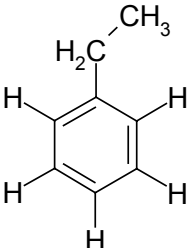
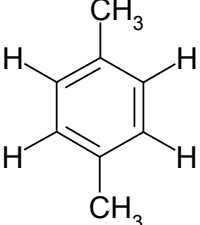


Figure 3-9: Absorption spectra of benzene, toluene, ethylbenzene, and xylene in the 0.38 μm – 2.5 μm wavelength region indicating their separability in this wavelength region.

Table 3-6: Characterization and separation of BTEX compounds in NIR spectra based on the 1.2 μm region absorption feature.

Substance	Benzene	Toluene	Ethylbenzene	Xylene
Structural Formula				 (Figure: o-Xylene)
Aromatic C-H stretches	6	5	5	4
Aliphatic C-H stretches	0	3	5	6
2 nd overtone aryl-H-stretch [μm]	1.140	1.142	1.143	1.148
2 nd overtone aryl-H-stretch [% reflectance]	76	81	83	85
2 nd overtone alkyl-H-stretch [μm]	N/A	1.189	1.188	1.190
2 nd overtone alkyl-H-stretch [% reflectance]	N/A	90	88	84

Absorption features of inorganics

Unlike organic substances, for which many important structural and functional groups are evident in near infrared spectra, most inorganic substances do not show any absorption features that allow a definite identification.

The reason for this is that most inorganics apart from water and some gases such as carbon dioxide, oxygen and ozone do not possess electrons in chemical bonds that are able to absorb near infrared wavelengths [ASD 2003]. This is evident in the spectra of six representative inorganic substances (metals, salts, oxides) depicted in figure 3-10.

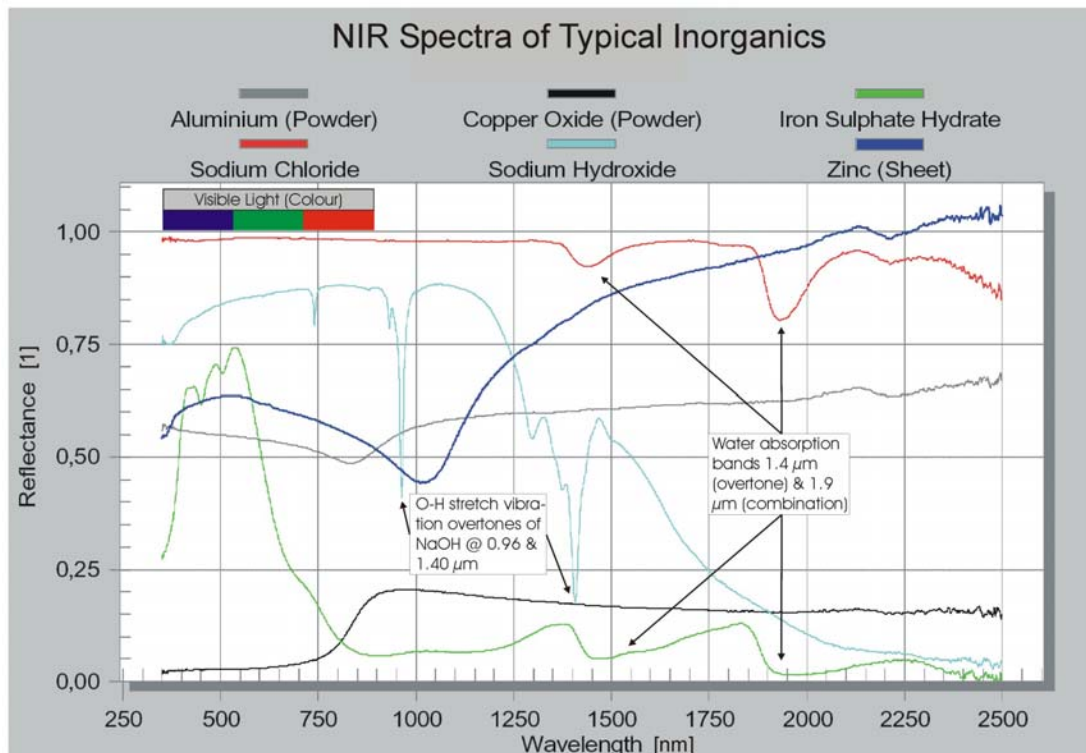


Figure 3-10: Example spectra of members of different groups of inorganics (e.g., metals, salts, oxides) proving the absence of characteristic absorption features for inorganics.

Aluminum (gray line) and zinc (blue line) as representatives for metals do not show major absorption features. Both exhibit a medium reflectance in the visible wavelength region (approximately 50 – 65 % reflectance) that increases towards longer wavelengths beyond 800 nm and 1,000 nm, respectively. The reflectance in the visible wavelength regions between 400 nm and 800 nm represents simply the color of the substance. With a reflectance of 50 to 65 % in the visible wavelength regions, both aluminum and zinc appear light gray or silvery gray.

The copper oxide measured (black line) was a dark black powder. This is again evident in the visible wavelength regions where almost no radiation is reflected.

Towards longer wavelengths beyond 800 nm, the reflectance of copper oxide increases but never exceeds 25 %.

Sodium chloride, a white crystalline substance (red line), shows no absorption features except two water absorption features at around 1,400 nm and 1,900 nm due to its moisture content. This is valid for all crystalline salts measured. All are white, crystalline substances that reflect almost 100 % of incident radiation in the 250 nm to 2,500 nm wavelength range with slightly decreasing reflectance beyond 2,000 nm.

Iron sulphate hydrate, a bluish-green, crystalline salt (green line) shows a triple peak in the 350 nm to 600 nm visible wavelength region, reflecting 60 – 70 % of the incident radiation while absorbing almost all radiation beyond 600 nm and therefore appearing bluish-green. Beyond 600 nm, reflection is generally lower than 15 % with two broad but weak peak/absorption features around 1,400 nm and 1,900 nm, obviously due to hydrated water.

Water free sodium hydroxide, measured as white pellets, are an exception compared to the other inorganics. Reflecting 75 – 80 % in the visible wavelength regions and therefore appearing white, reflectance decreases almost linearly beyond 1,000 nm (80 % reflectance) towards 2,500 nm (< 5 % reflectance). In contrast to the other inorganics investigated, sodium hydroxide exhibits two sharp and relatively strong absorption features at 950 nm and 1,400 nm, respectively. Obviously, these two bands are O-H stretch overtones (that can not be compared to the O-H absorption overtones of alcohols described above).

The results presented here are consistent with the spectra measured for more than 40 inorganic substances including elemental non-metals, metals, oxides, acids, and salts in laboratory reflectance measurements using an ASD Field Spec Pro FR.

Summary: Capabilities of NIR spectroscopy

As shown above, near infrared spectroscopy does not only hold a huge potential for quantitative analysis but also for qualitative analysis or combinations of both qualitative and quantitative chemical analysis.

Many, though not all, groups of organic chemical compounds (aliphatics, olefins, alkynes, aromatics, alcohols) can be easily distinguished using near infrared spectroscopy. If calibration standards are used, the identification of known substances in a mixture and the determination of their concentrations are also possible. Furthermore, it seems likely that the identification of substances based on their near infrared spectra in the 0.2 μm to 2.5 μm wavelength region is possible. This would require a comparison of the analyte spectrum to a spectral library containing spectra of the analyte or related substances. However, it seems unlikely that isomers can be differentiated using near infrared spectroscopy.

Inorganic compounds can usually not be distinguished or detected using near infrared spectroscopy because they usually exhibit not characteristic absorption features in the 0.2 μm to 2.5 μm wavelength region.

To what extent the possibilities of near infrared spectroscopy for qualitative and quantitative analysis of fuel hydrocarbons can be utilized in remote sensing imaging spectrometry of soils contaminated with fuel hydrocarbons will be investigated in sections 5, 6 and 7.

3.2 – Remote sensing imaging spectrometry

Near infrared spectroscopy was transferred from the laboratory to field applications and even adapted for remote sensing applications because it works in the wavelength ranges between 0.2 μm and 2.5 μm (in which range the sun also illuminates the Earth's surface and where the atmosphere is transparent for the most part) and because no sample preparation is required. This remote sensing technology is now known as imaging spectrometry, imaging spectroscopy or hyperspectral imaging. It was developed beginning in the 1970s and required significant developments with respect to data acquisition systems, data processing, data correction, and data interpretation. Now sharing only the fundamentals of infrared and near infrared spectroscopy with the laboratory methods described above, it has become a full-grown remote sensing tool that has opened completely new possibilities in remote sensing of the Earth's environment. However, terrestrial near infrared spectroscopy in field applications is still an important tool for the calibration ("ground-truthing") of remote sensing imaging spectrometry data.

Remote sensing imaging spectrometry (or hyperspectral imaging) is the application of near infrared spectroscopy as a remote sensing method from both aircrafts and spacecraft platforms. Instead of acquiring multitemporal measurements in the same location or medium (i.e. repeated single spectra at scheduled times) remote sensing imaging spectrometry means the acquisition of spectra for hundreds of sampling areas (pixels) simultaneously. Thus, imaging spectrometry data may be represented as both spectra for single pixels and images for single spectral bands. While the emphasis of near infrared laboratory or process analysis is quantitative analysis against comprehensive calibration models, the objective of remote sensing imaging spectrometry is both qualitative and quantitative analysis. In laboratory analysis or process control near infrared spectroscopy measurements, the environmental conditions are usually controlled and optimized with respect to near-optimal conditions for measurement. In contrast, remote sensing imaging spectrometry is an analytical chemistry method carried out in an "uncontrolled environment" [Goetz 1996a]. Both the target materials (varying areas of the Earth's surface with different land cover types) and the atmosphere, with considerably varying water vapor content, contribute to the "uncontrolled environment" and present considerable

challenges with respect to data acquisition, data processing and data interpretation. While the objective of laboratory or process control of near infrared spectroscopy is typically quantitative analysis of mixtures with known constituents, the objective of remote sensing imaging spectrometry is usually both qualitative and quantitative analysis of unknown target materials.

Because imaging spectrometry in the 0.2 μm to 2.5 μm wavelength region is the first remote sensing technology that provides analytical chemistry possibilities and precision in the field of remote sensing, many new applications have been developed and are still being developed. Where aerial photographs and multispectral remote sensing data allowed only the differentiation of major classes of vegetation (e.g. coniferous forest, deciduous forest, shrub land, etc.), imaging spectrometry now allows the identification of vegetation species rather than classes comprising many different species. Providing new possibilities to map vegetation biochemistry and detect vegetation stress and its sources (e.g., nutrient stress, water stress, pest stress, heavy metal stress, etc.), imaging spectrometry is also a promising technology for precision agriculture and forestry (forest damage mapping, pest infestation, etc.). With its proven potential for geologic mapping and mineral and hydrocarbon exploration, imaging spectrometry has already become a state of the art technology in industrial geologic exploration. Soil type and soil properties mapping, the remote sensing investigation of limnic, coastal and marine water bodies (e.g. determination of suspended matter, phytoplankton, bathymetry, submerged vegetation mapping, coral species and coral health mapping, etc.) are other applications that are gaining interest. Mostly unknown are the military applications of hyperspectral remote sensing and its implementation. However, recent publications hint at applications such as friend-foe identification (using paints with characteristic absorption features (“fingerprints”) in the 0.2 – 2.5 μm region to reduce so-called “friendly fire” incidents), battlefield (terrain) analysis, land mine detection, and the detection of chemical warfare agents (atmospheric application of imaging spectrometry). In the law enforcement sector, imaging spectrometry can be assumed to have gained significance in the detection and mapping of drug plant plantations (a special application of vegetation species mapping) in Central and South America but also other regions of the world. Still under investigation are atmospheric and urban applications of imaging spectrometry. Both fields of application pose considerable challenges. Because of the atmospheric interference measured against the terrestrial background from airborne and spaceborne imaging spectrometry systems, atmospheric applications make up only a fraction of the overall signal received compared with the terrestrial background. Nevertheless, the potential of imaging spectrometry data for atmospheric water vapor mapping, the mapping of atmospheric gases and larger exhaust plumes has been demonstrated in several studies. Urban applications pose considerable challenges because the target area is typically highly complex with many different surface materials varying over small areas (numerous different pavement and roofing materials, varying vegetation, water bodies, plastics, paint (cars), etc.). However, urban environment mapping, urban planning and tax

adjustment are considered as potential applications of imaging spectrometry investigations of urban areas.

Environmental applications with respect to the detection and/or mapping of contaminated sites, stressed vegetation, waste deposits or areas with other undesired anthropogenic impacts are typically special applications of the imaging spectrometry investigation of soil, geology, vegetation or urban areas. The subjects of environmental applications in the original field of imaging spectrometry are, for example:

- Soil salinisation detection, quantification and mapping (soil)
- Oil spill detection on water (water)
- Oil contamination mapping of soil and detection of geogenic hydrocarbon micro-seepage and macro-seepage in hydrocarbon exploration (geology)
- Analysis of lignite overburden dumps and metal mining overburden dumps with respect to acidic drainage and heavy metal release
- Vegetation stress mapping as an indicator for soil contamination that is induced by metals, salt and organic contaminants or general vegetation stress around known hazardous waste sites such as landfills (vegetation/agriculture)
- Wildfire damage and post fire succession monitoring (vegetation/forestry)
- Detection of illegal dumps (environment)
- Asbestos sheeting detection and mapping (urban)

Environmental applications with a focus on the detection of contaminated sites and soil contaminations, in particular with organic contaminants will be investigated in detail in section 4. Based on the objective of this study, this summary of a comprehensive literature survey will focus on the spectral properties and the imaging spectrometry investigation of soil properties (moisture, soil type, soil contamination, salinisation, etc.), vegetation stress related to contaminated soil (heavy metals, salts, organic contaminants), the detection of fuel hydrocarbons in the environment, the detection of waste deposits, and the detection of acidic leachates from metal mining overburden dumps.

In the context of recent applications of imaging spectrometry and their development, it should be noted that the first generation applications of imaging spectrometry were limited to highly homogeneous systems, namely to the mapping of surface mineralogy in arid regions. The mapping of the mineralogy of arid regions depends on only one variable, namely different minerals and their spectra. Soil moisture (water), vegetation cover or anthropogenic materials are typically nonexistent here. Mixed pixels in these applications therefore represent only mixtures of different minerals.

$$\textit{Mineral spectra (arid regions)} = f(\textit{mineralogy})$$

In the second generation of applications, imaging spectrometry was extended to other homogeneous systems, namely vegetation analysis (natural vegetation and agricultural vegetation), and the investigation of water bodies. For vegetation species mapping, measured spectra are compared to spectra from spectral libraries in order to match the measured spectra to known vegetation species. For vegetation stress mapping, usually applied to stands of homogeneous species, anomaly detection algorithms are applied. In water body investigation, minor spectral signatures of suspended matter, chlorophyll and other parameters of interest are detected in a dominating but homogeneous water background spectrum (even among different water bodies). Water and vegetation spectra are, therefore, determined by the following variables with water and vegetation species being the dominant factor determining the spectra. The “normal” water and vegetation species spectra can be considered the background in which “anomalies” are detected or mapped:

$$\text{Water spectra} = f(\text{water, suspended matter/turbidity, chlorophyll, submerged vegetation})$$

$$\text{Vegetation spectra} = f(\text{vegetation species, moisture, water / nutrient / contaminant stress})$$

The third generation of imaging spectrometry applications, namely the investigation of complex and inhomogeneous systems or targets such as urban areas and environmental contaminations involves many different variables. Typically, soil contaminations occur near or in urban areas, in particular industrial zones. Often contaminated sites are located on abandoned industrial brownfields. While urban areas are always heterogeneous, abandoned industrial brownfields are often even more heterogeneous with different pavement and roofing materials, varying vegetation cover (species, canopy closure, health) due to succession, material and waste deposits, painted and rusting metal structures, etc. In this heterogeneous background, different contaminants subject to such an investigation, are typically found in relatively low concentrations (usual contaminant concentrations of less than 3 wt.%). Furthermore, the extent of surface contaminations apart from waste deposits (that might even be covered) is usually small. Sometimes, contaminations are, as discussed earlier, limited to the subsurface without any surface expression as contaminated soil or stressed vegetation. Spectra of contaminated soil are therefore determined by four major variables of which the contaminants are typically the least dominant:

$$\text{Contaminated soil spectra} = f(\text{soil, vegetation cover, moisture, contaminant(s)})$$

In both urban applications of imaging spectrometry and the mapping/detection of contaminated sites, mixed pixels combining the spectra of different materials (either occurring as spatially neighboring materials or as mixtures) must to be considered normal, thus increasing the complexity of the detection problem.

Data acquisition and processing

Besides careful mission planning considering the objectives of an imaging spectrometry campaign and the technological possibilities, data acquisition and post-flight data processing are of particular importance in imaging spectrometry.

Imaging spectrometry utilizes reflected solar radiation in the $0.4\ \mu\text{m} - 2.5\ \mu\text{m}$ wavelength region as illumination source. As described in section 3 and illustrated in figure 3-2, the total radiance decreases from its maximum of approximately $1,500\ \text{W m}^{-2}\ \mu\text{m}^{-1}$ at $0.7\ \mu\text{m}$ to $100\ \text{W m}^{-2}\ \mu\text{m}^{-1}$ and less between $2.0\ \mu\text{m}$ and $2.5\ \mu\text{m}$. The radiance intensity is further decreased by atmospheric absorption bands of water vapor, carbon dioxide, oxygen, ozone and – in urban areas – atmospheric pollutants. Haze (water vapor or smog) attenuate the reflected solar radiation considerably, making data acquisition in perfect weather conditions (clear sky, dry atmosphere) preferable. Atmospheric interference is also crucial to the signal-to-noise ratio of imaging spectrometry data. The higher the absolute radiance is during data acquisition, the higher the signal-to-noise ratio will be and vice versa.

Post-flight data processing consists of three major components, namely atmospheric correction, conversion of radiance data to reflectance data, and geometric correction.

After being reflected by the target, usually the Earth's surface, the radiation passes through the atmosphere between the target and the sensor. On this path, atmospheric gases interact as described with the reflected radiation containing the target information, adding additional absorption features to the spectrum. In order to retrieve the radiation-surface interactions it is therefore necessary to remove these atmospheric absorption features from the data on a band by band basis because the atmospheric absorption is highly wavelength-dependent. Several atmospheric correction methods and algorithms based on different atmospheric radiative transfer models have been developed for this purpose. One common method is based on the comparison of the spectra of calibration targets measured by the airborne instrument and a ground based spectrometer. Subtracting the airborne measurement from the ground measurement yields the atmospheric interference that can then be subtracted from every pixel in the remote sensing imaging spectrometry data. Because this method does not take into account spatial atmospheric variations due to wind, topography or different ground cover, some instruments measure atmospheric calibration spectra for each ground spectrum or line of ground spectra collected (horizontal or off-axis measurement of atmospheric spectra). These atmospheric reference spectra are then used for a pixel-by-pixel correction of atmospheric effects in hyperspectral data.

For visual interpretation of hyperspectral spectra, and for most digital data interpretation methods, it is necessary to convert the acquired radiance spectra, which in most cases represent the solar irradiation curve, with the Earth's surface absorption bands into normalized relative reflectance spectra. In most cases, the radiance-to-reflectance conversion is now implemented in atmospheric correction models taking into account the solar radiation curve derived based on atmospheric data.

The geometric distortions of airborne scanner data that result from the unsystematic roll, crab and pitch movements of the platform are usually corrected using time-coded three-dimensional orientation data from the aircraft's inertial navigation system (INS). In a second step after the correction of these unsystematic distortions, systematic distortions such as the tangential distortion and resolution cell size variations in across-track scanner data can be corrected using simple mathematical models.

3.3 – Imaging spectrometry systems

More than 100 imaging spectrometry systems have been developed since the 1970s when the development of imaging spectrometry began in the wake of the advent of digital multispectral imaging systems (e.g., the first LANDSAT satellites) [Harrison 2003]. While most systems were developed in research and development projects in the United States, several commercial systems have been developed since the mid-1990s in the United States, Australia, Canada, and Finland.

In comparison to multispectral remote sensing systems such as the well-known spaceborne LANDSAT and SPOT systems, hyperspectral remote sensing systems required considerable advancements with respect to system optics, system mechanics, data compression and storage and data transfer. In contrast to multispectral systems that record electromagnetic radiation over a broad range of around 100 nm to 300 nm in four to ten independent bands, hyperspectral remote sensing systems record electromagnetic radiation in dozens to hundreds of small, contiguous bands. This implies several consequences with respect to the design and data handling in hyperspectral remote sensing systems. First, hyperspectral remote sensing systems produce multiple data volumes compared to multispectral systems with a similar spatial resolution. Second, the total radiance that is recorded in each band is only a fraction of that recorded by multispectral systems. While multispectral imaging systems integrate radiation over a wavelength range of 100 nm to 300 nm, hyperspectral remote sensing systems integrate electromagnetic radiation over bands that are typically only 2 nm to 10 nm wide.

To date, all known imaging spectrometry systems are passive system acquiring spectra in the 0.4 μm to 2.5 μm wavelength region (VIS, NIR, SWIR). As discussed before, the radiation received by an airborne or spaceborne instrument in this

wavelength region is sunlight reflected by the Earth's surface. However, the development of active hyperspectral imaging systems with an independent illumination source integrated in the system to enable the acquisition of hyperspectral data at nighttime and in adverse weather conditions for military purposes are under investigation [Nischan 2000].

Recently, several instruments have been developed that acquire spectra in the thermal infrared wavelength regions between 3 – 5 μm and 8 – 12 μm , respectively. As the main focus of these instruments is the investigation of atmospheric, fire and geologic features, they are not discussed in detail here.

Imaging spectrometry systems designs

Three major types of imaging spectrometry systems must be distinguished: across-track scanners (whisk-broom), along-track scanners (push-broom) and framing cameras [Harrison 2003, Puschell 2000].

Across-track scanners scan a single pixel at a time, with the scanning element moving continuously at right angles to the platform flight line. The radiation thus collected over the 0.4 – 2.5 μm range is dispersed using an optical grating, prism or a similar dispersing element and is detected, wavelength by wavelength, by a line detector array. Thus, across-track scanners have one detector element for each wavelength (spectral band) recorded. The size of the ground element recorded is referred to as instantaneous field of view, varying with the scan angle. The advantage of across-track scanning systems is that they are easily calibrated. Their main disadvantage is a relatively short residence or dwell time over each pixel. This design has been implemented in several imaging spectrometry systems such as AVIRIS and HyMap [Lillesand 1999, Goetz 1992a, Puschell 2000, Kruse 2000a, Harrison 2003].

Along-track scanners record a whole line of an image rather than a single pixel at a time using a two-dimensional dispersing element (grating) and a two-dimensional detector array. The main advantage compared to across-track scanners is their much higher dwell time for each pixel, thus increasing the signal-to-noise ratio considerably. The disadvantage of this kind of system is the difficult and time-consuming calibration of the two-dimensional detector array [Goetz 1992a, Puschell 2000, Harrison 2003].

Hyperspectral framing cameras (also: step-stare imagers) acquire hyperspectral data for an area simultaneously using one area array detector for every spectral band, thus taking dozens or hundreds of pictures in different wavelength bands simultaneously. The opto-mechanical challenge in the design of this type of instrument is considerable as the incoming radiation has to be split into wavelength bands for whole images. Furthermore, the system is required not to move relative to its target area during the necessary acquisition time. This design concept has to date only been implemented in the Geostationary Imaging Fourier Transform Spectrometer (GIFTS) [Harrison 2003, Puschell 2000].

The detectors used in imaging spectrometers are generally photovoltaic semiconductor detectors, so-called charge-coupled devices (CCD's). Semiconductor line or area arrays typically used in imaging spectrometers include silicon (Si) arrays, indium antimonide (InSb) arrays, mercury cadmium telluride (HgCdTe) arrays and indium gallium arsenide (InGaAs) arrays. Silicon arrays are sensitive to radiation in the 0.4 – 1.0 μm wavelength range, InSb, HgCdTe and InGaAs arrays at longer wavelengths between 1 μm and 5 μm . In some instruments, several different and overlapping detector elements are used for optimized sensitivity in different wavelength regions [Goetz 2000a].

Important System Parameters

The main system parameters to describe the capabilities of imaging spectrometers include the spectral range over which the instruments operate, the number of bands sampling the spectrum, the bandwidth (also referred to as spectral resolution), the signal-to-noise ratio, and the radiometric resolution. These main parameters are explained below.

Spectral range

The spectral range describes the wavelength areas covered by an imaging spectrometer. Most imaging spectrometers cover the whole 0.4 μm – 2.5 μm region, while some instrument that are tailored to vegetation analysis cover only the visible and near infrared wavelengths between 0.4 μm and 1.0 μm . Most imaging spectrometers do not acquire data in the spectral bands around the 1.4 (± 0.05) μm and 1.9 (± 0.05) μm atmospheric water vapor absorption bands.

Band number

The number of bands is one of the main parameters of hyperspectral systems. Most hyperspectral systems now have between 10 and 50 spectral bands over a 100 nm range of the electromagnetic spectrum or 100 – 250 spectral bands in total. However, the band number is not the only and decisive criterion. Some imaging spectrometers sampling certain, selected wavelength regions have only 20 – 50 spectral bands. The second important criterion is bandwidth (see below).

Bandwidth

The main criterion of the definition of imaging spectrometers or hyperspectral systems is the bandwidth, also referred to as spatial resolution. In order to resolve typical absorption features of natural and man-made structures that are typically between 20 nm and several hundred nanometers wide, it is necessary to sample

(integrate) the spectrum over short intervals. The bandwidth is a parameter that is defined as the full width at half maximum (FWHM) response to a spectral line source, describing the narrowest spectral feature that can be resolved by an imaging spectrometer [ASD 2002a]. Bandwidth should not be interchanged with the spectral sampling interval, indicating the spectral distance between two contiguous bands without referring to their bandwidth.

Signal-to-Noise-Ratio The signal-to-noise ratio (SNR or S/N) is the ratio of the radiance measured to the noise created by the detector and the instrument electronics. For imaging spectrometers, the signal-to-noise ratio is always wavelength-dependent because of overall decreasing radiance intensity towards longer wavelengths and atmospheric interferences (atmospheric absorption bands).

Spatial resolution The spatial resolution is defined as the ground area that is represented by one image pixel. Except for spaceborne instruments, the spatial resolution is not fixed. The parameter most commonly used to describe the spatial resolution of an instrument is the aperture angle for a single pixel or instantaneous field of view (IFOV), usually given in milliradians [mrad]. Multiplying the IFOV in radians with the platform (flying) height in meters yields the actual spatial resolution in meters. However, this is only valid at Nadir, i.e., exactly vertically below the platform. Airborne instruments typically yield a spatial resolution between 0.5 m and 20 m, spaceborne instruments between 30 m and 1,000 m.

Radiometric resolution Radiometric resolution is the ability of the sensor to resolve the signal intensity. It is usually expressed in digitization levels (bits). Recent imaging spectrometers digitize radiance data in 4,096 levels (12 bit) to 65,536 levels (16 bit), with the levels also being referred to as digital number (DN) values.

Platforms Most recent imaging spectrometers are airborne instruments that are usually applied from flying heights between 1,000 m and 5,000 m. Some coarse spatial resolution imaging spectrometers are spaceborne (e.g., MODIS with a spatial resolution of 250 – 1,000 m aboard the EO-1 satellite). A high spatial resolution spaceborne imaging spectrometer is the military Warfighter-1 instrument aboard

the OrbView-4 satellite delivering 8-m spatial resolution hyperspectral data from space.

Ten important recent and operational imaging spectrometry systems and important system parameters are summarized in table 3-7.

Table 3-7: System characteristics of important recent imaging spectrometry instruments. For the systems DAIS 7915, EPS-H, and MODIS, spectral bands in the thermal wavelength regions beyond 2.5 μm are left out.

System	Spectral Bands	Spectral Range [μm]	Bandwidth [nm]	IFOV [mrad]	Spatial Resol. [m]	Radiometric Resol. [bit]	SNR	Platform	Funding / Ownership	Company/ Country
AISA Eagle ¹	244	0.4 – 0.97	2.9	0.5 – 0.7	ca. 0.5 – 0.7 (@1,000 m)	12	N/A	airborne	commercial	Specim/ Finland
AISA Hawk ¹	254	1.0 – 2.4	8	1	ca. 1 (@ 1,000 m)	14	N/A	airborne	commercial	Specim/ Finland
AVIRIS ^{2, 10}	224	0.41 – 2.45	9.4 – 9.7	1	2 (low alt.) - 20 (high alt.)	12	150 – 1,100	airborne	research	Jet Propuls. Laboratory/ USA
CASI-3 ³	1 - 288	0.4 – 1.05	~2.2	0.49	ca. 0.5 (@ 1,000 m)	14	~480 : 1 (peak)	airborne	commercial	Itres Res./ Canada
DAIS 7915 ⁴	72 1	0.43 – 2.5 3 – 5	15-45 2	3.3	5 - 20	15	N/A	airborne	commercial / reserach	GER/ USA
EPS-H ⁵	76 64	0.4 – 1.01 1.0 – 2.5	8 16-50	1.25 - 5	1.25 – 5 (@ 1,000 m)	16	150 - 300	airborne	commercial	GER/ USA
HyMap ^{6, 10}	128	0.4 – 2.504	10 - 20	1 - 3	1.5 – 13.5	12 – 16	> 500 : 1	airborne	commercial	Int. Spectr./ Australia
Hyperion ⁷	220	0.4 – 2.5	10	N/A	30	N/A	N/A	spaceborne	research	NASA/ USA
MODIS ⁸	36	0.46 – 2.5 8 – 14.39	10 – 50 30 – 300	N/A	250 – 1,000	12	57 – 1,087 : 1	spaceborne	research	NASA/ USA
Warfighter ^{9, 10}	280	0.45 – 5.0	11.3 – 25.0	~0.02	8	N/A	50 - 400	spaceborne	military	US DOD/ USA

[Sources: ¹www.specim.fi, ²www.aviris.jpo.nasa.gov, ³www.itres.com, ⁴www.op.dlr.de/dais/dais-ser.htm, ⁵www.ger.com, ⁶www.intspec.com, ⁷www.eo1.gsfc.nasa.gov, ⁸www.modis.gsfc.nasa.gov, ⁹www.fas.org, ¹⁰Scriptum Short Course Hyperspectral Imaging & Data Analysis, CSES; University of Colorado 2000]

3.4 – Imaging spectrometry data interpretation

The objective of imaging spectrometry data interpretation, as for all remote sensing data interpretation, is the derivation of information on surface composition and properties from the image data. Because of its high spectral resolution, imaging spectrometry data can be analyzed for both qualitative and quantitative surface composition information and yield results that go beyond that of other remote sensing methods. In contrast to broadband spectral data, imaging spectrometer data can be used (in principle) to uniquely characterize and identify many materials [Shaw 2002, Goetz 1992a]. Depending on the objective of the investigation, the data interpretation might be targeted at a full-scale analysis of a particular scene resulting in a full-scale land cover analysis, the detection of known or expected spectral signatures or the detection of anomalies, i.e. unexpected spectra.

However, besides its possibilities, imaging spectrometry data also represents considerable challenges with respect to data interpretation. One of the main problems is coping with the high spectral dimensionality of imaging spectrometer data resulting in huge datasets that contain much redundant information and pose considerable computational challenges [van der Meer 2001b].

The general approach to imaging spectrometry data interpretation comprises the reduction of data redundancy, the identification of pure spectra in the dataset under investigation, and, finally, the identification of the spectral constituents of every single pixel over the whole scene.

The subsequent paragraphs will outline the general data interpretation approaches, problems, terminology and data interpretation techniques used in imaging spectrometry data interpretation.

Data interpretation objectives

The objectives of an investigation using imaging spectrometry can be organized according to the following application specific tasks [Shaw 2002a, Landgrebe 2002, Richards 1999, Chang 2003b, van der Meer 2001b, Manolakis 2002a]:

Classification

Grouping of pixels of a hyperspectral data set into classes according to common spectral properties using user-defined classes (supervised classification) or calculated classes of similar spectra (unsupervised classification)

Imaging spectrometry data allows, in contrast to multispectral data classification, a more detailed classification (e.g. classification of vegetation species rather than vegetation classes such as “grass”, “deciduous forest” and “coniferous forest”). Using spectral libraries, many

different vegetation species, minerals and man-made materials can be uniquely identified using classification methods developed for the interpretation of imaging spectrometry data.

Mapping

Distribution mapping of abundant materials with known spectral characteristics (“ground-truthing” or image derived) in a scene, e.g., dominant surface materials or vegetation species in a scene that are easily identified or known.

Anomaly detection

Detection of spectral anomalies in a “normal”, i.e. relatively homogeneous spectral background without a priori knowledge about the spectral characteristics of the “anomaly”

Typically, spectral anomalies are small compared to other objects or surface materials in the scene investigated. Usually, “anomalous” spectra can be identified after detection using spectral libraries.

Target detection

Detection of expected (or known) spectral signatures in a large, homogeneous or heterogeneous background

Usually, the target is small and its occurrence of low probability compared to the spectral background, i.e. it covers only few small areas of an imaging spectrometry dataset. Because of this, classification approaches based on statistical approaches are not applicable. If the target is actually smaller than a pixel, i.e. hidden in larger pixel, it is referred to as subpixel target detection. Target detection always requires a priori knowledge or assumptions about spectral characteristics of the target. Typically, target spectra searched for in imaging spectrometry dataset are taken from spectral libraries.

Abundancy mapping

Quantitative analysis with respect to the fractions of different materials that make up a pixel

Depending on the spatial resolution of an imaging spectrometry dataset, more or less pixels represent “mixed” spectra of different surface materials that were integrated into one pixel or spectrum. Spectral unmixing algorithms

that identify and quantify the spectral fractions of different materials in a pixel can be used to estimate the fractions of surface materials that make up a pixel. Spectral unmixing always requires the identification of the major spectral constituents that make up a spectrum (see below, spectral unmixing).

Change detection

Determination of changes between two or more multitemporal imaging spectrometry datasets of the same area, e.g. phenological changes of vegetation during different seasons or urban development between different years

Classification and mapping are qualitative analysis methods with a focus on spatial distribution, while anomaly detection and target detection are qualitative analysis methods with a focus on detection. Abundance mapping is a quantitative and qualitative analysis method with a focus on quantitative distribution mapping. Change detection comprises elements of both quantitative and qualitative analysis as changes might be both quantitative (e.g. increase in the density of certain surface materials) and qualitative (e.g., appearance of new surface materials).

Spectra

For the subsequent discussion of hyperspectral data characteristics, data interpretation preprocessing, and analytical processing techniques, several concepts with respect to the definition and description of spectral absorption features need to be described (figure 3-11).

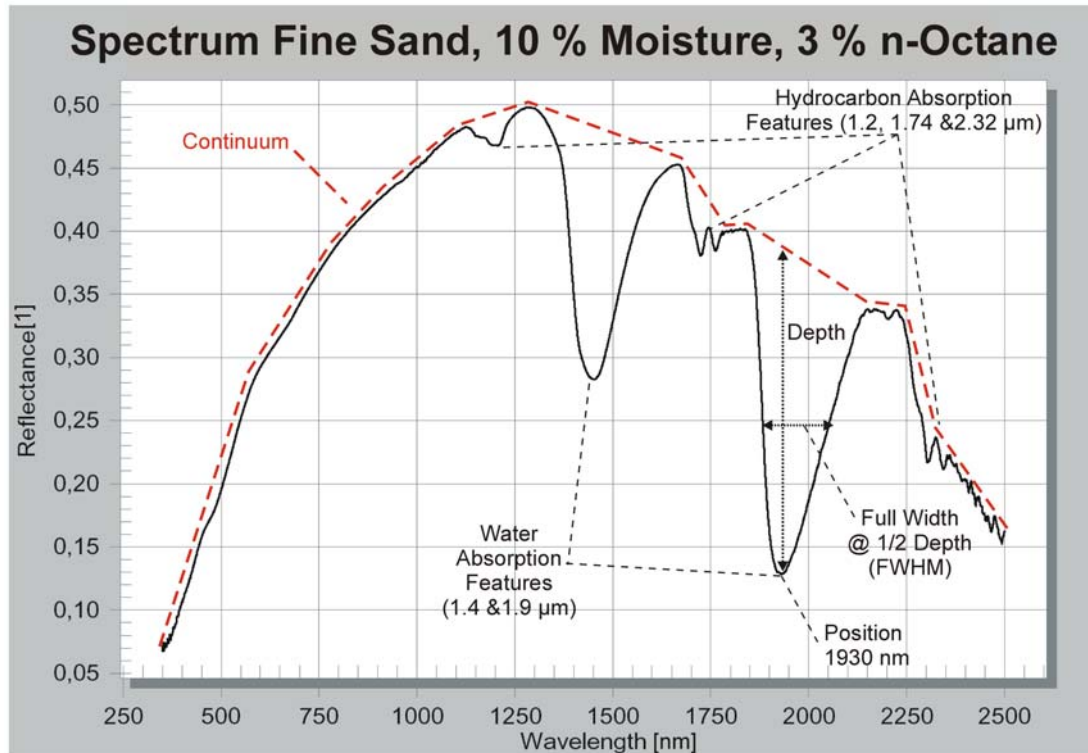


Figure 3-11: Important concepts, definitions and characteristics of near infrared spectra.

Absorption features are local minima in the reflectance spectra. They are described by both their position, i.e. the wavelength of their reflectance minimum, and their width. Because absorption features are usually wide at top and narrow towards the bottom, the width used to describe is the full-width-at-half-maximum (FWHM). It is defined as the width at half the absorption feature depth. Typical absorption features of solid and liquid surface materials observed in imaging spectrometry data are between several tens to a few hundreds of nanometers wide [Clark 2003b, Goetz 1996a].

In some cases, spectra are normalized for the investigation and comparison of absorption features by removing the continuum covering the spectrum. The continuum is defined as a convex hull fit over the top of a spectrum utilizing straight line segments that connect local spectra maxima [RSI 2001].

Characteristics of imaging spectrometry datasets

Spectra recorded in imaging spectrometry or hyperspectral data are usually oversampled, i.e., single absorption features are typically covered by several and not only single wavelength bands (hyperspectral – “too many bands”). General oversampling of imaging spectrometry data is necessary in order to ensure that narrow absorption features of all kinds of different surface materials can be recorded simultaneously. Therefore, imaging spectrometry spectra contain an abundance of

redundant information where single absorption features are covered by multiple wavelength bands.

As described above, depending on the spatial resolution, spectra of an imaging spectrometry dataset represent mixed spectra consisting of several constituents (pure substances, so called spectral endmembers) that covered the ground area represented by the pixel at the time of acquisition. For the spectral unmixing process described above, it is important whether a spectral mixture is based on linear or nonlinear mixing processes. Usually, linear mixing models are assumed for spectral unmixing.

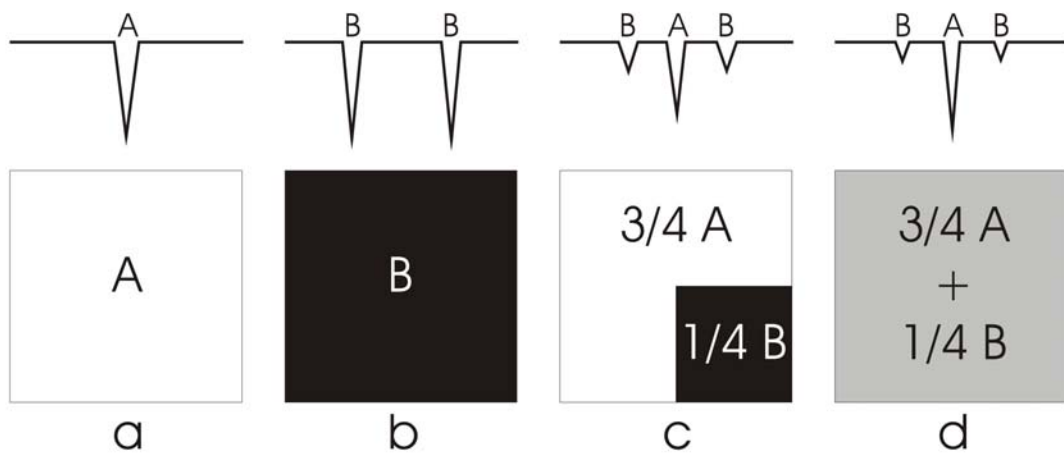


Figure 3-12: Spectral mixing concept with two basic mechanisms: linear mixing (c) and non-linear mixing (d) of two single components.

Figure 3-12 depicts two spectral mixing models. Figure 3-12 a and b represent two spectral endmembers and their spectral responses. Figure 3-12 c represents a linear mixing of the two spectral endmembers where pure A covers 3/4 of the pixel and pure B covers 1/4 of the pixel. The spectrum that results fulfills the linear mixing concept as a linear combination of the endmember spectra weighted by their area coverage fraction. The absorption feature depth of A is reduced to 3/4 and the absorption feature depth of B is reduced to 1/4. Figure 3-12 d illustrates a nonlinear mixing of the two components that is usually observed if two components are intimately mixed. In this case, absorption features might result in nonlinearly mixed spectrum where the absorption feature of B is less than 1/4 of the full absorption feature and the absorption feature of A is more than 3/4 of the full absorption feature. Two reasons for nonlinear mixing processes are, among others, absorption effects where one component is absorbed by the other and therefore not exposed at the surface and masking effects where the absorption spectrum of one component dominates over the other. Generally, nonlinear spectral mixtures occur if the endmember materials are mixed on a spatial scale that is smaller than the path length of photons in the mixture [Keshava 2002b, van der Meer 2001b].

Although it is not of particular importance for the investigation of the spectral response of soil (i.e. moisture) contaminant systems it should be noted that for some surface materials, the surface reflectance response (intensity) is highly dependent on the illumination and viewing angles. It is of particular importance for vegetation studies, resulting from architectural patterns and general orientation of plant canopies induced for example by wind and rain. Vegetation is therefore referred to as an anisotropic scatterer, reflecting radiance differently in different directions. This effect is described by the bi-directional reflectance distribution function (BRDF). The BRDF is a mathematical description of how reflectance varies for all possible combinations of illumination and viewing angles at a given wavelength [Kumar 2001a, Schott 1997, van der Meer 2001b].

Data interpretation preprocessing

Probably the most important step of preprocessing of imaging spectrometry data prior to image analysis is redundancy (or dimensionality) and noise reduction. The objective is to reduce the computational requirements for subsequent image analysis steps, to eliminate noise from the data that interferes with the interpretation, and to determine the inherent dimensionality (or information content) of the data.

The minimum noise fraction (MNF) algorithm developed for this purpose is a method of generating a reduced number of new, uncorrelated datasets or bands with accumulated information content from hyperspectral datasets consisting of hundreds of often highly correlated spectral bands. MNF utilizes the fact that while the spectral information content in hyperspectral data sets is often highly correlated, noise inherent in the data is typically uncorrelated. The MNF approach is based on the principal components transformation that was developed to uncorrelate multispectral datasets [Richards 1999, Goetz 2000a].

As described above, an imaging spectrometry dataset consists of m pixels each comprising n spectral bands. Each spectral band has an associated brightness value that was registered as the spectral response of the sampled area (pixel) by the instrument and can also be referred to as its digital number (DN) value. Thus, single spectra can be considered n -dimensional vectors with n indicating the number of spectral bands.

$$m = \begin{bmatrix} n_1 \\ n_2 \\ \dots \\ n_n \end{bmatrix}$$

with

m – Spectrum vector of pixel m

$n_1..n_n$ – Spectral response of band n

The vector concept assumed for imaging spectrometry data is illustrated in figure 3-12. Figure 3-13 a illustrates the concept for a three-dimensional (three-band) case. Expanding the concept to the number of n bands of a hyperspectral dataset yields an n -dimensional vector for each pixel spectrum of a dataset. The n -dimensional pixel vector can be defined by either n values or an angle and a length in n -dimensional space. Figure 3-12 b depicts a so called two-dimensional scatterplot in which all pixels of a scene are mapped according to their DN values in two user-selected bands. The pixel distribution pattern shown in b illustrates a case commonly observed when mapping multi- or hyperspectral data in scatterplots. Obviously, the DN values of the pixels in the spectral bands x and y are correlated linearly. Figure 3-13 c finally illustrates the principle of the principal components transformation. Based on the data (in this case for the two-dimensional case), a new orthogonal coordinate system is calculated thus that the data is uncorrelated in the new coordinate system. By means of linear combination of original, correlated bands, uncorrelated bands are produced [Richards 1999, Goetz 2000a, RSI 2001].

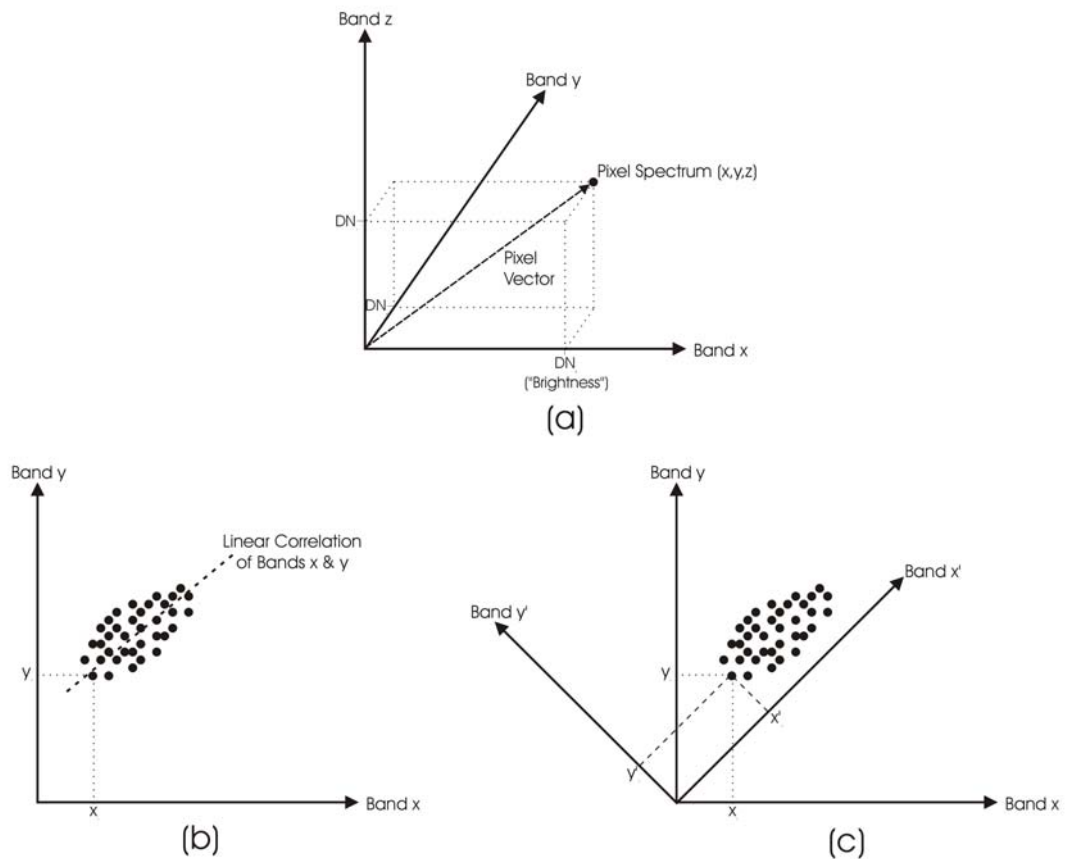


Figure 3-13: Concepts of n-dimensional spectrum (pixel) vectors (a) and coordinate transformations for dimensionality reduction (b), (c).

The MNF transformation developed for hyperspectral datasets that are more complex than multispectral data sets is essentially two cascaded principal components transformations. In MNF transformations, the first transformation is used to eliminate noise in the data while the second is used to apply a principal components transformation on the noise-whitened data.

The resulting MNF output bands are sorted by decreasing signal-to-noise-ratio (SNR), with the first band containing the highest information content and the last bands containing virtually only noise. The information content of MNF output bands is assessed by comparing the eigenvalues of the output bands, with high values indicating a high information content and eigenvalues around one indicating bands that contain almost only noise [Richards 1999, RSI 2001, Goetz 2000a].

Analytical data interpretation

Following the comprehensive preprocessing of the data including atmospheric correction, geometric correction, noise removal and redundancy reduction as described above, data interpretation can be carried out. Typically, data interpretation

techniques applied to imaging spectrometry data include elements of both classification approaches originally developed for the interpretation of multispectral data and spectrum interpretation methods developed for qualitative and quantitative chemical laboratory analysis. Some important data interpretation approaches applied to imaging spectrometry data will be discussed subsequently.

The primary objective of every analytical data interpretation applied to imaging spectrometry data is the identification of spectral signatures and their assessment with respect to quantitative abundance. This general approach is always valid, regardless of the overall objective of the imaging spectrometry campaign, be it mapping, classification, target detection, anomaly detection or abundance mapping. However, many specific methods have been developed that are optimized for mapping, classification or detection purposes.

The selection of spectral endmembers is an important step in data analysis except for anomaly detection where the “target” spectrum is unknown by definition. Spectral endmembers are “spectrally pure”, i.e. single-component spectra of which all or most mixed spectra found in a scene are composed. For target detection, endmembers can also be expected target spectra derived from earlier investigations or spectral libraries. Spectral endmembers can be chosen from an existing spectral library (e.g., for target detection) or extracted from a dataset using tools such as the pixel purity index (PPI), an algorithm that extracts “extreme” (pure) pixels from n-dimensional spectral vector datasets. Another data analysis approach is to compare every single pixel spectrum of an imaging spectrometry dataset to comprehensive spectral libraries calculating similarities. For some applications, e.g. classification, it might also be sufficient to build classes from an imaging spectrometry dataset first and then identify the classes. The subsequent paragraphs will outline the principle of some important analytical tools for imaging spectrometry data.

Spectral library comparison techniques

The simplest approach to imaging spectrometry data analysis is the comparison of image spectra to spectra from a spectral library on a band by band basis and calculating an overall similarity for an image spectrum with respect to spectral library matches. This approach has a number of drawbacks. First, this approach requires virtually indefinite spectral libraries covering all kinds of surface materials that are encountered in the image scenes under investigation. Second, the comparison is computationally demanding as the similarity of an image pixel must be calculated for every single spectrum in the spectral library. Third, usually only pure materials are covered by spectral libraries. Therefore, simple library comparison on a band by band basis does not identify spectral mixtures but rather calculates a high similarity value for the dominating material in a pixel. In some cases, results may be inaccurate because spectral mixtures might resemble spectral responses of materials not present in the pixel.

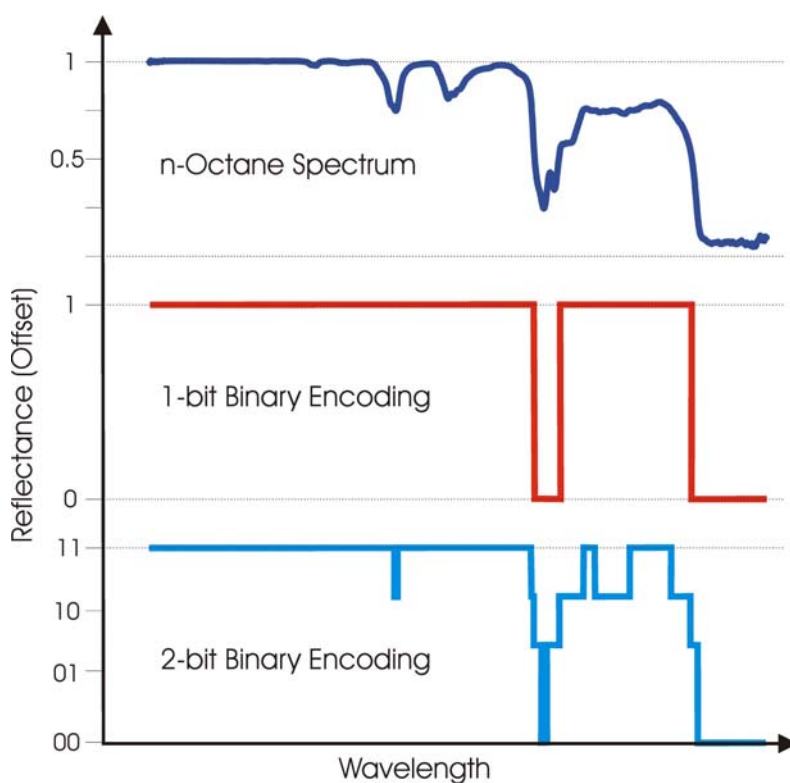


Figure 3-14: Concept of 1-bit and 2-bit binary encoding.

Binary encoding was developed in an early stage of imaging spectrometry data analysis to reduce the computational loads required for a band by band comparison of image and library spectra. In binary encoding, the spectrum is encoded into two values, zero and one based on a threshold value.

For example, all reflectance band values above 0.5 are assigned the value “1”, all reflectance values below 0.5 are assigned the value “0”. By applying binary encoding to both imaging spectrometry data and spectral libraries used for comparison, the computational load can be reduced considerably as the band by band comparison is reduced to a simple yes / no comparison between the image spectrum and the library spectra. The most probable match is that with the highest number of matches. Because simple binary encoding using only a 1-bit encoding (values 0, 1) and a single threshold reduces the separability of spectra of similar materials considerably, 2-bit binary encoding using four values (00, 01, 10, 11) was developed. With three user-defined thresholds and four different values to encode a spectrum, 2-bit binary encoding resembles the overall shape of a spectrum much better than 1-bit encoding. Figure 3-14 illustrates 1-bit and 2-bit binary encoding for the spectrum of liquid n-Octane [Richards 1999, Goetz 1992a, Goetz 2000a, RSI 2001].

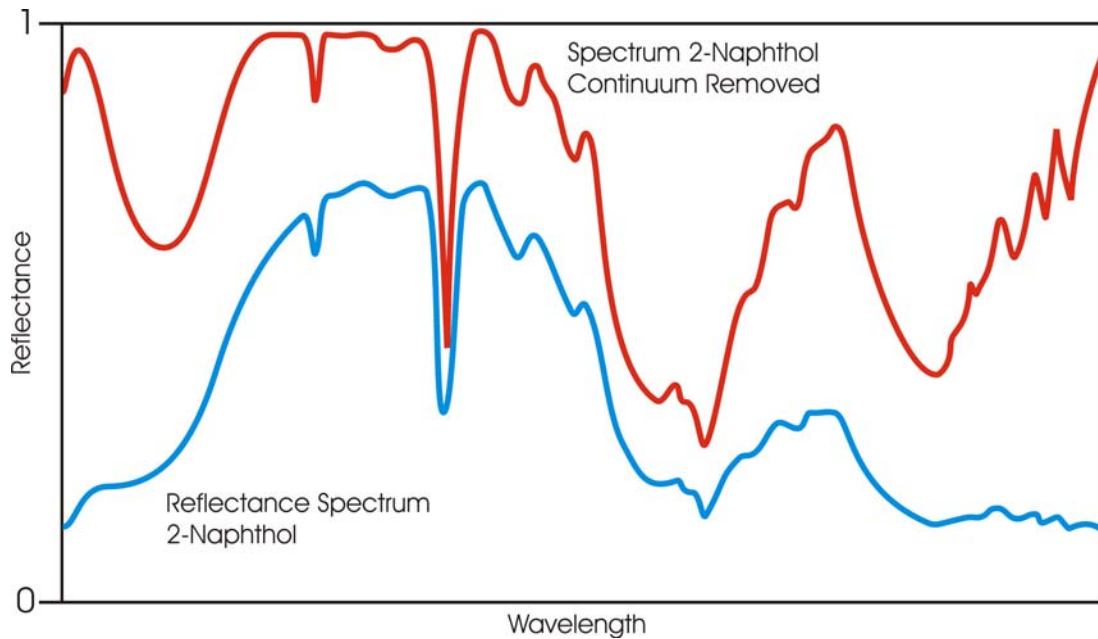


Figure 3-15: Continuum removal calculated for the spectrum of solid 2-naphthol. Blue: reflectance spectrum, red: continuum-removed spectrum.

More advanced forms of image library spectra comparison algorithms are *waveform characterization* and *spectral feature fitting (SFF)*. For these algorithms (see above), in a first step the continuum must be removed from the spectra for normalization. Figure 3-15 illustrates the effect of continuum removal for the reflectance spectrum of 2-Naphthol. In a second step, the normalized spectra are then used to characterize the absorption features with respect to their position (minimum wavelength), FWHM, depth, slope, and (a)symmetry. These parameters are then compared between image and library spectra calculating the similarity. The algorithms can usually be restricted to wavelength regions of interest to enhance computational efficiency [Clark 2003b, van der Meer 2001b, Richards 1999].

Spectral angle mapping (SAM) utilizes the angle of the n-dimensional vector characterizing the spectral response of a pixel or a group of spectrally similar pixels and does not take into account the magnitude (length) of the vector. The method is based on the assumption that classes of spectral endmembers are spectrally distinct from another such that angles in n-dimensional space are sufficient to differentiate groups that are spectrally similar from another. Angles can either characterize the mean of predefined classes or boundaries between classes. The spectral angle mapping algorithm calculates the similarity between image spectra and library or image derived endmember spectra by calculating the n-dimensional angle between the spectral endmember and each pixel spectrum. The resulting angle describes the similarity between the endmember spectrum and the pixel spectrum. The smaller the angle is, the closer the match to the endmember spectrum will be. According to user-defined threshold values as deviations from the endmember angle, pixels are either

assigned to an endmember class or left unassigned (unclassified). The advantage of the SAM algorithm is that it is largely insensitive to slope and illumination effects. The disadvantage is that SAM does not take into account the intensity of spectral absorption bands (vector length) which often plays an important role in spectrum discrimination. Figure 3-16 illustrates the spectral angle mapping principle [Richards 1999, RSI 2001, Goetz 2000a].

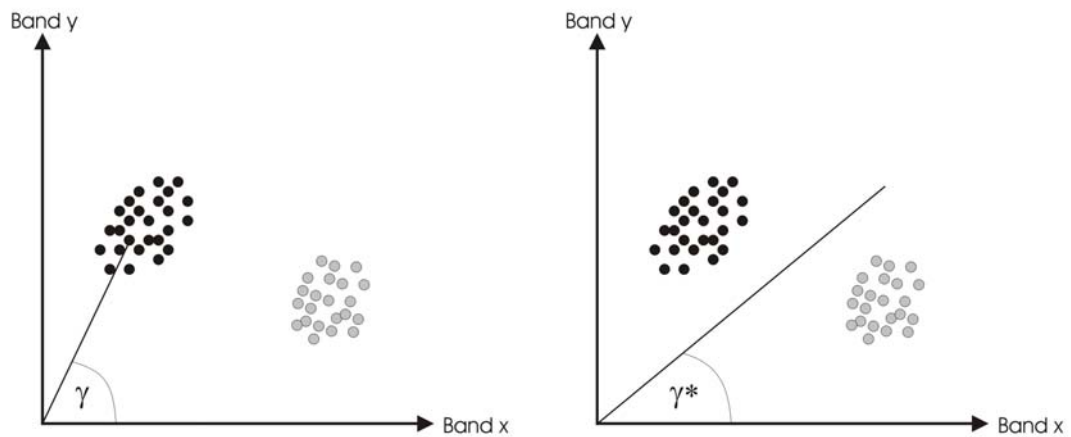


Figure 3-16: Spectral angle mapping classification concept.

Target detection techniques

For target detection, and the detection of known or expected spectral endmembers, the *matched filtering* and *mixture tuned matched filtering (MTMF)* algorithms have been developed. Based on the input of single or multiple endmember spectra, the response of the endmember(s) in the image pixel spectra are maximized while the spectral responses of background and non-target materials are suppressed. This process is also referred to as partial unmixing based on linear unmixing algorithms. It returns a single value between approximately 0 and +1 for every image pixel spectrum, the value representing the approximate sub-pixel abundance of the endmember spectrum under investigation with 1.0 indicating a pure target spectrum [RSI 2001]. Unfortunately, matched filtering sometimes returns a considerable number of false positives. MTMF is an enhanced matched filtering algorithm that, in addition to the result indicating the abundance of the endmember in a pixel, also calculates an “infeasibility value” for every pixel. Typically, false positives show a high infeasibility value. Correctly detected pixel spectra have both a high matched filter score above the background mean and a low infeasibility value [RSI 2001].

Anomaly detection

The objective of ***anomaly detection*** algorithms is to distinguish spectra of “unusual” materials in a scene from typical background materials without a priori knowledge about the target spectra. Anomalies are detected by comparing single pixel spectra of an imaging spectrometry dataset to average spectra (“normal spectra”) with a defined range of “allowed” deviations of either a whole scene, the wider neighborhood of the pixel under investigation or a limited number of abundant or expected spectral classes. Which of these three basic approaches is used mainly depends on the homogeneity of the scene under investigation. If a spectrum does not fall into the “normal” spectra of a scene, it is assigned an anomaly [Stein 2002b, Ren 2002, Penn 2003, Chang 2003b].

Spectral mixture analysis

Spectral mixture analysis is a classification approach that allows the designation of several classes to a single pixel based on the unmixing of the sum spectral responses of two or more materials covering the area represented by an image pixel. Spectral mixture analysis implemented in recent software packages for imaging spectrometry data interpretation is usually based on linear spectral unmixing, assuming that all spectral mixtures in a scene are linear mixtures [RSI 2001, van der Meer 2001b, Richards 1999]. However, as described above (figure 3-12), spectral mixtures can only be assumed to be linear mixtures if the two or more components involved are not intimately mixed but exist as spatially discrete units in a pixel. If two or more components are intimately mixed, spectral mixing processes usually have to be assumed non-linear. This fact will be of particular importance for the soil (moisture) contaminant mixtures considered in later sections [Keshava 2002b]. In some cases, however, non-linear mixture problems are made linear by changing variables [Goetz 1992a, Keshava 2002b].

Spectral mixture analysis requires the identification of all endmembers present in an imaging spectrometer dataset. It is then assumed that all pixel spectra of an imaging spectrometry dataset are linear combinations of the endmembers identified by the user or by automatic means. Based on this assumption, the measured spectra (most of which are mixed spectra to some degree) are decomposed into a combination of endmembers predefined by the user, and their fractional abundances are determined. This process is also referred to as inversion. The results of linear spectral mixture analysis are highly dependent on the identification of all correct spectral endmembers of an imaging spectrometry dataset, which is often impossible due to the huge number of different surface materials found in particular in urban areas. Linear unmixing algorithms have been shown to be accurate to approximately 3 – 5 % of absolute abundance of a material in a pixel [Keshava 2002b, RSI 1999, Richards 1999, Goetz 2000a].

Other analysis tools

Band ratios and ***band differences*** are simple transformations based on two spectral bands of a dataset that can be used as a quick-check tool for examining hyperspectral datasets for the presence of certain materials with known spectral absorption features. They are calculated from reflectance or radiance data using two bands in the area of sharp and specific absorption features of the target material [Penn 2002b, Richards 1999].

Band ratios should be calculated features for bands that are not more than several tens of nanometers apart in order to prevent that uncorrelated absorption features of materials other than the target material show up in the band ratio results. Usually, spectral bands used for band ratios are located such that one band lies in the center of a sharp, intense absorption feature and the other band lies on the shoulder of the same feature [Penn 2002b].

Neural networks are defined as large numbers of relatively simple processors (or neurons / units) that are operating in parallel and that are connected to each other by a defined system of links. They are promising alternatives to conventional detection and classification approaches based on class statistics and band by band comparison of image and library spectra. As far as their principal mode of operation is concerned, neural networks resemble animal brains. When a neural network is fed with information, the information is split into many small portions and processed in parallel over several cascades, with neighboring (connected) processors interchanging results. Resembling the animal brain, neural networks cannot be programmed to perform certain tasks but have to be trained in order to learn to make correct decisions. Training of neural networks means to adjust the parameters of the processors and to configure the connections between its processors. Neural networks can be implemented as either hardware solutions or software simulating a neural network. However, applications of neural networks for the interpretation of imaging spectrometry data reported in recent literature show that conventional approaches still dominate the interpretation of imaging spectrometry data. Furthermore, the application of neural networks to this task is still limited to few experiments for both classification and target detection [Carling 1992, Richards 1999, Udelhoven 1998, Rogers 1995, RSI 2001].

Probably the most widely used approach to hyperspectral data interpretation is a cascaded combination of the preprocessing and data interpretation techniques introduced above. Following atmospheric and geometric correction, an MNF transformation is applied to reduce noise in the data. Using the pixel purity index, spectral endmembers are then selected by the user. Applying linear unmixing and one or several of the data interpretation methods introduced above, endmember classes are finally mapped and identified.

4 – Environmental applications of imaging spectrometry

Imaging spectrometry has found many applications in different fields during the last decade. Originally developed by NASA scientists for geologic mapping in arid regions, the potential of imaging spectrometry for military, espionage and law enforcement applications was soon recognized in the United States. During the 1990s and still today, military interest and funding has been a driving force in the technological development of imaging spectrometry. Although only few publications are known in this particular field, funding acknowledgements to military and security-related government agencies and known instruments and missions (e.g., Hydice, Warfighter/Orb-View 4) indicate that much of the development was driven by a high interest in military and strategic applications of imaging spectrometry. However, civilian applications were also extended to many different fields from its early origins concerning the geology of arid regions. Recent applications include research and commercial applications in geology and mineral exploration, agriculture, forestry and ecology, limnology and oceanography, atmospheric sciences, and the military, espionage and law enforcement sectors. The objective of this section is to give an overview of imaging spectrometry applications in different fields and to provide a detailed analysis of environmental applications, in particular the detection and mapping of contaminations, overburden dumps, and waste deposits.

4.1 – Applications of imaging spectrometry

Table 4-1 gives an overview of recent remote sensing applications of imaging spectrometry in the different fields of application plus terrestrial applications of imaging spectrometry on laboratory scale (imaging spectrometry photography, imaging spectrometry microscopy) along with key references.

Table 4-1: Overview of the applications of imaging spectrometry sorted by fields of applications.

Field of Application	<i>Application Examples and Selected References</i>
Military and Espionage	Tactical reconnaissance [Lareau 2002, NN 2002c, Wall 2001]
	Target detection [Ashton 1999, Kailey 2000, Kailey 1996, McGregor 1998, Olsen 1997]
	Friend-foe identification (related to target detection)
	Terrain (battlefield) analysis [McGregor 1998]
	Mine detection [Achal 1995, Azimi-Sadjadi 1995, DePersia 1995, Kenton 1999, Smith 1999a]
	Detection of chemical warfare agents (early warning and risk assessment after application) [Ifarraguerra 1999a]
	Strategic surveillance of mining activity (e.g. for uranium and other strategic resources) [Levesque 2000]

Law Enforcement	Detection and mapping of narcotics plantations (e.g. in Central & South America, Middle East) [Kailey 2000]
	Border control (target detection of persons and vehicles) [Kailey 2000]
	Policing of agricultural subsidies (mapping of crop species and fallow land for subsidies fraud detection)
	Tax assessment (e.g. in case of taxes for certain roofing materials, surface sealing, etc. in urban areas)
Geology [van der Meer 1999b, van der Meer 2001c]	Geology and mineralogy mapping [Clark 1998b, Hook 1990, Kruse 1988c, Kruse 1992b, Swayze 1999, Wang 1998b]
	Mineral and ore exploration [Ma 1998, Sabins 1999, Wu 1996]
	Hydrocarbon exploration (detection of natural micro- and macroseeps) [Bammel 1994, De Oliveira 1996, Ellis 2001, van der Meer 2000d, van der Meer 2001d]
	Mapping of swelling clays [Chabrillat 2001, Chabrillat 2002]
Agriculture [Clevers 1999, Clevers 2001]	Crop species mapping and phenological characterization [Kneubühler 2001, Xiang 1998]
	Crop stress detection in homogeneous stands (nutrient stress, water stress, salt stress) [Cassady 2001, Goel 2003a, Kneubühler 2000, Lelong 1998, Lobell 2003]
	Crop biochemistry (chlorophyll content, leaf nitrogen concentration, leaf area index, water content, etc.) [Bach 1994, Blackmer 1996, Boggs 2003, Christensen 2004, Haboudane 2004, Oppelt 2000, Strachan 2002]
	Investigation of effects of pesticide applications on target and non-target species [Farone 1993, Henry 2004]
	Crop productivity and yield prediction [Fourty 1996, Gat 2000]
	Soil properties mapping (soil salinisation, soil crusting, organic material content, iron oxide content, texture, soil moisture, clay content and species) [Baumgardner 1985, Ben-Dor 1998a, Dehaan 2002, Dehaan 2003, Howari 2000, Ingleby 2000, Irons 1989, Metternicht 2003, Nagler 2000, Whiting 1999, Whiting 2001, Whiting 2003]
	Invasive species and weed detection and mapping [Borregaard 2000, Goel 2003a, Goel 2003b, Lass 2002, Smith 2003b]
Precision agriculture (weed selective spraying, selective fertilization, selective irrigation) [Feyaerts 1999, Gat 1999b, Staenz 1998a, Udelhoven 2000]	
Forestry and Ecology [Ustin 2004, Köhl 2001, Curran 2000]	Vegetation species detection and mapping [Clark 1995b, Curran 2000, Goodenough 2003, Martin 1996, Ustin 2004]
	Forest damage and vegetation stress mapping [Atzberger 1998, Banninger 1994, Carter 1994, Clark 1995b, Curtiss 1991, Howard 1971, Hoque 1992, Jackson 1986, Rock 1990, Singhroy 2000b]
	Succession monitoring [Qiu 1998, Sabol 1996]
	Vegetation senescence and dry plant materials mapping [Ben-Dor 1997b, Elvidge 1990a, Ustin 2004]
	Forest biochemistry mapping (chlorophyll content, metal stress, water content/stress, weed infestation) [Asner 2001b, Curran 2000, Martin 1993, Ustin 2004, Zarco-Tejada 2001b]
	Vegetation – substrate investigations [Howard 1971, van de Ven 2000]

Limnology and Oceanography [Dekker 2001, Mueksch 1998]	Water constituents mapping (chlorophyll, yellow substance, nonchlorophyllus particles, turbidity) [Fraser 1998, Jiang 1998, Kallio 2003, Lee 1999, Melack 2001, Olbert 2000]
	Characterization of acidic residual mining lakes [Boine 1999a, Boine 1999b]
	Bathymetry [Bagheri 1998, Dierssen 2003, Holyer 1996, Kappus 1998, Roberts 1999a, Sandidge 1998]
	Submerged vegetation recognition and mapping [Albertonza 1999b, Armstrong 1993, Williams 2002b]
	Plankton mapping (phytoplankton) [Lee 2004c, Melack 1992, Oliver 2004, Richardson 1999, Richardson 2000, Tester 1998]
	Coral species mapping and coral health / mortality mapping [Andrefouet 2003a, Clark 2000, Hochberg 2003, Holden 1999, Mumby 2004]
	Water quality mapping / contamination monitoring (oil spills) [Flanders 1997, Hamilton 1992, Kallio 2001, Keller 2001b, Salem 2002, Shafique 2002]
Urban Geography [Ben-Dor 2001a]	Urban land cover mapping / classification [Chen 2001, Rössner 1998, Rössner 2001, Segl 2000]
	Urban environment assessment [Ben-Dor 2001a, Rössner 2000]
	Monitoring of urban encroachment [Zhang 1998a]
Environmental Engineering	Contamination mapping [McCubbin 1999, Cloutis 1989, King 1989, Cloutis 1994, Hörig 2004, Finston 2000, Kühn 2004, Cloutis 1995, Sanchez 2003]
	Detection of illegal waste dumps [Notarnicola 2004]
	Soil contamination mapping (vegetation stress indicator) [Kooistra 2003, Lehmann 1990, Wilson 2004]
	Analysis of lignite mining overburden dumps [Kaufmann 1998, Krüger 1998, Müller 1996, Olbert 1999, Reinhäkel 1998b]
	Release of acidic mine drainage and mobilization of heavy metals from ore mining overburden dumps [Hauff 1999a, Hauff 1999b, Hauff 2000, Kruse 1996b, Levesque 1997c, Levesque 2000, Livo 1998, Mars 2003, Ong 2002, Shang 1999b, Swayze 1996, Swayze 1998a, Swayze 2000]
Atmospheric Sciences	Gas plume detection [Gallagher 2003c, Griffin 2000a, Hinnrichs 1999, Lane 1999, Marion 2004, Miller 2004, Thomas 2002]
	Atmospheric gas distribution mapping [Ben-Dor 1996, Green 1993g, Laan 2000]
	Cloud identification and thickness determination [Adler-Golden 1999a, Berendes 1991, Knap 2000, Kuo 1990]
Planetary Sciences	Compositional analysis of planets and stars using spaceborne and terrestrial imaging spectrometers connected to telescopes [Bell 1999, Christensen 2003]
Non-Remote Sensing Imaging Spectrometry Applications	Food analysis (fruit ripeness, major constituents) [Peirs 2003, Polder 2002, Tsuta 2004]
	Geologic exploration (mineral mapping in drill cores) [Kruse 1996a]
	Forensic Sciences (on-site trace characterization) [Drollette 2000b, Malkoff 2000]
	Pathology (histological examinations, tumor characterization) [Papadakis 2003, Tsurui 1999]
	Human medicine (cytological and histological examinations, identification of bacteria) [Goodacre 1998, Rothmann 1999, Shah 2003, Sowa 2002, Wennberg 1999]
	Veterinary medicine (chicken skin tumor detection, heart disease characterization) [Chao 2001, Chao 2002]
	Quality assurance in industry (ceramics, plastics, etc.) [Kulcke 2003]
	Concrete analysis [ASD 2002b]
	Food safety (apple diseases, fecal bacteria on surfaces) [Kim 2002b, Lawrence 2003c, Lu 2003, Park 2003]

4.2 – Environmental applications

This section aims to review previous work carried out in the field of detection and mapping of anthropogenic contaminations of environmental media using imaging spectrometry. This section provides an assessment of the possibilities and restrictions involved in using imaging spectrometry for environmental applications. Both direct and indirect detection of small contaminant concentrations, or contamination indicators in dominating matrices such as soil and vegetation cover, will be considered along with the detection of anthropogenic deposits (waste dumps, overburden dumps, and mine tailings).

In some cases, there is no clear dividing line between environmental applications and other application fields. Therefore, some of the “contamination” examples described below could also be assigned to other fields of application. For example, soil salinisation is a typical problem that occurs through improper irrigation and high evaporation rates. It is, therefore, primarily associated with the field of agricultural applications and soil science. However, other anthropogenic impacts, such as the production of mixtures of light crude oil and water from oil wells in Azerbaijan and their spillage into the surrounding environment, might also result in highly salinized soils. Another example is heavy metal stress found in vegetation. This can originate from both geogenic and anthropogenic sources. In the first case, the detection and mapping of metal-induced vegetation stress might well be associated with geologic (mineral mapping) or ecologic applications. In the latter case, it can clearly be associated with the detection and mapping of contaminated sites of anthropogenic origin. All environment-specific fields of application reviewed below have in common that they are related to the investigation, characterization, assessment, and monitoring of adverse impacts of anthropogenic origin on the environmental media soil and water. The adverse impacts considered in this review are limited to the deposition of both organic and inorganic substances of anthropogenic origin (wastes), the redeposition of natural materials due to mining activities (overburden dumps, mine tailings) and subsequent adverse chemical reactions, and the effects of soil contaminations on its vegetation cover. Other adverse anthropogenic impacts such as soil compaction and soil erosion will not be considered.

The focus of this review revolves around the direct and indirect detection, by means of remote sensing imaging spectrometry, of soils that have been contaminated with fuel hydrocarbons. Because only very few studies have been carried out in this particular field, the review also includes the detection of natural hydrocarbon seepages (so called microseeps and macroseeps) as they are in some aspects related to soil hydrocarbon contaminations of anthropogenic origin.

Fuel hydrocarbon soil contaminations

The first basic investigations on the potential of remote sensing for the detection and mapping of terrestrial and extraterrestrial hydrocarbons in the 0.35 μm to 2.6 μm wavelength region were carried out in the late 1980s [Cloutis 1989]. With the purpose of investigating the planets and their moons for hydrocarbon occurrences and aiming to explore and investigate tar containing sands, specific absorption bands of hydrocarbons were investigated acquiring laboratory and field spectra. While considering the fundamental bands known in the infrared wavelength region (2.5 μm – 20 μm) and their combination bands and overtones, it was concluded that the most promising absorption features occur near 1.7 μm and between 2.2 μm and 2.6 μm wavelength. Laboratory reflectance spectra of Athabasca (Canada) tar containing sands were acquired consisting largely of quartz containing sands, clay minerals, water and containing bitumen in concentrations of 0 to 15 % by weight. The results showed that for low-bitumen samples (0 – 5 %), absorption features characteristic for hydrocarbons are barely detectable. These spectra were found to be dominated by soil (clay) and water absorption features, in particular around 1.4 μm and 1.9 μm . Spectra acquired for the medium-bitumen samples (5 – 10 %) were found to be richer in detail and to exhibit significant hydrocarbon absorption features around 1.7 μm and 2.3 μm . Also, the 2.2 μm to 2.6 μm wavelength region exhibited a positive slope in the medium-bitumen samples in contrast to a negative slope observed for low-bitumen samples. In addition, the depth of the 1.9 μm water absorption band was found to be considerably reduced in comparison to low-bitumen samples. High-bitumen sample spectra (10 – 15 %) were found to be dominated by intense bitumen absorption features (hydrocarbon, C-H stretch overtone), in particular around 1.7 μm and 2.3 μm . The positive slope in the 2.3 μm to 2.6 μm wavelength region was more intense than for the medium-bitumen samples. Soil (clay) and water absorption bands were virtually absent in these spectra. It was also found that for the samples investigated, no simple correlation between spectral albedo (overall reflectance intensity) and major phase abundances could be established. Comparing clay and hydrocarbon absorption features it was found that both exhibit absorption features around 2.3 μm but that clays generally show a negative slope in the 2.3 μm to 2.6 μm region while hydrocarbons generally exhibit a positive slope in this region. The 1.7 μm absorption features was only found when hydrocarbons were present in the sample, independent of the clay and quartz content [Cloutis 1989]. Later investigations confirmed that the overall reflectance of oil containing sands decreases with bitumen content and thus darker sample colors in the visible wavelength range [Cloutis 1995]. Similar results were obtained in another study on the spectral responses of mixtures of montmorillonite, a clay mineral, and high quantities of different organics, including super unleaded fuel, benzene, toluene and trichloroethylene in the 0.8 μm to 3.0 μm wavelength region. Hydrocarbon absorption features around 1.7 μm and 2.3 μm were found to be most pronounced in spectra of hydrocarbon contaminated soils. While the spectra of montmorillonite contaminated with super unleaded fuel, benzene and toluene were found to be similar

except for small differences in the hydrocarbon absorption features, trichloroethylene exhibited extended and strong absorption bands around 1.7 μm and 2.3 μm plus a major absorption feature around 2.4 μm and a minor absorption features around 1.2 μm [King 1989].

Later investigations, mainly aimed at the spectral analysis of extraterrestrial bodies, included other materials containing carbon and hydrocarbons. Pure powdered carbon samples including natural and synthetic graphite and synthetic carbon black were found to exhibit no characteristic narrowband absorption features. Instead, all samples showed overall concave shaped spectra with an overall positive slope in the 0.3 μm to 2.5 μm region. The maximum reflectance of dark samples such as graphite and carbon black was found to be low with 10 – 14 % and less than 1 %, respectively. Spectral behavior similar to that of graphite (with different shapes in the visible range) was found for oil shale and coal tar extract. Coal was found to show a behavior similar to that of graphite with minor absorption features in the 2.3 μm region. Only dark oil containing sands were found to exhibit distinct C-H stretch overtones characteristic for hydrocarbons at around 1.7 μm and 2.3 μm . Accordingly, it was concluded that the carbon-hydrogen ratio (or the coalification) governs the occurrence and intensity of C-H stretch overtones [Cloutis 1994].

A study conducted in 1998 and published in 2001 investigated the detectability of hydrocarbons using HyMap imaging spectrometry data. Several material samples covering areas between one and 48 square meters, among others bitumen roofing felt, plastic tarpaulins and two oil-contaminated sand targets of 4 \times 4 m classified “highly oil-contaminated” (containing circa 80 g/kg = 80,000 mg/kg lubricating oil/sand or 8 wt.%) and “slightly oil-contaminated” (containing circa 20 g/kg = 20,000 mg/kg of lubricating oil/sand or 2 wt.%) were laid out and mapped by the HyMap instrument in 128 bands covering the 0.44 μm – 2.54 μm wavelength range with a spatial resolution of approximately 2.3 meters. The study confirmed the absorption features near 1.73 μm and 2.31 μm described earlier for bitumen (tar and oil sand samples), with the 2.31 μm feature being more pronounced. When it came to distinguishing oil contaminated soil and rock from plastics in imaging spectrometry data it was found that the 1.73 μm absorption feature is more pronounced for plastics samples than for oil contaminated soil and rock samples. The authors also described the use of a common method to visualize absorption features of hydrocarbons by placing the three display color bands (RGB – red, green, blue) such that the green display band is placed in the center of the 1.73 μm absorption feature and both the red and the blue display bands on the shoulder of the absorption feature. Thus, all surface materials bearing considerable portions of hydrocarbon materials (spectra representing hydrocarbon-bearing materials) were displayed in pinkish to reddish color. Rather than using atmospherically corrected relative reflectance data, the authors applied this method successfully to uncorrected radiance data (raw output data from the HyMap imaging spectrometer) [Hörig 2001]. The same authors propose a hydrocarbon index (HI) based on their findings that the 1.73 μm absorption feature is a specific characteristic for hydrocarbon-bearing materials.

Based on continuum removal for the 1.73 μm hydrocarbon absorption feature, the hydrocarbon index basically describes the depth of the absorption feature at its local minimum. If hydrocarbon materials are represented in the spectrum, the index value is generally higher than zero. If no hydrocarbon materials are represented in the spectrum, the index is generally expected to equal zero or to yield negative values because the absorption feature was found to be characteristic for hydrocarbons. Applying the index to an imaging spectrometry dataset and displaying the index as a grayscale image with brightness increasing with HI value will display hydrocarbon-bearing materials as brighter pixels. The output image provided does not allow for differentiation between different hydrocarbon materials and serves only as an occurrence map including all kinds of hydrocarbon bearing materials such as fuel hydrocarbon contaminated soil, plastics, asphalt roads, bitumen roofing felt, artificial turf, and paint. The proposed hydrocarbon index can be applied to both radiance and reflectance data. However, the authors observed that HI images appear often noisy for areas covered by vegetation while HI images for urban areas and bare ground can be used to accurately detect hydrocarbon-bearing materials. The index is illustrated in figure 4-1 and given in the below equation [Kühn 2004].

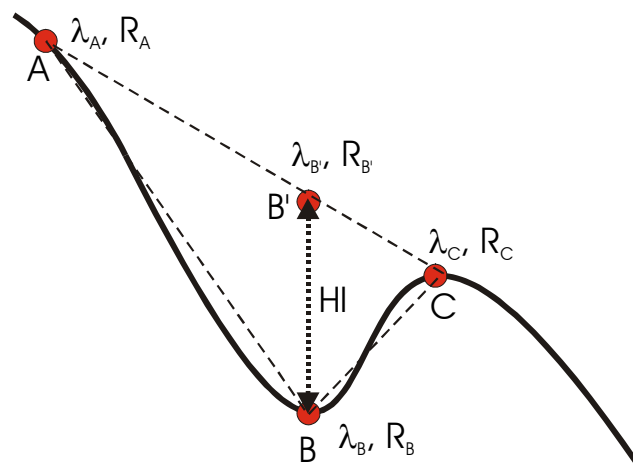


Figure 4-1: Concept of the hydrocarbon index (HI) [after Kühn 2004]

$$\text{Hydrocarbon Index (HI)} = \frac{(\lambda_B - \lambda_A)}{(\lambda_C - \lambda_A)} \times (R_C - R_A) + R_A - R_B \approx \frac{2}{3} \times (R_C - R_A) + R_A - R_B$$

where

$\lambda_A, \lambda_B, \lambda_C$ – Band position [nm]

R_A, R_B, R_C – Reflectance or radiance value at this wavelength

Several publications dated 2000 and 2001 report the investigation of imaging spectrometry as a tool for environmental applications such as the detection of oil-impacted soils, the monitoring of pipeline spills, and hydrocarbon exploration by detecting natural hydrocarbon seeps from crude oil deposits (resulting in crude oil “contaminated” soil or rock) for hydrocarbon exploration by commercial service providers associated with the oil industry. The studies included both instruments in the 0.3 μm – 2.5 μm wavelength region and the 3 μm – 5 μm thermal infrared wavelength region. One study stated that asphalts and plastics exhibit absorption features similar to those observed in natural hydrocarbons which might cause false positives in interpretation results. These materials, therefore, need to be eliminated in data interpretation. Furthermore, it was observed that calcite and dolomite exhibit a pronounced absorption feature in the 2.3 μm wavelength region that is, however, different in shape from the hydrocarbon absorption features occurring at approximately the same wavelength [Finston 2000, Taylor 2000, Ellis 2001].

To date, only few studies have addressed the indirect detection of hydrocarbon soil contaminations through vegetation stress response mapping. Historically, the detection of non-specific vegetation stress by remote means goes back to the advent of false color near infrared aerial photography and multispectral sensor systems; and was often based on reflectance ratios between the red and near infrared wavelength bands. More recent studies have been focusing on the detection of vegetation stress and the determination of its source by means of the affected vegetation spectra. While some success has been made with respect to the source-specific detection of nutrient and water stress in agricultural stands and heavy metal stress in forest stands, no results have been reported concerning the source-specific detection of vegetation stress with respect to organic or inorganic contaminants.

Vegetation stress in natural and agricultural stands or forests can be induced by a large number of agents, among others adverse climatic conditions, nutrient deficiency, water deficiency or surplus, weed infestation, pest infestation, soil salinisation, soil acidification, high carbon dioxide concentrations in soil vapor, and contamination with heavy metals or organics [Lerner 1999b, Martini 2000, Brunold 1996]. Even though agricultural stands are relatively homogeneous over larger areas (single species in similar phenological state), natural vegetation stands tend to be more diversified (multiple species of different phenological states). For this reason one must question whether a source-specific detection of vegetation stress using imaging spectrometry data is feasible or to what extent a priori knowledge about occurring stress agents is necessary [Martini 2000].

Investigations showed that both common organic and inorganic soil contaminants are stress agents for many species of plants [Wilson 2004, Folkard 1998, Martini 2000]. However, it was also acknowledged that some species are insensitive to certain stress agents. Nevertheless, there are examples of positive application of imaging spectrometry in the detection of contaminations. One study reported the successful detection of pipeline leakages by vegetation stress mapping along a known fuel hydrocarbon pipeline using imaging spectrometry data [Taylor 2000]. Another study

indicated that stress-agent specific detection and mapping of vegetation stress with respect to organic contaminants, inorganic contaminants and nutrients might be possible, though requiring highly complex research. The study focused on the detection of vegetation stress induced by landfill leachates in vegetation surrounding the landfills [Folkard 1998].

Because the literature survey on spectroscopic analysis and detection of fuel hydrocarbons through imaging spectrometry did not return many results, the survey was extended to the exploration of natural hydrocarbon resources by imaging spectrometry. From petroleum geology it is known that many natural hydrocarbon reservoirs exhibit surface expressions. These surface expressions are referred to as macroseeps and microseeps. Macroseepage is the visible presence of fuel hydrocarbons at the surface due to the upward vertical migration of fuel hydrocarbons [van der Meer 2001d]. Macroseeps have been observed on land and at sea in many regions worldwide, among others in Azerbaijan [Zeinalov 2000]. Macroseeps are similar to soil contaminations by fuel hydrocarbons; hence they have been included in the above section. Microseeps, however, are different. Microseepages can be described as a near-vertical, long-term, continuous leakage of small quantities of typically light hydrocarbons from their underground deposits to the surface. Microseeps are associated with geochemically induced alterations of surface and near-surface mineralogy, some of which are listed below [Schumacher 1996, Saunders 1999]:

- Formation of “paraffin dirt” as a product of microbial oxidation of hydrocarbons
- Mineralogical changes such as the formation of calcite, pyrite, elemental sulfur, iron oxides and iron sulfides
- Clay mineral alterations (alteration of illite to kaolinite)
- Biogeochemical and geobotanical anomalies

The formation of “paraffin dirt” as a product of microbial oxidation of hydrocarbons in soils is typically observed in humid to temperate climates where these yellow-brown waxy appearing soils containing large quantities of dead cell walls can be observed at the surface [Schumacher 1996]. “Paraffin dirt” soils can therefore be expected to exhibit absorption features similar to those of soil contaminated with hydrocarbons. Microbial degradation of light hydrocarbons percolating through soils consumes either free or chemically bound oxygen (sulphates, nitrates). Depending on the local conditions, “paraffin dirt” can be produced in both aerobic and anaerobic conditions, in any case altering geochemical conditions towards more reducing conditions.

As a by-product of hydrocarbon oxidation and its changes to the surrounding mineralogical environment (release of carbon dioxide → reaction of carbon dioxide with water to form hydronium ions → dissolution of subsurface calcite or gypsum → release of calcium ions), diagenetic carbonates (calcite CaCO_3 , siderite FeCO_3) are

formed near and at the surface. Other reaction products associated with geochemical processes at hydrocarbon microseepages include pyrite, elemental sulfur, uraninite, and iron sulfides [Klusman 1992, Schumacher 1996, Saunders 1999]. According to recent studies, these mineralogical anomalies can be detected by means of imaging spectrometry if exhibited at the surface [van der Meer 2000d, Yang 1999b, Yang 2000b, van der Meer 2002a].

The release of light hydrocarbons has also been observed to result in geobotanical anomalies at the location of hydrocarbon microseeps. The microbial degradation of light hydrocarbons in the soil matrix decreases soil oxygen concentration while significantly increasing the concentration of carbon dioxide and organic acids. Increased acidity results in the mobilization of some trace elements and metals, thus increasing their availability to plants while reducing the availability of alkaline (earth) elements such as potassium, calcium, strontium and barium [Bammel 1994, Saunders 1999, Schumacher 1996]. In investigations focusing on the spectral response of plant species and communities at the sites of hydrocarbon microseepages, observations showed vegetation stress expressing itself in a shift of the so called red edge (the edge observed in spectra between 0.7 μm to 0.8 μm wavelength between the absorption minimum in the red and the maximum in the near infrared) and an overall decrease of reflectance in stressed vegetation. In all studies, vegetation stress was attributed to inorganic stress agents that resulted from geochemical changes induced by the seeping hydrocarbons. Stress-agent specific spectral responses or significant correlations between vegetation stress and the occurrence or absence of hydrocarbons in the soil matrix were not found. Furthermore, other factors such as soil-moisture were found to have generally a more pronounced effect on vegetation stress than the presence of hydrocarbons [Bammel 1994, Yang 1999b, Yang 1999c, van der Meer 2002a, Klusman 1992, Cwick 1995]

In summary, it must be stated that most effects described for hydrocarbon microseepages are uncommon at sites with anthropogenic hydrocarbon contaminations. Both the formation of “paraffin wax” and altered mineralogy require long-term exposure to hydrocarbons on a scale of centuries to millennia. However, changes in soil geochemistry, expressed as vegetation stress, can be expected at the sites of hydrocarbon spills, since these processes occur on a scale of months to years. The stress expressions depend on the contaminant’s biodegradability, the availability of electron donors, nutrients for the microorganisms involved, and other environmental parameters such as moisture and temperature.

Heavy metal soil contaminations

Heavy metals (e.g., Pb, Cu, Ni, Zn, Cr, Cd, Co, Mo, As, Hg) as soil contaminants typically occur in concentrations well below 1 % (10,000 mg/kg dry soil). Depending on soil geochemical conditions (pH, pE) and the presence of inorganic anions such as sulphate, carbonate, nitrate, etc., heavy metals tend to form different types of soluble cations and anions with more or less soluble carbonates, hydroxides, oxides,

chlorides and sulfides. Furthermore, as discussed above (section 3), inorganics in general do not exhibit characteristic absorption features in the 0.3 μm to 2.5 μm wavelength region. For these reasons it is considered impossible to directly detect general inorganic soil contaminants, in particular heavy metals, by means of imaging spectrometry. Therefore, most studies have focused on the detection of vegetation stress caused by increased heavy metal concentrations in the soil. Some studies also have addressed the mapping of certain clay minerals or mud that had been known to correlate with heavy metal concentrations.

Vegetation stress caused by heavy metal toxicity can have different expressions, depending on the heavy metal type, its concentration and the sensitivity of the species affected. Effects typically observed include physiological, morphological and ecological changes such as chlorosis (reduced production of chlorophyll and hence reduced photosynthetic activity), leaf wilting, needle retention, decrease in branch density, defoliation, growth inhibition, flowering and fruiting changes, dwarf growth and gigantism, changes in plant species distribution and the establishment of adapted species, and the dying-off of whole plants or communities. In some cases, whole areas might stay void of vegetation due to highly toxic concentrations of heavy metals¹ [Press 1974, Jackson 1986, Curtiss 1991, Horler 1980]. However, as mentioned above, all these effects could also be observed resulting from other stress agents.

All studies on the spectral response of heavy metal stressed vegetation observed differences between the spectra of metal-stressed vegetation and unstressed controls. These effects usually included a blue-shift of the red edge of metal-stressed vegetation, increased reflectance in the 0.4 μm to 0.7 μm (signs of reduced photosynthetic activity due to chlorosis) and decreased reflectance in the 0.7 μm to 2.5 μm wavelength region [Curtiss 1991, Lehmann 1991, Yost 1971, Banninger 1990, Rothfuß 1994, Horler 1980, Howard 1971, Kooistra 2003, Schuerger 2003]. Vegetation stress symptoms that could be correlated specifically to heavy metal stress have not been reported. Some heavy metals considered as contaminants are also essential micronutrients to all vegetation species, in particular copper and zinc. Therefore, in some cases even positive effects in reflectance spectra could be observed where one of the elements under investigation obviously was a micronutrient with limited availability. Such effects included a red-shift of the red edge and decreased reflection in the visible wavelength region (indicating increased photosynthetic activity) [Horler 1980].

Several studies have addressed the detection of heavy metal stress in plants and have reported successful applications of imaging spectrometry to perform this task. However, no instance has reported metal-stressed vegetation being specifically detected without a priori knowledge of the occurrence of metal stress in the particular

¹ The latter was utilized for mineral exploration by means of remote sensing as early as the 1930s, when large parts of the “Copperbelt” region in Rhodesia and Katanga (today’s Zimbabwe and SE Congo) were mapped with panchromatic photography in the search for vegetation clearings resulting from metal toxicity associated with large copper deposits [Press 1974].

area of investigation. However, stressed vegetation was always distinguishable as “anomalous vegetation” from unstressed background vegetation, and usually other stress agents such as nutrient deficiency, water deficiency or pest infestation could be ruled out using additional information. Thus, for known locations of metal-induced stress, the spatial distribution and extent can usually be mapped using imaging spectrometry data.

Although metals, in particular at low concentrations, do not have detectable absorption features, another study proposes a direct mapping of heavy metal concentrations based on direct correlations between heavy metal concentrations and organic material and clay content of bare soils in river floodplains. Earlier investigations have shown that the clay content and the content of organic material can be determined through the interpretation of imaging spectrometry data. The method has been applied toward predicting elevated metal concentrations in floodplains along the river Waal in the Netherlands. However, the method requires a certain number of reference samples from the area under investigation in order to correlate metal concentrations with organic material and clay content in soils. This must be accomplished before quantitative predictions and spatial distributions can be mapped by means of imaging spectrometry [Kooistra 2000]. A similar approach was applied following the mining accident that endangered the Doñana National Park in Spain, in which large wetland areas upstream of the national park were covered with sludge containing high concentrations of heavy metals and cyanides. Here, residual sludge was mapped in order to predict heavy metal concentrations. Using chemical analysis of the sludge and imaging spectrometry to map sludge occurrence, mapping showed areas of remaining heavy metal contaminations after major clean-up operations [Kemper 2000].

Soil salinisation

Soil salinisation mainly occurs in arid and semi-arid regions and can have natural (e.g., evaporation of near-surface groundwater) or anthropogenic causes (improper irrigation, discharge of salt water onto soil). Usually, soil salinisation expresses itself as mineral crystallizations (salts) on soil, with the most important mineral types being chlorides, sulfates and carbonates [Baumgardner 1985, Metternicht 2003].

Pure salt spectra (e.g., halite / sodium chloride, potassium chloride) are usually featureless, while other salt spectra (sulfates, carbonates) exhibit minor absorption features. The spectral signature of a saline soil however, can be a result of the salt itself (salt crystals), or indirectly from other chromophores related to the presence of the salt (e.g., organic matter). It can also be a result of masking of other absorption features (e.g., masking of ferric ion absorption features in the visible wavelength region) or changes in surface roughness of soils due to soil crystallization [Ben-Dor 1998a, Metternicht 2003]. Soil salinity expressing itself in salt crystals typically increases the overall reflectance (albedo) of the affected soil in comparison to non-salinized soil of similar composition. Comparing reflectance over wavelength

regions or for single bands with respect to brightness can be used to characterize soil salinisation [Ben-Dor 1998a, Baumgardner 1985, Metternicht 2003, Whiting 1999]. However, some studies also report a contrary behavior with decreasing reflectance as an indicator of soil salinisation, obviously due to salinisation of high reflectance soils where the salt crystals lead to increased diffuse scattering and decreased reflectance [Dehaan 2002, Zhou 2003]. Other studies conclude that dominant salt crystallization on soils (halite, calcium carbonate, gypsum, sodium bicarbonate) and highly saline soils can be identified and distinguished to some extent although salts have only minor absorption features (in particular around 1.78 μm and 2.2 μm) and although non-linear mixture processes were observed when several different salt species were involved [Howari 2000, Dehaan 2002, Dehaan 2003].

Vegetation affected by salt shows stress symptoms similar to those induced by heavy metals. Hence, the above mentioned considerations for the remote sensing imaging spectrometry detection of heavy metal-induced stress are also valid for the detection of salt-induced vegetation stress. In addition, the use of halophytic vegetation species as indicators for soil salinisation has been proposed [Lauten 1992, Dehaan 2002, Dehaan 2003].

Mine tailing characterization (ore mining)

The application of imaging spectrometry to the characterization of mine tailings from ore mining was one of the first environmental engineering applications of imaging spectrometry. As will be outlined below the characterization of mine tailings is based on mineral and geologic mapping of dominating minerals in non-vegetated areas, which is the origination of imaging spectrometry. Analysis is conducted with respect to the mineralogy and associated concentrations of inorganic contaminants found in mine tailings and their oxidation state, the formation of acidic mine drainage, and the distribution of fluvially distributed mine tailing sediments.

The most common metal ores of elements like iron, lead, copper, zinc, nickel, lead, chromium, uranium, and others are sulfides and oxides, and, to a lesser extent, carbonates. Due to natural concentration processes, ores usually do not occur as single elements or mineral species but are associated with other metals and minerals. Ore mining usually yields small quantities of target ore encapsulated in large quantities of non-target minerals and rock (spoil). Although the “spoil” fraction, usually generated when accessing ore veins, is usually dumped on spoil dumps at the surface, the fraction containing the target ore is typically processed on-site to concentrate the ore and thus reduce transportation costs. There are several ways ores may be treated in order to separate them from spoil rock, such as flotation by means of surfactant agents or by water and pressurized air processing to separate fine-pulverized ore from non-target residues. Cyanidation of pulverized raw ore with sodium cyanide is also used to dissolve target elements like metal-cyanide complexes for precipitation with non-noble metals like zinc. Leaching of pulverized raw ore with sulphuric acid is another way to dissolve target elements like metal sulphate for

electrolytic separation. Finally, liquifaction refining conducted by heating the ores to above the melting point of the target separates it from the non-target rock that remains solid [Mortimer 1987, King 2000b]. Depending on the ore treatment process applied, large quantities of wastes are generated, including smelter slags, highly acidic wastewater, sludge containing cyanides or organic surfactants, and fine pulverized tailings. Typically, these wastes are stored on-site, forming huge mine tailings, spoil and smelter slag deposits, and sludge landfills. In the past, acidic wastewaters from ore leaching were typically discharged into streams and rivers. The wastes generated by ore treatment usually contain large quantities of sulfide minerals (e.g., pyrite) and non-target heavy metals that are associated with every type of target ore plus agents used for ore processing, including sulfuric acid, cyanide, mercury and surfactants. Deposited at the surface and exposed to water and oxygen, sulfide minerals are oxidized to form sulfuric acid. This process is usually enhanced by microbiological processes also referred to as bioleaching. Thus, leaching processes continue in spoil deposits and mine tailings, generating acidic mine drainage that contains high concentrations of heavy metals that are released at increased rates relative to unmined areas with lower exposure of sulfide minerals sensitive to these processes. All processes and wastes described above, whether natural or man-made, include alterations of minerals and the deposition of minerals typically only occurring in the subsurface. In addition mine tailings, spoil and slag deposits usually remain void of vegetation unless recultivated. This is due to their high acidity, high concentrations of heavy metals, low water retention and virtually no substrate suitable for plant colonization [Mortimer 1987, King 2000b]. Common countermeasures to prevent the formation of acidic drainage and the release of heavy metals in mine tailings and spoil dumps include the application of limestone or recultivation including the construction of a surface sealing [Levesque 1997c]. The fact that mine tailings and other affected areas are typically free of vegetation and their limited water retention capacity holds little moisture, makes them highly suitable for remote sensing investigations and particularly the application of imaging spectrometry. This is because endmember spectra mainly comprise minerals and only few mixed pixel spectra are expected to occur in these types of areas.

As for heavy metal soil contaminations, imaging spectrometers can not directly map heavy metals or acidity. Imaging spectrometry can, however, be applied to map surface mineralogy and minerals that are found at the surface as a result of ore treatment and weathering, oxidation, other alteration processes, and countermeasures such as the distribution of limestone on deposits [Levesque 1997c, Kruse 1996b].

Several studies have demonstrated the ability of imaging spectrometry data to detect and map mine tailings based on the known presence of characteristic primary minerals or secondary alteration minerals (e.g., illite as an alteration product of muscovite at the location of a lead and zinc mine; dolomite, limestone and phosphoritic mudstone at the location of a phosphorite mine) [Hauff 1999b, Mars 2003]. The potential of imaging spectrometry to map acidic mine drainage based on the formation and precipitation of different secondary iron-bearing minerals has been

demonstrated in other investigations. This approach utilizes the fact that acidic mine drainage is continually neutralized as it drains away from its point of origin, depositing different secondary iron-bearing minerals whose type is controlled by pH, degree of oxidation, moisture content, and solution composition. Among others, the iron mineral of interest for this application are jarosite, schwertmannite, ferrihydrite, goethite, and haematite. The reflectance spectra of each of these and other iron-bearing secondary minerals have been shown to be characteristic. Mapping their abundance around mine tailings and along river valleys into which acidic mine drainage has been discharged can therefore be used to derive information on correlated geochemical parameters [Swayze 1996, Farrand 1997a, Farrand 1997b, Farrand 1995, Shang 1999a, Shang 1999b, Cudahy 2000, Hauff 2000, Swayze 2000]. Further correlating heavy metal concentrations and mobility from laboratory analyses with the occurrence of these iron minerals has been used to map heavy metal concentrations and mobility [Fenstermaker 1994, Hauff 1999b]. Correlating the occurrence of secondary iron-bearing minerals to the pH value range in which they occur can be used to indirectly map soil surface pH [Ong 2002]. Similar to the approach of mapping heavy metal-contaminated soil through vegetation stress mapping in imaging spectrometry data, areas affected by heavy metals released from mine tailings or mine wastewater discharge have been mapped using vegetation stress as an indicator [Mars 2003].

Similarly, the spread of other minerals from mining areas and the buffering potential of sediments and rocks occurring naturally in its surroundings (e.g., dolomite, calcite) can be mapped to assess environmental impacts of mining activities [Livo 1998].

Overburden dump and residual lake characterization (surface lignite mining)

Surface mining for lignite is common in Germany with the Lusatian lignite mining district, the Central German lignite mining district and the Rhine lignite mining district being the major mining regions. In the Lusatian and Central German mining districts, extensive surface mining for lignite during the time of the former German Democratic Republic has left a legacy of more than 440 square kilometers (as of 1995) of devastated land, which has not been recultivated [Wittig 1998, Vogler 1995]. As described above for mine tailings, oxidation of pyrite from tertiary sediments and associated acidification of overburden pose severe problems with respect to the recultivation of these areas.

An investigation of the applicability of imaging spectrometry for the geochemical and mineralogical characterization of lignite mining overburden dumps has demonstrated that major constituents of overburden substrates such as clay minerals, quartz, organic carbon, and pyrite can be detected and quantitatively determined. The study was carried out using imaging spectrometry data of a 79-channel imaging spectrometer covering the visible through thermal infrared wavelength regions (DAIS 7915), field and laboratory spectral measurements and analyses of

representative soil samples of two overburden dumps in the Central German Lignite Mining District (Zwenkau, Espenhain). Based on reflectance spectra and specific absorption features, kaolinite and organic carbon occurring in a range between 0 – 15 wt.% and 0 – 60 wt.%, respectively, were mapped with an accuracy of 2 wt.%. Pyrite occurring in concentrations between 0 – 4 wt.% was determined with an accuracy of 0.8 wt.% [Kaufmann 1998, Krüger 1998]. Other parameters such as secondary iron-bearing minerals or the correlation of mineral abundance to geochemical parameters such as pH were not investigated.

Another study investigated the applicability of imaging spectrometry data for the investigation of residual mining lakes left behind by lignite surface mining. These lakes are typically characterized by low pH values, high concentrations of Fe(II) and low concentrations of phytoplankton, hence low chlorophyll concentrations. Results show that indicators of iron content, pH, and chlorophyll content can be derived from imaging spectrometry data in the 0.4 – 0.9 μm wavelength region. Highly acidic lakes containing high iron concentrations were shown to have a low reflectance maximum (< 5 % reflectance) near 0.65 μm , while near-neutral lakes with a low iron content exhibited a high reflectance (ca. 20 % reflectance) with a maximum near 0.6 μm [Boine 1999a, Boine 1999b].

Water contamination monitoring

While considerable research has addressed the application of imaging spectrometry to the characterization of water bodies (suspended matter content, phytoplankton concentration, submerged vegetation mapping and identification), only few studies to date have addressed the detection and monitoring of dynamic contamination processes and plumes in rivers, lakes, estuaries and at sea.

The detection and characterization of oil spills on water with respect to oil film thickness and oil type has been shown to be possible in a recent study. Water spectra in the 0.5 μm to 0.85 μm wavelength region generally have a low reflectance with a peak around 0.55 – 0.6 μm . Oil floating on water was found to result in a sharp absorption feature centered around 0.68 μm and associated with a second peak at around 0.71 μm [Salem 2002].

An earlier laboratory study investigated the reflectance spectra of several industrial liquid wastes and their effect on water spectra if discharged into natural waters. The study included liquid cannery wastes, milk wastes, municipal sewage, tannery wastes, sulphite liquor, and paper mill wastes. Spectra were acquired for a wavelength range of 0.2 μm to 1.2 μm . Significant differences between the waste spectra were found with respect to both absorption features and overall reflectance. Experiments with 0.5 %, 2.0 % and 8.0 % solutions of liquid paper mill wastes in natural water showed that even though the overall reflectance is low (< 12 %), the different concentrations could clearly be distinguished in reflectance spectra [Mishev 1986].

Another investigation addressed the characterization of an ocean wastewater plume (discharge of treated wastewater into the ocean) with respect to photosynthesis rates, suspended matter, and transport [Hamilton 1992].

Other Applications

Other applications of imaging spectrometry remote sensing for environmental engineering applications include the identification and mapping of asbestos concrete roof sheeting consisting of approximately 80 % concrete and 20 % asbestos fibers. Using relatively low spectral resolution data with 92 bands covering the 0.3 μm to 2.5 μm wavelength region, a classification accuracy of 92 % was obtained [Marino 2000]. Asbestos minerals such as chrysotile and amphibole exhibit characteristic absorption features around 2.3 – 2.4 μm .

Another application addressed the assessment and monitoring of iron ore dust (mainly consisting of iron oxides) that is covering mangrove vegetation near a loading dock for iron ores. Iron ore dust was found to reduce the overall reflectance of the vegetation affected. Utilizing a specific iron oxide absorption feature at around 0.9 μm and the decrease in reflectance in comparison with field sampling of iron dust loads on leaves, a correlation was established that allows for the determination and spatial distribution mapping of iron ore dust on mangrove vegetation in units of milligrams of iron dust per square centimeter of mangrove foliage [Ong 2003].

Summary, conclusions, and critique on recent applications

The above summary of recent applications of imaging spectrometry to environmental applications with respect to the detection, mapping and characterization of organic and inorganic contaminants in the environment shows that research and applications in this field are still limited. An exception is the investigation and characterization of (ore) mine tailings which is closely related to the origins of imaging spectrometry in the mapping of surface mineralogy in arid regions. However, reported research results indicate the potential that imaging spectrometry holds for direct and indirect mapping of numerous effects related to environmental pollution. Also, the limitations of imaging spectrometry with respect to the direct and specific determination of inorganic contaminants and vegetation stress agents have been shown. In any case, the objectives of an application must be considered carefully, and the potential of imaging spectrometry for the particular investigation must be assessed thoroughly by preliminary laboratory investigations prior to field applications.

As far as the detection of fuel hydrocarbons is concerned, it must be stated that until now, only high concentrations of fuel hydrocarbons ($\gg 2 - 5 \text{ wt.}\%$) in single soil and rock matrices have been investigated with respect to their detectability by means of imaging spectrometry with a focus on two major absorption features around 1,730 nm and 2,350 nm.

The following issues that are important for the detection and mapping of fuel hydrocarbon contaminations of soil have not yet been investigated:

- Distinction of fuel hydrocarbon classes by optical spectrometry in the 0.4 – 2.5 μm wavelength region
- Differentiation between classes of hydrocarbons, in particular the differentiation of plastics and fuel hydrocarbons in imaging spectrometry data
- Detection limits for different fuel hydrocarbons in a non-interfering matrix (pure silica sand)
- Detection limits for fuel hydrocarbons in different soil types (e.g., sands, clays, organic soils) with different moisture grades
- Characteristics of spectral mixing processes of fuel hydrocarbons, soils and soil moisture

Even though some experiments have already addressed the detection and mapping of pure liquid and solid fuel hydrocarbons and fuel hydrocarbon contaminations of soils by means of imaging spectrometry, no systematic approach has yet been made to the differentiation of different types of (fuel) hydrocarbons (chemical types, solids, liquids, natural hydrocarbons, plastics, refined hydrocarbons), their discrimination in different background matrices (different soil types and moisture levels) and detection limits in environmental media, in particular soil.

The objective of this study is to investigate the applicability of imaging spectrometry with respect to the detection and mapping of fuel hydrocarbon soil contaminations. General considerations of imaging spectrometry's application for contaminated site detection and investigation, the experimental approach to this problem, and the results obtained will be described in the next chapters.

5 – Applicability of imaging spectrometry for contaminated site detection and investigation

Fuel hydrocarbon contaminations of soil can be considered as a mixture of varying fractions of soil, water (soil moisture), fuel hydrocarbons, and sometimes other minor constituents such as salt. For the purpose of remote sensing and, in particular, the detection and investigation of soils contaminated by fuel hydrocarbon through imaging spectrometry, it is necessary to consider the composition and properties of the components of a fuel hydrocarbon contamination along with their interactions and macro- and microscopic distribution.

5.1 – Soils and soil spectral properties

Soils

Soils are highly differentiated. Depending on the parent rock's mineral composition and physico-chemical properties, on climatic conditions, local biocenosis and topography, soils may range from purely organic to purely mineral, from dry to moist soils and with different mineralogical composition and varying geochemical conditions. For pedological, agricultural and forestry purposes, soils are typically characterized by macroscopic properties describing their fertility and water capacity. The main parameters are the structure of its horizontal layers (horizons), layer color, layer texture, grain size distribution, visually identifiable components (e.g., iron concretions, organic material) and soil moisture. However, only the open surface of top soils is accessible to retrieve information on the soil by means of remote sensing investigation. Top (top) soil can be considered a mixture of different solid, mineral and organic constituents of varying grain size mixed with water in varying proportions.

The dominating primary minerals in most soils worldwide are quartz (amorphous SiO_2), feldspars (orthoclase, plagioclase), mica (muscovite, biotite), and dark minerals (e.g., augite, hornblende). Important secondary minerals formed as a product of weathering and pedogenesis from primary minerals include carbonates (calcite, dolomite), gypsum, iron oxides and hydroxides (hematite, goethite, gibbsite), and silicate clay minerals (e.g., kaolinite, illite, montmorillonite). In addition, oxides and hydroxides of other elements such as aluminum, manganese and titanium may occur. Depending on the state of pedogenesis, certain primary or secondary minerals might dominate in a soil or single horizons of a soil. Minor fractions of soils typically below 2 wt.% may also include heavy minerals, salts (e.g., chlorides, nitrates), and sulfides [Schachtschabel 1998, Miller 2001, Kuntze 1994, Bohn 2001].

Organic materials in soils and on soil surfaces may include more or less dry organic matter (dead plant material), itself consisting of lignin, cellulose, proteins, tannins, sugars, cuticular wax, and other plant constituents. These substances, together with biochemically altered plant material in various stages of decomposition, which often form highly complex organic molecules or complexes, usually make up the largest part of soil organic matter, also referred to as humus. Depending on the environmental conditions, mineral soils that make up about 98 % of the world's soils typically contain between 0.5 wt.% and 10 wt.% organic matter. Organic soils (e.g., peat) mainly contain organic material and only minor fractions of minerals [Schachtschabel 1998, Miller 2001, Kuntze 1994, Bohn 2001].

In geology and soil science, sediment soils are classified by their dominating grain size fraction and their grain size distribution. The major classes of sediments textures by grain size are, from coarse to fine: gravel, sand, silt, and clay, each representing a soil parent material and/or stage of pedogenesis. Each textural class can also be categorized into major mineral classes. Gravels, as the coarsest class (grain size > 2 mm) consists of fluviably transported and rounded pieces of different rocks, including plutonites such as granite, vulcanites such as basalt, sedimentary rocks such as shale or breccias and metamorphic rocks such as gneiss or dolomite. Gravels contain many different minerals, depending on their parent materials. Sand (grain size 0.05 – 2 mm) is typically a weathering product of gravel, containing small particles of pure minerals of its parent material. Most sands mainly consist of quartz (amorphous SiO₂) and contain smaller quantities of feldspars, mica, carbonate, and other minerals. Silt (grain size 0.002 – 0.05 mm) consists of even finer mineral particles with a composition similar to that of sand. Silt typically contains fine grained quartz, silica and carbonate minerals. Clay (grain size < 0.002 mm) consists of weathered silica minerals known as clay minerals such as kaolinite, illite, and montmorillonite. Mixtures of sand, silt and clay are referred to as loam, containing varying quantities of all single compounds (minerals) of the three major classes [Schachtschabel 1998, Kuntze 1994, Miller 2001]. The approximate composition of sands, silts and clays with respect to the main components quartz, primary silicates (e.g., feldspar, mica), secondary silicate minerals (clay minerals) and other secondary minerals (e.g., iron oxides, iron hydroxides, etc.) is illustrated in figure 5-1 [Irons 1989].

Surface soil color is mainly determined by the presence of iron, geochemical soil conditions (moisture, pH, Eh), and the iron oxides, hydroxides, or sulfides formed. Also, organic material can influence soil color considerably. Surface soil colors typically range from bright to dark, yellowish-white to shades and mixtures of brown, red, gray and black [Schachtschabel 1998, Sponagel 1994].

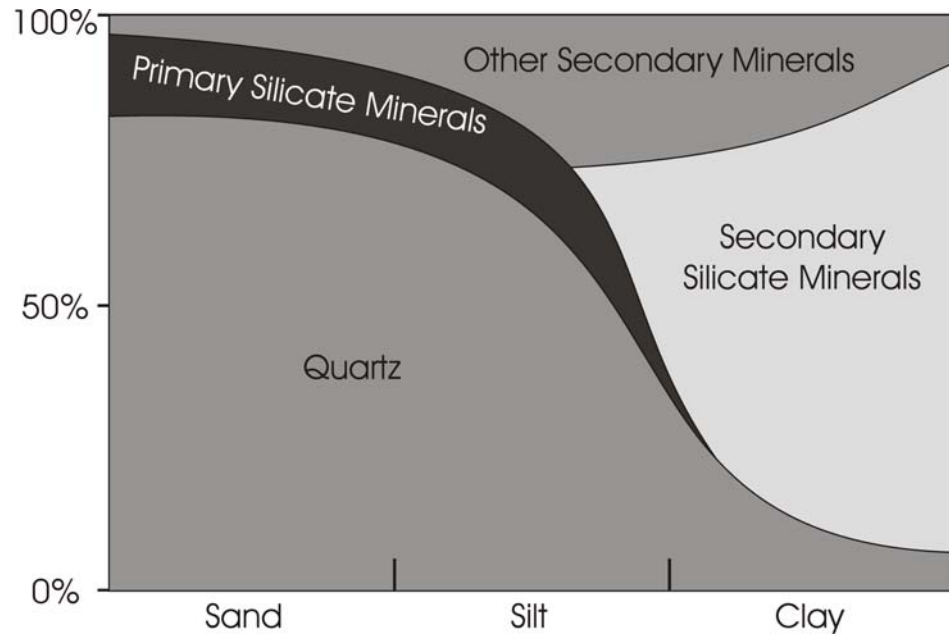


Figure 5-1: Composition of sand, silt and clay of quartz, primary and secondary silicate minerals, and other secondary (e.g., iron) minerals [after Irons 1989].

The surface exposed by soils often can not be considered to be representative for the properties of subsurface soil. Precipitation, soil encrustments, wind deposition, and the formation of salt crystalizations due to irrigation or discharge of salt water, form surface structures and encrustments that are different in composition from the subjacent and even near-surface soil layers.

Water (soil moisture)

Depending on the soil type and structure (sand, silt, clay, loam) as well as local climatic and topographic conditions, soils contain different quantities of water, also referred to as soil moisture. The water contents of soil typically ranges between slightly above zero for sands in arid regions to approximately 60 wt.% for clays and organic soil in temperate and humid climate regions. While the largest part of soil water (retained water) can be evaporated in higher temperatures, small quantities of water remain in the soil as crystal water, adsorbed onto grain surfaces and as capillary water [Scheffer 1998, Kuntze 1994]. Again, surface soil moisture does not usually represent the soil moisture of deeper soil horizons because the surface is directly exposed to precipitation, solar irradiation, diurnal temperature changes and wind. All these factors result in short-term alterations in soil moisture at the surface.

However, approaches have been made to correlate soil properties exhibited at the surface to subsurface soil properties, thus making them detectable by imaging spectrometry remote sensing.

Spectral properties of soils

All the above components, namely minerals (in particular iron oxides, carbonate and clay minerals), organic matter, surface structures (grain size), surface crusts (salt) and water (soil moisture) contribute to the reflectance spectra of soils. In this section, the spectral response of different soil types will be considered, taking into account different conditions and considerations of the spectral responses of single components, as well as soils as linear mixtures of certain components in the 0.4 μm to 2.5 μm wavelength region.

The interaction of electromagnetic radiation with a soil surface can be described as a multiple-scattering by different atoms, molecules, and crystals. The sum of all single radiation-matter interactions within the field of view of a given sensor is the reflectance spectrum of the soil over the wavelength region sampled. Grain size has an effect on the overall spectral response as illustrated in Figure 5-2. Typically, absorption features of soils of similar mineral composition are more pronounced for coarse grain soils than for fine grain soils. This is observed because of multiple scattering at different grains in coarse grain soils while in fine grain soils a more direct reflection is observed. Accordingly, the overall reflectance is lower for coarse grain soils compared to similar chemical composition fine grain soils because of increased absorption. Some light entering coarse textures of soils can even be assumed to be extinguished in the process [Ben-Dor 1998a, Baumgardner 1985, Irons 1989].

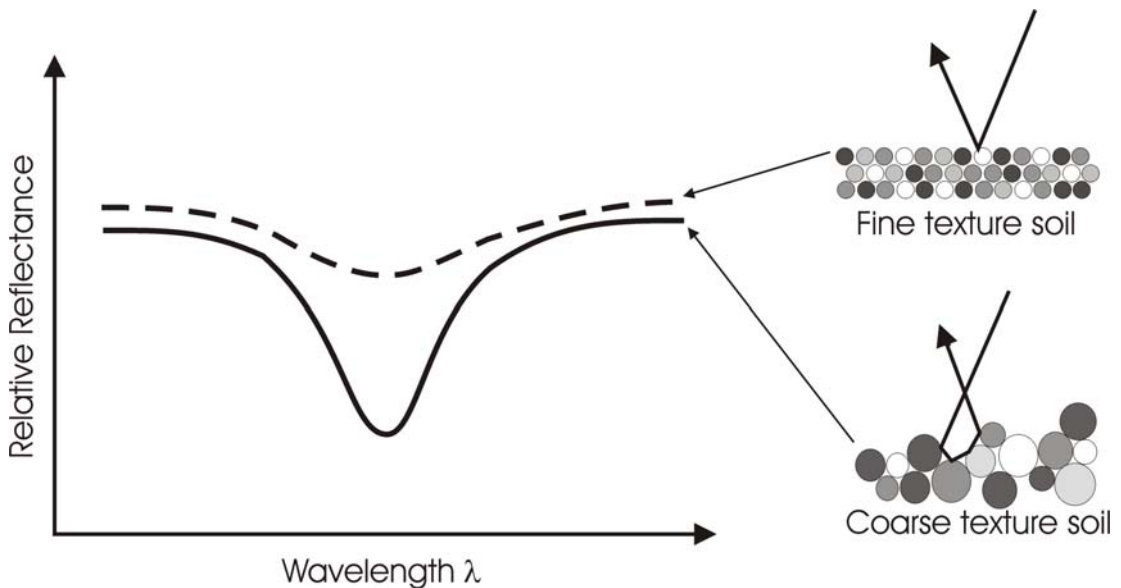


Figure 5-2: Influence of soil texture on reflectance, in particular the intensity of each absorption feature.

The overall spectral response of soils in the 0.4 μm – 2.5 μm wavelength region is typically described by a more or less convex hull with two major absorption features due to water absorption at around 1.4 μm and 1.9 μm . In the near infrared and shortwave infrared wavelength regions, reflectance is typically higher than towards the ends of the spectrum at 0.4 μm and 2.5 μm . Depending on soil color, reflection in the visible wavelength region might vary. Absorption features that allow for the specific identification of many minerals are mainly found in the 2.1 μm to 2.5 μm wavelength region. Several smaller specific absorption features that are related to specific minerals, organic matter, and water, can be found in the 0.5 μm – 2.0 μm region.

Spectral reflectance measurements of several hundred soil samples of mineral soils have shown that five major groups of soil spectral reflectance curves stand out with respect to basic soil composition (figure 5-3): organic dominated soils (organic carbon $\gg 4\%$, iron oxide $< 1\%$, fine texture, E), minimally altered soils (organic carbon $< 2\%$, iron oxide $< 1\%$, B), iron affected soils (organic carbon $< 2\%$, iron oxide 1..4%, C), organic affected soils (organic carbon $> 2\%$, iron oxides $< 1\%$, A), and iron dominated soils (iron oxides $\gg 4\%$, D) [Stoner 1981]. Figure 5-3 shows the average reflectance spectra of these five major soil reflectance classes.

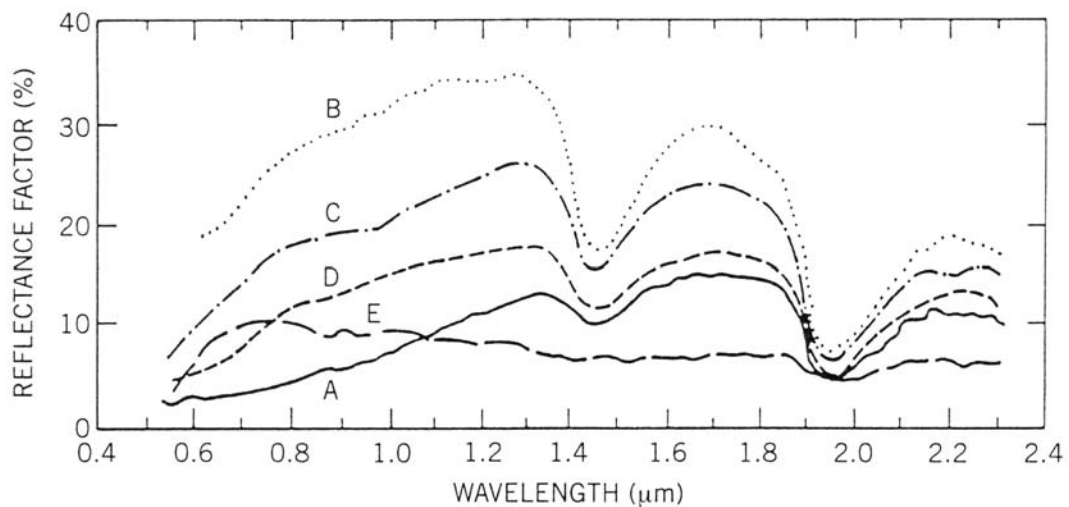


Figure 5-3: Typical reflectance of five major groups of soil types [from Ben-Dor 1998, after Stoner 1981].

Spectral reflectance of soils in the visible wavelength region, or color, can be related to certain physical and chemical properties of soils [Baumgardner 1985]. In contrast to the common method of comparing soil color to Munsell color chips, imaging spectrometry can be used to acquire measurements of soil reflectance in the visible wavelength, providing an unambiguous and objective measure of surface soil color.

To a great extent, soil moisture determines the shortwave infrared spectra of soils. Two dominating water absorption bands appear around 1.45 μm and 1.95 μm and an overall decreasing reflectance occurs with increasing soil moisture. Minor absorption bands attributed to liquid water are observed at 0.97 μm , 1.2 μm and 1.77 μm [Ben-Dor 1998a, Irons 1989, Baumgardner 1985].

Soil organic matter has a strong influence on soil reflectance, with overall soil reflectance strongly decreasing with increasing organic matter content. With increasing organic matter content, usually associated with low reflectance and dark colors in the visible wavelength range, absorption features of other materials are masked, i.e. extinguished from the spectrum. Different minimum values for soil organic matter content were found to have a masking effects, ranging from 2 % to as high as 9 %, depending on the type of soil organic matter. Soils with high contents of organic matter rarely exhibit a relative reflectance above 20 %, with soil moisture further decreasing overall reflectance [Baumgardner 1985, Ben-Dor 1998a, Irons 1989]. Recent investigations have found that imaging spectrometry data can be utilized to predict soil organic matter content and provide some information on the degree of decomposition of soil organic matter [McMorrow 2004, Ben-Dor 1998a, Ingleby 2000].

Most soil minerals, such as the most abundant minerals in soil feldspars, mica, carbonates, clay minerals, iron oxides and iron hydroxides, exhibit specific absorption spectra allowing their identification in hyperspectral remote sensing data. Only quartz, the most ubiquitous mineral and main component of most inorganic soils, and some other primary silicate minerals, do not exhibit any absorption features that allow for their identification in the 0.4 μm – 2.5 μm region. Only minor absorption features are exhibited by apatite and orthoclase. All clay minerals, mica, carbonate, dolomite, gypsum and hematite, however, exhibit unique absorption features that allow for their identification. These absorption features, mainly located in the 2.2 μm – 2.5 μm region, are attributed to the OH-groups found as part of the mineral structure (Si-OH) or adsorbed water in the clay mineral layers. Carbonates exhibit specific absorption features at 2.16 μm (only calcite), 2.23 μm – 2.27 μm and 2.31 μm – 2.35 μm (calcite and dolomite) ranges. Magnesium and impurities of iron have been shown to shift the latter absorption feature towards shorter and longer wavelengths, respectively. A double absorption feature at 1.87 μm and 1.99 μm is not visible in remote sensing data or spectra of wet carbonates due to the 1.9 μm atmospheric water absorption band [Ben-Dor 1998a, Baumgardner 1985].

Iron oxides and hydroxides that are abundant in many soils exhibit broad absorption features in the visible and near infrared wavelength regions between 0.5 μm and 1.3 μm . However, the iron content of soils has also been shown to have an influence on the overall spectral response of soils, obviously due to its typically fine distribution on the surface of larger soil particles. Therefore, linear relationships were also found between iron contents and the reflectance at shortwave infrared wavelengths [Ben-Dor 1998a].

Soluble salts, among others sodium chloride, sodium carbonate and magnesium chloride, often encrust soil surfaces resulting in overall increased soil reflectance compared to spectra of similar soils without a salt encrustment. Other non-soluble salts such as gypsum exhibit specific absorption features that allow for their direct identification [Ben-Dor 1998a].

It has been shown in many different applications that, although often no specific absorption features are known, close relationships between spectral response and soil constituents or properties could be found. These properties include, for example, soil encrusting and infiltration rates, soil pH, soil organic matter content, soil surface moisture, inorganic soil carbon, soil degradation, and different minerals at low concentrations (minimum 1 %) [Kaufmann 1998, Whiting 2003, Leone 1999, Leone 2000, Ben-Dor 2003a]. To some extent it is therefore possible to draw conclusions on the constituents and geochemical properties of the relatively homogeneous topsoil layers (upper 15 – 30 cm) by using surface soil properties (spectral response of the upper 1 μm – 2 mm) and imaging spectrometry data.

5.2 – Fuel hydrocarbons and their spectral characteristics

Fuel hydrocarbons

The absorption features of basic organic compounds of the fuel hydrocarbon group (alkanes, alkenes, alkynes, aromatics, alcohols, carbonyls, carboxyls, chlorinated organics, nitrated organics) were discussed in section 3. However, although used in large quantities as feedstock in the chemical industries these pure, single compounds of the group rarely occur as soil contaminants. Rather, they are found as groundwater contaminants due to leaking pipeline systems at production facilities in the chemical industry. Most soil contaminations are a result of spills, leakages and deposition of crude oil, fuels, fuel oils, lubricants, and refinery and coking residues during production, transport, storage and use. These fuel hydrocarbons are highly complex mixtures of a variety of basic compounds. The spectral response of mixtures of single fuel hydrocarbon compounds adds up to form the spectral response of the mixture. Therefore, the composition of several important commercial fuel hydrocarbon compounds will be considered here in addition to the spectral response of single compounds discussed in section 3.

Crude oils are yellowish to black liquids consisting of more than 500 single compounds, mainly alkanes (usually $\text{CH}_4 - \text{C}_{30}\text{H}_{62}$), cycloalkanes (usually cyclopentane, cyclohexane, and cycloheptane) and aromatics (usually alkylbenzenes). Depending on the deposit and its genesis, either aromatic or aliphatic compounds may dominate. The boiling point of compounds contained in crude oil typically ranges from 50°C to 350°C . The density ranges from 0.65 g/cm^3 to 1.02 g/cm^3 , with most crude oils in the range of 0.82 g/cm^3 and 0.94 g/cm^3 . The viscosity of crude oil ranges from liquid to viscous, since longer exposure to atmospheric conditions results in the evaporation of volatile compounds, thus increasing viscosity [Römpf 1995].

Important commercial fuels used for fueling all kinds of vehicles, power generation and heating include regular gasoline (95 fuel), premium gasoline (98 fuel), kerosene, diesel, light fuel oil, and heavy fuel oil. Depending on their composition of volatile or non-volatile, low or high density, mobile liquid or viscous to solid compounds, fuel hydrocarbons, when spilled, exhibit a different environmental behavior with respect to their distribution in terrestrial, aquatic and atmospheric systems. Table 5-1 summarizes important properties of widely used commercial fuel hydrocarbon products.

Table 5-1: Characteristics of important fuel hydrocarbon products [Compiled from Römpp 1995, HSDB 2004].

	<i>Main Components</i>	<i>Color</i>	<i>Boiling Range 90% [°C]</i>	<i>Melting Point [°C]</i>	<i>Density [g/cm³]</i>	<i>Viscosity</i>
95 Fuel	alkanes, cycloalkanes, monoaromatics (C ₅ -C ₁₂)	clear, colorless – slightly yellow	80 – 130	-90 - -95	0.72 – 0.76	mobile liquid
98 Fuel	monoaromatics , alkanes, cycloalkanes (C ₅ -C ₉)	clear, colorless	80 – 130	-90 - -95	0.72 – 0.76	mobile liquid
Kerosene	alkanes (C ₁₀ -C ₁₆), aromatics (C ₆ +C ₁₀)	clear, colorless - yellow	180 – 270	N/A	ca. 0.8	mobile – oily liquid
Diesel	alkanes, cycloalkanes, alkenes, naphthenes	clear, dark yellow – light brown	170 - 360	70 – 100	0.83 – 0.86	mobile – oily liquid
Lubricating Oil (Mineral Oil)	medium – high molecular weight aliphatics	clear, yellow - brown	> 260	> -60	0.8 – 1.0	oily – slightly viscous liquid
Synthetic Lubricating Oil	polyethers, phosphate esters, silicone oils	clear, yellow - brown	> 260	> -60	0.8 – 1.0	oily – slightly viscous liquid
Light Fuel Oil	alkanes, aromatics (1-3 rings)	clear, light brown, often dyed (red, green)	282 – 338	≥ -6	0.86 – 1.10	oily – slightly viscous liquid
Heavy Fuel Oil / Bunker Oil	refinery residues, long-chain alkanes, polynuclear aromatics	dark brown - black	> 300	≥ 10	> 1.10	viscous liquid
Tar	mainly polynuclear aromatics	dark brown – black	> 210	> 80	> 1.0	viscous liquid – solid
Bitumen / Asphalt	high molecular weight hydrocarbons (aliphatics & aromatics)	dark brown – black	> 700	> 90	1.0 – 1.18	solid

Based on the parameters given in table 5-1, fuel hydrocarbon products can be categorized in the following classes:

- Highly mobile, volatile and colorless fuel hydrocarbons consisting mainly of monoaromatics (95 fuel, 98 fuel)
- Mobile and colorless fuel hydrocarbons consisting mainly of alkanes (kerosene, light fuel oil)
- Oily to slightly viscous, dark fuel hydrocarbons consisting mainly of alkanes (lubricating oil, heavy fuel oil)
- Viscous to solid, black fuel hydrocarbons, consisting mainly of high molecular weight aromatics and/or aliphatics (heavy fuel oil, coal tar, bitumen/asphalt)

All fuel hydrocarbons share in common their hydrophobic nature and hence are almost insoluble in water. Water solubility for these materials ranges from one to ten milligrams per liter. Typically viscosity, melting point and boiling points increase with increasing lengths of the carbon skeleton chain. Whereas fuel hydrocarbons with smaller carbon skeleton chain lengths usually range from clear and colorless to yellowish, longer chained carbon skeleton fuel hydrocarbons tend to be brown to black. The density of all clear and only slightly colored fuel hydrocarbons (clear, colorless to clear, brown) is lower than that of water ($< 1 \text{ g/cm}^3$).

Spectral response of fuel hydrocarbons

Apart from the prominent C-H-stretch overtone vibrations of liquid and solid fuel hydrocarbons that were discussed in sections 3 and 4 (at around $2.3 \mu\text{m}$, $1.7 \mu\text{m}$, $1.4 \mu\text{m}$ and $1.2 \mu\text{m}$), not many results concerning the spectral response of fuel hydrocarbons and their distinction ability in visible, near and shortwave infrared spectra have been published. Also, the ability to decipher liquid and solid fuel hydrocarbons from other natural and synthetic organic materials containing hydrocarbons has not been explicitly addressed. However, much research has addressed the NIR analysis of organic (food) materials, plastics, and fuel hydrocarbon products in industrial process analysis. These works were usually focused on chemometric applications of NIR analysis in controlled environments, determining correlations between selected parameters and reflection or transmission at certain wavelengths. These works generally did not address characteristic absorption features of different hydrocarbon classes and other products containing hydrocarbons [Workman 1996, Buchanan 1992, Stark 1992, Cermelli 1992, Murray 1992, Burns 1992, Hildrum 1992].

5.3 – Fuel hydrocarbon soil contaminations and spectral properties

Fuel hydrocarbon soil contaminations

For the purpose of remote sensing imaging detection and investigation of fuel hydrocarbons in and on surface soils it is necessary to consider the distribution of fuel hydrocarbons in and on soil, their interactions with soil particles and soil moisture, and the typical concentration range of fuel hydrocarbons observed in soil contaminations on a microscopic scale. Although soil contaminations visible at the surface typically make up only a small part of a fuel hydrocarbon soil contamination, the macroscopic distribution and environmental behavior of fuel hydrocarbon contaminations of soil and groundwater, as discussed in section 2, must be considered, even though the largest part of the contamination is usually hidden in the subsurface. However, from a remote sensing point of view, only the behavior and interactions of fuel hydrocarbons and the soil matrix on a microscopic scale are of interest because only the upper few micrometers to millimeters of a soil surface interact with electromagnetic radiation in the visible, near infrared and shortwave infrared wavelength regions, returning the reflectance spectrum to an imaging spectrometry sensor system.

Fuel hydrocarbon contaminations of soils are typically observed in a concentration range between 100 mg/kg (0.01 wt.%) and more than 100,000 mg/kg (10 wt.%), with the actual concentration depending on exposure history and soil and fuel hydrocarbon properties. In Germany, typical remediation threshold concentrations for fuel hydrocarbons in soils are in the range of 1,000 mg/kg (0.1 wt.%), and soils with concentrations above 100 mg/kg (0.01 wt.%) are required to be monitored on a regular basis. However, fuel hydrocarbon concentrations in spill centers or heavily contaminated soils readily exceed 10,000 mg/kg (1.0 wt.%). The concentration of fuel hydrocarbons observed in soils some period of time after the actual spill is usually referred to as the residual concentration. The residual concentration is defined as the quantity of fuel hydrocarbons held in the soil matrix against the force of gravity by capillary forces or adsorbed to soil particle surfaces. Several processes further decrease the concentration of fuel hydrocarbons in the soil matrix over time. Volatile compounds (C₁-C₈ alkanes, monoaromatics) tend to evaporate over time, and percolation of water through the soil matrix dissolves soluble compounds and washes insoluble compounds into deeper soil horizons. With increasing viscosity, smaller quantities penetrate into the soil matrix and higher quantities are held back as residual concentration. Microbial activity results in the degradation of biodegradable compounds. Adaptation of the microflora to fuel hydrocarbons has been observed to result in the degradation of less biodegradable compounds over longer periods of time. However, viscous and high molecular weight hydrocarbon compounds (long-chain aliphatics, polynuclear aromatics, heavy oils, bitumen, tars, asphalt) are typically not dissolved, washed out, evaporated or biodegraded and thus remain in the soil matrix over long periods of time.

Different classes of hydrocarbons, soil types and moisture levels must be considered concerning the distribution and behavior of fuel hydrocarbons in a soil matrix with its mineral and organic components, soil constituents and water (soil moisture) on a microscopic scale. Generally, fuel hydrocarbon spills occur on more or less moist soils, i.e. fuel hydrocarbons are added to a system of fine-grained mineral or organic soil particles containing water adsorbed to the particle surfaces or trapped in the pore spaces between the soil particles. Depending on their viscosity, soil properties (grain size distribution, soil crusts) and environmental (climatic) conditions, fuel hydrocarbons may or may not penetrate the soil matrix. Usually, light crude oils and refined fuels (95 fuel, 98 fuel, diesel, kerosene, fuel oil) penetrate into the soil matrix, while viscous fuel hydrocarbons (heavy fuel oil, heavy crude oil, tars, bitumen, asphaltics) tend not to penetrate the soil matrix and cover the soil surface. Because their density is generally lower than that of water and because fuel hydrocarbons are generally hydrophobic, fuel hydrocarbons that penetrate into the soil matrix are expected to mainly "float" on the soil moisture covering the soil particles and fill void spaces (soil-vapor filled) in the pore volume of the soil. Dry soil particles, usually found at the surface in arid regions, might adsorb fuel hydrocarbons to their surfaces, thus being coated or "impregnated" against soil moisture. Although quartz and primary silicate minerals are not expected to adsorb fuel hydrocarbons except to their surfaces if dry, secondary silicate (clay) minerals and organic material in soils can be expected to strongly absorb fuel hydrocarbons into voids in the mineral structure (clay) or to adsorption sites of humic substances (organic matter). Fuel hydrocarbons may even displace other adsorbed chemicals in these structures. Adsorption (residual concentration) is generally expected to increase in the case of decreasing soil particle size and increasing fractions of secondary silicate minerals and soil organic matter on the one hand, or also in the case of increasing viscosity and increasing boiling temperatures of the fuel hydrocarbons involved.

When covering the soil surface as a separate phase, the state of aggregation of the fuel hydrocarbons might undergo diurnal changes, being solid during the night and melting into liquid state with increasing temperature during daylight.

In the event of precipitation, if pools of water form on the fuel hydrocarbon contaminated soil surface, small quantities of free fuel hydrocarbon from the pore spaces and the soil surface can be expected to be released and float on the water's surface.

In arid regions, contaminations of soils with fuel hydrocarbons are often covered by a thin layer of fine soil particles from the erosion of adjacent areas of open soil and atmospheric deposition of the particles. These particles are held at the surface of the contaminated area by adhesive forces of liquid and largely viscous fuel hydrocarbons. Thus, no hydrocarbon contaminated soil may be exhibited at the surface although only covered by a thin layer of uncontaminated soil.

In the case of high concentrations of fuel hydrocarbons in soils, plant growth may be prevented due to the toxicity of certain fuel hydrocarbons, decreased availability of water in the rhizosphere (caused by impregnation of the soil matrix with hydrophobic fuel hydrocarbons), and increased carbon dioxide and decreased oxygen concentrations in soil vapor due to microbial degradation of fuel hydrocarbons.

Expected spectral behavior of soil contaminated with fuel hydrocarbons

Based on the above considerations of the composition and physico-chemical properties of soils and fuel hydrocarbons, the spectral response of soils and fuel hydrocarbons as single components, and the distribution pattern and environmental behavior of fuel hydrocarbons as contaminants in soils, the following assumptions on the spectral response of soil contaminated with fuel hydrocarbons can be made. For the subsequent assumptions it is anticipated that both uncontaminated soil and soil contaminated with fuel hydrocarbons that are exposed at the surface are relatively homogeneous media over larger areas.

Because of the adsorption of fuel hydrocarbons to soil organic matter and clay minerals, it is expected that contaminations of soils containing large amounts of either soil organic matter or clay minerals (humic soils, boulder till, clays) are spectrally masked, i.e. the absorption features of fuel hydrocarbons are attenuated considerably or even undetectable in reflectance spectra in the 0.4 μm – 2.5 μm wavelength region. On the other hand, a reverse effect can be expected for mineral soils containing large fractions of quartz and primary silicate minerals without adsorptive capacities. In this case, the presence of fuel hydrocarbons may be pronounced because the contaminants are covering the mineral surfaces and "floating" on the soil moisture, thus masking the spectral response of water (soil moisture) and that of the mineral soil matrix. The spectral response of individual fuel hydrocarbons, particularly with respect to the intensity of the prominent absorption bands in the 1.73 μm and 2.35 μm wavelength region and the overall reflectance, are also expected to play an important role in the ability to detect typically low concentrations of fuel hydrocarbons in a soil matrix.

In either case, spectral mixing can be assumed to be non-linear.

For every imaging spectrometry application aimed at the detection of fuel hydrocarbon soil contaminations, the possibility that areas of contaminated soil have been covered with uncontaminated material due to natural erosion and deposition processes should be considered.

5.4 – Research objectives

Fuel hydrocarbon spectra

While prominent absorption features of fuel hydrocarbons as a major chemical class have been described (1.7 μm , 2.3 μm) and applied in remote sensing imaging spectrometry, it has not yet been determined to what extent different classes of typical fuel hydrocarbons occurring as soil contaminants can be distinguished in reflectance spectra and imaging spectrometry data in the 0.5 μm – 2.5 μm region. Furthermore, it has not been investigated in detail if the deposition of other natural and synthetic organic materials on soil surfaces (dry organic matter such as wood/lignin, cellulose, etc. and plastics) can result in false positives when trying to detect fuel hydrocarbon soil contaminations using only single prominent absorption features or single band correlations. Therefore, the ability to separate different hydrocarbon classes including fuel hydrocarbons, plastics and natural materials needs to be investigated.

Spectral response of fuel hydrocarbon soil contaminations

Recent research on the application of imaging spectrometry and reflectance spectroscopy for the detection of fuel hydrocarbons in soils has been limited to the qualitative detection of rather high concentrations of fuel hydrocarbons in single soil matrices. Also, detection limits for different classes of fuel hydrocarbons (e.g., aliphatics, aromatics) and related compounds (e.g., phenols, chlorinated hydrocarbons, explosives) in different soil types (i.e., sand, silt, clay, humic soil) composed of different mineral and organic constituents and at different moisture grades have not yet been addressed and require investigation.

Instrumentation and remote sensing parameters

With the development of instruments that allow for user-defined spectral resolution (FWHM) and sampling intervals, variable spatial resolution depending on instrument foreoptics and flight altitude during data acquisition and user-defined radiometric resolution, it becomes possible to adapt imaging spectrometry instruments to the application rather than the application to the instrument. Therefore it is necessary to define instrumentation and data acquisition parameters with respect to spectral and radiometric resolution based on the absorption features observed in the target material (i.e., fuel hydrocarbon contaminated soils) in order to ensure both the detection and separation of different absorption features. Since the occurrence and intensity of mixed spectra in imaging spectrometry data largely depends on spatial resolution (variability of surface materials typically increases with sampled area, in particular in urban areas) and because fuel hydrocarbons as soil contaminants

typically occur in relatively low concentrations (see above), high spatial resolution of imaging spectrometry data is preferable from a solitary spectrometry point of view. On the other hand, the data volume of imaging spectrometry datasets increases exponentially with spatial resolution, setting limitations with respect to data acquisition (data storage during data acquisition) and data processing and interpretation. Therefore, recommendations for required spatial, spectral and radiometric resolution for the application of imaging spectrometry for the detection and investigation of fuel hydrocarbon soil contaminations need to be derived based on spectral properties and spatial distribution patterns observed.

Because soil moisture is expected to play an important role in the detectability of fuel hydrocarbons in different soil types, it is also necessary to derive recommendations with respect to pre-data-acquisition weather conditions.

Possibilities and restrictions of remote sensing in contaminated site investigation

Given the ability to determine the possibilities and limitations of imaging spectrometry in the 0.4 μm – 2.5 μm wavelength region and to define the instrumentation and data acquisition parameters for the detection and analysis of fuel hydrocarbon soil contaminations, it must be said that the results obtained are only valid for scenes consisting of relatively large and homogeneous entities of soil and fuel hydrocarbon contaminated soil and minor abundances of other spectral endmembers. Therefore, it is especially important to extend the considerations of the applicability of imaging spectrometry for contaminated site detection and investigation to common patterns and environments at brownfields and contaminated sites. Also, the total area of contaminated sites, the exposure of contaminants, wastes and contaminated media at the surface, the overall homogeneity and distribution pattern of different surface materials (spectral variability), and secondary indicators that might hint at subsurface contaminations (vegetation stress) should be taken into account. Additional environmental applications should be considered together with findings concerning the ability to separate different classes of fuel hydrocarbons, other synthetic hydrocarbon-bearing materials and organic materials, and their detection limits.

The limitations and restrictions of imaging spectrometry and other remote sensing methods for contaminated site detection and investigation also should be considered in the context of surface structures, exposition and distribution patterns of contaminations and waste deposits. On the other hand, the possible fields of applications should be outlined.

Data interpretation approaches

Finally, the issue of data interpretation needs to be addressed. Because soil contaminations are typically limited to relatively small areas within larger scenes,

and because the “contamination-specific” spectral response is expected to be relatively small compared to background features (e.g., soil matrix), appropriate data interpretation methods have to be applied. Considering contaminated sites as an anomaly within a normal background and hydrocarbon soil contaminations as a more or less known target spectrum, anomaly and target detection algorithms need to be tested and adapted. Furthermore, a general algorithm for data interpretation with respect to the detection of fuel hydrocarbon soil contaminations needs to be outlined. However, data interpretation is not the primary focus of this study, which aims primarily at the applicability of imaging spectrometry for contaminated site investigation rather than the development or enhancement of data interpretation methods and techniques for this purpose.

The laboratory and field spectrometry and data interpretation experiments presented in the subsequent sections address the problems outlined above. Based on the results obtained in these experiments and the description of typical contaminated sites provided in section 2, conclusions are drawn and the possibilities and limitations of application of imaging spectrometry for contaminated site detection and investigation are determined. Furthermore, recommendations for the application of imaging spectrometry for contaminated site investigation with respect to remote sensing instrumentation, data acquisition and data interpretation are derived.

6 – Spectrometry experiments

To address the problems outlined in section 5 involving the application of imaging spectrometry for the detection and investigation of contaminated sites, particularly those sites with fuel hydrocarbon soil contaminations, a series of laboratory spectrometry, field spectrometry and data interpretation experiments was designed and carried out. While this section addresses the laboratory and field spectrometry experiments and their results, the data interpretation experiments will be addressed separately in section 7.

The laboratory experiments were designed to provide results with respect to the ability to separate and detect spectra in the 0.4 μm – 2.5 μm wavelength range depending on the following variables:

- Different classes of hydrocarbon compounds (alkanes, monoaromatics, polynuclear hydrocarbons, alcohols, explosives, chlorinated organics, etc.)
- Different inorganic compounds (metals, metal oxides, salts, etc.)
- Different commercial fuel hydrocarbon products as mixtures of different classes of hydrocarbon compounds,
- Hydrocarbon compounds and fuel hydrocarbon products from other natural and anthropogenic hydrocarbon-bearing materials (plastics, wood, paper, etc.)
- Different soil types (dry and at different moisture levels)
- Selected, representative fuel hydrocarbon compounds at typical contaminant concentrations in different soil types at different moisture levels

In addition, spectra from several authentic samples of contaminated soils were measured in the laboratory and in the field at the former glassworks Haidemühl, an industrial brownfield. These spectra were measured to test the results of the laboratory experiments against real-life soil contaminations and the applicability in the field. Four major groups of experiments were conducted under defined experimental conditions:

- Spectral measurements of a variety of organic and inorganic chemical compounds, and commercial chemical products and materials (potential contaminants)
- Spectral measurements of different soil types (dry and different moisture contents)
- Spectral measurements of seven different soil types contaminated with twelve representative contaminants of the fuel hydrocarbon group at different soil moisture levels
- Spectral measurements of samples of contaminated soils from different industrial brownfields

In the subsequent sections, first the chemicals, soils, substances, products and materials used in the experiments will be described. Then, the experimental methods, instrumentation and the experimental set-up will be described along with sample preparation procedures, and sample nomenclature. Finally, the results obtained for artificially contaminated soil samples, detection thresholds, and real-life contaminated soil samples will be discussed.

6.1 – Sample materials

Organic and inorganic chemicals

In order to identify specific absorption features and spectral properties of different classes of hydrocarbons and to determine the spectral uniqueness of fuel hydrocarbons from other classes of chemicals, spectra of more than 120 selected chemical compounds, commercial chemical products and fuel hydrocarbons were acquired in experiments under controlled laboratory conditions. In order to assess the applicability of imaging spectrometry for detecting contaminations with inorganic pollutants and to assure their distinction from hydrocarbons in spectra in the 0.4 μm to 2.5 μm wavelength region, a number of inorganics with a focus on heavy metal compounds and salts was also included. Although they were expected to be spectrally featureless, major classes of organics included aliphatics, monoaromatics, polynuclear aromatic hydrocarbons, alcohols, phenols, explosives, chlorinated hydrocarbons, fuel hydrocarbons and other commercial products consisting of hydrocarbons. Major classes of inorganics included elemental metals and heavy metals, metal oxides, metal sulfates, metal salts, and salts.

Table 6-1 lists the compounds and products included in the experiments. Liquid and solid compounds are listed in separate columns because the measurement methods applied varied depending on the state of aggregation and the opacity or transmissivity of the sample. Those chemicals selected for the subsequent experiments on soil contaminations are highlighted in the table.

Anthropogenic materials

In order to determine the uniqueness of fuel hydrocarbon contaminants from materials of anthropogenic origin abundant in urban scenes of remote sensing data, spectra of about 30 wide-spread anthropogenic materials were acquired (plastics, paints, ceramics, paper, fabric, wood products) in a large number of varieties (different colors, surface structures, material thickness, etc.). Anthropogenic materials that were expected to exhibit similar spectral characteristic as soils (brick, concrete) were also included in the measurements. Table 6-2 lists the materials included in these measurements.

Table 6-1: Chemicals and chemical products investigated with respect to their spectral characteristics in the 0.38 μm to 2.5 μm wavelength region. Those compounds and products selected as contaminants for the soil – moisture contaminant experiments are marked bold and italic.

Group	Liquid Compounds	Solid Compounds
Aliphatics	n-Hexane, n-Heptane, <i>n-Octane</i> , 1-Octene, 1-Octyne	
Monoaromatics	Benzene, Toluene, Ethylbenzene, <i>Xylene</i> , 1,2,4-Trimethylbenzene	1,3,5-Trimethylbenzene, 1,2,4,5-Tetramethylbenzene
Polycyclic Aromatic Hydrocarbons	1-Methylnaphthalene, <i>1-Acetylnaphthalene</i>	<i>Naphthalene</i> , 1-Naphthol, 2-Naphthol, 2-Methylnaphthalene
Alcohols	Methanol, Ethanol, 1-Octene-3-ol, 1,8-Octanediol, 2-Octanol, 3-Octanol	
Phenols	<i>2,4-Dimethylphenol</i>	<i>Phenol</i> , 2,5 / 2,6 / 3,4 / 3,5-Dimethylphenol, 2-Amino-4-Methylphenol, 4-Chloro-3,5-Dimethylphenol, Pyrogallol
Explosives	4-Nitrotoluene	2,4,6-Trinitrotoluene (TNT), Hexogen, <i>2,4-Dinitrotoluene</i> , Octogen
Chlorinated Hydrocarbons	Dichloromethane, Trichloromethane, Chlorobenzene, 1,2-Dichlorobenzene, <i>1,2,4-Trichlorobenzene</i>	1,2,3,4-Tetrachlorobenzene
Fuel Hydrocarbons	Regular Gasoline (95), Premium Gasoline (98), <i>Diesel</i> , Kerosene F-34, <i>Kerosene R-1</i> , Fuel Oil, Synthetic Motor Oil, <i>Crude Oil</i> , <i>Waste Oil</i>	
Lubricants, Cleaning Fluids, Sealings	Cleaners Naphtha, Bitumen Lacquer, Cutting Oil, Mechanics Lubricant Oil, Precision Mechanics Lubricant Oil, Boiled Linseed Oil	Bitumen Paste, All-Purpose Grease
Other Organics	Acetic Acid, Acetone, Glycerin, Sodium Acetate, 1-Octanal, 2-Octanone, 3-Octanone, Octanoic Acid	Triphenylarsine
Metals, Metal Sulfates, Metal Oxides, Metal Salts, etc.		Al (powder), AlO, AlCl ₂ , Cu (powder), CuO, CuSO ₄ , CuSO ₄ •H ₂ O, CuCl ₂ , Zn (powder), ZnO, ZnCl ₂ , ZnSO ₄ , Fe (powder), FeCl ₂ , Fe ₂ O ₃ , FeSO ₄ •H ₂ O, MnCl ₂ , V ₂ O ₅ , As ₂ O ₃ , CoCl ₂ , Pb(NO ₃) ₂ , AgCl ₂
Salts	NaCl solution (aq.), KCl solution (aq.)	NaCl, NaNO ₃ , KCl, KBr, KNO ₃ , NH ₄ NO ₃
Others Inorganics	NH ₃ (aq.), H ₂ O	B(OH) ₃ , NaOH, NaN ₃ , NaHSO ₃ , CO(NH ₂) ₂ , SiO ₂ , S, C (powder, graphite)

Table 6-2: Anthropogenic hydrocarbon-bearing materials investigated to determine their uniqueness when compared to fuel hydrocarbon soil contaminations.

<i>Group</i>	<i>Materials</i>
Paints	Acrylic Lacquers, Alkyd Paint, Synthetic Resin Varnish, ZK-Pur Lacquer (different colors of each)
<i>Plastics</i>	Acrylic Plastic (PMMA), Polyethylene (PE-LD), Polypropylene (PP), Polystyrene (PS), Polyurethane (PU), Polyvinyl chloride (PVC), Latex, Nitrile, Nylon, Rubber, Silicone, Styrofoam (different colors of each)
<i>Paper & Cardboard</i>	Cardboard, Cellulose Fiber Cloth, Paper (different colors of each)
<i>Fabric</i>	Cotton Cloth
<i>Natural Materials</i>	Cork bark, Wood
<i>Concrete & Ceramics</i>	Brick (red, yellow), Concrete
Metals	Aluminum Sheet, Brass Sheet, Copper Sheet, Steel Sheet (not oxidized)

All granular or powdered solid and all liquid substances were prepared in Duroplan glass Petri dish bottoms with an inner diameter of 68 millimeters for the spectral measurements. For translucent liquids, the samples were prepared with a thickness of one millimeter, equivalent to 3.6 ml of liquid in the Petri dish bottom and yielding an effective absorption path length (dual-pass) of two millimeters. Non-transparent liquids and solids were prepared to cover the whole bottom of the Petri dish.

Other material samples (e.g., plastic sheets, wood, paper, painted materials, metal sheets, etc.) were prepared in squares of minimum 8 × 8 centimeters.

Soil samples

For the experiments on the detectability and separability of different fuel hydrocarbons in soils at different soil moisture contents, six different soil types were selected. The soils were selected to contain different fractions of quartz, primary silicate minerals, secondary (clay) minerals, iron, and soil organic matter.

The soil types included *pure silica sand* (commercial product, laboratory grade), *fine sand* containing quartz and primary silicate minerals, *coarse sand* containing some organic matter and iron in addition to quartz and primary silicate minerals, *boulder till* containing quartz, clay and organic matter, *clay*, and *humic topsoil* dominated by organic matter and containing high concentrations of iron.

Because the handling of clay, even if ground, proved highly difficult with respect to sample homogenization when adding water for soil moisture and contaminants, *clay granulate* (fine grain clay cat litter, a commercial product) was included in the experiments.

For each soil, the following parameters were determined (where applicable): natural (sampling) moisture content, ignition loss (organic material), grain size distribution, carbonate content, iron content, and background concentration of fuel hydrocarbons. The soil types, their sampling sites and their physico-chemical properties (table 6-3) are described as follows. Each soil type was assigned a symbol to identify it in the experiments.

Sea Sand (symbol SS)

Description: Fine sea sand, washed and purified with acid and calcined at 1,000 °C to yield pure silica sand, color yellowish-white, sieved, grain size 0.1 – 0.3 mm

Source: VWR International, order no. 1.07712.5000

Fine Sand (symbol fS)

Description: Yellowish-gray fine grain sand with darker and brighter grains (primary silicate minerals), sieved, maximum grain size 0.4 mm

Sampling site: Gravel and clay pit at Calau-Plieskendorf ca. 25 kilometers southwest of Cottbus (Brandenburg / Germany)

Sampling coordinates: 13.9660 °E (approx.)
(WGS84, decimal) 51.7187 °N (approx.)

Coarse Sand (symbol cS)

Description: Yellowish – brown, mainly coarse sand with smaller fractions of medium sand and gravel

Sampling site: Heathland near Taubendorf ca. 23 kilometers northeast of Cottbus (Brandenburg / Germany)

Sampling coordinates: 14.59037 °E
(WGS84, decimal) 51.88763 °N

Boulder Till (symbol BT)

Description: Fine to medium grain soil with medium to coarse gravel portions, containing organic matter

Sampling site: Agricultural field (corn) on the “Hornoer Berg” ca. 19 kilometers northeast of Cottbus (Brandenburg / Germany)

Sampling coordinates: 14.58543 °E
(WGS84, decimal) 51.84074 °N

Clay (symbol Cv)

Description: Light gray (some parts dark gray and yellowish-brown), mainly clay, highly cohesive, high water content

The clay deposit is reported to consist mainly of kaolinite with smaller fractions of mica, montmorillonite, and halloysite [Schroeder 1995].

Sampling site: Gravel and clay pit at Calau-Plieskendorf ca. 25 kilometers southwest of Cottbus (Brandenburg / Germany)

Sampling coordinates: 13.96655 °E
(WGS84, decimal) 51.71874 °N

Humic Soil (symbol Hu)

Description: Dark brown – black, fine to medium grain soil with high organic material content, obviously high iron content, and small fine sand fraction

Sampling site: Pasture land at Peitzer Laßzinswiesen ca. 16 kilometers northeast of Cottbus (Brandenburg / Germany)

Sampling coordinates: 14.43984 °E
(WGS84, decimal) 51.88291 °N

Clay Granulate (symbol Cg)

Description: Medium gray, natural clay granulate (bentonite), grain size 1 – 2 mm (cat litter “Catsan”)

Source: Masterfoods GmbH, “Catsan Ultra Klumpende Katzenstreu”, article no. 947765 D/A

Table 6-3: Important characteristics of the soils used for the soil – moisture – contaminant experiments.

Soil Type	<i>Symbol</i>	<i>Grain Size</i>		<i>CaCO₃</i> [%]	<i>Fe</i> [mg/kg]	<i>FHC</i> [mg/kg]	<i>Ignition Loss</i> [%]	<i>Natural</i> Moisture [%]	<i>Color</i>
		[mm]	[%]						
Sea Sand (pure silica sand)	SS	> 2	0	max. 0.02	max. 10	0	max. 0.05	ca. 10	light gray - white
		0.3 - 2	0						
		0.1 – 0.3	100						
Fine sand	fS	>2	0	0.41	730	6.6	0.1 – 0.3	ca. 10	light gray – yellowish
		0.4 - 1	0						
		< 0.4	100						
Coarse sand	cS	> 2	11.6	0.41	3,620	7.9	1	3 – 4	yellow – brown
		1 – 2	8.7						
		< 1	79.7						
Humic topsoil	Hu	> 1	34.5	N/A	20,200	12	25 – 55	50 – 70	dark brown – black
		< 1	65.5						
Boulder till	BT	> 1	3.9	0.46	4,370	9	2 – 3	6 - 7	brown
		< 1	96.1						
Clay	Cy	> 1	0	0.57	14,900	12	5 – 7	20 – 22	gray
		< 1	100						
Clay granulate	Cg	> 2	0	N/A	N/A	0	7 – 8	ca. 12	gray
		1 – 2	100						

In preparation of the soil / moisture / contaminant experiments, the soils were oven-dried at 105°C for a minimum of 24 hours. All materials with a diameter of more than two millimeters were separated from the dry soils by sieving. Because of the small scale of the laboratory spectral measurements (samples in Petri dishes with a diameter of 68 mm), the maximum particle size was further reduced to a maximum of one millimeter by sieving. The grain size distribution of this fraction used for the subsequent experiments was determined in a grain size analysis. Not included in this analysis were pure silica sand (SS, grain size 0.1 – 0.3 mm) and clay granulate (Cg, grain size 1 – 2 mm) because the grain size distribution was known and clay (Cy) because the grain size was too small for sieving analysis. The results for fine sand (fS), coarse sand (cS), boulder till (BT) and humic soil (Hu) are presented in table 6-4.

Table 6-4: Particle size distribution 0.04 mm – 1.0 mm of fine sand, coarse sand, boulder till, and humic soil.

Particle Size	Fine Sand (fS) [%]	Coarse Sand (cS) [%]	Boulder Till (BT) [%]	Humic Soil (Hu) [%]
1 - 0.63 mm	0.00	16.95	6.14	17.48
0.63 - 0.25 mm	47.35	53.06	25.68	41.35
0.25 - 0.125 mm	46.46	23.92	37.58	32.53
0.125 - 0.080 mm	3.99	2.86	14.78	4.76
0.080 - 0.040 mm	0.64	0.66	9.09	2.90
< 0.040 mm	1.56	3.45	6.73	0.98

Based on this analysis, the soils can be described as follows:

Sea sand (SS): pure silica (quartz) sand, fine grain sand, containing no iron, carbonate or organic matter

Fine sand (fS): fine grain sand consisting of quartz and primary silicate minerals, low iron content, free of organic matter

Coarse sand (cS): coarse grain sand, quartz-dominated, medium iron content, containing small fraction of organic matter

Boulder till (BT): fine grain soil containing quartz and secondary silicate minerals, with medium iron and organic matter content

Clay (Cy): finest grain soil, consisting of secondary silicate minerals, containing high concentrations of iron and no soil organic matter (loss on ignition due to evaporation of crystal water)

Humic Soil (Hu): organic soil with high iron content

Clay Granulate (Cg): fine grained clay consisting of secondary silicate minerals

In the analyses, all soil samples were found to be virtually free of fuel hydrocarbons with concentrations in the range of 6 mg/kg – 12 mg/kg that can be attributed to hydrocarbon-bearing soil organic matter. However, the concentrations found are irrelevant compared to the target concentrations investigated in the soil / moisture / contaminant experiments.

6.2 – Experiment design – fuel hydrocarbon contaminated soils

Soil moisture level selection

For the investigation of soil spectra of different moisture grades contaminated with fuel hydrocarbons, the seven soil types described above were prepared at three defined moisture contents and mixed with twelve selected (fuel) hydrocarbons at three different concentrations. Based on pretests (mixing the dry, sieved soils < 1mm grain size with different quantities of water) and the natural moisture content of the soil samples, the moisture levels listed in table 6-5 were selected for these experiments. An important criterion was to prevent liquid water floating on the samples to ensure the comparability of the spectral measurements. For coarse sand (cS), clay (Cy) and boulder till (BT), the maximum soil moisture for the experiments was selected to coincide with the moisture of the soil samples taken in the field, 4 %, 20 % and 6 %, respectively. For humic soil (Hu), the soil moisture of the field samples was about 60 %. However, the sieved fraction < 1 mm used for the experiments was found to take up only about 30 % moisture at maximum without liquid water floating on the sample. Therefore, the maximum soil moisture for humic soil was selected at 30 %. To determine the maximum soil moisture content of sea sand (SS) and fine sand (fS), several samples of oven-dried soil were saturated with water and drained for three days. The soil moisture determined for these samples was about 20 % for both soils. However, when mixing these saturated samples with contaminants, liquid water formed on the surface. Therefore, the maximum soil moisture level for sea sand (SS) and fine sand (fS) was selected to be 10 %. In addition to the selected maximum soil moisture level, experiments were conducted with soil samples containing half of the maximum soil moisture level selected and with dry soils (oven-dried at 105°C).

Table 6-5: Soil moisture levels selected for the experiments for the different soil types.

<i>Soil Type</i>	<i>Dry Soil [%]</i>	<i>Moisture Level 1 [%]</i>	<i>Moisture Level 2 [%]</i>
<i>Sea Sand (SS)</i>	0	5.0	10.0
<i>Fine Sand (fS)</i>	0	5.0	10.0
<i>Coarse Sand (cS)</i>	0	2.0	4.0
<i>Boulder Till (BT)</i>	0	3.0	6.0
<i>Humic Soil (Hu)</i>	0	15.0	30.0
<i>Clay (Cy)</i>	0	10.0	20.0
<i>Clay Granulate (Cg)</i>	0	10.0	20.0

Note: For soil moisture calculations, the US definition was applied (soil moisture [%] = water content [g] / dry soil [g] * 100) rather than the German definition according to DIN 18121 (soil moisture [%] = water content [g] / moist soil [g] * 100).

Contaminant selection

Based on the comparison of the spectra of different classes of fuel hydrocarbons, twelve different hydrocarbon compounds and commercial fuel hydrocarbon products were selected as contaminants for the experiments. Basic chemical compounds (alkane, monoaromatics, polynuclear aromatic hydrocarbons), important functional groups as well as important and representative classes of environmental contaminants were included in the selection such as fuel hydrocarbons, chlorinated hydrocarbons, persistent organic pollutants, phenols, explosives, polynuclear aromatic hydrocarbons. The selected compounds exhibited distinct absorption features that allowed their identification, at least with respect to major compounds (alkane, aromatics, functional groups).

The selected contaminants are known to be resident in soils (i.e. adsorb to soil minerals and organic matter and not to volatilize easily or dissolve in water). Volatile and water-soluble contaminants were not selected because they can be expected to be evaporated or washed out of the soil matrix over short periods of time, therefore being irrelevant as soil contaminants that are typically expected to be detected at the surface for longer periods of time. Where the primary target substance exists as a solid under standard conditions, a related, liquid compound exhibiting similar spectral characteristics was selected as an additional contaminant when possible (phenol / 2,4-dimethylphenol and naphthalene / 1-acetylnaphthalene). The contaminants selected for the experiments are listed in table 6-7.

Contaminant concentrations selection

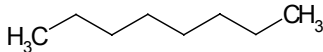
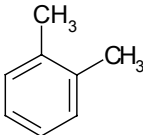
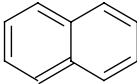
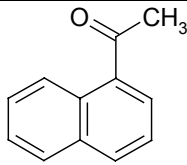
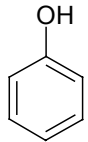
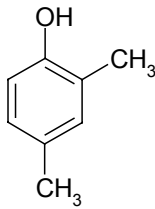
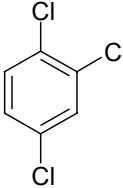
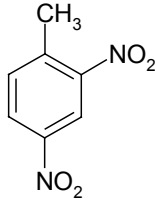
The contaminant concentrations for the experiments were selected based on both realistic contaminant concentrations observed at contaminated sites and pretests with varying concentrations of the selected contaminants in the different soils and at different soil moisture levels. The minimum concentration was selected to be detectable only in some soil samples and under certain environmental conditions. The maximum concentration was selected to be detectable in every soil type at least at one moisture level. As a result, the following contaminant concentration levels (mg contaminant per kg dry soil or %) were selected for the experiments (Table 6-6):

Table 6-6: Contaminant concentration levels selected for the experiments.

<i>Concentration</i>	<i>mg / kg dry soil</i>	<i>mg / 50 g dry soil</i>	<i>mg / 30 g dry soil</i>
<i>0.5 %</i>	5,000	250	150
<i>1.0 %</i>	10,000	500	300
<i>3.0 %</i>	30,000	1,500	900

Note: Analogously to the soil moisture definition, the calculation basis applied was (contaminant [%] = g contaminant per g uncontaminated dry soil).

Table 6-7: Contaminants selected for the experiments with composition, structural formula and state of aggregation in standard (experiment) conditions.

<i>Contaminant</i>	<i>Symbol</i>	<i>Class</i>	Structural formula	<i>State of Aggregation</i>
<i>n-Octane</i>	OCT	Alkane		liquid
<i>Xylene</i>	XYL	Monoaromatic, substituted with alkyl group		liquid
<i>Naphthalene</i>	NAP	Polynuclear hydrocarbon		solid
<i>Kerosene</i>	KER	Jet fuel: mainly aliphatics + some aromatics	N/A	liquid
<i>Diesel</i>	DIS	Automotive fuel: mainly aliphatics	N/A	liquid
<i>Waste Oil</i>	WO	Waste product: mainly aliphatics	N/A	liquid
<i>Crude Oil</i>	CRO	Light crude oil: mainly aliphatics	N/A	liquid
<i>1-Acetylnaphthalene</i>	ANA	Polynuclear hydrocarbon, substituted with acetyl (CO-CH ₃) group		liquid
<i>Phenol</i>	PHE	Phenol, monoaromatic, substituted with OH group		solid
<i>2,4-Dimethylphenol</i>	DMP	Phenol, monoaromatic, substituted with OH group and alkyl (CH ₃) groups		liquid
<i>1,2,4-Trichlorobenzene</i>	TCB	Monoaromatic, substituted with chlorine		liquid
<i>Dinitrotoluene</i>	DNT	Explosive, monoaromatic, substituted with nitro groups (NO ₂)		solid

6.3 – Sample Preparation

With twelve different organic contaminants, three contaminant concentration levels, seven soil types and three soil moisture levels, a total of 756 single samples with a unique combination of soil type, contaminant, contaminant concentration, and soil moisture level had to be prepared and the spectrum measured. For quality assurance, 25 % of the experiments were repeated independently once, and 5 % of the experiments were repeated independently twice. Comparison of the spectra of independently repeated measurements showed that the repeatability of the measurements was good.

Sample Description System

In order to uniquely identify every sample and every single spectrum measured, the following sample description system was used. The first two letters describe the soil type. The two following digits indicate the soil moisture in whole percentages, and the next two digits the contaminant concentration as a percentage. The two or three letter symbol following indicates the contaminant used, and the final six digit combination is the date of sample preparation and the spectrum measurement (generally on the same day). The three digit file suffix identifies the number of a spectrum measured in a series. The sample descriptions were also used as file names for the spectrum files saved. Examples:

cS-02-05-OCT_041012.009 coarse sand, 2 % moisture, 0.5 % n-octane, spectrum no. 009 measured on Oct. 12, 2004

Hu-15-30-ANA_041117.084 humic soil, 15 % moisture, 3.0 % 1-acetylnaphthalene, spectrum no. 084 measured on Nov. 17, 2004

The additional file suffix *.sco after the file/spectrum number indicates that the splice correction function of the ASD View Spec Pro® software was applied to the spectrum to correct for erroneous offsets between the three different sensors of the instruments (at 1,000 nm and 1,780 nm).

Preparation of moist soil samples

The dry, sieved soil with grain sizes < 1 mm prepared as described above was used for the experiments with dry soil and contaminants at different concentrations and to prepare soils with the defined moisture levels. For this, one kilogram of soil was given into a 2-liter PE-LD wide-mouth bottle and the appropriate quantity of distilled water was added to the sample. The sample was then shaken thoroughly to mix water and soil homogeneously. To allow for an equal distribution of the water in the soil matrix, the soils were left to rest for a minimum of 24 hours and shaken from time to time. Table 6-8 lists the moisture levels and water quantities added to prepare the moist soil samples.

Tabelle 6-8: Soil moisture level sample preparation.

	<i>Moisture Level 1</i>		<i>Moisture Level 2</i>	
	<i>[%]</i>	<i>ml H₂O / kg dry soil</i>	<i>[%]</i>	<i>ml H₂O / kg dry soil</i>
<i>Sea Sand (SS)</i>	5	50	10	100
<i>Fine Sand (fS)</i>	5	50	10	100
<i>Coarse Sand (cS)</i>	2	20	4	40
<i>Boulder Till (BT)</i>	3	30	6	60
<i>Clay (Cy)</i>	10	100	20	200
<i>Clay Granulate (Cg)</i>	10	100	20	200
<i>Humic Soil (Hu)</i>	15	150	30	300

Preparation of soil samples with liquid contaminants

For the spectral measurements of liquid contaminants in dry and moist soil samples, defined quantities of dry or moist soil were weighed into Petri dish (bottoms) so that every Petri dish contained the same quantity of soil (without moisture), generally 50.00 ±0.01g for the mineral soils, and 30.00 ±0.01 g for the humic soil (Hu). Depending on the soil moisture content, different quantities had to be weighed out for every individual soil type and moisture level. For each contaminant, three soil samples of all three moisture levels were prepared, and 0.5 %, 1.0 % and 3.0 % of the contaminant under investigation were added to the soil samples (equivalent to 250 mg, 500 mg, and 1,500 mg for mineral soils and 150 mg, 300 mg, and 900 mg for humic soil). The relatively small quantities of liquid contaminant were generally added to the samples using a micropipette and a laboratory balance to double-check the quantity of contaminant added to the sample. The sample containing soil and contaminant was then thoroughly mixed for a minimum period of three minutes using a glass rod to assure a homogeneous distribution of the components in the sample. To prevent the volatilization of contaminants and moisture from the samples, the Petri dishes were generally covered with the Petri dish top when the sample was not being worked on.

Table 6-9 gives an overview of the soil samples prepared for the experiments with every liquid contaminant.

Table 6-9: Soil quantities and contaminant quantities used to prepare soil samples with defined contaminant concentrations.

<i>Soil/ Moisture Level</i>	<i>0.5 % Contaminant (-05)</i>		<i>1.0 % Contaminant (-10)</i>		<i>3.0 % Contaminant (-30)</i>	
	<i>g soil</i>	<i>mg contaminant</i>	<i>g soil</i>	<i>mg contaminant</i>	<i>g soil</i>	<i>mg contaminant</i>
<i>SS-00</i>	50.0	250	50.0	500	50.0	1,500
<i>SS-05</i>	52.5	250	52.5	500	52.5	1,500
<i>SS-10</i>	55.0	250	55.0	500	55.0	1,500
<i>fS-00</i>	50.0	250	50.0	500	50.0	1,500
<i>fS-05</i>	52.5	250	52.5	500	52.5	1,500
<i>fS-10</i>	55.0	250	55.0	500	55.0	1,500
<i>cS-00</i>	50.0	250	50.0	500	50.0	1,500
<i>cS-02</i>	51.0	250	51.0	500	51.0	1,500
<i>cS-04</i>	52.0	250	52.0	500	52.0	1,500
<i>BT-00</i>	50.0	250	50.0	500	50.0	1,500
<i>BT-03</i>	51.5	250	51.5	500	51.5	1,500
<i>BT-06</i>	53.0	250	53.0	500	53.0	1,500
<i>Hu-00</i>	30.0	150	30.0	300	30.0	900
<i>Hu-15</i>	34.5	150	34.5	300	34.5	900
<i>Hu-30</i>	39.0	150	39.0	300	39.0	900
<i>Cy-00</i>	50.0	250	50.0	500	50.0	1,500
<i>Cy-10</i>	55.0	250	55.0	500	55.0	1,500
<i>Cy-20</i>	60.0	250	60.0	500	60.0	1,500
<i>Cg-00</i>	50.0	250	50.0	500	50.0	1,500
<i>Cg-10</i>	55.0	250	55.0	500	55.0	1,500
<i>Cg-20</i>	60.0	250	60.0	500	60.0	1,500

Preparation of soil samples with solid contaminants

To ensure a homogeneous distribution of the solid contaminants (naphthalene, phenol, 2,4-dinitrotoluene) in the soil samples, it was necessary to first dissolve the contaminants in an organic solvent, add the solvent to dry soil samples in the amount required to reach the desired contaminant concentrations in the soil samples and then evaporate the solvent from the soil samples. Only after the contaminant had been added to the soil sample and the solvent removed, was distilled water added to adjust the required soil moisture level.

To ensure high volatility even from soil samples containing high levels of adsorptive material (clay minerals, organic matter), trichloromethane and diethylether, which were also found to dissolve large quantities of the three solid contaminants, were selected as solvents.

Twenty grams of naphthalene was dissolved in non-polar trichloromethane and had a total volume of 100 ml in a measuring flask. Forty grams of phenol and 30 grams of 2,4-dinitrotoluene were each dissolved in diethylether, a more polar solvent, which allowed for higher concentrations of the contaminants to be dissolved, also with a total volume of 100 ml in the measuring flask. One hundred grams of dry soil of each type were measured into washing bottles and the total weight was noted. Next, depending on the concentration of the solution, different volumes of contaminants were added to the washing bottles to yield concentrations of 1.0 % and 3.0 %, respectively. The solution was thoroughly mixed with the soil and flushed with pressurized air under a venting hood until weight equilibrium was reached. Usually, small differences (± 0.2 g) to the expected sum weight of soil and contaminant (101.00 g @ 1.0 % and 103.00 g @ 3.0 %, respectively) were observed, obviously due to the absorption of the solvent or fine soil particles being blown out of the washing bottle. The dry soil samples containing the contaminant at concentrations of 1.0 % or 3.0 % were then weighed into Petri dishes, and distilled water was added to reach the soil moisture levels defined for each soil type. Finally, the sample was manually homogenized before measurement as described above.

Table 6-10: Contaminant-solvent mixtures added to dry soil to prepare defined contaminant concentration soil samples with solid contaminants.

	<i>Solution / 100 g Dry Soil for Contaminant Concentration 1.0 %</i>	<i>Solution / 100 g Dry Soil for Contaminant Concentration 3.0 %</i>
<i>Solution 20 g Naphthalene / 100 ml Trichloromethane</i>	5.0 ml	15.0 ml
<i>Solution 40 g Phenol / 100 ml Diethylether</i>	2.5 ml	7.5 ml
<i>Solution 30 g 2,4-Dinitrotoluene / 100 ml Diethylether</i>	3.33 ml	10 ml

Because of difficulties concerning the homogeneous distribution of relatively low quantities of liquid contaminants in the dry soil samples (1,25 ml – 2,5 ml / 100 g dry soil), samples containing 0.5 % of contaminant were only prepared for solid contaminants that could be dissolved in a highly volatile solvent and for some liquid contaminants with a very low viscosity.

6.4 – Instrumentation and measurement set-up

For the laboratory spectral measurements, an Analytical Spectral Devices, Inc. Field Spec Pro FR® spectrometer (instrument no. 6199, calibration 1) covering the 0.38 μm to 2.5 μm wavelength region was used. Being a passive sensor instrument, a Lowel ProLamp® was used for the illumination of the samples. Because the instrument measures the intensity of light and thus needs a reference standard for the computation of relative reflectance, a 3.6 inch (9.1 cm) diameter dish of white Spectralon® was used as a white reference for the spectral measurements.

To prevent stray light from other sources of illumination and reflections of non-sample materials being measured by the instrument, the lamp, sensor and target were set up in a housing of black cotton cloth. In order to prevent overheating of the Lowel ProLamp® illumination source, the outer body of the reflector was continuously ventilated with pressurized air.

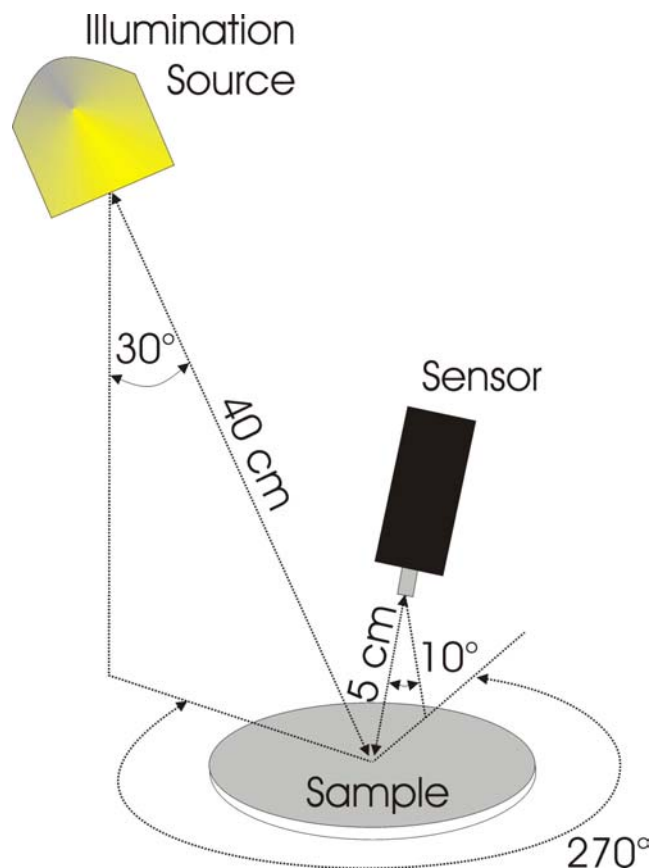


Figure 6-1: Measurement setup for laboratory reflectance measurements.

The illumination source was adjusted at a distance of 40 cm from the sample with an illumination angle of 30° off the vertical. The sensor was oriented at an angle of 90° to the illumination source with a viewing angle at the sample of about 10 – 15° off the vertical, to prevent shadows on the sample during the measurement, and a distance to the sample of about 5 – 6 centimeters. With the sensor orientation and sensor at a given sample distance, the diameter of the sensor field of view was about 2.5 centimeters. Figure 6-1 depicts the measurement set-up.

Prior to the measurements, the instrument was allowed to warm up for a minimum of 60 minutes. Before the first and during the measurements at intervals of about five minutes, the instrument was optimized and a new white reference was taken.

For each recorded spectrum, 64 single spectra were acquired and averaged by the instruments. For the dark current measurement 128 single measurements were averaged, for white reference measurements 64 measurements were averaged. To determine the number of spectra to be averaged, an experiment was conducted with 1, 2, 4, 8, 16, 32, 64, 128, and 256 spectra of the same sample at the same viewing geometry being averaged for each spectrum saved. As expected, noise in the data, in particular at the infrared wavelengths between 2,000 nm and 2,500 nm was observed to decrease with an increase in the number of spectra averaged for each spectrum saved. However, limitations of the instrument required to set the maximum of spectra averaged for each spectrum averaged to 64. At higher numbers of spectra averaged, the instrument was experienced to return errors that necessitated a re-start of the instrument without the spectrum averaged being saved.

At the beginning and at the end of each measurement series, three standard materials were measured and their spectra saved for measurement quality assurance, namely transparent Mylar film, transparent NIST 126635A plastic film, and white polyester NIST 126636.

Samples of clear, translucent liquids in Petri dishes were placed on the white reference for the measurements. The optimization and the white reference measurements for these samples were conducted with an empty Duroplan Petri dish on the white reference to include the (weak) absorption of the Petri dish glass in the white reference measurement. With a liquid thickness of one millimeter, the effective absorption path length for the measurement was two millimeters: 1 mm sample – glass – white reference – glass – 1 mm sample.

Samples of opaque materials (opaque liquids, soil samples, powdery or granular solids, solid material samples) were placed directly under the sensor. Optimization and white reference measurements prior to the spectral measurements were conducted with only the white reference material.

Each spectral measurement was documented immediately after the measurement in a laboratory journal using the sample description system explained above. The sample description was later used as the file name for each spectrum. In some cases, offset errors between the three detectors of the instruments (occurring at 1,000 nm and 1,780 nm) had to be corrected using the splice correction function of the processing and viewing software ASD View Spec Pro®.

6.5 – Results and Discussion

The spectra of organic and inorganic chemicals, dry and moist soils, soils contaminated with different contaminants at varying concentrations and moisture levels, different anthropogenic materials (plastics, paper, paint) and natural materials (wood, cork, bark, cotton, etc.) were interpreted with respect to specific absorption features. The primary objective of the interpretation was to determine whether specific absorption features allow for the unambiguous identification of individual compounds and chemical groups in remote sensing applications, as well as to identify similarities between contaminants and related (non-contaminant) materials, and to determine detection of limits in different soil types at different moisture levels.

The result is a description of the possibilities and restrictions of the detection, detection limits and discrimination of organic contaminants in soils by means of imaging spectrometry remote sensing. In addition, a comprehensive spectral library is compiled, consisting of about 100 different chemicals (contaminants), seven different soils, related anthropogenic materials, and contaminated soils with twelve different contaminants in seven different soil types and at three moisture levels for remote sensing applications.

Spectral characteristics of major groups of organic chemicals

A first step in this process included an investigation of the absorption features of the major organic chemical classes, particularly focusing on fuel hydrocarbons. For basic organic compounds, like alkanes and aromatics, six wavelength regions with major absorption features could be identified at around 900 nm, 1,200 nm, 1,380 nm, 1,700 nm, 2,150 nm, and 2,300 nm. Usually, the first three exhibit only weak to medium absorption features, while the latter three are typically strong absorption features. Except for in the 2,150 nm wavelength region, where only aromatics and not aliphatics exhibit absorption features, both aliphatics and aromatics exhibit absorption features in these regions. However, the absorption features of aliphatics and aromatics in these regions are typically distinct with respect to the minimum position of an absorption feature, its width (FWHM) and its intensity. For alkanes (aliphatic C-H-stretch), the absorption feature in the 900 nm region the minimum is observed between 914 nm and 930 nm wavelength. The corresponding absorption feature of aromatics (aryl-C-H-stretch) is shifted by about 40 – 50 nm towards shorter wavelengths and can be observed between 870 nm and 880 nm. The absorption feature of aromatics is usually more intense compared to that of aliphatics but sharper (smaller FWHM). Likewise, a shift towards shorter wavelengths by about 50 – 60 nm is observed in the 1,200 nm region where aliphatics typically exhibit absorption features between 1,190 and 1,210 nm, and aromatics exhibit absorption features between 1,140 and 1,150 nm. In the 1,380 nm wavelength region, absorption features of aromatics are observed at both longer and shorter wavelengths than those

of aliphatics (at around 1,390 nm). However, because these absorption features overlap with the prominent, intense absorption bands of liquid water and water vapor. Therefore, this absorption feature is not suitable for both field spectrometry and remote sensing applications.

A similar spectral behavior is observed for the strong absorption feature at around 1,700 nm. The absorption feature minima of aromatic compounds are shifted by about 25 – 65 nm towards shorter wavelengths (1,670 nm – 1,700 nm) compared to aliphatics (around 1,725 nm).

The strong and relatively sharp absorption feature at around 2,150 nm is observed only for aromatic compounds. The absorption feature at around 2,300 nm shows a reverse behavior with a small shift of about 10 – 20 nm towards longer wavelengths.

Another absorption feature that is only observed for aromatics is the aromatic C=C-stretch absorption feature between 2,400 nm and 2,500 nm that is about 100 nm wide. However, this feature is often superimposed by stronger and broader aliphatic C-H-stretch absorption features of substituted alkyl groups or aliphatics in mixtures with aromatics (strong, broad absorption feature with a minimum at around 2,305 nm extending from 2,200 nm to well beyond 2,500 nm).

Table 6-11 compares the absorption features of basic aliphatics (alkanes) and aromatics in the six wavelength regions discussed above with respect to the position of the absorption feature minimum, the full-width-at-half-maximum (FWHM) of the absorption features and its intensity (W – weak, M – medium, S – strong).

Table 6-11: Characteristic differences of aromatics and aliphatics in the absorption feature wavelength regions.

	900 nm Region			1,200 nm Region			1,380 nm Region		
	Min. [nm]	FWHM [nm]	Inten -sity	Min. [nm]	FWHM [nm]	Inten -sity	Min. [nm]	FWHM [nm]	Inten -sity
ALIPHATICS	914-930	20-30	W	1191-1208	20-60	M	1388-1391	50-90	W-M
AROMATICS	872-878	10-20	W-M	1139-1148	20-80	M-S	1381-1410	70-160	W-M

	1,700 nm Region			2,150 nm Region			2,300nm Region		
	Min. [nm]	FWHM [nm]	Inten -sity	Min. [nm]	FWHM [nm]	Inten -sity	Min. [nm]	FWHM [nm]	Inten -sity
ALIPHATICS	1723-1725	90-110	M-S	-	-	-	2300-2309	250	S
AROMATICS	1670-1700	30->300	S	2140-2180	70-80	S	2320-2330	250	S

Figure 6-2 depicts the spectra of n-octane, benzene and xylene, illustrating individual absorption features, the shifts of common absorption features of both groups and the combinations of the absorption features in xylene, a monoaromatic compound substituted with two methyl groups (here: spectrum of a mixture of the three isomers ortho-, meta- and para-xylene).

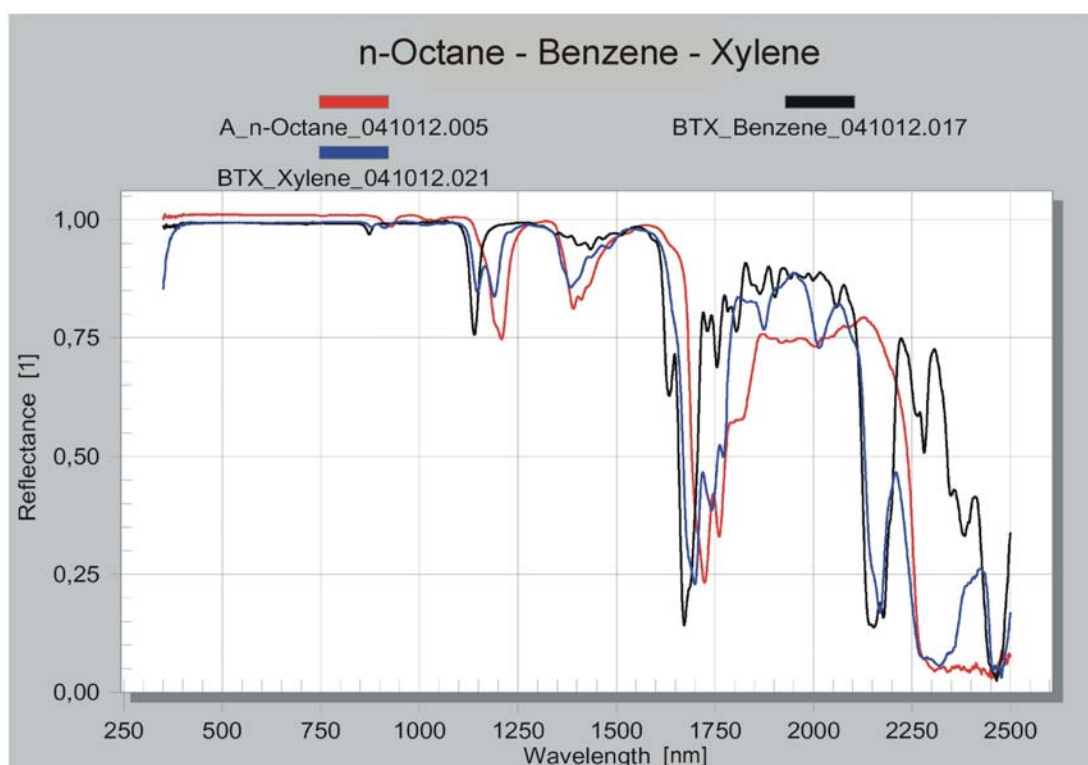


Figure 6-2: Spectra of n-octane, benzene and xylene illustrating characteristic absorption feature differences.

While different substituted monoaromatics have been shown to be distinct in spectra in the 350 nm to 2,500 nm wavelength region, it has been found impossible to discriminate different alkanes (n-hexane, n-heptane, n-octane) in these spectra. However, different groups of aliphatics (alkanes, alkenes, alkynes) and many functional groups (alcohols, substituted chlorine, nitro-groups, and aldehydes) have been found to exhibit distinct absorption features that allow for the determination and discrimination of different functional groups. Table 6-12 summarizes the results obtained with respect to spectral absorption features that allow for an identification of structural groups of organic chemicals in 0.35 μm – 2.5 μm spectra. Figures 6-3 and 6-4 illustrate the distinguishing absorption features of several functional and structural groups of organic compounds.

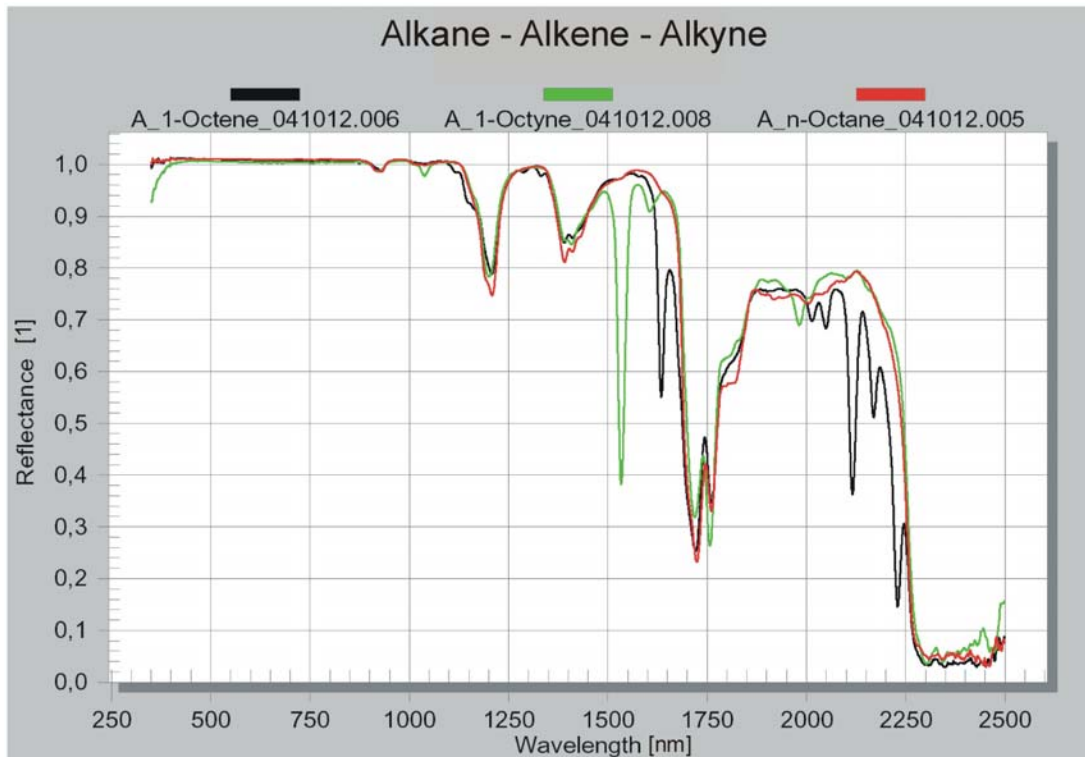


Figure 6-3: Spectra of alkanes, alkenes, and alkynes (n-octane, 1-octene, and 1-octyne, respectively).

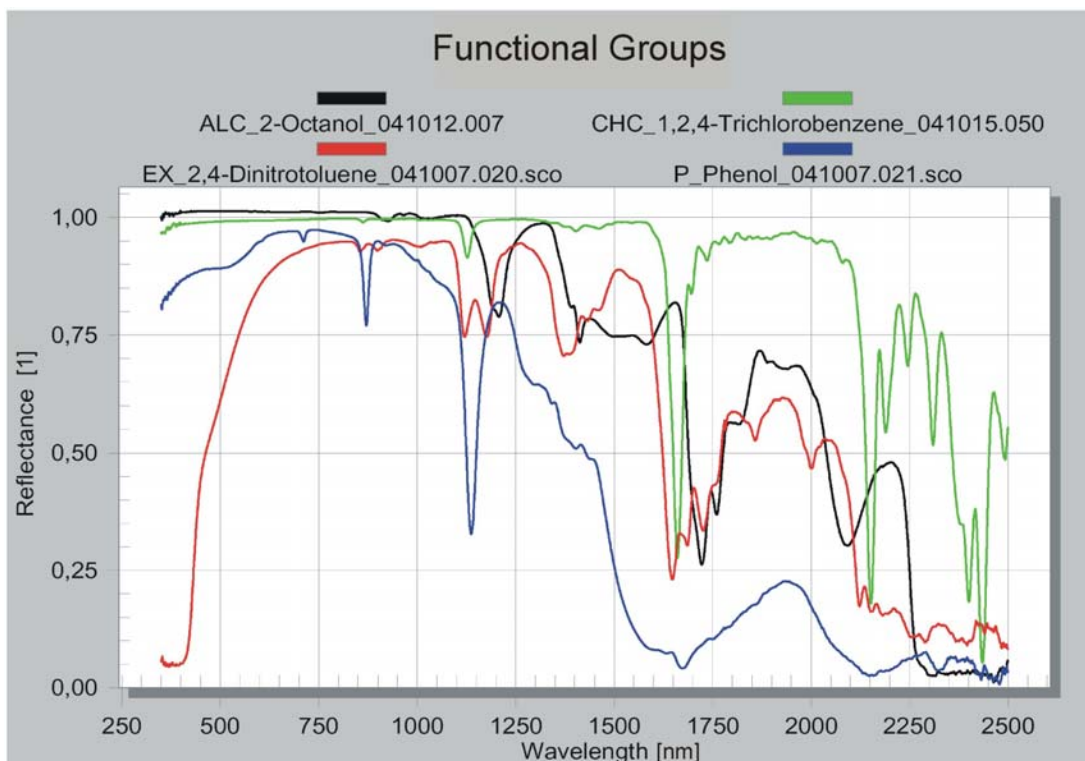


Figure 6-4: Spectral characteristics determined by functional groups (-OH, -Cl, -NO₂)

Table 6-12: Characteristics absorption features of functional groups compared to basic organic compounds.

<i>Group</i>	Characteristic Absorption Features of Functional Groups Compared to Basic Compounds (Alkanes & Monoaromatics)
C=C (Alkenes)	<ul style="list-style-type: none"> sharp, strong absorption features at 1,634 nm, 2,115 nm and 2,230 nm
C≡C (Alkynes)	<ul style="list-style-type: none"> 1,533 nm sharp, strong absorption feature
OH (Alcohols)	<ul style="list-style-type: none"> broad, intense absorption feature between 1,400-1,650 nm relatively broad (FWHM 100 – 150 nm), strong absorption feature at 2,070 – 2,090 nm, in aromatic compounds (phenols) overlapping with 2,150 nm absorption feature
CHO (Aldehydes)	<ul style="list-style-type: none"> 1,390 nm alkyl-C-H absorption feature shifted towards longer wavelengths (~1,420 nm), overall reflectance decreased by ca. 5 % in the 1,420 - 1,600 nm region compared to alkanes Sharp absorption feature of medium intensity at 2,200 nm, overall reflectance decreased by approx. 10 – 15 % in the 2,000 nm to 2,250 nm region compared to alkanes
CO	<ul style="list-style-type: none"> Weak to medium, but sharp absorption features at around 1,930 – 1,950 nm and 2,120 – 2,160 nm, in organic acids superimposed by OH-absorption features
Aryl-NO₂ (Explosives)	<ul style="list-style-type: none"> absorption feature doublets at 865 nm + 905 nm and at 1,130 nm + 1,185 nm broad, intense absorption feature around 1,400nm, more pronounced than similar absorption feature of aliphatics and aromatics C-NO₂ absorption feature (1,640 – 1,690 nm) shifted towards shorter wavelengths compared to C-H absorption features (~1,700 - 1,724 nm), generally broader than that of C-H
Alkyl-Cl	<ul style="list-style-type: none"> Alkyl-Cl absorption feature (1,150 nm & 1690 nm) shifted towards shorter wavelengths compared to comparable alkane C-H absorption features (~1,200 nm & 1,724 nm) Alkyl-Cl absorption feature around 1,410 – 1,430 nm, shifted towards longer wavelengths compared to Alkyl-H (~ 1,390 nm) One or more sharp absorption features (FWHM 50 – 80 nm) in the 2,200 – 2,500 nm wavelength region rather than broad absorption features as observed for alkanes
Aryl-Cl	<ul style="list-style-type: none"> Aryl-Cl absorption feature (1,127-1,139 nm) shifted towards shorter wavelengths compared to Aryl-H absorption feature at 1139 nm Aryl-Cl (1,660-1,667 nm) absorption feature shifted towards shorter wavelengths compared to Aryl-H absorption feature at 1,673 nm nm 2,150 nm absorption feature of Aryl-Cl sharper than Aryl-H absorption feature

Spectral uniqueness of organic contaminants and other materials

Also under investigation was the ability to distinguish between chemical compounds occurring as soil contaminants in the environment from natural and synthetic materials containing hydrocarbon compounds. For this purpose, the spectra of aliphatics and aromatics were compared to the spectra of hydrocarbon-bearing materials such as paper, plastics (polymers of aliphatics or aromatics), rubber, paints and natural materials such as wood, bark and cotton. The six wavelength regions around 900 nm, 1,200 nm, 1,380 nm, 1,700 nm, 2,150 nm and 2,300 nm were the focus of this investigation because the major characteristic absorption features of organic compounds in general and fuel hydrocarbons in particular are observed in these regions.

As expected, plastics consisting of either aromatic or aliphatic compounds were found to exhibit absorption features in the same wavelength regions as liquid or solid aliphatics and aromatics. Usually, the absorption features of plastics were found to be much stronger and often also sharper than those of the chemical compounds, in particular in the 1,200 nm, 1,380 nm, and 1,700 nm regions. Remarkably, it was also observed that the position of absorption features of plastics consisting of aromatic compounds were found to coincide with those of aliphatic chemical compounds; and the absorption features of plastics consisting of aliphatic chemical compounds coincided with those consisting of aromatic chemical compounds. Rubber types were found to behave spectrally similar to (aliphatic) plastics with usually somewhat lower intensities of absorption features.

The comparison of aliphatic and aromatic compounds spectra with spectra of paper, cardboard, wood, bark, cork, and cotton showed that single absorption features of hydrocarbon-bearing compounds coincide with single absorption features of the chemicals. However, while some materials had some similarities with one absorption feature (e.g., the spectra of cork and aliphatics match at around 1,725 nm and 2,305 nm), the overall spectra were found to be distinct and no complete or near-complete matches of whole spectra or all major absorption features were observed. Usually, the absorption features of these natural materials were also found to be weaker but at the same time sharper than those observed for the chemical compounds. Generally, the hydrocarbon absorption features at around 900 nm and 1,200 nm are observed as strong absorption features for all natural and synthetic materials consisting of hydrocarbons or containing large fractions of hydrocarbons. These absorption features do not appear in the spectra of hydrocarbon contaminated soils and are therefore a distinguishing feature of separate natural and synthetic hydrocarbon bearing materials (plastics, wood, paper, etc.) from hydrocarbon contaminated soils. In this context it should be noted that pure solid or liquid organic chemicals do exhibit similar absorption features.

It also should be noted that a number of dark hydrocarbon-bearing materials were found to exhibit virtually no characteristic absorption features and only reflect a small fraction of the incident radiation over the whole wavelength region sampled

(0.38 μm – 2.5 μm), even though they were known to consist mainly of aliphatics and aromatics as basic compounds. This was found in particular for gray and black rubber materials, black plastics and dark paints. As the behavior is similar to that observed for pure black carbon such as graphite, coal and activated carbon, it can be assumed that lampblack used as a coloring agent in these materials absorbs electromagnetic radiation at a constant rate over the whole sampled wavelength region.

Table 6-13 summarizes the findings of the comparison of contaminant spectra with hydrocarbon-bearing materials of anthropogenic and natural origin.

Table 6-13: Comparison of absorption features of natural and man-made hydrocarbon bearing materials and hydrocarbon compounds.

	900 nm Region			1,200 nm Region			1,380 nm Region			1,700 nm Region			2,150 nm Region			2,300nm Region		
	Min. [nm]	FWHM [nm]	Intensity	Min. [nm]	FWHM [nm]	Intensity	Min. [nm]	FWHM [nm]	Intensity	Min. [nm]	FWHM [nm]	Intensity	Min. [nm]	FWHM [nm]	Intensity	Min. [nm]	FWHM [nm]	Intensity
ALIPHATICS	914-930	20-30	W	1191-1208	20-60	M	1388-1391	50-90	W-M	1723-1725	90-110	M-S	-	-	-	2300-2309	250	S
AROMATICS	872-878	10-20	W-M	1139-1148	20-80	M-S	1381-1410	70-160	W-M	1670-1700	30->300	S	2140-2180	70-80	S	2320-2330	250	S
PAPER	-	-	-	1200-1210	40	W	-	-	-	-	-	-	-	-	-	2330	40-60	W-M
PLASTICS ALIPHATICS	910-930	20-30	M	1190-1210	20-60	S-M	1390-1420	50-100	M-S	1720-1730	100-150	S	-	-	-	ca. 2310	200	S
PLASTICS AROMATICS	875	10-20	M	1143	20-40	W-M	ca. 1410	50-100	S-M	ca. 1680	50-150	M-S	ca. 2165	50-100	M-S	ca. 2310	100-200	S
RUBBER	-	-	(W)	1200-1210	50-80	M	1390-1420	80-100	M	1720-1730	ca. 100	M-S	-	-	(W)	ca. 2310	100-250	M-S
NATURAL MATERIALS	-	-	M	ca. 1210	50-100	W-M	ca. 1370	20-40	W	ca. 1725	50-80	W-M	ca. 2100	50-100	W-M	ca. 2303	100-200	M-S
				(cork, cotton, wood)			(cotton, wood)			(cork, wood)			(cotton, wood)			(cork, wood)		
PAINTS	-	-	-	1190-1220	50-70	W	-	-	-	1700-1720	50-80	W-M	ca. 2139	50	(W)	2264 / 2304	250	M-S

W – weak (1..10 % rel. absorption), M – medium (10 .. 40 % rel. absorption), S – strong (> 40 % rel. absorption)

Spectral characteristics of selected soil contaminants

The spectra of the contaminants selected for the soil contamination experiments can be distinguished in three major groups. The first group of fuel hydrocarbons, comprising n-octane, diesel, kerosene, crude oil and waste oil, is dominated by aliphatic compounds. This becomes evident when comparing the spectrum of n-octane to those of the other fuel hydrocarbons. However, diesel, kerosene and crude oil seem to contain small fractions of aromatic hydrocarbons, which is indicated by a small absorption feature that appears at 2,150 nm in the spectra characteristic for aromatic hydrocarbons. The 1,200 nm absorption feature of diesel and kerosene also exhibits a shoulder in the aliphatic C-H-stretch overtone absorption below 1,200 nm. The position of the minimum of this shoulder at around 1,150 nm (i.e., shifted towards smaller wavelengths) indicates that the small overlapping absorption feature is caused by aromatics, probably small quantities of monoaromatics and/or naphthalene in these fuel hydrocarbons. The spectra of n-octane and the fuel hydrocarbons used for the soil contamination experiments are depicted in figure 6-5.

The second group comprises xylene and naphthalene, a monoaromatic compound substituted with two alkyl (methyl) groups, naphthalene, a two-ring polynuclear aromatic hydrocarbon and 1-acetylnaphthalene, a naphthalene molecule substituted with an acetyl (COCH₃) group. However, as discussed above, C=O groups exhibit only minor absorption features in spectra in the visible, near infrared and shortwave infrared wavelength regions and therefore resemble the spectrum of the basic compound, in this case naphthalene. Because of this, and because 1-acetylnaphthalene is, in contrast to naphthalene, a liquid compound and therefore easier to handle, 1-acetylnaphthalene was selected for the experiments. Comparing the spectra of the three compounds it is obvious that xylene unites both the absorption features of aliphatics and aromatics. The spectrum is dominated by the aromatic absorption features with minima at 1,149 nm, 1,705 nm, and 2,168 nm. The aliphatic absorption features however, are also pronounced, with absorption feature minima at 1,190 nm, 1,743 nm, and 2,320 nm. A shift of the aliphatic absorption features towards longer wavelengths (e.g., 1,725 nm → 1,743 nm) is obvious. Comparing the spectra of the two polynuclear aromatic compounds, naphthalene and 1-acetylnaphthalene to the spectrum of xylene shows that the aromatic absorption features are generally shifted further towards shorter wavelengths in polynuclear compounds (e.g., 1,147 nm for xylene compared to 1,140 nm for naphthalene and 1-acetylnaphthalene, 1,698 nm compared to 1,680 nm, and 2,168 nm compared to 2,150 nm - 2,153 nm, respectively). Furthermore, it is observed that the absorption features of the solid naphthalene (clear crystals) are much stronger than the absorption features of the dual-pass through one millimeter of liquid 1-acetylnaphthalene. The same effect was observed for solid phenol and liquid 2,4-dimethylphenol (see below). The spectra of xylene, naphthalene and 1-acetylnaphthalene are depicted in figure 6-6.

The third group comprises aromatics that have been substituted with either only functional groups (-OH, -NO₂, -Cl) or functional groups and alkyl rests. Namely, solid phenol, liquid 2,4-dimethylphenol, liquid 2,4-dinitrotoluene, and liquid

1,2,4-trichlorobenzene have been selected and investigated in this group. The spectra of these compounds are, along with the spectrum of xylene as a reference, depicted in the figures 6-7 and 6-8. The aliphatic and aromatic absorption features of 2,4-dimethylphenol are almost identical with those of xylene, which is hardly surprising since both comprise a benzene ring with two substituted methyl groups. However, the aromatic absorption features of 2,4-dimethylphenol are slightly weaker than those of xylene, probably due to the reduced number of aryl-H-stretches (four in xylene, three in 2,4-dimethylphenol). Additionally, 2,4-dimethylphenol exhibits two strong and broad absorption features with minima at 1,440 nm and 2,160 nm, covering the wavelength regions between 1,390 nm – 1,630 nm and 1,890 nm – 2,160 nm, respectively. The 1,390 nm – 1,630 nm absorption feature comprises both the dominating O-H stretch absorption feature (first overtone) with a minimum at 1,440 nm and a weaker, unexplained absorption feature that expresses itself in a shoulder in the O-H stretch absorption feature at around 1,550 nm. The second large absorption feature between 1,890 nm and 2,160 nm obviously also consists of two combined absorption features. Also, the 2,150 nm aromatic absorption feature is overlapping with this absorption feature. Solid phenol exhibits the same absorption features as 2,4-dimethylphenol, which are more pronounced. In addition, a third broad and strong absorption feature appears in the spectrum of solid phenol in the 1,450 nm – 1,950 nm region, fully overlapping with the hydrocarbon absorption feature around 1,700 nm.

Compared to the spectrum of xylene, the major aromatic C-H absorption features in the spectra of both 2,4-dinitrotoluene and 1,2,4-trichlorobenzene are considerably shifted towards shorter wavelengths. In contrast to aromatics substituted with alkyl groups, 2,4-dinitrotoluene absorbs electromagnetic radiation beyond 2,100 nm almost completely and does not exhibit the characteristic aromatic 2,150 nm absorption feature. The 1,200 nm, 1,380 nm and 1,700 nm absorption features clearly exhibit characteristic aromatic absorption features. At the same time, these absorption features are stronger and broader than those of alkyl-substituted aromatics. Also, an increased absorption in the 1,750 nm to 2,100 nm region is observed while the overall shape remains similar to that of alkyl-substituted aromatics. 1,2,4-trichlorobenzene exhibits, although only half of the molecules' hydrogen atoms are substituted by chlorine atoms, sharp, single absorption features at 1,126 nm, 1,660 nm, 2,150 nm, 2,400 nm, and 2,435 nm. The 1,380 nm absorption feature is very weak. Besides the two absorption features mentioned above, the 2,000 nm – 2,500 nm wavelength region comprises several sharp absorption features of medium strength.

The hydrocarbon absorption features including the characteristic shifts of all selected contaminants for the soil contamination experiments are summarized in table 6-14 (absorption features of basic aliphatic and aromatic compounds). The absorption features of the functional groups are summarized in table 6-12 (see above).

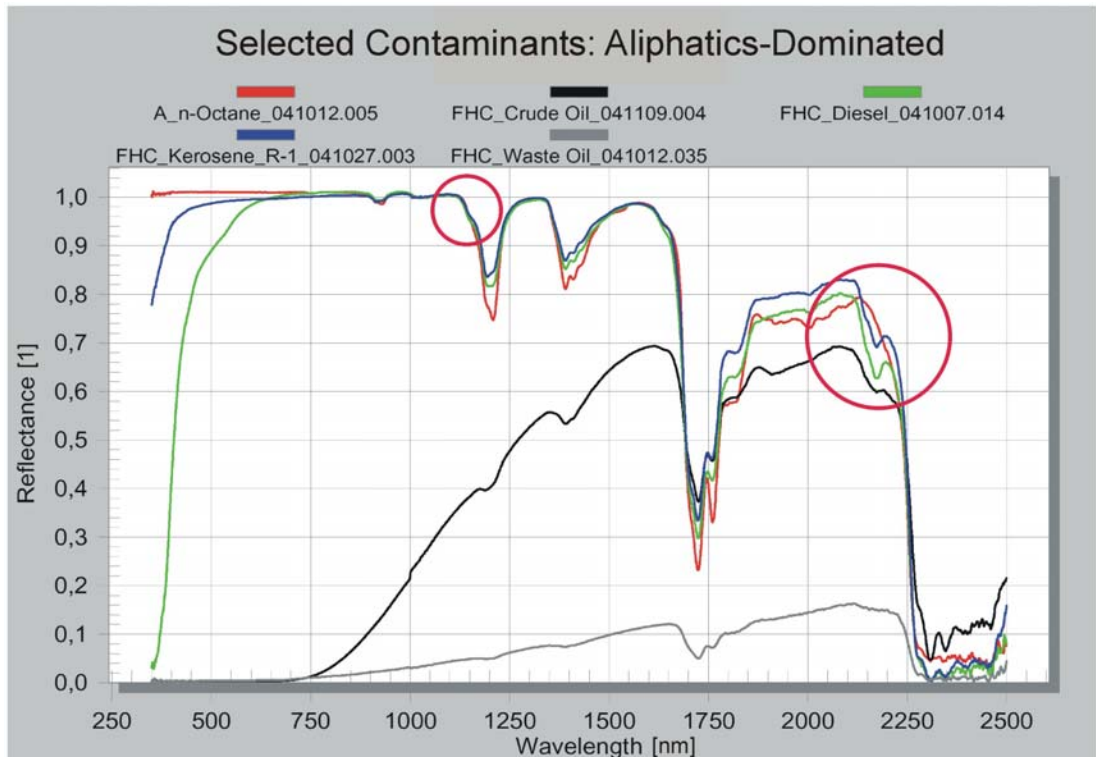


Figure 6-5: Spectra of aliphatics-dominated contaminants selected for the experiments. The circles indicate minor aromatic absorption features observed in the spectra of the fuels, hinting at small fractions of aromatics.

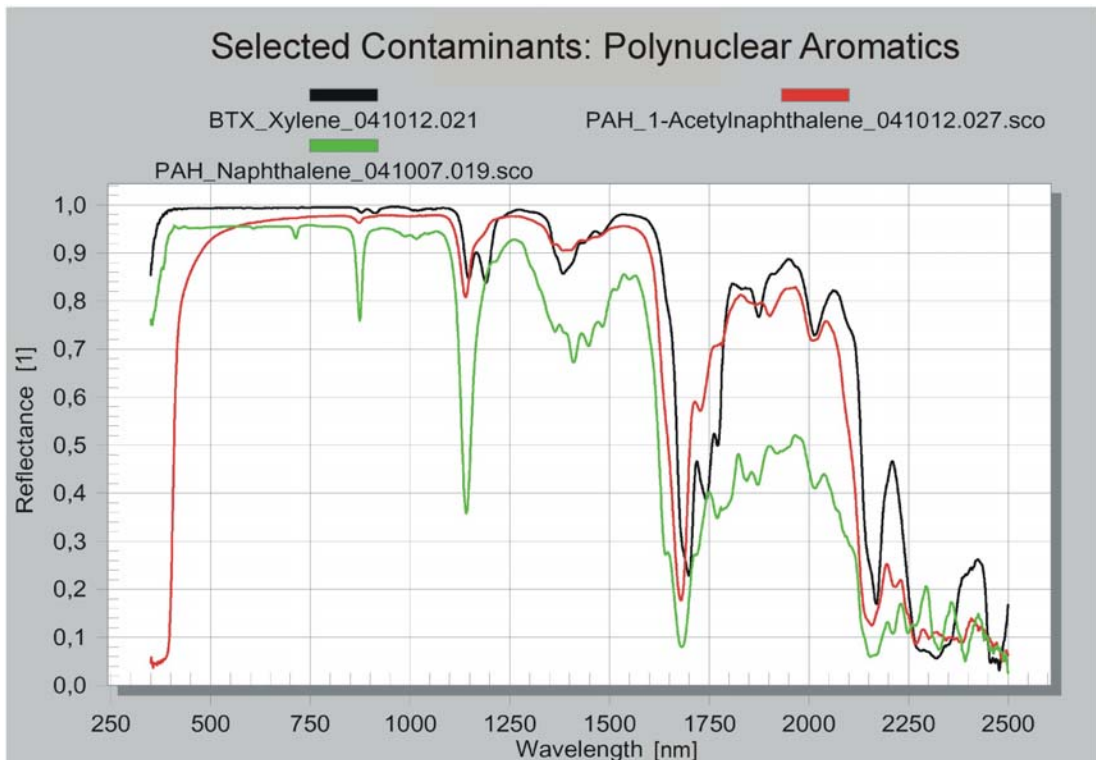


Figure 6-6: Spectra of the aromatic contaminants selected for the experiments, namely xylene, naphthalene and 1-acetylnaphthalene.

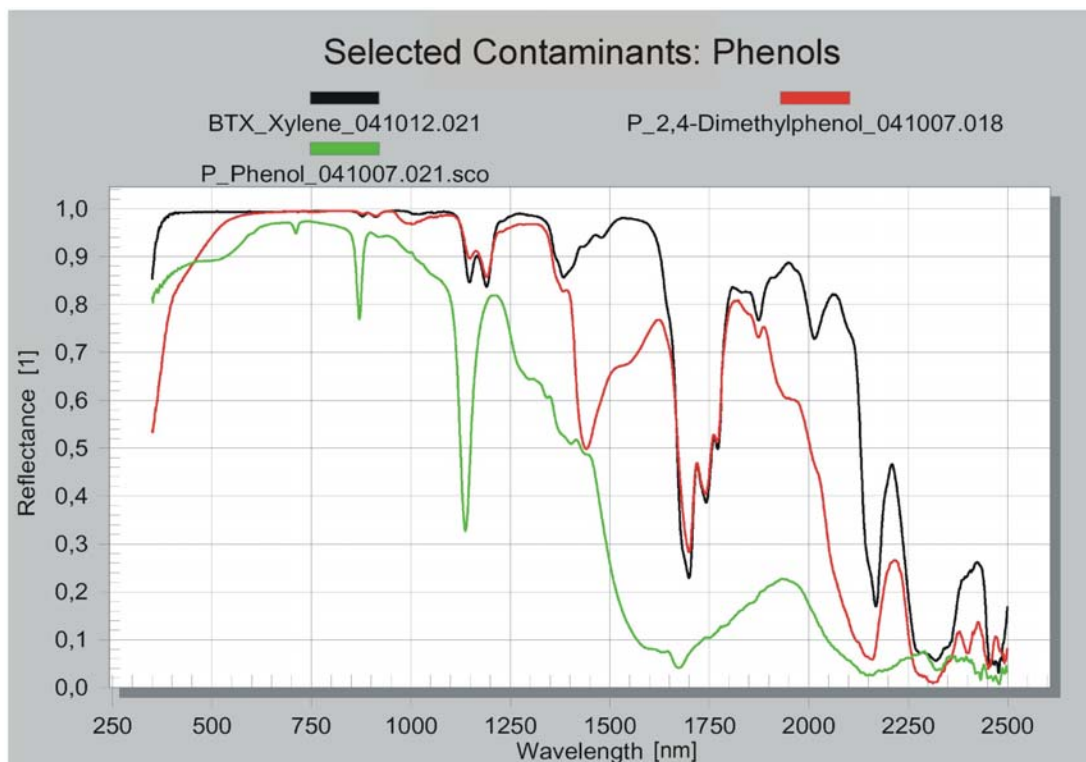


Figure 6-7: Spectra of phenol (solid) and 2,4-dimethylphenol (liquid), selected as contaminants, compared to the spectrum of xylene.

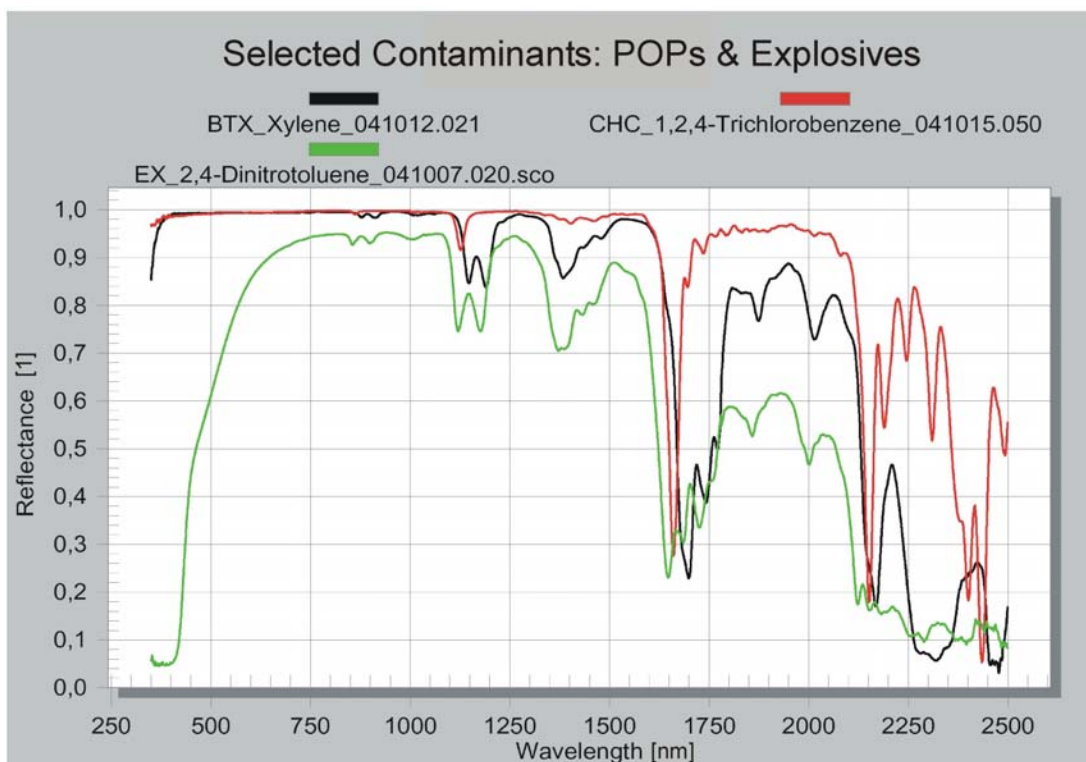


Figure 6-8: Spectra of 1,2,4-trichlorobenzene and 2,4-dinitrotoluene, also selected as contaminants, compared to the spectrum of xylene.

Table 6-14: Exact location of aliphatic and aromatic absorption features of the selected contaminants.

	900 nm Region			1200 nm Region			1380 nm Region			1700 nm Region			2150 nm Region			2300nm Region		
	Min. [nm]	FWHM [nm]	Inten-sity	Min. [nm]	FWHM [nm]	Inten-sity	Min. [nm]	FWHM [nm]	Inten-sity	Min. [nm]	FWHM [nm]	Inten-sity	Min. [nm]	FWHM [nm]	Inten-sity	Min. [nm]	FWHM [nm]	Inten-sity
OCT	930	20	W	1208	50	M	1390	80	M	1723	90	S	-	-	-	~2300	250	S
DIS	921	30	W	1196	55	M	1390	85	M	1724	100	S	2172	50	W	2309	250	S
KER	914	25	W	1193	60	M	1391	90	M	1723	90	S	2172	30	W	2309	250	S
CRO	-	-	-	1191	30	W	1390	70	W	1725	110	M	2172	40	W	2309	250	S
WO	-	-	-	1191	20	W	1388	50	W	1724	90	M	-	-	-	~2300	250	S
XYL	878/ 912	10-20	W	1147/ 1189	80	M	1383	80	M	1698	50	S	2168	50	S	2319	> 150	S
NAP	874	14	M	1141	35	S	1409	160	M	1680	110	S	2153	> 100	S	2362/ 2391	250	S
ANA	873	30	W	1140	32	M	1383	110	W	1680	60	S	2150	60	M	2270	250	S
DMP	-	-	-	1148/ 1192	80	M	1440	150	M	1700	110	S	2158	> 100	S	2316	250	S
DNT	855/ 890	20	W	1120/ 1176	80	M	1371	> 100	M	1647	150	S	2000	50	M	2288	300	S
PHE	870	15	M	1136	35	S	-	-	-	1674	> 300	S	2150	> 200	S	2200- 2500	300	S
TCB	-	-	-	1125	20	W	-	-	-	1660	30	S	2150/ 2190	25/30	S/M	2309	20	M

W – weak (1..10 % rel. absorption), M – medium (10 .. 40 % rel. absorption), S – strong (> 40 % rel. absorption)

Spectral characteristics of selected soils

The soil types selected for the soil contamination experiments can be distinguished into three groups: quartz-dominated sand soils, clays, and organic matter dominated soils. The spectra of dry and moist soils, their characteristic absorption features and similarities will be discussed subsequently.

Dry soil spectra

The spectra of dry soils (oven-dried at 105°C for 24hrs), depicted in figure 6-9, exhibit absorption features that result from the soil mineralogy, soil organic matter and iron content, and adsorbed, crystal water in the soil matrix that is not evaporated when heated to 105 °C.

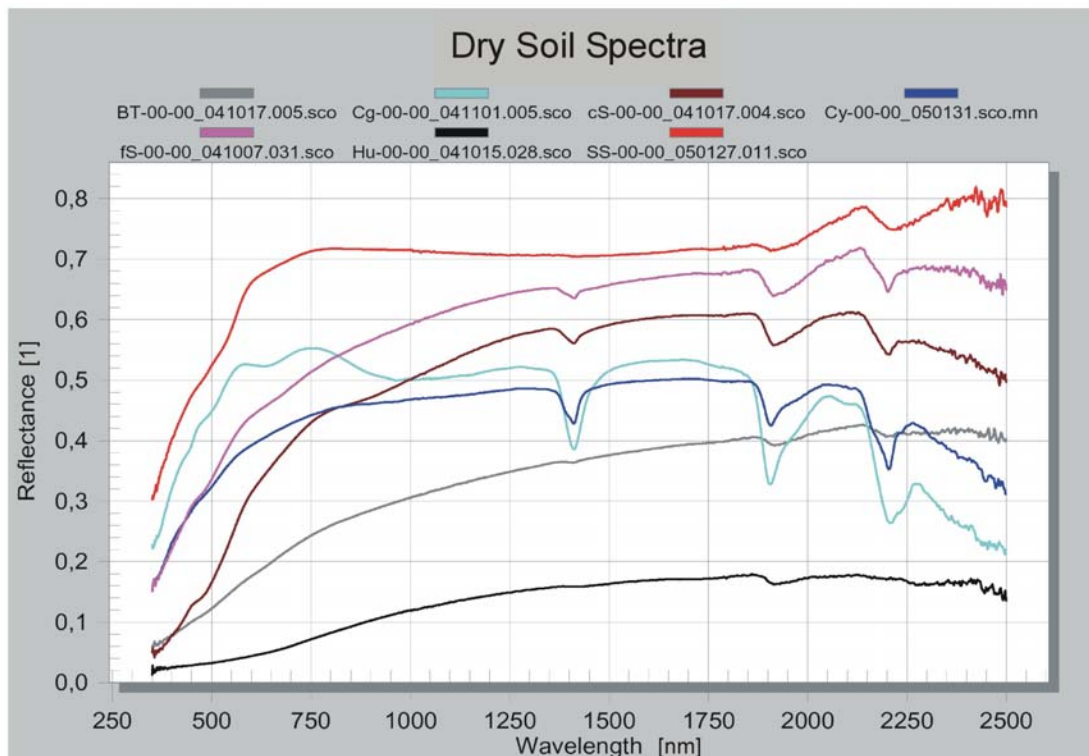


Figure 6-9: Spectra of the seven soils selected for the experiments (dried soils).

The spectra of all dry and moist soils have in common that the reflectance generally increases throughout the visible wavelengths up to 750 nm - 1,000 nm, reaching a more or less flat plateau in the near infrared wavelength regions beyond 1,000 nm and decreasing beyond 2,200 nm towards 2,500 nm. Exceptions from this general spectral behavior are soils that are dominated by soil organic matter (exhibiting a positive slope throughout the spectrum), and pure silica sand (sea sand), which exhibits a positive slope beyond 2,200 nm.

The highest overall reflectance is observed for yellowish-white sea sand, with a reflectance of circa 70 % in the infrared. Fine and coarse sand, both containing some iron, finer materials and organic matter, show an overall reflectance between 55 % and 65 % in the infrared. Similarly, both clays reflect about 50 % of the incident radiation in the infrared with reflectance decreasing considerably beyond 2,100 nm. Boulder till and humic soil, both having their spectral behaviors determined by larger quantities of soil organic matter, show an overall increasing reflectance from the visible towards the shortwave infrared. The reflectance of boulder till increases from about 5 % at 350 nm to a maximum of 42 % at 2,140 nm, decreasing only slightly beyond this wavelength range. The reflectance of humic soil shows a similar behavior, but on a lower level, increasing from about 2 % at 300 nm to 18 % at 2,120 nm.

All dry soil spectra have a water absorption feature at 1,915 nm in common. The second important water absorption feature at 1,417 nm is evident in all dry soils except for sea sand. It can be assumed that only very low quantities of adsorbed or crystal water remained on the sea sand (pure silica) soil particles, thus only exhibiting the generally stronger water absorption feature at 1,915 nm. However, for boulder till and humic soil, the absorption feature in the 1,400 nm region is very weak, probably due to masking effects by dark material (soil organic matter). These are similar to those masking effects observed in dark plastics and rubber, where pure carbon reduced the overall absorption to a relatively even level while at the same time masking all absorption features. Fine and coarse sand and both clay types exhibit relatively strong water absorption features, hinting at crystal water in the samples.

Mineral absorption features in the soils selected are limited to the 2,100 nm to 2,300 nm wavelength range. The three sands (SS, fS, cS) and the two clays (Cg, Cy) exhibit relatively strong absorption features, all with a minimum between 2,200 nm and 2,210 nm.

Clay (Cy) exhibits a characteristic absorption feature with a minimum at 2,205 nm and a shoulder in the same absorption feature at 2,165 nm. This absorption feature coincides with that of kaolinite. The absorption feature of clay granulate (Cg) has its minimum at 2,208 nm and a shoulder at 2,231 nm. This absorption feature coincides with that of montmorillonite (based on a comparison with spectral library spectra of clay minerals), a clay mineral known for its swelling capacity and likely to be utilized as cat litter. Both fine sand and coarse sand exhibit a mineral absorption feature with a minimum at 2,202 nm, a broader shoulder towards shorter wavelengths and a steeper one towards longer wavelengths. However, the absorption feature could not be identified uniquely but it can be assumed that small quantities primary and secondary clay minerals, probably muscovite and kaolinite, contribute to this absorption feature because both minerals have an absorption feature with a corresponding minimum and are likely to occur in the two soil samples. The fine sand sample was taken from the same gravel and clay pit as the clay (Cy), which has

been proven to consist mainly of kaolinite and is known to contain mica. The coarse sand is likely to contain muscovite because of its geologic origin.

No mineral absorption feature is observed in the spectrum of humic soil (Hu). Boulder till, even though known to contain larger fractions of clay minerals besides quartz, primary silicate minerals and soil organic matter, exhibits only a weak, minor absorption feature in the 2,100 nm – 2,300 nm wavelength region. As with other absorption features, it must be assumed that the mineral absorption features are masked by the soil organic matter content.

Except for the few absorption features (water, minerals) described above, the (dry) soil samples have been found to exhibit no significant absorption features that interfere with the characteristic absorption features of hydrocarbons. However, smaller shoulders in the increasing reflectance in the visible wavelength regions, in particular observed in coarse sand (cS), can be attributed to iron absorption features but can not be considered major absorption features.

Moist soil spectra

The spectra of the all soil types, two of which (coarse sand and clay), are depicted at different moisture levels in Figures 6-10 and 6-11 have in common that the overall reflectance decreases with increasing moisture content. An exception to this observation is the humic soil sample, which exhibits an increasing reflectance at low to medium moisture contents compared to the reflectance of dry samples which decreases with increasing moisture level.

The two major water absorption features around 1,400 nm and 1,900 nm broaden with increasing moisture content. Their absorption depth also increases relative to overall reflectance. At high moisture contents other smaller water absorption features are observed to appear at around 980 nm, 1,190 nm, and 1,780 nm. Also, the negative slope generally observed beyond 2,200 nm increases.

At the same time, as the moisture content increases, other absorption features (e.g., mineral features) in the spectra are observed to become weaker or even to be extinguished from the spectra completely.

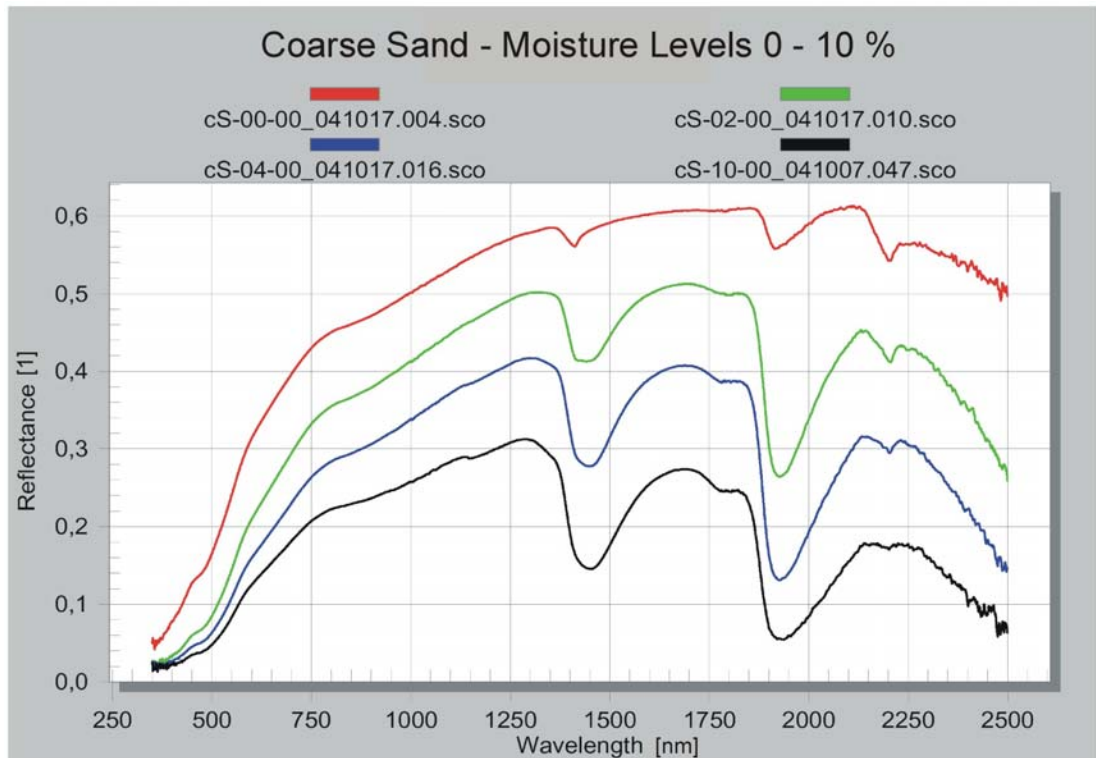


Figure 6-10: Spectra of dry (red) and moist (green, blue, black) coarse sand samples containing 0 %, 2 %, 4 % and 10 % moisture, respectively.

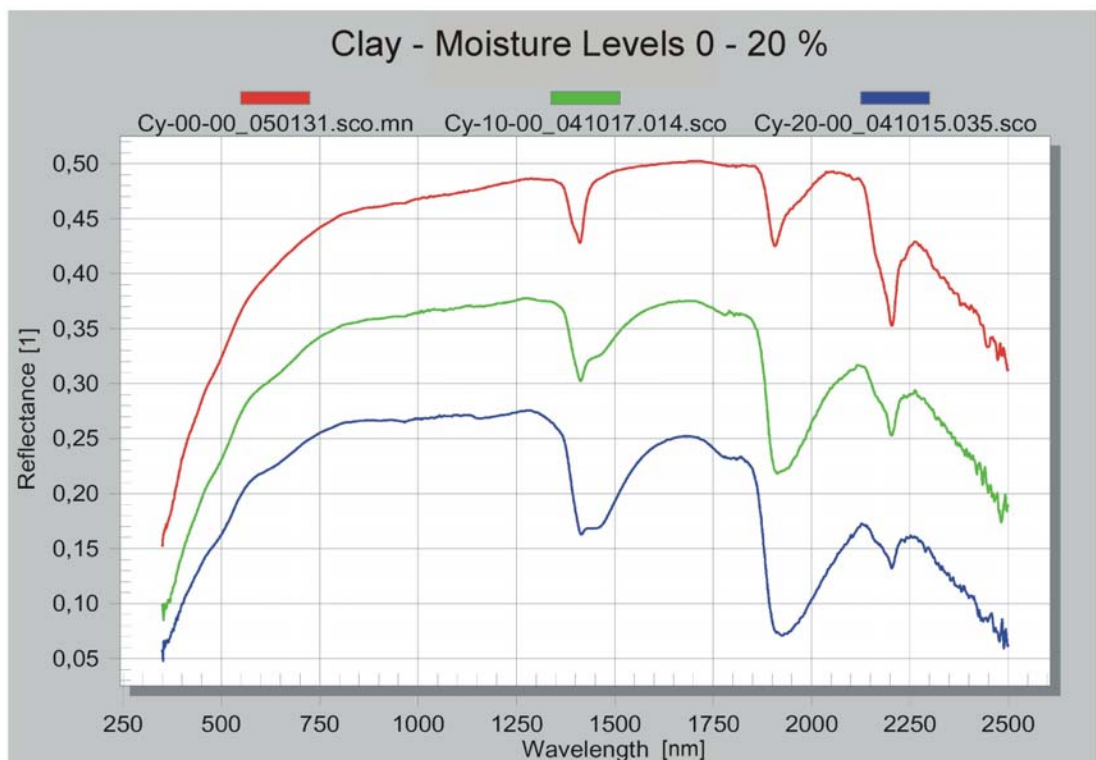


Figure 6-11: Spectra of dry (red) and moist (green, blue) clay samples containing 0 %, 10 % and 20 % moisture, respectively.

Contaminated soil experiments

The spectra acquired of seven different soils at three different moisture levels contaminated with twelve different contaminants at three concentration levels were interpreted with respect to:

- Detection limits in different soils at different soil moisture levels
- Possibilities and limitations of remote sensing quantitative analysis
- The ability to distinguish different groups of contaminants
- The ability to distinguish hydrocarbon-contaminated soils from plastics (wastes) distributed on soil
- The nature of spectral mixing of the components soil and contaminant in dry and moist soils
- The influence of viewing geometry and the ability to reproduce measurements

In a spectral library found on the enclosed CD-ROM and in the Excel files prepared for the interpretation, spectra of all measured soil contaminant concentrations can be found, along with spectra from the contaminants themselves, the dry and moist soils used for the experiments, additional potential contaminants, natural and anthropogenic materials exhibiting properties similar to those of the contaminants or contaminated soils, and a selection of spectra of contaminated media from contaminated sites.

General observations

The overall shape of the contaminated dry and moist soil spectra is usually determined by the spectrum of the respective soil sample, keeping in mind its particular level of moisture. Depending on the contaminant concentration, the overall reflectance of the soil sample and the soil moisture content, the contaminants are found to more or less alter the overall reflectance of the sample and / or the reflectance in the region of their specific absorption features. Noise in the spectra is found to sharply increase with overall decrease in reflectance. In particular the wavelength region beyond 2,200 nm is heavily affected by noise expressing itself in random peaks of usually one or two and up to four percent of total reflectance. The noise ratio is observed to increase towards longer wavelengths. It was also found to be increased by increasing soil moisture contents and overall decreasing reflectance of soil samples, usually due to high content of organic material (“black material”). Noise is generally expected to increase in this wavelength region because the artificial illumination source used for the experiments – like the sun as the illumination source in remote sensing applications – emits comparably low quantities of energy in the wavelength regions beyond 2,000 nm (comparable to the solar irradiation curve, figure 3-2). The noise in this wavelength region thereby obscures

important absorption features of organic chemicals and fuel hydrocarbons in the 2,300 nm and 2,400 nm wavelength region. Between 2,000 nm and 2,200 nm, noise is generally found to equal 0.1 % to 0.5 % of total reflectance. Noise in the other wavelength regions smaller than 2,000 nm is generally found to be smaller than 0.1 % of total reflectance, except for in the case of humic soil, which exhibit an overall reflectance of less than 20 % and thus sharply increased noise levels (see figure 6-12).

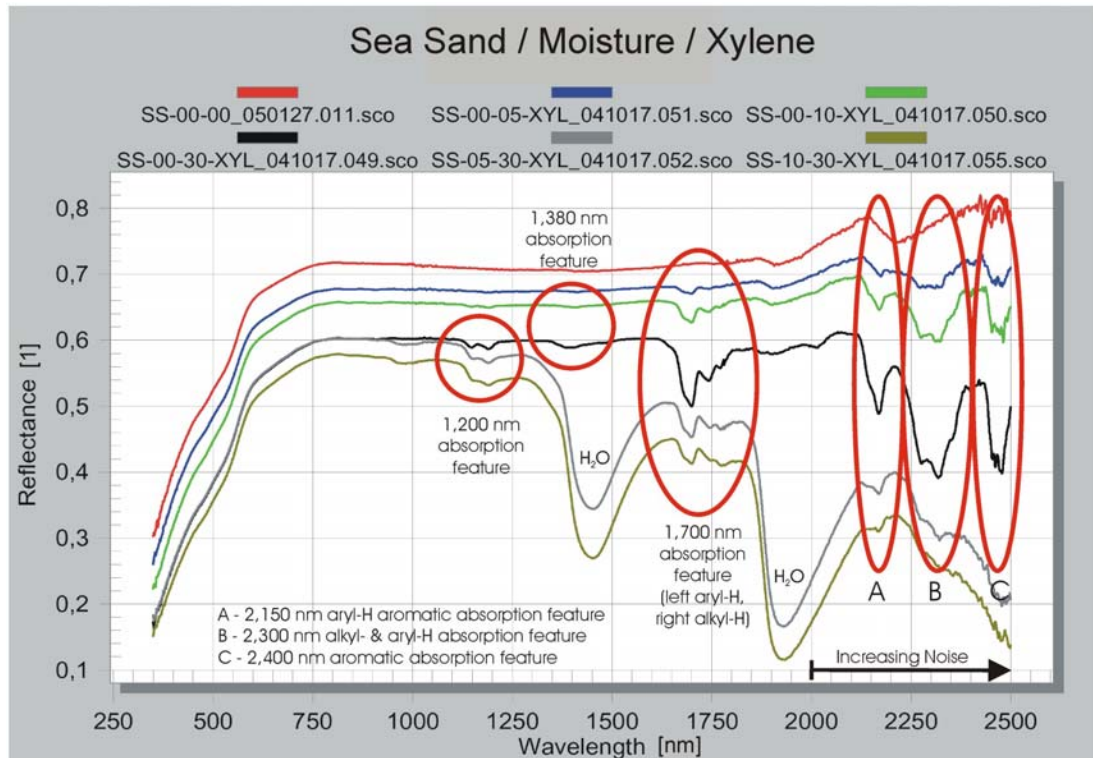


Figure 6-12: Absorption features of xylene at different concentrations in dry and moist sea sand.

In general, liquid and solid contaminants added in increasing concentrations to soil samples of similar moisture contents are found to decrease the overall reflectance of the sample if measured under identical conditions (illumination source, viewing geometry). Exceptions with an unchanged or even increased overall reflectance are rarely observed for solid and liquid contaminants that are added to dark soil types (humic soil, boulder till) or clays. This is obviously due to the formation of crystals or oil films on the soil surfaces, which exhibit a higher reflectance than the pure soil sample. To quantify this effect, the total relative reflectance of spectra was measured at 850 nm, a wavelength region that is typically unaffected by absorption features of organic chemicals. Because the overall reflectance depends on viewing geometry, including sample orientation and sensor viewing angle, as well as the strength of the illumination source and other external factors, the overall change in reflectance caused by contaminants is not a suitable measure to detect and quantify the concentration of a contaminant. However, under certain circumstances it might be used in remote sensing applications to correlate contaminant concentration to overall

reflectance (see below). Tables 6-15 and 6-16 summarize and illustrate the reflectance observed at a wavelength of 850 nm for sea sand and clay at different moisture levels, contaminated with different concentrations of crude oil and diesel fuel, respectively.

Table 6-15: Effects of crude oil contaminations of sea sand on the reflectance intensity (measured at 850 nm) at different moisture and contaminant concentration levels. A general, overall decrease in reflectance is observed.

Contaminant Concentration	Dry	5 % Moisture	10 % Moisture
0.0 %	72 %	62 %	57 %
0.5 %	60 %	54 %	52 %
1.0 %	54 %	48 %	46 %
3.0 %	37 %	38 %	36 %

Table 6-16: Effect of diesel fuel contaminations of clay on the reflectance intensity (measured at 850 nm) at different moisture and contaminant concentration levels. A general, overall decrease in reflectance is observed.

Contaminant Concentration	Dry	10 % Moisture	20 % Moisture
0.0 %	46 %	36 %	27 %
0.5 %	43 %	36 %	23 %
1.0 %	41 %	34 %	22 %
3.0 %	44 %	25 %	18 %

Typically, only the medium and strong absorption features observed in pure contaminant spectra (see table 6-14) can also be observed in contaminated soil spectra. Generally, the weak 900 nm absorption feature observed in pure contaminant spectra is not found in contaminated soil spectra. Both the 1,200 nm and 1,380 nm absorption features that are observed in the spectra of aliphatic and aromatic contaminants are only observed in contaminated soil spectra at high contaminant concentrations or at medium concentrations in dry (oven-dried) contaminated soils. In moist contaminated soil samples, both absorption features overlap with the 1,200 nm and 1,400 nm water absorption bands. While the 1,380 nm absorption feature is generally fully masked by the water absorption band, the 1,200 nm feature is typically found at the edges of the water absorption feature, thus being observable even in moist soil samples. The prominent 1,700 nm and 2,300 nm hydrocarbon absorption features, along with the aromatic 2,150 nm absorption feature, are the strongest absorption feature of organic contaminants observed in contaminated soil samples. Aromatic compounds are also observed to exhibit absorption features in the 2,400 nm region that are, however, often obscured by increased noise levels in this wavelength region.

The minima of contaminant absorption features are generally found to appear at the same wavelength (± 3 nm) as in pure contaminant spectra, i.e. the 1,700 nm feature is

found to appear at wavelengths smaller than 1,700 nm for aromatic compounds and at wavelengths larger than 1,700 nm for aliphatic compounds. This, in turn, allows for an identification of the contaminant group. The same observation can be made for the 2,300 nm absorption feature.

The absorption feature depth is generally found to increase with increasing contaminant concentration in a soil sample. With increasing soil moisture, clay, and organic (“black”) matter content, the total depth of absorption feature caused by similar contaminant concentrations is found to decrease, obviously due to masking effects and contaminant absorption in clay minerals and organic matter.

Aliphatic contaminants (OCT, DIS, KER, CRO, WO) and aromatic compounds that are substituted with alkyl groups (XYL, DNT, DMP) were found to exhibit doublet absorption features at both the 1,700 nm and 2,300 nm absorption features because of both alkyl-H ($\text{CH}_2 / \text{CH}_3$) and aryl-H stretch overtones present in the molecules. The intensity of the two peaks in the doublet was found to depend on the number and relation of alkyl-H and aryl-H present in the molecules. Aromatics that contained no or only minor fractions of substituted alkyl groups (NAP, ANA, PHE, TCB) were found to exhibit single absorption peaks in the 1,700 nm and 2,300 nm absorption feature regions. The 2,150 nm absorption feature was only observed for aromatic compounds and always appears as a single absorption feature. In soils containing secondary silicate minerals, the 2,150 nm aromatic absorption feature was usually observed to overlap with characteristic and strong absorption features of these minerals, thus being obscured by these dominating matrix absorption features. Figures 6-13 and 6-14 illustrate these effects.

Despite the local, intense absorption features in the 2,300 nm wavelength region, all organic contaminants used in the experiments were found to increase the overall absorption in the 2,100 nm to 2,500 nm wavelength region. While the effect was particularly pronounced in dry soils, it was found to decrease with increasing soil moisture and to diminish at high soil moisture levels. The 2,300 nm absorption feature is also observed to diminish with increasing soil moisture and decreasing overall reflectance.

While increasing contaminant concentrations were found to further increase the absorption in the minimum of the water absorption bands, the contaminant concentration was found to have no influence on the width or shape of the water absorption bands. However, as will be discussed later, reflectance in the water absorption bands is not important in remote sensing applications because of the impermeability of the atmosphere in these water (vapor) absorption bands.

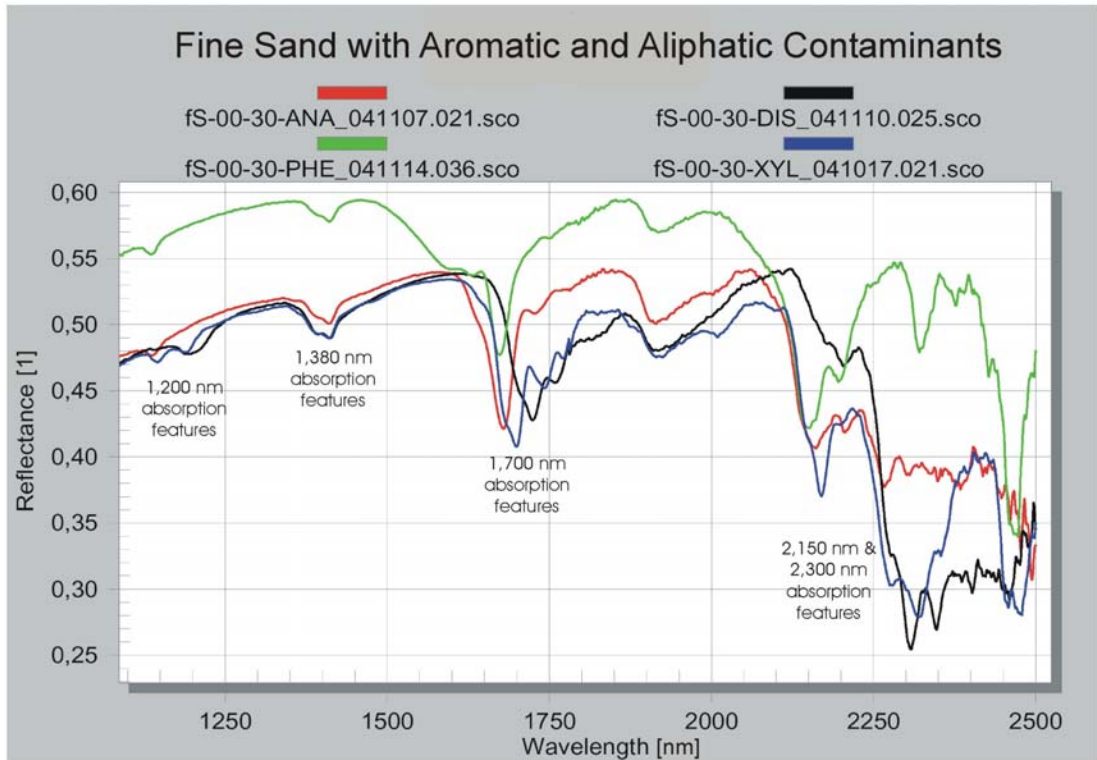


Figure 6-13: Absorption features of different contaminants in dry fine sand. The absorption feature minima appear at the same wavelengths as for pure contaminants (subset of the 1,200 nm – 2,500 nm wavelength region).

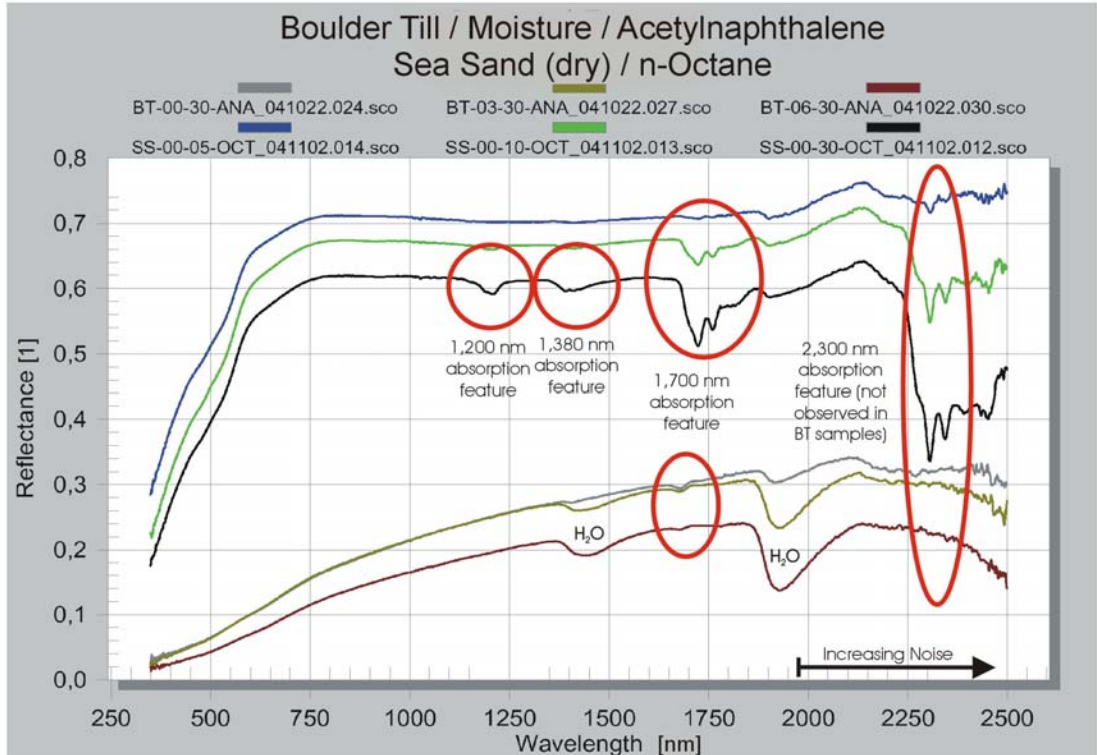


Figure 6-14: Effects of soil moisture and soil type on absorption feature depths. Dry sea sand contaminated with n-octane (0.5%, 1.0%, 3.0%) and boulder till at different moisture levels (0%, 3%, 6%), contaminated with 3 % 1-acetylnaphthalene.

The overall detectability that will be discussed in more detail in the next paragraphs was found to be best in dry, sandy (quartz / primary silicate) soils and was found to decrease with increasing content of secondary silicate (clay) minerals, soil organic matter, and soil moisture. All contaminants were found to be almost undetectable in dry and moist humic soil (Hu) samples in the more than 150 combinations of humic soils with moisture and contaminants investigated.

Spectral mixing behavior of soil / moisture / organic contaminant spectra

For the following discussion addressing the detection limits of fuel hydrocarbon contaminations in dry and moist soils and the prospects of remote quantitative analysis, it is necessary to determine the spectral mixing behavior of fuel hydrocarbon soil contaminations and their single spectral constituents soil, water and hydrocarbon contaminants. As discussed in section 3, linear spectral mixing has been proven to be most common for geological, agricultural and urban applications, as well as vegetation analysis where different materials and surfaces are present in one pixel. Examples include spatially separated units of roofing material, pavement and green vegetation that might be combined in a random pixel from an urban imaging spectrometry scene or mixtures of soil and vegetation in an agricultural imaging spectrometry scene where the vegetation canopy covers the soil only partially. These components covering the surface area of a pixel in different proportions are linearly spectrally combined to form a common pixel's spectral response. Applying linear spectral unmixing algorithms, these spectra can be unmixed to yield the endmember spectra that make up the combined pixel spectrum. To describe the linear composition of spectral responses to a spectrum consisting of two components, the following equation can be applied to both the whole spectrum and to the reflectance at single wavelengths:

$$R_{MIX} = f_A \times R_A + (1-f_A) \times R_B$$

where

R_{MIX} – spectral response of a mixed spectrum

f_A – factor describing the abundance of material A in the pixel

R_A – spectral response of material A

R_B – spectral response of material B

For fuel hydrocarbon soil contaminations, however, non-linear spectral mixing was expected due, on one hand to masking effects in soils with high adsorptive capacities such as organic soils and clays, and on the other hand to the exhibition of fuel hydrocarbons on soils with low adsorptive capacities (section 5).

This expectation is confirmed by the results of the measurements of the different combinations of soil, moisture, contaminant type and contaminant concentration. Different liquid contaminants (n-octane, xylene, diesel, crude oil) were found to exhibit similar absorption feature depths as shown for the examples of dry sea sand contaminated with different concentrations of n-octane, xylene, diesel and crude oil at the 1,700 nm absorption feature in Table 6-17. Minor differences in the absorption feature depth at similar concentrations can be attributed to different colors (e.g. dark crude oil, clear n-octane). This results in changes of overall reflectance and viscosity (e.g. viscous crude oil vs. liquid n-octane) which, in turn, results in a different distribution in the soil matrix.

Table 6-17: Absorption feature depth (total reflectance percentage) of the 1,700 nm feature of different contaminants at different concentrations in an identical matrix (dry sea sand).

	SS-00- XX-OCT	SS-00- XX-XYL	SS-00- XX-DIS	SS-00- XX-CRO
XX = 0.5 %	0.70	1.57	2.52	2.02
XX = 1.0 %	4.31	3.86	4.33	3.31
XX = 3.0 %	10.73	10.94	11.10	8.33

At the same time, the absorption feature depth of similar contaminants in different matrices (different dry soils) was found to differ considerably as shown for the 1,700 nm absorption feature of n-octane in four different matrices in table 6-18. Also, soil moisture was found to have a significant effect on the reflectance of similar contaminant concentrations in identical soil types with different moisture levels as shown in table 6-19.

Table 6-18: Absorption feature depth (total reflectance percentage) of the 1,700 nm feature of n-octane in different dry soil types.

	SS-00- XX-OCT	cS-00- XX-OCT	Cy-00- XX-OCT	BT-00- XX-OCT
XX = 05	0.70	0.53	0.29	0.00
XX = 10	4.31	1.80	0.77	0.18
XX = 30	10.73	6.79	1.56	0.84

Table 6-19: Absorption feature depth (total reflectance percentage) of the 1,700 nm feature of crude oil in a soil sample with different moisture levels (fine sand dry and with 5 % and 10 % moisture, respectively).

	fS-00- XX-CRO	fS-05- XX-CRO	fS-10- XX-CRO
XX = 05	1.90	1.20	1.05
XX = 10	4.74	2.59	1.74
XX = 30	8.40	6.27	4.31

In summary, the absorption feature depth of different contaminants in different matrices was found to primarily depend on soil type and soil moisture level rather than contaminant type. A similar behavior was found for solid contaminants. This behavior was found to be valid throughout the experimental series and proves that spectral mixing for fuel hydrocarbons in soils is non-linear. Furthermore, hydrocarbon concentrations were found to contribute to absorption feature intensities that do not equal their proportion as a constituent of the sample measured as assumed in linear mixing models.

To further demonstrate the non-linear nature of spectral mixing processes of soil, moisture and contaminant combinations, linear mathematical combinations of the pure component spectra of contaminants and soils were compared to contaminated soil spectra according to the above equation. Figure 6-15 depicts the spectra of pure n-octane (dual-pass absorption through 1 mm of liquid n-octane) and dry sea sand together with the spectrum measured for dry sea sand contaminated with 3 wt.% n-octane and two spectral math spectra that were calculated to model the spectral response of the latter through combinations of the pure sea sand and n-octane spectra. There are two limitations to the model. First, the n-octane spectrum used is an absorption spectrum rather than a reflectance spectrum (which is impossible to obtain for a clear liquid such as n-octane except at extremely low temperatures). Second, there is full absorption of liquid n-octane in the pure n-octane spectrum beyond the 2,200 nm wavelength. Nevertheless, the results demonstrate the non-applicability of the linear mixing model to fuel hydrocarbon soil contaminations. However, the application of the dual-pass absorption feature is justified because the dual-pass absorption spectrum of n-octane is expected to exhibit even stronger absorption features than a theoretical spectrum of solid n-octane because of its larger optical thickness compared to a (hypothetical) solid, and because the absorption feature depths observed at hydrocarbon absorption features of more than 3 % at 3 % contaminant concentration.

The comparison of the calculated spectra for n-octane-contaminated dry sea sand and the spectrum measured for n-octane-contaminated dry sea sand shows that the spectral mixing behavior of hydrocarbons and soils does not fulfill the paradigm of linear spectral mixing where components are supposed to contribute to the resulting spectrum according to their proportional abundance (figure 6-15). This is best demonstrated for the 1,726 nm absorption feature of n-octane. Linear mixtures of 97 % dry sea sand spectrum (factor 0.97) and 3 % n-octane spectrum (factor 0.03) yield a spectrum (dark red line) which, as is to be expected, does not differ much from the spectrum of pure dry sea sand (light blue line) and is not comparable to the spectrum measured for dry sea sand contaminated with 3 % n-octane (green line). When calculating a mixed spectrum with fractions of 85 % dry sea sand (factor 0.85) and 15 % n-octane (factor 0.15), and multiplying this with a factor of 0.85, the resulting spectrum matches the spectrum measured for dry sea sand contaminated with 3 % of n-octane in the wavelength range between 750 nm and 2,200 nm with only minor deviations. In the visible (350 nm – 750 nm) and shortwave infrared

wavelength region (2,200 nm – 2,500 nm), the spectrum still does not match the measured spectrum. The much lower reflectance of the measured spectrum versus the calculated spectrum in both wavelength regions indicates that the spectral mixing of soil and contaminant combinations is not only non-linear, but also wavelength-dependent. Furthermore, the doublet absorption feature observed in the spectrum measured for the contaminated sample appears neither in the absorption feature of pure n-octane nor in the spectrum of the calculated spectra due to the high absorption of pure n-octane in this wavelength region.

Table 6-20 shows the absorption feature depths of the 1,726 nm absorption feature for the one measured and two calculated spectra for comparison. Each is compared to the reflectance at 1,650 nm at the shoulder of the absorption feature, which is not affected by the hydrocarbon concentration in the soil matrix.

Table 6-20: Absorption feature depths of measured and calculated spectra for dry sea sand contaminated with 3.0% n-octane.

	Reflectance @ 1650 nm	Reflectance @ 1726 nm	Delta R = Absorption feature depth
SS-00-30 OCT (measured)	0.6146	0.5131	0.1015 (10.15 %)
SS-00-30-OCT (calculated 97% SS, 3%OCT)	0.7187	0.7024	0.0163 (1.63 %)
Calculation adapted to match the measure spectrum SS-00-30-OCT	0.6033	0.5175	0.858 (8.58 %)

In the case of dry sea sand and other contaminated soil samples lacking moisture and adsorptive capacities, the absorption features have been found to be stronger than expected when assuming linear mixture models (figure 6-15). The reverse effect has been found in soils with high adsorptive capacities and high moisture levels. In these samples, the absorption feature depths were found to be weaker than expected when assuming linear mixture models. This is demonstrated in Table 6-21 and figure 6-16 by the example of boulder till with 3 % moisture and contaminated with 3 % xylene. The endmember spectra used were the spectrum of moist boulder till with a moisture content of 3 % and the transmittance spectrum of xylene. In this case, the best fit for the measured spectrum was calculated with fractions of 98 % moist boulder till (factor 0,98) and 2 % xylene (factor 0.02), and this combination was raised to a power of 1.4. The resulting spectrum matches the measured spectrum well with only minor deviations that occur in particular at the wavelengths of the 1,693 nm and 2,320 nm absorption features of xylene. Again, as already observed for the sea sand and n-octane spectrum combinations, the 2,300 nm feature is weaker in the calculated spectrum compared to the measured spectrum.

Table 6-21: Absorption feature depths of measured and calculated spectra for moist boulder till contaminated with 3.0% xylene.

	Reflectance @ 1650 nm	Reflectance @ 1693 nm	Delta R = Absorption feature depth
BT-03-30 XYL (measured)	0.2579	0.2529	0.0050 (0.5 %)
BT-03-30 XYL (calculated)	0.3720	0.3656	0.0064 (0.64 %)
Calculation adapted to match the measure spectrum BT-03-30 XYL	0.2504	0.2445	0.0059 (0.59 %)

A similar behavior was found for other soil/moisture/contaminant combinations with each belonging to one of two major groups. Generally, contaminants in dry soils with low adsorptive capacities (namely sands) were found to exhibit absorption features that are stronger than expected when assuming linear mixing models. On the contrary, contaminants in moist soils and soils with high adsorptive capacities (namely clays and soils with high organic matter contents) were found to exhibit absorption features that are weaker than expected when assuming linear mixture models. The results thus indicate that the spectral response of organic contaminants depends largely on soil properties rather than contaminant properties and concentration. Also, spectral mixing for soil/moisture/contaminant combinations must be assumed to be wavelength-dependent.

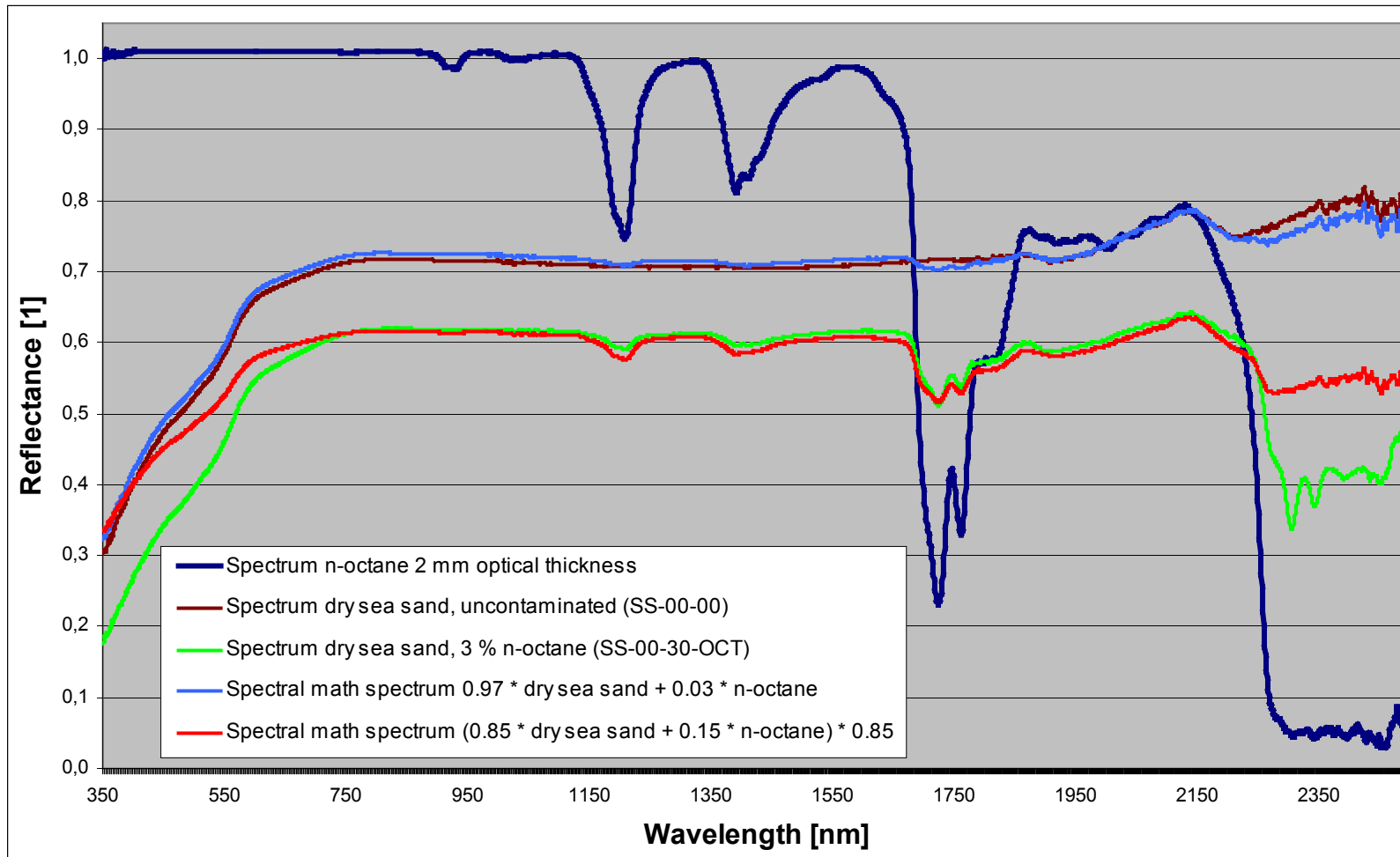


Figure 6-15: Measured spectra of pure n-octane, dry sea sand and dry sea sand contaminated with 3% n-octane compared to calculated spectra. The comparison proves the non-linear mixing behavior of contaminants and soils.

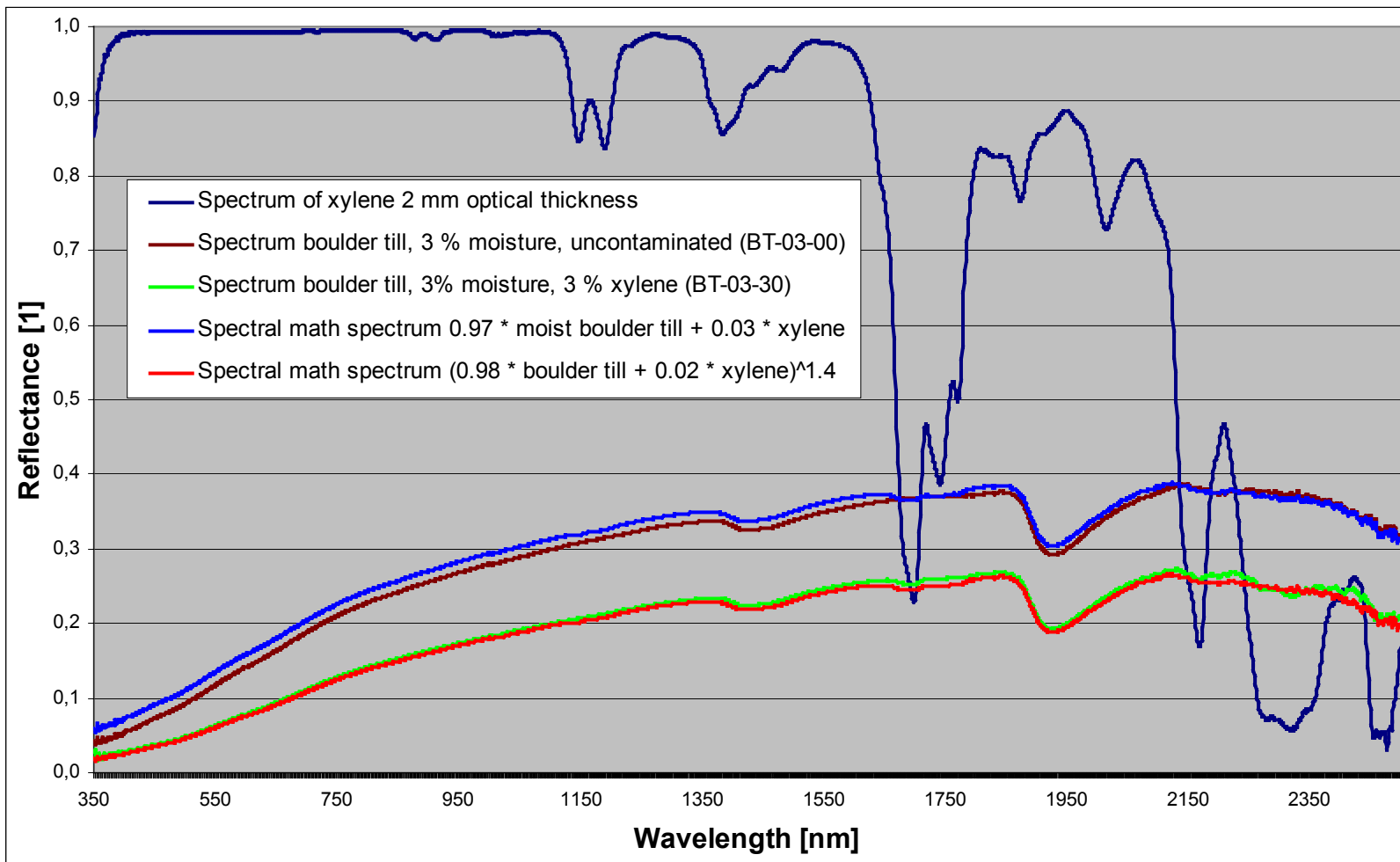


Figure 6-16: Measured spectra of pure xylene, moist boulder till, and moist boulder till contaminated with 3% xylene compared to calculated spectra. The comparison proves the non-linear mixing behavior of contaminants and soils.

Detection limits

For the detection of fuel hydrocarbon contaminations in soils, the detection limit is a crucial parameter. However, unlike in analytical chemistry where measurements are carried out in a controlled environment with carefully prepared calibration models (constant illumination and viewing geometry, diluted sample in well-described solute) where detection limits can be determined using standards and statistical analysis, the definition of a detection limit for remote sensing applications is more difficult.

In remote sensing imaging spectrometry applications, the measurement environment is uncontrolled, with changing illumination, atmospheric effects and viewing geometry (that can be corrected), and hundreds to thousands of different surface materials with an almost infinite number of combinations of factors in single pixel spectra. Therefore, aside from imaging spectrometry applications over large, uniform areas (e.g., large, mono-cultured agriculture fields), it is impossible to develop universal calibration models.

This is particularly true for the problem of detecting fuel hydrocarbon soil contaminations discussed here. Because of the non-linear nature of spectral mixing demonstrated above and the spatial variability of soils and soil properties (e.g. soil moisture and organic material content variations due to topography and land use effects), it would be necessary to develop calibration models for each soil type and moisture level.

However, for the interpretation of remote sensing imaging data interpretation and the application of linear unmixing and spectral feature detection algorithms, it has been reported that, as a minimum, 3 – 5 % levels of a material in a pixel can be reliably detected in imaging spectrometry datasets (see above, section 3). Assuming the linear mixing model, it follows that in order for the absorption feature of a material or substance to be detected in a remote sensing dataset it must contribute at least 3 – 5 % to the total spectrum. That is to say, the characteristic absorption features of the substance or material to be detected must exhibit a depth of at least 3 –5 % relative to the spectrum continuum.

Accordingly, a 3 % detection limit can be defined for a contributor to a spectral response with respect to the qualitative detection of fuel hydrocarbon contaminants in soils. As shown above, two major effects can be observed in the spectra of soils contaminated with fuel hydrocarbons compared to uncontaminated soil samples of identical composition. First, a decrease in the overall reflectance of a sample is typically observed. Second, several characteristic absorption features appear in the contaminated soil spectra, most prominently the hydrocarbon absorption features around 1,700 nm and 2,300 nm. While an overall decrease in reflectance can result from different factors such as increased soil moisture or slope effects, the 1,700 nm and 2,300 nm absorption features have been found to be characteristic for hydrocarbons. Therefore, the 3 % threshold with respect to the absorption depth as a detection limit should be applied to these absorption features. With this detection limit, absorption features of fuel hydrocarbons in soil spectra can typically be detected visually in soil spectra.

To determine the detection limits of fuel hydrocarbon soil contaminations in different soil and moisture matrices with the 3 % absorption feature threshold, the absorption feature depth of the 1,700 nm and 2,300 nm (and other important absorption features where applicable) was determined for all spectra measured for the contaminants n-octane, xylene, diesel, crude oil, naphthalene, and phenol. In total, the absorption feature depths were determined for about 400 spectra of the investigated soil/moisture/contaminant combinations. The absorption feature depths were determined by reading the reflectance at both the individual reflectance minimum of the absorption feature (1,725 nm in figure 6-17) and its shoulder, which was selected to be both on the direct shoulder of the absorption feature and also not be affected by the fuel hydrocarbon concentration in the sample (1,650 nm in figure 6-17). The reflectance at the feature minimum was then subtracted from the reflectance on the feature's shoulder and normalized for the reflectance difference observed in the uncontaminated but otherwise identical sample spectrum. This corrected any differences caused by soil features. The feature depth determination and normalization with respect to the uncontaminated sample is illustrated for the example of fine sand in figure 6-17.

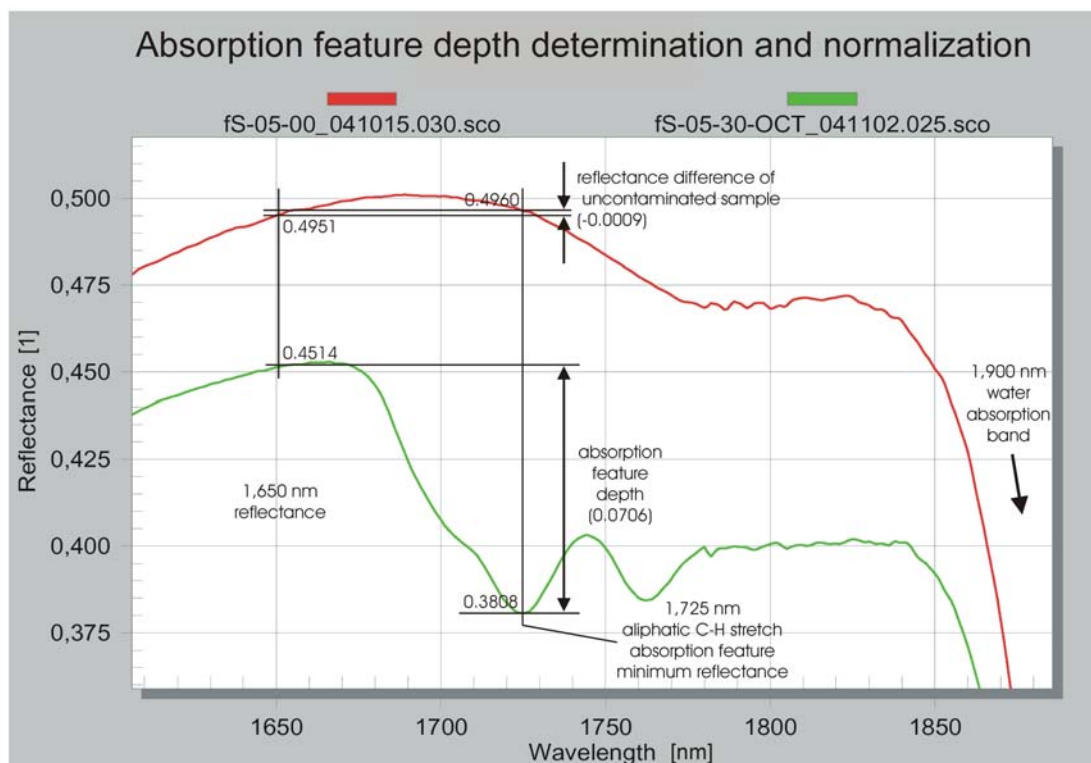


Figure 6-17: Illustration showing the absorption feature depth determination and normalization applied to the analysis of contaminated soil sample spectra.

With the defined threshold detection limit of a 3 % contribution to a spectral response, the detection limit also becomes dependent on the overall reflectance of a sample. The relative reflectance and resulting detection limits of 3 % of uncontaminated soil samples of various moisture levels measured in the important 1,700 nm and 2,300 nm wavelength regions are listed in Table 6-22. The detection

limits, calculated in terms of reflectance percentage, show that the detection limits generally decrease with overall decreasing reflectance (i.e., increasing moisture content or increasing adsorptive capacities). Considering the above discussion of the spectral mixing behavior, this does not indicate that lower contaminant concentrations are detectable.

Table 6-22: Relative reflectance of different soil samples at different moisture levels in the important 1,700 nm and 2,300 nm wavelength regions. The detection limit is defined as 3% of the relative reflectance measured at the respective wavelength.

Moisture	Wavelength		SS [%]	fS [%]	cS [%]	Cy [%]	Cg [%]	BT [%]	Hu [%]
Dry	1700 nm	Reflectance	71.6	67.5	60.7	50.2	53.3	39.4	17.1
		Detection Limit	2.1	2.0	1.8	1.5	1.6	1.2	0.5
	2300 nm	Reflectance	77.3	68.2	55.8	41.5	31.3	41.4	16.3
		Detection Limit	2.3	2.0	1.7	1.2	0.9	1.2	0.5
Moisture Level 1 (M1)	1700 nm	Reflectance	54.7	50.1	51.2	37.5	45.7	36.9	18.4
		Detection Limit	1.6	1.5	1.5	1.1	1.4	1.1	0.6
	2300 nm	Reflectance	42.4	36.9	41.5	27.9	24.2	37.2	16.5
		Detection Limit	1.3	1.1	1.2	0.8	0.7	1.1	0.5
Moisture Level 2 (M2)	1700 nm	Reflectance	43.4	39.0	40.7	25.2	37.7	29.8	15.4
		Detection Limit	1.3	1.2	1.2	0.8	1.1	0.9	0.5
	2300 nm	Reflectance	29.4	24.4	28.5	14.9	18.4	29.3	13.3
		Detection Limit	0.9	0.7	0.9	0.4	0.6	0.9	0.4

To determine the detection limits of the contaminant concentration in a given soil/moisture matrix, the absorption feature depths of the 1,700 nm level for different soil/moisture combinations contaminated with crude oil were compared to the detection limits calculated and listed in table 6-23.

Table 6-23: Detection limits of crude oil in different soil type and moisture matrices for the 1,700 nm absorption feature. Absorption feature depths marked bold and italic are above the individual detection limit determined by the reflectance of the soil-moisture combination contaminated.

	XX = SS	XX = fS	XX = cS	XX = Cy	XX = Cg	XX = BT	XX = Hu
XX-00-05-CRO	2.02	1.90	1.17	0.14	0.62	-0.01	-0.08
XX-00-10-CRO	<i>3.31</i>	<i>4.74</i>	1.78	0.21	0.97	0.06	-0.04
XX-00-30-CRO	<i>8.33</i>	<i>8.40</i>	<i>4.09</i>	0.48	<i>2.61</i>	0.62	0.04
XX-M1-05-CRO	1.11	1.20	0.95	0.01	0.54	0.12	0.00
XX-M1-10-CRO	<i>1.99</i>	<i>2.59</i>	<i>1.80</i>	0.30	0.65	0.27	0.05
XX-M1-30-CRO	<i>5.72</i>	<i>6.27</i>	<i>4.64</i>	1.01	1.33	0.77	0.14
XX-M2-05-CRO	0.89	1.05	0.87	0.21	0.25	0.16	0.03
XX-M2-10-CRO	<i>1.65</i>	<i>1.74</i>	<i>1.54</i>	0.35	0.62	0.30	0.06
XX-M2-30-CRO	<i>4.31</i>	<i>4.31</i>	<i>3.94</i>	<i>1.04</i>	<i>1.29</i>	<i>0.90</i>	<i>1.16</i>

Similarly, the absorption feature depths were determined for the 2,300 nm absorption feature and summarized in table 6-24. However, the detection limits defined in table 6-24 were found to be too low because of the increased noise levels beyond 2,200 nm discussed earlier. Instead, a minimum absorption feature depth (absolute reflectance) of 2 % in sand soils and 3 % in clay and organic matter soils was found to be necessary to detect fuel hydrocarbon contaminations using the 2,300 nm feature, despite increased noise levels in this wavelength range. In tables 6-23 to 6-26, the absorption features marked bold and italic are above the detection limit.

Table 6-24: Detection limits of crude oil in different soil type and moisture matrices for the 2,300 nm absorption feature. Absorption feature depths marked bold and italic are above the individual detection limit determined by the reflectance of the soil-moisture combination contaminated.

	XX = SS	XX = fS	XX = cS	XX = Cy	XX = Cg	XX = BT	XX = Hu
XX-00-05-CRO	<i>9.96</i>	<i>7.71</i>	<i>3.40</i>	0.58	0.85	0.18	0.05
XX-00-10-CRO	<i>14.67</i>	<i>15.23</i>	<i>5.65</i>	0.57	1.55	1.45	0.36
XX-00-30-CRO	<i>26.12</i>	<i>21.24</i>	<i>11.89</i>	1.41	2.90	<i>3.05</i>	0.37
XX-M1-05-CRO	<i>2.49</i>	1.42	<i>2.51</i>	0.27	-0.05	0.29	0.72
XX-M1-10-CRO	<i>3.66</i>	<i>3.43</i>	<i>4.74</i>	0.44	0.49	1.30	0.47
XX-M1-30-CRO	<i>10.77</i>	<i>7.66</i>	<i>8.99</i>	2.11	1.81	2.84	1.14
XX-M2-05-CRO	1.73	0.73	0.98	-0.21	0.24	0.21	-0.26
XX-M2-10-CRO	<i>2.79</i>	1.62	<i>2.79</i>	0.82	0.30	0.49	-0.59
XX-M2-30-CRO	<i>6.24</i>	<i>3.83</i>	<i>5.89</i>	0.69	0.24	<i>3.13</i>	-0.43

The investigation of the 1,700 nm and 2,300 nm absorption features of diesel fuel returned similar results (table 6-25 and 6-26).

Table 6-25: Detection limits of diesel in different soil type and moisture matrices for the 1,700 nm absorption feature. Absorption feature depths marked bold and italic are above the individual detection limit determined by the reflectance of the soil-moisture combination contaminated.

	XX = SS	XX = fS	XX = cS	XX = Cy	XX = Cg	XX = BT	XX = Hu
XX-00-05-DIS	<i>2.52</i>	<i>2.75</i>	1.32	0.31	0.35	0.15	-0.01
XX-00-10-DIS	<i>4.33</i>	<i>4.92</i>	<i>2.32</i>	0.40	<i>1.70</i>	0.21	0.00
XX-00-30-DIS	<i>11.20</i>	<i>11.26</i>	<i>5.46</i>	0.98	<i>2.65</i>	0.95	0.17
XX-M1-05-DIS	1.43	<i>1.52</i>	0.90	0.40	0.60	0.23	0.09
XX-M1-10-DIS	<i>2.48</i>	<i>3.52</i>	<i>2.33</i>	0.39	0.93	0.43	0.07
XX-M1-30-DIS	<i>6.52</i>	<i>6.90</i>	<i>5.47</i>	<i>1.20</i>	<i>2.06</i>	1.00	0.17
XX-M2-05-DIS	1.08	1.08	0.85	0.13	0.55	0.19	0.06
XX-M2-10-DIS	<i>1.79</i>	<i>1.92</i>	<i>1.82</i>	0.33	0.60	0.34	0.16
XX-M2-30-DIS	<i>4.24</i>	<i>3.73</i>	<i>3.87</i>	<i>1.42</i>	<i>1.43</i>	0.97	0.21

Table 6-26: Detection limits of diesel in different soil type and moisture matrices for the 2,300 nm absorption feature. Absorption feature depths above the individual detection limit determined by the reflectance of the soil-moisture marked bold and italic combination contaminated.

	XX = SS	XX = fS	XX = cS	XX = Cy	XX = Cg	XX = BT	XX = Hu
XX-00-05-DIS	<i>11.53</i>	<i>9.39</i>	<i>4.38</i>	0.16	0.52	1.10	0.76
XX-00-10-DIS	<i>16.72</i>	<i>14.61</i>	<i>6.96</i>	0.91	1.81	1.73	-0.04
XX-00-30-DIS	<i>30.47</i>	<i>23.59</i>	<i>12.74</i>	2.86	2.18	<i>4.47</i>	1.45
XX-M1-05-DIS	<i>2.76</i>	<i>2.51</i>	<i>2.64</i>	1.59	-0.01	0.72	1.01
XX-M1-10-DIS	<i>4.74</i>	<i>14.61</i>	<i>5.02</i>	1.75	0.36	1.42	0.96
XX-M1-30-DIS	<i>10.93</i>	<i>23.59</i>	<i>9.75</i>	2.70	0.69	<i>3.29</i>	0.54
XX-M2-05-DIS	<i>2.05</i>	<i>2.51</i>	<i>1.33</i>	-0.08	0.67	0.62	0.09
XX-M2-10-DIS	<i>2.83</i>	<i>4.92</i>	<i>2.85</i>	0.21	0.25	1.46	0.47
XX-M2-30-DIS	<i>5.51</i>	<i>8.62</i>	<i>5.24</i>	1.22	0.63	2.74	0.16

The results show that fuel hydrocarbon contaminations in primary silicate (sand) soils with low adsorptive capacities can usually be detected at concentrations of more than 1.0 wt.% (10,000 mg/kg). Under certain circumstances, even lower concentrations of 0.5 wt.% (5,000 mg/kg) can be detected, particularly in dry to moderately moist soils. In soils with high adsorptive capacities (clays, humic soils and soils with increased organic and clay mineral content like boulder till), even high concentrations of fuel hydrocarbons can only be detected in some cases.

In primary silicate (sand) soils, the 2,300 nm absorption feature of fuel hydrocarbons is generally found to be stronger than the 1,700 nm absorption feature, often allowing for the detection of low contaminant concentrations that cannot be detected through the 1,700 nm absorption feature.

In clay soils, even contaminant concentrations as high as 3.0 wt.% were only detectable in some cases with no clear pattern of soil moisture dependence. Based on the measured absorption feature depths, it is assumed that fuel hydrocarbons in clays

can only be reliably detected if the concentration exceeds 5.0 wt.% (50,000 mg/kg). Boulder till containing both primary and secondary silicate minerals and a significant amount of organic matter was found to behave similar to clays. In humic soil, all contaminants were found to be non-detectable at concentrations of 3.0 wt.%, regardless of the soil moisture level. With only minor absorption feature depths even at this concentration level, no prediction can be made as to the concentration at which hydrocarbon contaminants are detectable in soils with high organic matter content.

Quantitative analysis

Experience shows that overall reflectance and absorption feature depths are primarily determined by soil properties (adsorptive capacities, organic “dark” material content and soil moisture), not by the concentration of the hydrocarbon contaminant in the soil. Therefore it is obvious that quantitative analysis based on absorption feature depths in imaging spectrometry datasets is not possible, because the soil properties are usually unknown and vary within a scene (data set).

However, for large areas of homogeneous soil types and soil properties, calibration models can be established, similar to those used in laboratory analytical chemistry, by correlating the characteristics of absorption feature depths to hydrocarbon contaminant concentrations determined by standard laboratory analysis. Despite minor differences in soil composition (iron content, small quantities of organic matter and clay minerals), the results obtained for the sand soils (SS, fS, cS), with similar absorption feature depths for similar contaminant concentrations, indicate that this approach may also be valid for groups of similar soils like sands or clays.

If in an area of homogeneous soil type and properties (i.e. homogeneous marshlands as described for the Abadan crude oil spill in section 2), where the only variable is fuel hydrocarbon abundance or concentration, the detection and quantification might also be based on solely the overall reflectance decrease observed, rather than characteristic absorption features.

6.6 – Field samples of contaminated soils and related materials

To verify the results of the laboratory experiments with carefully prepared contaminated soil samples and to assess the applicability to real contaminated sites in field and remote sensing applications, selected samples of contaminated soils from contaminated sites were investigated in laboratory and field experiments. Additionally, other materials were investigated that are expected to exhibit similar absorption features to the fuel hydrocarbon soil contaminations, particularly with respect to the characteristic fuel hydrocarbon absorption features. In particular, household wastes and plastics were included in these measurements.

The investigated fuel hydrocarbon contaminated soils included a sample of soil taken from the oilfields around Baku in Azerbaijan, which was contaminated with crude oil, samples of soils, wood and concrete contaminated with heavy fuel oil, lubricant oil and diesel fuel from the site of the former glassworks Haidemühl, and a sample of tar-contaminated soil from the site of the former chemical processing plant in Cottbus. Soil samples highly contaminated with explosives (mainly trinitrotoluene) from the burning site of the former explosives production facilities at Torgau-Elsnig were also investigated.

Materials with related or similar absorption features investigated included unsorted household wastes collected in Cottbus, and plastics wastes and wood chips deposited on the site of the former glassworks Haidemühl.

The soil sample from Baku, Azerbaijan, was highly contaminated with crude oil, and therefore dark to black in color, showing an overall reflectance of about 20 % at maximum. A laboratory analysis of the sample confirmed a high fuel hydrocarbon contamination in excess of 200,000 mg/kg (20 wt.%). Both the 1,700 nm absorption feature and the 2,300 nm absorption feature were clearly visible in the reflectance spectrum with absorption feature depths of 1.87 % and 2.34 %, respectively. With a reflectance of 15.6 % and 11.4 % at 1,700 nm and 2,300 nm, the detection limits are calculated at 0.5 % and 0.4 % reflectance, respectively. Because of the intensity of the 1,700 nm absorption feature and the low noise level observed around 2,300 nm, both features can be assumed to be detectable in remote sensing imaging spectrometry applications. No water absorption features are observed in the sample, obviously due to an impregnation of the soil matrix with hydrophobic fuel hydrocarbons contained in high concentrations.

Tar and fuel hydrocarbon contaminations of concrete pavements and soils at the former glassworks Haidemühl and the former chemical plant in Cottbus were found to exhibit the characteristic absorption features at 1,700 nm and 2,300 nm where a fuel hydrocarbon contamination could also clearly be detected by organoleptic means. Typically, the 1,700 nm absorption feature was found to be clearly detectable (visible) in these spectra although the overall relative reflectance of the spectra rarely exceeded 20 %. The 2,300 nm absorption feature was often obscured by noise in the region beyond 2,200 nm and only detectable in approximately half of the samples investigated. Figure 6-20 depicts a selection of spectra acquired in laboratory and field measurements for contaminated soil and concrete samples from contaminated sites.

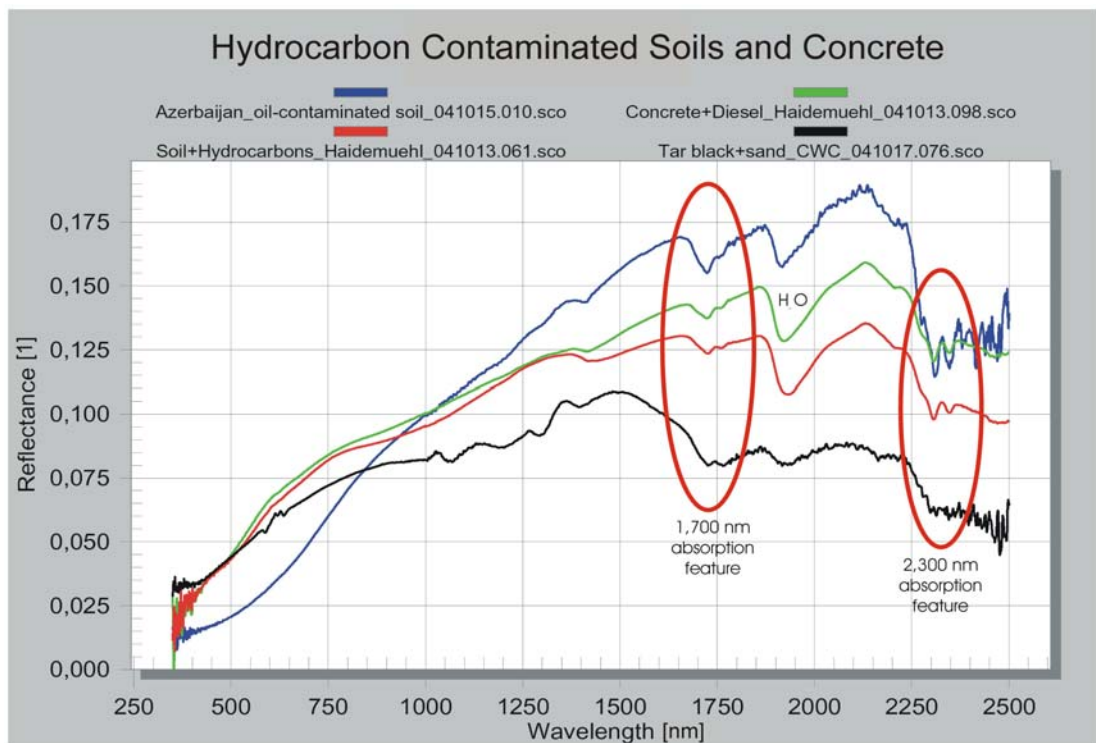


Figure 6-18: Spectra of various samples of soil and concrete contaminated with fuel hydrocarbons collected from contaminated sites.

In addition to a variety of fuel hydrocarbon contaminated samples from different sites, seven samples contaminated with explosives, explosives burn residues and by-products from the production of explosives were examined. The samples were taken from a dump containing residues from the uncontrolled burning of explosives, byproducts and wastes on the peripheries of the explosives production facility at Torgau-Elsnig in Saxony, Germany. Here, mainly trinitrotoluene (TNT) but also other explosives were produced for several decades. The residues of the burning process were piled up in a dump that is today enclosed in a containment for environmental safety reasons.

The samples consisted of dark brown to black, moderately moist soil known to contain large quantities of explosives and related compounds, as well as incineration residues (soot), which cause the dark color of the material. The explosives are not distributed finely in the soil. Instead, the explosives are typically found in the form of solid yellow particles with a diameter of one to several millimeters. The seven samples were taken from different locations in the dump during a sampling procedure in July 2004.

The spectra of the seven samples acquired in laboratory measurements were all found to exhibit a low relative reflectance of less than 20 %. Also, increased noise levels were found in the wavelength region beyond 1,800 nm with extreme noise levels (up to 5 % relative reflectance differences over a wavelength range of only several nanometers) beyond 2,300 nm. Generally, the spectra were found to resemble those measured for humic soil (Hu).

In only one out of the seven samples investigated, could a characteristic hydrocarbon absorption feature (aromatic C-H) be determined, having a minimum at 1,648 nm and an absorption feature depth (shoulder at 1,625 nm – minimum at 1,648 nm) of 0.36 %. A second, weaker absorption feature can be observed on the longer wavelength shoulder of this feature with a minimum at around 1,668 nm. A comparison of this absorption feature to the spectra acquired generally for chemicals and particularly for explosives showed that only 2,4,6-trinitrotoluene exhibits a similar, almost identical pattern of absorption features with minima at 1,648 nm and a second feature merged into the first one with a minimum at 1,672 nm. The absorption features of dinitrotoluene were also found to be similar. However, the second absorption feature of dinitrotoluene is shifted to longer wavelengths, appearing at around 1,680 nm. All other aromatic compounds investigated exhibit absorption features between 1,670 nm and 1,700 nm only, and aliphatics exhibit absorption features in the 1,700 nm region, generally beyond 1,700 nm. The spectrum of the sample in which TNT could be detected is depicted in figure 6-21, along with five of the other spectra of samples contaminated with explosives.

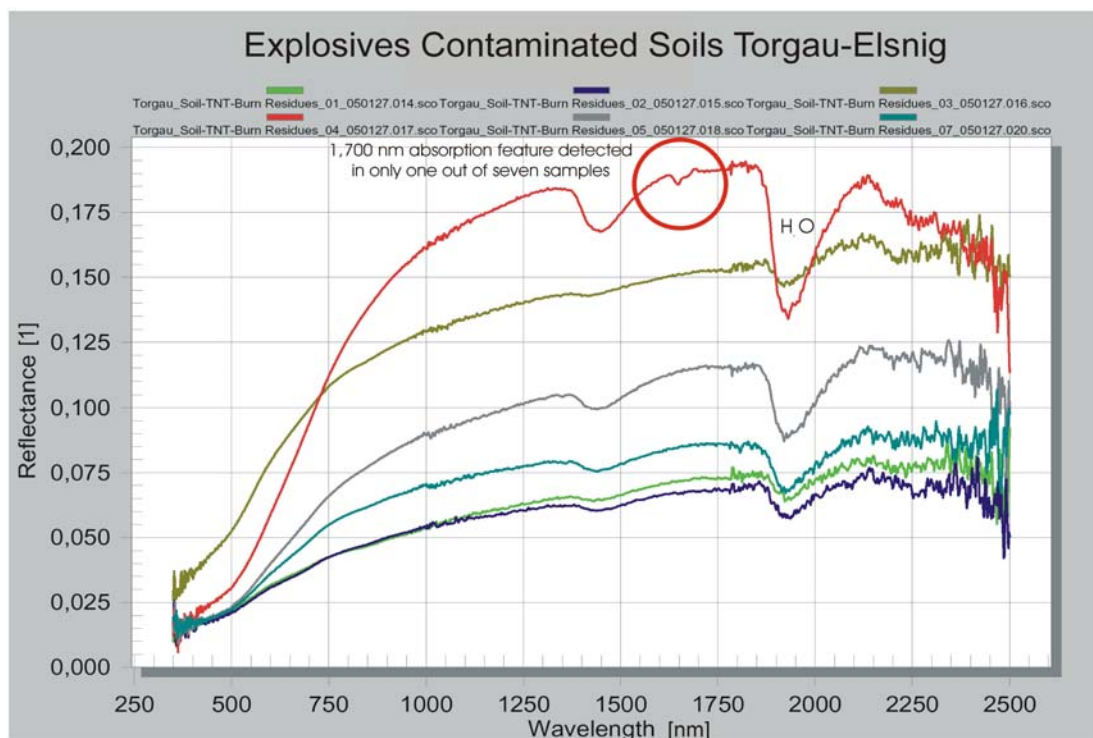


Figure 6-19: Spectra of soil samples containing high concentrations of explosives (obviously TNT) and soot. The TNT is detectable in the spectrum (red circle) exhibiting the highest overall reflectance.

Although all samples have been proven to contain high concentrations of explosives and related compounds, only one spectrum showed a characteristic absorption feature that could be related to explosives contained in the sample. This can be attributed to two reasons. First, all samples contain large quantities of soot (carbon black) that reduces the overall reflectance of the samples and masks absorption features of substances and materials contained in the matrix (as observed for humic soils in the

systematic experiments described and discussed above). This is supported by the fact that the explosive (TNT) was detected in the “brightest” dark brown sample while all other (darker) samples did not exhibit characteristic absorption features. Second, the explosives are, as described above, found as rather large solid particles in the soil matrix. Therefore, only where these particles are exhibited at the surface they can be detected by optical spectrometry methods that record the reflectance of a surface over a certain wavelength area. Based on the results obtained for the samples from Torgau-Elsnig it must be stated that, in general, the detection of explosives and their separation from other chemicals in soils is possible only where other materials do not mask their presence. Furthermore, a (representative) quantitative analysis for particulate target materials in a dominating matrix is generally impossible.

Figure 6-22 depicts an average spectrum calculated from 15 single measurements plus two of the extreme spectra of unsorted household wastes collected in Cottbus for analysis by the Chair of Waste Management of the BTU Cottbus. Despite waste sorting efforts, household wastes still contain mainly plastics and a variety of decayed and partially-decayed natural organic materials (wood, food residues), plus smaller amounts of paper and cardboard, glass, metal and other materials (construction wastes, etc.). However, the main fraction is still made up by natural and synthetic materials consisting of or containing large fractions of various hydrocarbons. These hydrocarbon materials exhibit the characteristic absorption features in the 900 nm, 1,200 nm, 1,700 nm and 2,300 nm wavelength regions. The overall shape is determined by the color of the materials present, the hydrocarbon absorption features, and the high moisture content of the household. These major compounds express themselves in two strong water absorption features around 1,400 nm and 1,900 nm and decrease overall in reflectance in the shortwave infrared wavelength region between 1,300 and 2,500 nm. Beyond 1,800 nm wavelength, noise levels are found to increase considerably in the household waste spectra.

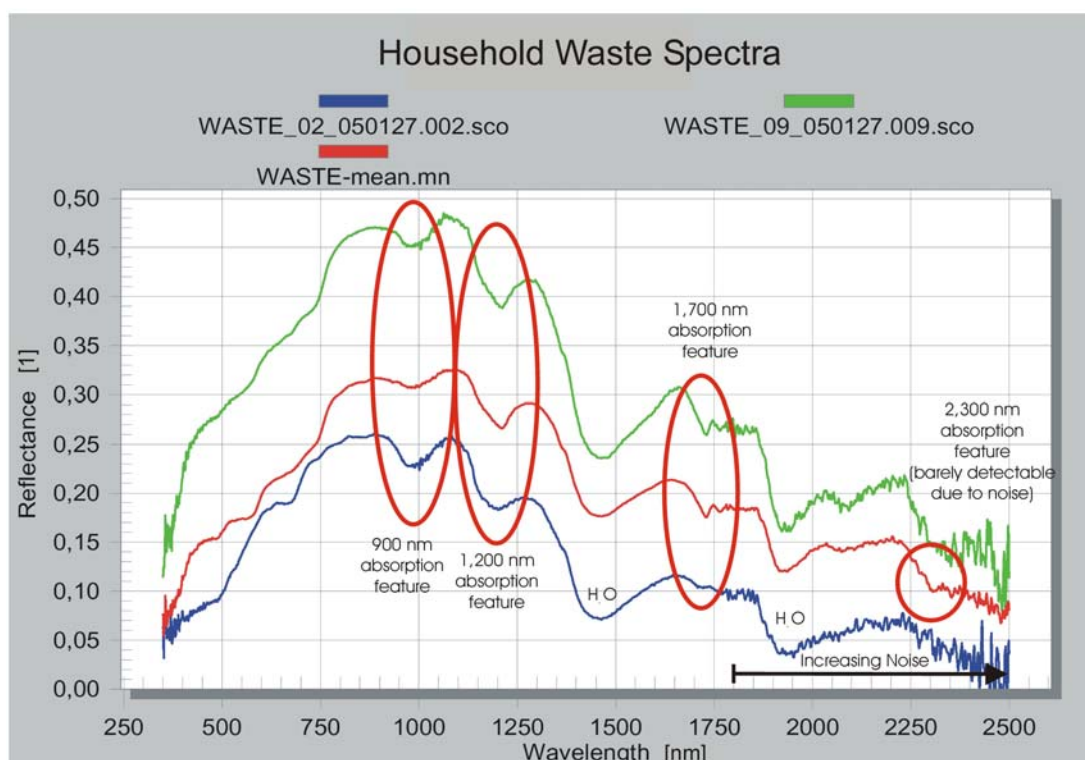


Figure 6-20: Extreme (green, blue) and average (red) spectra of household wastes containing large quantities of plastics and organic materials and exhibiting characteristic hydrocarbon absorption features.

The separation of household wastes, natural organic materials and plastics that exhibit both the characteristic 1,700 nm and 2,300 nm absorption features used to detect fuel hydrocarbon contaminations can be separated from the related materials based on the 900 nm and 1,200 nm absorption features that do not appear in hydrocarbon contaminated soil spectra. Rather they appear as strong absorption features in plastics and natural material spectra. Similarly, strong absorption features in the 900 nm and 1,200 nm regions in addition to the absorption features in the 1,700 nm and 2,300 nm regions were found in field and laboratory measurements of plastics and plastics wastes. Although no laboratory analyses were made to correlate absorption feature depth and fuel hydrocarbon concentration in the contaminated media, the results clearly indicate that imaging spectrometry could be applied to detect outdoor fuel hydrocarbon contaminations provided that the contaminated area is large enough and the spatial resolution high enough to resolve the characteristic absorption features in the spectra of an imaging spectrometry dataset. The results also indicate that a differentiation of fuel hydrocarbon soil contaminations and other materials exhibiting characteristic fuel hydrocarbon absorption features is possible based on the overall shape of the spectra of contaminated soils compared to household wastes, plastics, and paints. The latter materials typically exhibit a strong 1,200 nm hydrocarbon absorption feature that is not observed in fuel hydrocarbon contaminated soils.

7 – Data interpretation

An imaging spectrometry dataset was investigated for hydrocarbon absorption features in order to verify the results of the laboratory spectroscopy investigations with respect to the detectability of hydrocarbon materials, hydrocarbon soil contaminations and the ability to decipher different hydrocarbon-bearing materials, and also in order to develop an algorithm for the detection and separation of different hydrocarbon materials and classes in imaging spectrometry datasets.

First, the standard detection and classification methods and algorithms presented in section 3 were applied to the dataset for the detection of hydrocarbons.

Second, an algorithm applying relatively simple operations was developed to detect, map, and separate different classes of hydrocarbons.

Based on the results of the laboratory experiments, two principal approaches can be considered to detect hydrocarbons in imaging spectrometry datasets. One is based on the comparison of image spectra to an image-derived, non-affected reference spectrum. The other is based on information on the target material (hydrocarbons) inherent in each spectrum that contains the target material above a certain detection limit, that is to say, exhibits characteristic absorption features.

The first approach is based on the observation that soil contaminations with liquid hydrocarbons results in a decrease of the overall reflectance with only a few exceptions, which can be considered irrelevant for practical applications (e.g., dark humic soils in which fuel hydrocarbons cannot be detected anyway). In an area with homogeneous surface coverage over large areas, a simple approach to detect fuel hydrocarbon contaminations could be to compare the image spectra to that of a uncontaminated reference spectrum that was selected manually. Based on a decision criterion, e.g., a reflectance threshold value at a certain wavelength or an average reflectance threshold value for the whole spectrum under investigation, a simple 0/1 decision “contaminated” or “uncontaminated” could be made. Although the approach requires only minimal computational resources and skills, it would only prove applicable where surface coverage is homogeneous over large areas and no other target materials with a lower reflectance (e.g., asphalt road pavements, tar roofing) or natural variances in vegetation cover or soil reflectance occur (e.g., due to soil moisture differences). The approach would even be possible without imaging spectrometry data, instead being applied to digital aerial photographs, be it panchromatic, RGB or false color infrared aerial photographs or multispectral data. From the examples of contaminated sites considered in section 2, this approach would only be applicable to the crude oil spill in a marshland near Abadan, Iran, where large quantities of black crude oil were distributed over large areas of homogeneous marshland without settlements or major infrastructure in the area.

The second approach is based on the interpretation of characteristic differences observed in the response of different spectral bands for certain (target) materials. All data interpretation algorithms for imaging spectrometry datasets presented in section 2 make use of these absorption features of target materials by comparing the whole or only user-selected portions of all image spectra to reference (library)

spectra by different means (e.g., binary encoding, spectral feature fitting, spectral angle mapping, matched filtering, mixture tuned matched filtering, etc.).

Considering the examples of a variety of the typical contaminated site types introduced in section 2 and the results of the laboratory experiments presented in section 6, it is obvious that, depending on the specific case, two different applications of imaging spectrometry for the detection or investigation of fuel hydrocarbon contaminated soils are possible.

The first application case is the detection of relatively few and small areas of contaminated soil in a larger scene, with the targets to be detected being small-area hydrocarbon contaminations or deposits at the surface. Application examples include the filling station or the uncontrolled waste dump in Venezuela in the Rio Unare basin, hot spots on military brownfields like the former military training area Döberitzer Heide or industrial brownfields like the former glassworks Haidemühl and the Schwarze Pumpe industrial area. Despite several other problems that disallow the detection of contaminations hidden below natural or anthropogenic barriers (heterogeneous “chaotic” sites, shadow effects, surface sealing, or plant cover), the detection of small characteristic hydrocarbon features in spectra dominated by other materials (soil background, plant cover, etc.) is required for this application. The comparison of spectra to reference spectra of different mixtures of soils and various hydrocarbon contaminants in a spectral library has to be considered impossible, because the background spectrum of a hydrocarbon contamination or deposit can be made up of a large variety of different soils, concrete or other materials. In order for this to be possible, large spectral libraries containing all possible combinations of a huge variety of different soils, hydrocarbon contaminants and related materials would need to be produced. Therefore, other approaches focusing specifically on the characteristic absorption features of hydrocarbons must be developed to detect hydrocarbons and separate fuel hydrocarbon soil contaminations from related materials or material combinations exhibiting comparable spectra in imaging spectrometry datasets, e.g., plastic wastes on soil.

The second application case is the mapping of hydrocarbon soil contaminations, which make up a considerable portion of an imaging spectrometry dataset and exhibit significant, relatively homogeneous spectral responses, including some of the characteristic absorption features discussed above. In these cases, one example of which is the crude oil production on the oilfields of the Absheron Peninsula around Baku, Azerbaijan (with many similar areas in the Black Sea and Caspian Sea regions and the Middle East), the established remote sensing data interpretation approaches (based on statistical methods) can be applied. Generally, as described above, these methods are based on user-selected or calculated classes or spectral endmembers having a more or less high frequency in the investigated scene (so-called image-derived endmembers). These classes can thus be considered as a group of materials or spectral endmembers dominating the dataset. If fuel hydrocarbon soil contaminations make up a considerable part of such a dataset, the approach can therefore be applied to map the distribution and abundance of the contamination. However, it must be not be forgotten that the spectral mixture analysis and unmixing algorithms applied to imaging spectrometry data in these data interpretation

algorithms generally utilize linear mixture models, and that the spectral mixture behavior of fuel hydrocarbons in dry and moist soils has been proven to be non-linear in nature (section 6).

In the subsequent paragraphs, the dataset used for the investigations will be introduced, and several established data interpretation techniques will be evaluated with respect to the detection of fuel hydrocarbon soil contaminations. In addition, a method to detect and separate different classes of hydrocarbons regardless of background materials based on simple analysis tools will be developed.

For data processing and interpretation, ENVI® 3.6, a widely used software package for remote sensing data interpretation with a focus on imaging spectrometry data, was used.

7.1 – HyMap dataset military training area *Döberitzer Heide*

The dataset used for the data interpretation experiments was acquired with the HyMap instrument during the HyEurope campaign in 1999 on behalf of the *Geoforschungszentrum* (GFZ) Potsdam, Geodesy and Remote Sensing Department, Remote Sensing Section, Prof. Dr. Kaufmann. The dataset kindly provided for the purpose of this project is a subset of about a quarter of a flightline covering urban Potsdam and its northern and southern surroundings.

The subset covers the southern part of the former military training area *Döberitzer Heide* (today Natural Reserve *Döberitzer Heide* and *Standortübungsgelände Berlin* of the German Armed Forces) plus part of the Krampnitz barracks, the Krampnitz Bullenwinkel facility and the civilian areas of Krampnitz/Lehnitz Lake with the adjacent villages of Neu Fahrland and Krampnitz, which lie south of the former military training area. The former military training area *Döberitzer Heide* has been subject to a number of research projects of the Chair of Chemical Engineering and Hazardous Wastes of the Brandenburg University of Technology Cottbus between 1998 and 2004.

The aerial images were acquired on May 19, 1999 at 12.52 pm with the HyMap imaging spectrometer. The flight direction was north to south (heading 180.1°), the sun's azimuth was 223° (west-south-west) and the sun's zenith was 38.8° (off the vertical). With a flight altitude of approximately 2,570 meters and a swath width of 62°, the scene covered is approximately three kilometers wide. The provided scene subset was not geo-processed. The weather conditions during the data acquisition are described as sunny.

At that time, the HyMap whiskbroom scanner had the following parameters: 126 spectral bands with a spectral resolution (bandwidth) of 10 – 20 nanometers covering the wavelength regions between 457 nm and 2,480 nm and a signal-to-noise ratio of > 1,000 : 1 [Kruse 2000a]. No data was acquired by the instrument in the area of the two atmospheric water vapor absorption bands between 1,346 nm and 1,431 nm and 1,802 nm and 1,967 nm, respectively. In these wavelength regions, the spectra are

bridged when viewed with ENVI® image processing software, connecting the adjacent bands of the water vapor absorption features with a straight line.

The data were provided as both radiance and reflectance data. The radiance dataset comprises the original radiance values for the scene. The reflectance values were derived from the radiance dataset by empirical line correction.

The scene of 512 (west – east) by 956 (north – south) pixels covers a ground area of approximately 3.0 kilometers by 4.8 kilometers (14.4 square kilometers). From this, a spatial resolution of approximately five to six meters per pixel can be calculated. Also, the instantaneous field of view of the sensor (IFOV) can be calculated at approximately two milliradians.

7.2 – Data interpretation standard procedures

For data interpretation use with the HyMap dataset described above, the spectral library containing spectra of contaminated soils at different contaminant concentrations and moisture levels, chemicals, man-made materials, and soils with a spectral resolution of one to two nanometers in about 2,200 spectral bands was resampled to match the spectral characteristics of the 1999 HyMap sensor (126 bands, 10 – 20 nm spectral resolution). This was done in order to make it compatible with the dataset.

Detection of hydrocarbons

Among the established imaging spectrometry data interpretation tools that were tested with respect to their suitability for the detection and segregation of hydrocarbons in imaging spectrometry datasets were:

- Spectral angle mapper (SAM)
- Spectral feature fitting (SFF) and multi-range spectral feature fitting (MSFF)
- Matched filtering (MF) and mixture tuned matched filtering (MTMF)
- Hydrocarbon index (HI)

Several other tools, in particular linear spectral unmixing and binary encoding tools were not tested because they were not considered suitable detection tools based on the findings that a huge variety of hydrocarbon/matrix combinations might occur and mixture processes of fuel hydrocarbon soil contaminations are generally non-linear in nature. Matched filtering (MF) and mixture tuned matched filtering (MTMF) were tested although they apply linear spectral unmixing because they allow for spectral subsetting of datasets, thus focusing only on features of interest (characteristic absorption features).

The test was conducted using the HyMap dataset described above, and it was found to contain no fuel hydrocarbon soil contamination or pure fuel hydrocarbon spectra but a variety of pure and mixed plastics spectra.

The *spectral angle mapper* classification tool was used to map hydrocarbon abundances in the scene with reference spectra of hydrocarbon materials and fuel hydrocarbon contaminated soil samples selected from the spectral library compiled from the laboratory experiments. Several trials with different spectral subsets and different maximum angles as class threshold values were conducted. Spectral subsets included trials limited to 1,000 nm – 2,500 nm to exclude color effects in the visible / near infrared wavelength range and trials limited to ± 100 nm to the 1,700 nm and 2,300 nm characteristic hydrocarbon absorption features. The results were found to return a large number of false positives if too many reference spectra were selected. However, a number of aliphatic and aromatic-based plastics (polyethylene, polypropylene, polyvinylchloride, polystyrene) were found to be detectable when the number of input reference spectra was limited and the spectral angle thresholds were adapted. The plastic spectra detected were all situated in settlement areas and on the lake (boating harbors, boats). Several stationary objects detected could be verified despite the time span between data acquisition (1999) and interpretation (2004/5). A large area where polystyrene was detected coincided with a greenhouse in Krampnitz, while other features, mainly those of polypropylene and polyvinylchloride coincided with plastic canopy roofs attached to buildings. Within the former military training area *Döberitzer Heide*, no plastic spectra were detected. Test runs with coarse and fine sand (similar sediments to those found in the *Döberitzer Heide* where open soil is exposed) contaminated with different aliphatic and aromatic fuel hydrocarbons in different concentrations were found to return a large number of false positives of soil sparsely covered with dry vegetation (also known to exhibit similar, however not identical, absorption features as fuel hydrocarbons).

The *spectral feature fitting* algorithm (also known as tetracorder algorithm) was applied with similar input spectra from the spectral library as for the spectral angle mapper. Both single spectral subsets (1,000 nm – 2,500 nm) and multiple range spectral subsets restricted to one to three characteristic absorption features were used for several tests of the spectral feature fitting algorithm. It was generally found to detect only relatively pure spectra of plastics, while at smaller abundances in a pixel, plastics were usually not detected. Furthermore, the spectral feature fitting algorithm was found to return a large number of false positives, in particular in the area of shadows and water surfaces.

The *matched filtering* and *mixture tuned matched filtering* algorithms were also applied to the dataset, both applying linear unmixing to identify pure or partial spectra of user-selected endmembers (from either a spectral library or the image). With similar spectral endmembers selected from the spectral library and a spectral subset for the spectral range between 1,000 nm and 2,500 nm (again to exclude color effects in the visible wavelength range) both algorithms were found to detect only about half of the known abundances of plastics. However, few if any false positives were returned if the correct stretch was applied to the output image.

The application of the *hydrocarbon index* (see section 4 for a detailed explanation) as originally proposed by the inventors is generally found to be a suitable tool to map most hydrocarbon absorption features. However, as described in section 6, different hydrocarbons and plastics exhibit the 1,700 nm absorption feature at different wavelengths; aliphatic compounds generally beyond 1,700 nm and aromatic compounds (and plastics made from aromatics like polystyrene) generally at wavelengths shorter than 1,700 nm. Therefore, when only focused on the 1,730 nm aliphatic absorption feature, aromatic absorption features at wavelengths smaller than 1,700 nm are not detected. In particular, the polystyrene roofing of the greenhouse in Krampnitz identified by both the spectral angle mapper and spectral feature fitting algorithms is not detected using the hydrocarbon index as originally proposed by the inventors, because it exhibits a characteristic aromatic absorption feature around 1,670 nm. Also, wood and bark chips and some other natural organic materials are also found to be registered by the index. Exhibiting relatively strong absorption features with a minimum around 1,730 nm, ground truthing at several sites with corresponding absorption features in the *Döberitzer Heide* nature reserve (almost unchanged since 1999) showed that the soil surface at these sites was covered by wood bark chips, fine wood chips, and pine needles.

Apart from the detection of small areas affected by hydrocarbons (whether contaminated soils or plastics covering the soil), it might be desirable to map hydrocarbon abundance in imaging spectrometry datasets where these make up a considerable fraction of a scene, rather than occurring as a rare material. For the mapping of hydrocarbon contaminations of large areas or covered at least partially by plastics (wastes, agricultural covers, etc.), it can be assumed that the application of established imaging spectrometry data interpretation methodology consisting of several cascaded algorithms is possible. This cascaded methodology, sometimes also referred to as operational hyperspectral processing, consists in the correction of the input dataset to yield apparent reflectance (atmospheric correction), as well as the calculation of a minimum noise fraction for spectral dimensionality reduction, and subsequently the calculation of the pixel purity index for spatial data reduction and the extraction of spectrally pure pixels. Spectral endmembers for the analysis are then selected by the user, and finally the distribution and abundance of the selected endmembers is mapped using one of several mapping algorithms such as the spectral angle mapper or mixture tuned matched filtering. The method is definitely a promising alternative to the detection algorithms tested above where the contaminants are spectrally known, occur at high concentrations, and cover large areas of a scene. However, it must be noted that linear spectral unmixing is generally a core part of this data interpretation methodology. Therefore, while allowing for a reliable detection of fuel hydrocarbons in high concentrations and abundances in or on soil, this methodology will not allow for a reliable quantification because of the proven non-linear spectral mixture behavior of soils and hydrocarbon contaminants. If applied for quantitative analysis, fuel hydrocarbon contaminations of soils with low adsorptive capacities are expected to be attributed too high hydrocarbon concentrations while fuel hydrocarbon contaminations of soils with high adsorptive capacities are expected to be attributed too low hydrocarbon concentrations.

Because the detection algorithms tested above (spectral feature fitting, mixture tuned matched filtering, spectral angle mapper) require a priori knowledge of the contaminants to be detected (spectral endmembers), they are generally not well suited for the detection of unknown contaminations covering small areas (hot spots). As considered earlier, many different combinations of various soils, hydrocarbon contaminants and man-made hydrocarbon materials with different spectral characteristics, intensities and concentrations may occur, which all cannot be known a priori. Therefore, a more methodological approach applying knowledge of the general spectral characteristics of groups of important contaminants and materials and their interactions with background matrices (soils) will be proposed and demonstrated in the subsequent paragraphs.

7.3 – Data interpretation for the detection of fuel hydrocarbon soil contaminations

Based on the results of the characteristic spectral features of different fuel hydrocarbon materials and related natural and synthetic hydrocarbon-bearing materials, and the results obtained in data interpretation tests applying established data interpretation tools for imaging spectrometry, the following method is proposed to increase the detection rates of hydrocarbons and to separate different classes of hydrocarbons in imaging spectrometry datasets. The method proposed is based on the following observations and assumptions:

1. Usually, fuel hydrocarbon soil contaminations and related hydrocarbon materials of natural or synthetic origin make up only a minor fraction of an imaging spectrometry dataset.
2. Usually, fuel hydrocarbon soil (or concrete) contaminations exposed at the surface (open soil) are relatively small, covering only several to few hundred square meters.
3. Fuel hydrocarbon contaminated soils typically exhibit characteristic absorption features at around 1,700 nm and 2,300 nm, while the 1,200 nm absorption feature is generally weak.
4. Plastics generally also exhibit absorption features around 1,700 nm and 2,300 nm plus a medium to strong 1,200 nm absorption feature typically not found in the spectra of fuel hydrocarbon contaminated soils but also in the spectra of pure, basic hydrocarbon compounds.
5. The exact minimum locations of the hydrocarbon absorption features and additional absorption features (apart from the carbon-hydrogen backbone) allow for an identification of major chemical groups (alkanes, alkenes, alkynes, monoaromatics, polynuclear aromatics, alcohols, etc.) or groups of synthetic hydrocarbon-based materials.

6. Established data interpretation methods including the comparison of image spectra to reference target spectra selected from spectral libraries or image scenes are found to detect only a part of the hydrocarbon bearing materials or contaminated soils in the scene.
7. A huge variety of different hydrocarbon materials in different uses (construction/roofing material, lorry tarpaulins, commercial and household wastes, boats, painted surfaces, asphalts, etc.) typically occur together in an imaging spectrometry dataset. Contaminated soils with different hydrocarbon contaminants at different concentrations in different soil types are only one of a huge variety of similar hydrocarbon spectra to occur – if they occur in a dataset at all. Together, this makes the selection of a comprehensive set of reference spectra for data interpretation virtually impossible.

Basically, the method proposed consists of three major steps. First: the detection of all natural and man-made hydrocarbon-bearing materials and hydrocarbon contaminations using common absorption features like the 1,700 nm and 2,300 nm region absorption features. Second: the separation of different classes of hydrocarbons and natural and synthetic materials using specific absorption features and shifts of absorption features of the different classes. In particular, false positives like plastics and natural materials (wood, certain vegetation species) can be separated from other hydrocarbon species using the 1,200 nm absorption feature and absorption feature depths of the 1,700 nm and 2,300 nm absorption features that are typically deeper for pure hydrocarbon materials and weaker in fuel hydrocarbon soil contaminations and natural organic materials. Third: the detailed analysis of the selected hydrocarbon spectra of interest with respect to hydrocarbon species and background or matrix (soil) spectra. Additional steps might be added to enhance the detectability (amplification of characteristic absorption features as described in section 6) or to perform a quantitative analysis on pixel spectra of interest if appropriate calibration models can be established.

The detection was found best to be based on simple band differences between unaffected bands on the shoulder of characteristic absorption features and typical minima of characteristic hydrocarbon absorption features. These absorption features are similar to those used earlier for the determination of depths of hydrocarbon absorption features rather than spectrum matching methods or the hydrocarbon index introduced earlier.

A comparison of typical spectra of natural and synthetic materials bearing hydrocarbons and occurring in imaging spectrometry datasets (depicted in figure 7-1) shows that natural materials as well as man-made materials and contaminated soils all exhibit hydrocarbon absorption features around 1,200 nm, 1,700 nm, and 2,300 nm. However, depending on the material type and its basic organic (hydrocarbon) compounds, the absorption features are different with respect to their minimum position, width (FWHM), depth and the relation to neighboring bands on the shoulder of the hydrocarbon absorption features. Additionally, characteristic absorption features of some hydrocarbon classes can be observed in the 1,100 nm wavelength region.

The comparison shows that the target materials of interest in this study exhibit a clearly distinguishable absorption feature in the 1,700 nm wavelength region and in the 2,300 nm wavelength region. Considering only the 1,700 nm absorption feature, a very similar absorption feature with respect to minimum position and depth is observed for wood (both ranging from 1,718 nm – 1,730 nm, with depths of about 5%). Differences between both materials are observed in the 1,200 nm bands, which show strong and broad bands for wood and weak for hydrocarbon-contaminated soil. Another difference lies in a 2,096 nm absorption feature that is only observed for wood but no other hydrocarbon-bearing material.

For vital and dry vegetation, a 1,700 nm absorption feature with a minimum around 1,780 nm and a depth of about 2 – 3 % is generally observed. Also, a 1,200 nm absorption feature is typically observed in vegetation spectra with a minimum around 1,190 nm, a high reflectance difference compared to its left shoulder, and a low reflectance difference to its right shoulder.

As discussed earlier, pure hydrocarbon materials, in particular plastics, exhibit a very strong 1,700 nm absorption feature plus strong 1,200 nm and 2,300 nm absorption features and the characteristic aromatic 2,150 nm absorption feature when aromatic compounds are involved. Absorption feature depths are generally in the tens of percents rather than single-digit percents, as observed for natural materials and contaminated soils where hydrocarbons make up only a minor fraction of the total spectrum. Unlike in vegetation spectra, where the left shoulder is typically high and the right shoulder low, the 1,200 nm absorption feature of plastics and other pure, synthetic hydrocarbons is generally found to exhibit a similar reflectance on both shoulders.

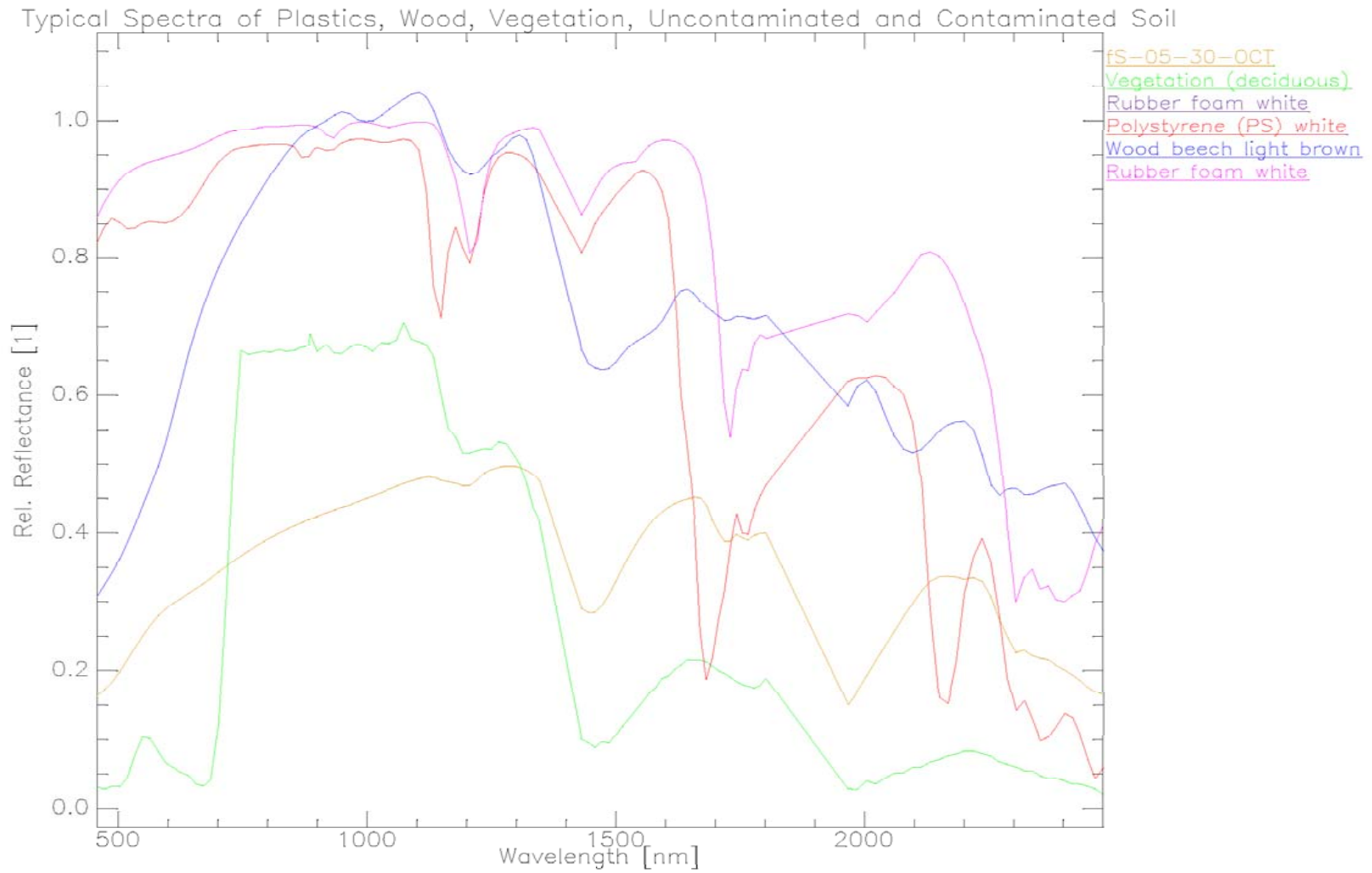


Figure 7-1: Comparison of absorption characteristics of different natural and man-made hydrocarbon-bearing materials and hydrocarbon soil contaminations.

The differences outlined above, and described in more detail in section 6, allow for the detection and differentiation of hydrocarbon abundances in imaging spectrometry datasets.

To detect hydrocarbons of different chemical compositions and origins, several different band differences were applied to the dataset, targeting characteristic absorption features of the different classes of hydrocarbons. Band differences are defined as simple subtraction operations where the reflectance at a known characteristic absorption feature minimum is subtracted from the reflectance on one of its shoulders. When this operation is applied to an imaging spectrometry dataset for a known absorption feature, it is expected to return positive values for spectra in the dataset containing this absorption feature and negative values or values around zero for spectra not containing this absorption feature, thus having a negative slope or no slope between the two bands involved in the operation. If applied to a relative reflectance dataset with values ranging from 0.0 (0% relative reflectance) to 1.0 (100 % relative reflectance), the values are generally expected to lie between -1.0 (positive slope over the full range from 0.0 and 1.0 between the two selected bands) and +1.0 (negative slope over the full range from 1.0 and 0.0 between the two selected bands). For hydrocarbons however, the values expected are generally in the positive range with values between 0.03 (3 % absorption feature depth) and 0.1 - 0.5 (10 - 50 % absorption feature depth). Of course, the absorption feature depth determined by this method does not take into account the hull or the slope on which an absorption feature is situated. It simplifies absorption feature depth to a simple difference between two bands rather than calculating the convex hull and determining the absorption depth at the minimum band compared to the hull (compare figure 4-1). In addition, there is no normalized absorption feature depth for the reference matrix or background material for slope effects, as was done in determining the threshold for hydrocarbon detection in soils in section 6. Such normalization is infeasible for an imaging spectrometry dataset comprising spectra of dozens to hundreds of materials in different combinations. The bands used for the band difference indices need to be carefully selected by the user to ensure that (as far as possible) only the target material exhibits a characteristic band difference (or absorption feature) in a given wavelength region. In the best case scenario, all other materials abundant in a scene will not exhibit a significant band difference between the two bands selected. To ensure this, the bands involved in the operation should be chosen to be no further apart than 100 nm to 150 nm.

The result of a band difference applied to an imaging spectrometry dataset can be displayed as a color-coded image having different grayscales or colors indicating different absorption feature depths. Generally, values below or only slightly above zero should be masked out using the stretching functions available in imaging processing software. Histogram stretching generally should be applied such that the pixels of interest with band difference values higher than 3 - 10 % (0.03 - 0.10) are displayed color-coded according to increasing values, while pixels with lower or negative values (background, non target materials) are masked.

Band differences as outlined above were applied to different characteristic absorption features of hydrocarbon-bearing materials in the 1,700 nm wavelength region. To specifically adapt the band differences of aliphatics and different aromatics, the following band differences were applied covering all possible absorption features of natural (except green vegetation) and man-made hydrocarbon-bearing materials:

$$\textit{Aliphatics 1 / Wood} = R(1,656 \text{ nm}) - R(1,730 \text{ nm})$$

$$\textit{Aliphatics 2} = R(1,656 \text{ nm}) - R(1,718 \text{ nm})$$

$$\textit{Aliphatics 3} = R(1,656 \text{ nm}) - R(1,706 \text{ nm})$$

$$\textit{Aromatics 1} = R(1,554 \text{ nm}) - R(1,694 \text{ nm})$$

$$\textit{Aromatics 2} = R(1,554 \text{ nm}) - R(1,681 \text{ nm})$$

$$\textit{Aromatics 3} = R(1,554 \text{ nm}) - R(1,669 \text{ nm})$$

with

$R(\lambda)$ – relative reflectance at wavelength λ

The resulting output datasets contained data ranges from -0.08 to $+0.16$, indicating maximum absorption feature depths of hydrocarbon absorption features in the imaging spectrometry dataset of up to 16 % (in terms of simple band differences). For data interpretation, histogram stretching was applied to the single output datasets such that all pixels with calculated band differences below 4 % (0.04) were displayed as black (masked), the grayscale color table was applied to all absorption feature depths between 4 % and 8 % (0.04 – 0.08) and all absorption feature differences of more than 8 % (0.08) were displayed in white indicating best hits for characteristic hydrocarbon absorption features. Comparing the different datasets, it was found that the band difference datasets calculated for different wavelength regions indicated different pixels with hydrocarbon absorption features in the 1,700 nm wavelength region depending on the wavelength bands for which the difference was calculated. However, neighboring difference indices partially returned similar pixels with positive values, indicating similar absorption features.

In order to unite the results obtained from the single band difference calculations, all resulting output datasets were added up to a single file in order to display all hydrocarbon absorption features detected in one image display. The dataset resulting from the addition of all single band differences comprised a data range from -0.17 to $+0.49$. Using the region of interest tools, all pixels of this dataset with a value equal to or larger than 0.08 (8 % relative reflectance) were selected using the *band threshold to region of interest* tool of ENVI® and displayed as pixels exhibiting a 1,700 nm absorption feature (Figure 7-2). A total of 289 pixels of the scene were

found to exhibit absorption features with band differences above this threshold. If the threshold was increased to 0.1 (10 % relative reflectance), only 217 pixels were found to fulfill the criterion, if it was decreased to 0.06 (6 % relative reflectance), 468 pixels fulfilled the criterion. With the threshold at this lower level, a larger number of mixed pixels (neighboring pixels to those also selected with higher thresholds) and a larger number of “wood” pixels were detected. Only few false positives were observed with the threshold at the lower level. The background image is a grayscale image of the 609 nm band of the HyMap dataset in figure 7-2.

To separate the detected hydrocarbon abundances into two groups, namely aromatics-based and aliphatics-based materials, the three single band differences calculated for each group were added to yield two output datasets, one for aromatics (absorption feature minimum at wavelengths < 1,700 nm) and one for aliphatics (absorption feature minimum at wavelengths > 1,700 nm). Both groups are depicted in Figure 7-3, the aliphatics-based materials in red and the aromatics-based materials in green. The detection threshold selected for both groups was 0.04 (4 % relative reflectance), which was half of the threshold value selected for the sum of all six datasets. With this threshold, 100 pixels of the dataset were found to contain aliphatics-based materials, and 87 pixels were found to contain aromatics-based materials.

The resulting comparison of the positive hits for hydrocarbon absorption features shows that the method returns few if any false positives for hydrocarbons. All detected hydrocarbon absorption features could be attributed to plausible ground targets by comparison to high-resolution aerial photographs from the years 1999 and 2000 and ground truthing in 2004 and 2005. Most hydrocarbon absorption features, in particular the more intensive ones, were found in settlement areas, while for vegetated areas and water surfaces no significant absorption features were returned by the application of the band difference method. Wood shown to exhibit similar absorption features to soils contaminated with aliphatics in the 1,730 nm region returned a few areas of interest on the grounds of the former military training area *Döberitzer Heide*. Closer investigation of the spectra, however, showed that all of these also exhibited the 2,100 nm wood absorption feature, thus excluding them as fuel hydrocarbons or plastics. Ground truthing, the collection of samples and laboratory spectrometry of these samples confirmed these results.



Figure 7-2: Hydrocarbon abundances (mainly plastics and wood) detected in the HyMap dataset of the former military training area *Döberitzer Heide* from 1999. Hydrocarbon abundances are pixels marked red and circled for better visibility. Summation of six band differences calculated for the region 1,669 nm – 1,730 nm, with a minimum threshold absorption feature depth (band difference) of 0.08 (8 % reflectance).



Figure 7-3: Hydrocarbon abundances (mainly plastics and wood) detected in the HyMap dataset of the former military training area *Döberitzer Heide* from 1999 and separated in two groups: aliphatics (green pixels, circled green) and aromatics (red pixels, circled red). Summation of three band differences calculated each for the region 1,669 nm–1,694 nm and 1,706 nm–1,730 nm, minimum threshold absorption feature depth (band difference) of 0.04 (4 % reflectance).

Band differences were also calculated for the 1,200 nm (plastics, pure hydrocarbons, vegetation), 2,100 nm (wood), 2,150 nm (aromatic hydrocarbons) and 2,300 nm (aliphatic and aromatic hydrocarbons) ranges in an attempt to separate the different classes of hydrocarbon materials. The following band differences were calculated:

$$1,200 \text{ nm Aromatics } 1 = R(1,235 \text{ nm}) - R(1,148 \text{ nm})$$

$$1,200 \text{ nm Aromatics } 2 = R(1,235 \text{ nm}) - R(1,133 \text{ nm})$$

$$1,200 \text{ nm Aliphatics } 1 = R(1,264 \text{ nm}) - R(1,207 \text{ nm})$$

$$1,200 \text{ nm Aliphatics } 2 = R(1,264 \text{ nm}) - R(1,192 \text{ nm})$$

$$2,100 \text{ nm Wood} = R(2,201 \text{ nm}) - R(2,114 \text{ nm})$$

$$2,150 \text{ nm Aromatics} = R(2,004 \text{ nm}) - R(2,150 \text{ nm})$$

$$2,300 \text{ nm Hydrocarbons} = R(2,219 \text{ nm}) - R(2,304 \text{ nm})$$

with

$R(\lambda)$ – relative reflectance at wavelength λ

The 1,200 nm band differences were calculated by subtracting the reflectance at the known absorption feature minima from the reflectance at a longer wavelength, rather than a shorter wavelength as applied for all other calculations, because vegetation was found to exhibit an absorption feature in this wavelength region with a high shoulder on its left (shorter wavelengths) and a low shoulder on its right (longer wavelengths). If the 1,200 nm band difference was calculated accordingly, all vegetation was found to return high band difference values. If, on the other hand, the 1,200 nm band difference was calculated using the lower shoulder as the minuend and the minimum as the subtrahend, vegetation was found to return low values around zero. However, although the sensitivity for the 1,200 nm vegetation absorption feature could thus be considerably reduced, the band differences calculated were found to be cross-sensitive to other materials with strong, continuous positive slopes in this wavelength region, such as burnt red clays (roofing tiles). Despite the cross-sensitivity with respect to materials exhibiting a strong positive slope in this wavelength region, the 1,200 nm absorption feature was found capable of indicating differences between aromatic and aliphatic hydrocarbons in imaging spectrometry data interpretation if the investigation of this feature is restricted to those pixels also exhibiting a 1,700 nm or another characteristic hydrocarbon absorption feature. The 1,200 nm absorption features were found to be specific from an absorption depth (band difference) threshold of at least 0.04 – 0.05 (4 – 5 % relative reflectance). With these thresholds applied to the band differences, vegetation-related false positives were typically not found in the dataset.

Investigating the 1,200 nm wavelength bands of different materials in the scene by means of band differences, it was also found that the difference calculated for the bands at around 716 nm and 1,100 nm (minuends) and at around 791 nm and 1,200 nm (subtrahends), respectively could be used to simply map areas of open soil and areas sparsely vegetated with dry vegetation. This or similar band differences could be used to restrict the area of investigation in an imaging spectrometry dataset to areas of open soil if the investigation is targeted at the detection of fuel hydrocarbon contaminated soils. The region of interest threshold tool referred to above could be used to subset the dataset accordingly for further investigation.

The 2,100 nm wood and 2,150 nm aromatics absorption features were found to be almost inseparable by means of band difference calculations, in particular because both absorption features are relatively wide and therefore overlapping despite the fact that their minimum wavebands are 40 nm to 60 nm apart. Both band differences calculated were therefore found to be relatively unspecific and to contain a larger number of the other component with values above 0.1 in the difference calculations. However, despite wood and aromatic absorption features, no other materials with an absorption feature in this wavelength region were found to interfere in the dataset under investigation. Based on the laboratory spectrometry experiments, however, mineral absorption features of some clays are expected to interfere with these absorption features where they are present and exposed to the surface. Although the 2,100 nm wood and 2,150 nm aromatic absorption features are thus found unsuitable with respect to the separation of different classes of hydrocarbon-bearing materials in the investigated imaging spectrometry dataset, both might prove a valuable tool for the differentiation of aliphatics and aromatics or aliphatics and wood in arid regions if the occurrence of one of the two and clay minerals with absorption features in the same region can be ruled out.

The 2,300 nm absorption feature was also found to be sensitive to wood and some other natural organic materials (dry vegetation). Therefore, the 2,300 nm absorption feature and band differences were found unsuitable for both the detection and the separation of hydrocarbons.

Figure 7-4 depicts the spectra of two hydrocarbon pixels detected and separated as aromatic-based and aliphatic based hydrocarbons using the 1,700 nm absorption features. The two spectra were selected from the image for identification. Figures 7-5 and 7-6 show a subset of an RGB aerial photograph acquired from the location of the two pixels identified as hydrocarbon-bearing and a subset of the imaging spectrometry dataset covering the same area. Ground truthing showed that the pixels identified as hydrocarbon-bearing represent a greenhouse with a transparent to white plastics roof (identified as aromatic hydrocarbons) and beds covered with transparent plastic sheets (identified as aliphatic hydrocarbons).

The greenhouse pixels identified as aromatic hydrocarbons have an absorption feature with a minimum at 1,669 nm (< 1,700 nm), indicating aromatic compounds in the material. The band difference calculated is about 0.15 (15 % relative

reflectance). The aliphatic absorption feature at the greenhouse entrance has an absorption minimum at 1,730 nm ($> 1,700$ nm), indicating aliphatic compounds. The absorption feature depth, calculated as band differences, is about 0.05 (5 % relative reflectance).

By comparing the image spectra to laboratory spectra resampled to match the wavebands of the HyMap instruments, the aromatic, greenhouse pixel spectra were identified as polystyrene (PS). The only other plastic material exhibiting similar absorption feature combinations in both the 1,200 nm and 1,700 nm regions was found to be acrylic plastic (PMMA). Acrylic plastic could be ruled out because of a characteristic absorption doublet of polystyrene at 1,133 nm and 1,207 nm compared to a single absorption feature of acrylic plastic with its minimum at 1,177 nm to 1,192 nm and the 1,700 nm of acrylic plastic slightly shifted towards longer wavelengths.

The aliphatic pixel spectra were identified as polyethylene (PE) based on the position of the 1,200 nm and 1,700 nm absorption features that were found to perfectly match the image spectrum with respect to the absorption feature minimum positions.

Most other pixel spectra detected as hydrocarbon spectra were also found to be specifically identifiable by means of manual image – library spectra comparison.



Figure 7-4: Color aerial image (RGB) acquired in 2000, Krampnitz village, resolution 0.5 m. The greenhouse and entrance, detected as aromatic and aliphatic plastic respectively, are noted.

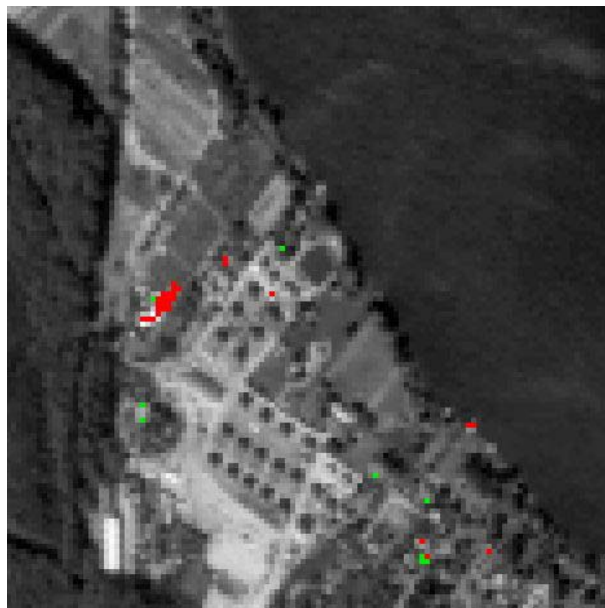


Figure 7-5: Subset (zoom) of the HyMap 1999 dataset (5-6 m spatial resolution) of the same area. Green pixels indicate aliphatic hydrocarbon features detected by the band difference method in the 1,700 nm region, red pixels indicate aromatic hydrocarbon features.

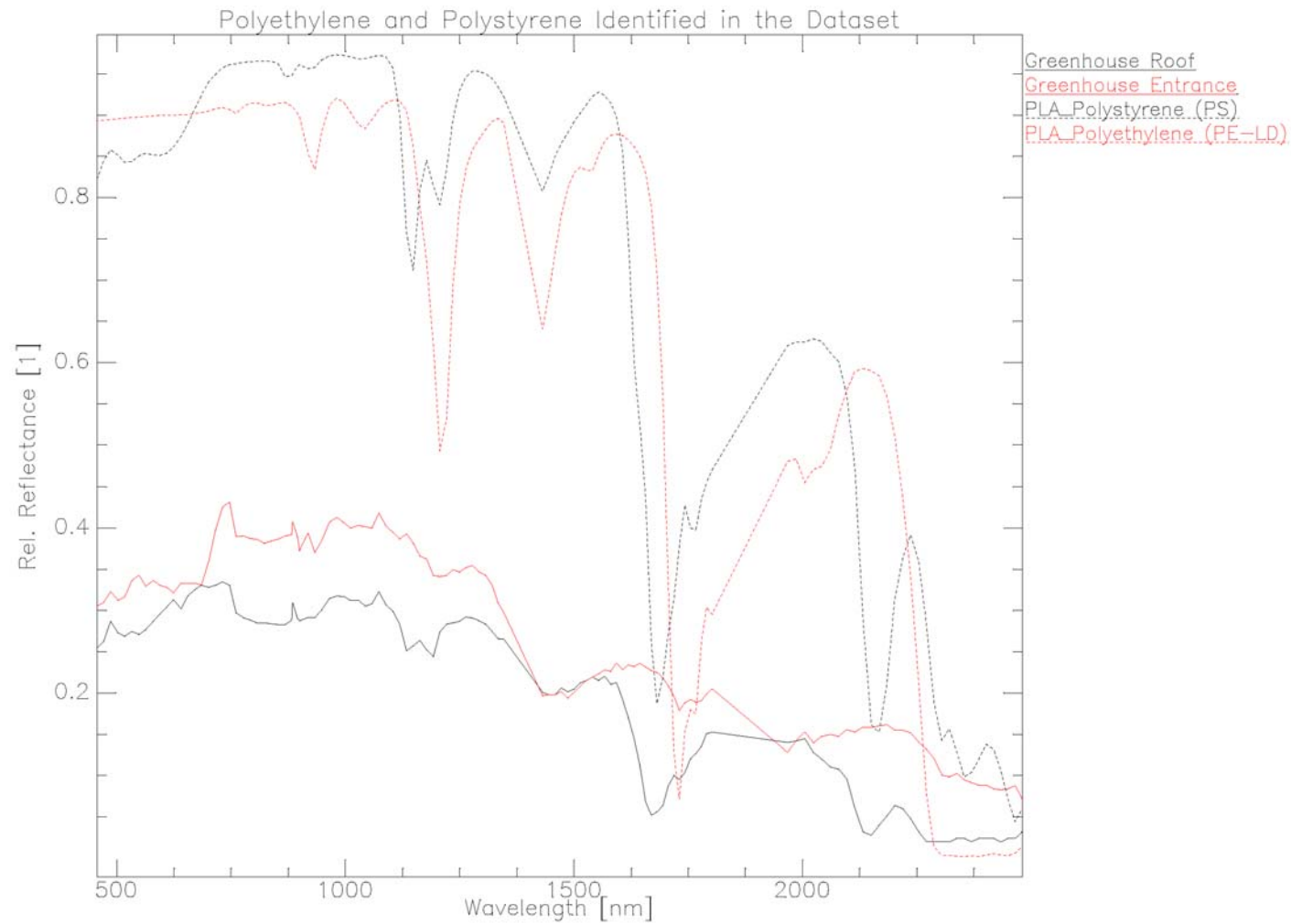


Figure 7-6: Comparison of the greenhouse (black) and greenhouse entrance (red) spectra from the imaging spectrometry dataset to the resampled laboratory spectra of polystyrene (dashed, black) and polyethylene (dashed, red).

The results show that applying simple band differences calculated by using carefully selected bands holds the potential for detecting hydrocarbons in imaging spectrometry datasets and distinguishing the two major groups, aliphatic and aromatic-based materials. Despite several cross-sensitivities to related materials, the above results also demonstrate that the proposed method particularly holds the potential to further differentiate classes of hydrocarbons. By applying the above method, i.e. using expert knowledge and visual analysis in comparing image and library spectra, several individual synthetic hydrocarbons were detected and identified in the investigated scene. In particular, the method applied was found to be return fewer false positives than the hydrocarbon index proposed by other authors because it is not only centered around a single absorption feature (1,730 nm).

Although the method was at first used to detect hydrocarbons in the investigated dataset, it could also be applied to map large contaminated areas with known or unknown hydrocarbons as contaminants. However, in these cases, matched filtering or operational hyperspectral data analysis might be easier and more reliable to apply, requiring less manual interpretation work.

Instead of band differences that were applied here, it would also be possible to adapt the hydrocarbon index (determination of continuum-removed absorption band depth) proposed by other authors to specifically detect different hydrocarbon classes. However, it might prove difficult to adapt the hydrocarbon index because it would require the definition of not only the minimum waveband but also the two shoulders of each absorption feature – which are found at different positions for different hydrocarbons. Therefore, band differences are simpler to apply and probably more reliable with respect to the approximate determination of absorption band depths.

Although the interpretation approach demonstrated here focused on the detection and mapping of hydrocarbons in imaging spectrometry dataset, based on manual interpretation and band difference calculations, it is possible to develop a cascaded automatic interpretation algorithm based on this. It would however, require further investigations with respect to cross-sensitivities and the implementation of a process chain algorithm. Because of the several varieties of different hydrocarbons and hydrocarbon-bearing materials, each with its own spectral characteristics and infinite combinations in imaging spectrometry datasets, such automated algorithms should still require for the user to determine the absorption features of interest and wavebands to be analyzed. This, in turn, will require the user to understand the spectra of the materials he is targeting.

8 – Synopsis, conclusions and vision

The subject of this study was the investigation of the applicability of imaging spectrometry for contaminated site investigation and particularly the detection of fuel hydrocarbon soil contaminations. Imaging spectrometry is defined as a remote sensing technique acquiring quasi-continuous reflectance spectra in the visible through shortwave infrared wavelength regions. Imaging spectrometry in principle allows for a detailed qualitative and quantitative analysis of the Earth's surface, providing high spatial and spectral resolution data. With contaminated sites endangering important natural resources like groundwater and arable land and posing severe problems worldwide, the potential of imaging spectrometry for the detection and investigation of contaminated sites is a potential tool for investigation.

General applicability of remote sensing for contaminated site investigation

The general advantage of remote sensing methods over other methods based on field-based data collection is that remote approaches allow for systematic surveys of large areas at relatively low costs and can be repeated regularly. Also, inaccessible and remote areas can be investigated with relatively few ground reference investigations. Since it provides spatial information about the surface, remote sensing methods can be applied to overview investigations and temporal monitoring only where relevant information expresses itself at the surface. Also, a suitable remote sensing detection system or method is required for detecting the concerned features. Thus, remote sensing systems provide information on the spatial distribution pattern of targets of interest. On the other hand, remote sensing methods have general disadvantages compared to ground-based methods. Since all optical remote sensing methods provide only information about the surface (the upper few micrometers determine the reflectance of a target), generally no direct information on the subsurface can be obtained by remote sensing methods. In some cases, indicators (e.g., vegetation stress, altered geology) might allow to correlate surface observations to subsurface properties. In most cases, however, contaminated sites are found on industrial and military brownfields and are usually connected to or covered by infrastructure installations or vegetation. Impermeable surfaces (traffic infrastructure), buildings, installations and shadowing effects caused by these, along with regrowth of plant cover on brownfields after years of lying fallow, prevent direct optical remote sensing access to contaminations. Other sites, in particular military training areas as an important type of military brownfields, are often highly complex and diversified with respect to their surface structure. Here, typically large areas are covered by vegetation, making them inaccessible to direct remote sensing investigation. In addition to these challenges, hot spots of contaminated soil are typically small, covering only a few tens of square meters. Therefore, remote sensing methods are best applied to contaminated site detection and investigation where targets (contaminated soils, waste deposits, mining wastes, etc.) are expected to be directly exposed at the surface.

Two basic application cases are under consideration. First, the detection of unknown contaminations or wastes deposits, and second, the mapping of known contaminations with known contaminants. Detection applications typically include imaging spectrometry surveys of larger areas and the application of detection algorithms to locate and identify hydrocarbon abundances of different types. Mapping applications would typically include imaging spectrometry surveys of an area of interest and an investigation of the abundance of one or more specific hydrocarbon species.

Since only surface information is provided, generally only those elements exposed at the surface of a contamination or waste deposits, can be detected, given they exhibit characteristic absorption features. This method is not applicable to the direct detection or mapping of inorganic contaminants (heavy metals, salts, nutrients, etc.) or other hazards found on some sites (e.g., unexploded ordnance on military sites and battlefields). For this reason, remote sensing and particularly imaging spectrometry can only be one of several tools used to detect, map and investigate hot spots of certain contaminations and wastes. Remote sensing methods in general do not hold the potential for comprehensive site investigation.

Spectral characteristics of fuel hydrocarbons

In laboratory investigations conducted with different classes of hydrocarbons, including basic organic compounds, substituted compounds, and commercial (fuel) hydrocarbon products, it has been shown that optical spectrometry in the visible through mid infrared spectrum (0.4 μm – 2.5 μm) allows for the identification of different groups of hydrocarbons. Above all, the differentiation between aliphatics and aromatics is possible and also a number of functional groups can be identified. Hydrocarbon absorption features were identified in the 900 nm, 1,200 nm, 1,380 nm, 1,700 nm, 2,150 nm and 2,300 nm wavelength regions. In general, absorption features were found to be strong and wide at longer wavelengths and to decrease in both intensity and width towards smaller wavelengths.

Considering remote sensing applications with respect to the detection and quantification of hydrocarbons in imaging spectrometry datasets, it was found that the 900 nm absorption feature is usually too weak to be utilized. However, for some synthetic hydrocarbon materials (plastics) this feature could play a role in identification. The 1,200 nm absorption feature is generally of medium to strong intensity in pure hydrocarbon compounds and hydrocarbon-based synthetic materials but very weak where hydrocarbons make up only a minor fraction. It was therefore found to play a particular role for the detection and identification of plastics and the differentiation of plastics from fuel hydrocarbon soil contaminations. The 1,380 nm absorption feature generally plays no role in remote sensing applications because it overlaps with the strong 1,400 nm atmospheric water vapor absorption band that prevents remote sensing in this wavelength region. The 1,700 nm absorption feature was found to be a characteristic and specific absorption feature for hydrocarbons. It

was not found to overlap with major absorption features of non-hydrocarbon materials.

The 2,150 nm (only aromatic) and 2,300 nm absorption features were found to be typically strong. However, both features might be found to overlap with major mineral absorption features (mainly of clays). Also, the data acquired in this region by imaging spectrometers might exhibit elevated noise levels, depending on sampling duration (dwell time) and bandwidth.

Ability to differentiate between different hydrocarbon classes

The experiments conducted showed that different classes and groups of basic hydrocarbon compounds (both pure and as contaminants in soils), man-made materials consisting of or containing hydrocarbons (plastics, paints, paper, cardboard, etc.) and natural hydrocarbon-bearing materials (wood, dry plant material, etc.) can be distinguished in reflectance spectra in the 0.4 μm to 2.5 μm wavelength region although different materials might exhibit similar absorption characteristics for single absorption features. Comparing two or more different absorption features based on minimum position, width, and depth, it was found that all hydrocarbon-bearing materials can be differentiated.

In particular it was found that aromatics and aliphatics and materials composed of either aromatics or aliphatics can be easily differentiated in imaging spectrometry datasets.

For the 1,200 nm and 1,700 nm absorption features it was found that aliphatic compounds tend to exhibit absorption features at longer wavelengths than aromatic absorption features. This was similarly observed for the other absorption features mentioned but not as evident as for these two absorption features.

Plastics were found to exhibit characteristic absorption features, which allow them to be differentiated from other targets (natural materials, hydrocarbon soil contaminations). Imaging spectrometry can also be used to detect and map uncontrolled waste deposits because plastics make up a major fraction of all household and commercial wastes disposed off.

Detectability and detection limits of fuel hydrocarbon soil contaminations

Experiments were conducted with twelve different organic contaminants (fuel hydrocarbons, monoaromatics and polynuclear aromatics, aliphatics, phenols, explosives, chlorinated aromatics) at three concentration levels (0.5 wt.%, 1.0 wt.%, 3.0 wt.%) in seven different soils (sands, clays, organic soils) at three moisture levels (0 % - max. 30 %, individual levels depending on the soil type). It was found that the detectability and the detection limit largely depends on the soil type and soil properties, in particular soil moisture, clay content, particle size, and organic matter content, and not on spectral characteristics of the contaminant and its concentration.

In laboratory investigations, different hydrocarbon contaminants were found to exhibit similar absorption feature characteristics in similar soil samples at similar concentrations. Absorption feature depths at identical contaminant concentrations in identical soil samples were found to sharply decrease with increasing soil moisture. Similarly, absorption feature depths were found to sharply increase with increasing contaminant concentrations in identical soil samples with identical soil moisture levels.

Generally, it was found in the laboratory investigations that hydrocarbon soil contaminations can be detected if the absorption feature depth is at minimum 3 % of the absolute reflectance at the absorption feature wavelength position. Because of this requirement, only the relatively strong 1,700 nm and 2,300 nm absorption features of fuel hydrocarbons are suitable for detection purposes in soil matrices.

While the detectability in primary silicate mineral soils (sand) was found to be good, the detectability in secondary silicate mineral (clay) and organic soils (humic soil, boulder till) was found to be generally poor. In sand soils, fuel hydrocarbon concentrations of 1.0 wt.% (10,000 mg/kg) were generally detectable using the 1,700 nm absorption feature, regardless of soil moisture levels. When using the 2,300 nm absorption feature, even the 0.5 wt.% (5,000 mg/kg) concentration was found to be detectable in most cases.

In clay soils, even contaminant concentrations as high as 3.0 wt.% were only detectable in some cases with no clear pattern with respect to soil moisture dependence. Based on the absorption feature depths measured, it is assumed that fuel hydrocarbons in clays can only be reliably detected if the concentration exceeds 5.0 wt.% (50,000 mg/kg). Boulder till containing both primary and secondary silicate minerals and a significant amount of organic matter was found to behave similar to clays. In humic soil, all contaminants were found to be typically non-detectable at concentrations of 3.0 wt.% regardless of the soil moisture level. With only minor absorption feature depths even at this concentration level, no prediction can be made of the concentration at which hydrocarbon contaminants are detectable in soils with high organic matter content.

Imaging spectrometry quantitative analysis of soil contaminations

The experiments conducted proved that fuel hydrocarbons in dry and moist soil samples generally exhibit a non-linear spectral mixing behavior. Therefore, linear mixing models widely used for imaging spectrometry data unmixing and quantitative analysis cannot be applied to fuel hydrocarbon contaminated soil spectra.

However, if larger areas with identical or similar soil types (with respect to soil composition and soil properties) are to be investigated for fuel hydrocarbon contaminations, calibration models could be developed to enable quantitative analysis of fuel hydrocarbon concentrations in soils.

Linear mixing models are applicable only if surfaces covered with pure, non-transparent hydrocarbons contribute to larger pixel spectra also comprised of other surface materials or where plastics (wastes) occur together with other materials that contribute to a common pixel spectrum.

Remote sensing implications

Considering the traits of the major characteristic absorption features concerning the detection of hydrocarbons as contaminants in soils and as pure hydrocarbon materials, the following requirements for remote sensing applications with respect to instrumentation and data acquisition parameters can be defined:

- Because hot spots of fuel hydrocarbon soil contaminations are typically small, and cover only a few to tens of square meters, spatial resolution of imaging spectrometry data acquired for their detection should be high, i.e. two or three meters per pixel. The higher the spatial resolution, the purer the pixel spectra, the lower the spatial resolution, the more spectral endmembers are typically combined in a pixel spectrum. This is particularly true for complex, diversified surface structures of contaminated sites.
- The absorption feature widths (FWHM) in the spectral regions up to 1,700 nm are often between ten and a few tens of nanometers. Therefore, the spectral resolution (FWHM bandwidth) of instruments used for data acquisition should be five nanometers in order to ensure a minimum of two, but more favorably five bands to cover a single absorption feature and determine the minimum position with a deviation of ± 5 nm. This is required due to specific absorption band positions of different hydrocarbon compounds and materials (aliphatics, aromatics, etc.). With absorption feature widths of 50 nm up to 250 nm in the wavelength regions beyond 1,700 nm, the minimum spectral resolution in this region should be ten nanometers.
- Because the visible wavebands do not contain important information about hydrocarbons, it is not necessary to cover this wavelength region with the full spectral resolution. A few bands to provide reference imagery (PAN, RGB, CIR) for the analysis will be sufficient. If, however, vegetation absorption features in this wavelength region (vitality, chlorophyll absorption, red edge, etc.) or soil color are of interest, this wavelength region should be covered spectrally.
- Radiometric resolution and signal-to-noise ratio should be as high as possible to ensure the detectability of low contaminant concentrations at wavelengths beyond 2,000 nm and to allow for the amplification as proposed. However, due to restrictions of the illumination source in remote sensing, atmospheric

interferences and thus the uncontrolled environment in which the method is applied, measurements cannot be repeated indefinitely like in analytical laboratory chemistry to eliminate noise. Due to the nature of remote sensing, the dwell time for each pixel is limited and noise in the data cannot always be prevented or eliminated. Increasing bandwidths and thus the wavelength region over which radiation is integrated during data acquisition in a single band may also be helpful in reducing noise in the data, particularly at longer wavelengths. However, the negative correlation of spatial resolution and radiometric resolution and signal-to-noise ratio requiring trade-offs have to be observed.

Data interpretation for hydrocarbon detection, mapping and separation

Established data interpretation approaches for imaging spectrometry data interpretation, such as spectral angle mapper, matched filtering, mixture tuned matched filtering, and spectral feature fitting were found to be unsuitable in detecting fuel hydrocarbon abundances in imaging spectrometry datasets. This is due to the huge variety of hydrocarbons exhibiting different specific absorption features with shifts of up to 100 nm for a single feature, depending on the chemical characteristics (aromatic, aliphatic, etc.), and because hydrocarbons typically make up only a minor fraction of the materials present in the datasets. It is therefore impossible to determine and select all relevant endmembers for these analysis approaches from spectral libraries. Also, the hydrocarbon index developed for the 1,730 nm aliphatic absorption feature was found to detect only a fraction of the many synthetic hydrocarbons present in a scene. It also returned a considerable number of false positives (vegetation, wood).

As an alternative, a data interpretation approach was developed, which applied several different simple band ratios with carefully selected bands at the expected absorption feature minimum and on of the shoulders of the major characteristic hydrocarbon absorption feature around 1,700 nm. When this method was applied to an imaging spectrometry dataset containing a number of hydrocarbon spectra (plastics), the method was found to correctly detect the abundance of synthetic hydrocarbons. By using characteristic shifts around the 1,700 nm absorption feature, this method also allowed for the differentiation of aromatic and aliphatic hydrocarbons. It also clearly limited the number of false positives when the detection threshold was reduced to a minimum of 3 – 4 % absolute reflectance.

This method was also shown to allow for the differentiation of different classes of natural and man-made hydrocarbon-bearing materials when other absorption features, in particular those around 1,200 nm and 2,150 nm, are included in the analysis.

Applicability to contaminated site types

The results obtained in the laboratory and data analysis experiments have clearly demonstrated that imaging spectrometry can detect organic contamination in soils, well justifying further investigation and development of field methods for detection. Considering the examples of contaminated sites introduced in section 2, this means that the uncontrolled waste dumps in the Rio Unare Basin in Venezuela, hydrocarbon soil contaminations observed at the diesel filling station (also in the Rio Unare Basin in Venezuela), and the soil contaminations at the Mingecevir fuel depot in Azerbaijan could all be detected by imaging spectrometry. In the latter case, soil color changes caused by the oxidation of iron in soil due to leakages of nitric acid could also be detected by analyzing the visible wavelength region of an imaging spectrometry dataset and comparison to unaffected, neighboring soil pixel spectra. A more detailed investigation apart from the detection is infeasible, due to the small size of these contaminated sites.

Imaging spectrometry can also be considered a feasible option for the detection, mapping, and investigation of large contaminated sites, in particular large mining dumps where organic wastes are also disposed, and the contamination of large areas from spills during production and transportation of crude oil. The large mining dumps in the manganese-producing district of Ordshonikidse in the Ukraine, the contamination of several hundred square kilometers of open soil with crude oil from oil production on the Absheron Peninsula in Azerbaijan, and the pollution of a marshland with crude oil after the destruction of a pipeline during the Iran-Iraq war near Abadan in southern Iran, as introduced in section 2, all fall in this category. For these large, homogeneous areas, quantitative analysis can be considered a feasible option as calibration models could be established for large areas of a similar matrix (soil) contaminated with one or few different contaminants.

Imaging spectrometry should not be considered for the detection and investigation of soil contaminations at industrial brownfields where large areas are covered with buildings, plants, and traffic infrastructure or are hidden in the shadow of installations and buildings. Although soil and groundwater contaminations are frequently observed at these sites, they are typically covered and not exposed at the surface. Although a few points of interest could be detectable if exposed at the surface, it must be assumed that the vast majority is not detectable by remote sensing methods. Imaging spectrometry – along with other remote sensing techniques – has therefore been deemed inapplicable to industrial brownfields like the former glassworks Haidemühl or the Schwarze Pumpe industrial facility introduced in section 2.

Similarly, the applicability to sites of buried wastes or sites with large fractions covered by vegetation is limited. The uncontrolled waste burials near Groß Pinnow or the former military training area Döberitzer Heide in Brandenburg fall into this category. Here, soil contaminations are typically not directly detectable because the soils are covered by vegetation. Apart from the direct detection of contaminants in

soils, however, the use of imaging spectrometry data can aid in the location of vegetation stress indicators.

Because soil moisture and vegetation cover limit the detection of fuel hydrocarbons in soils, the applicability in general must be assumed better in arid and semiarid regions, where both factors have limited influence and do not interfere as much as in humid and temperate climate regions. The higher solar radiance and the lower atmospheric interferences (due to lower atmospheric water vapor concentrations) also allow for higher signal-to-noise ratios and better detectability of concerned targets in these regions.

Vision

Based on laboratory results, imaging spectrometry could be applied immediately to (1) the detection, mapping and quantification fuel hydrocarbon contaminations in soil or surface area in regions where crude oil is produced (e.g., Middle East, Caspian Sea Region, Siberia, Northeastern Venezuela) and (2) to the detection and mapping of locations of uncontrolled waste dumping found at the surface in virtually every region of the world.

Similarly, the use of portable field spectrometers could be applied in the detection and identification of organic soil contaminants during overview site investigations in order to identify hot spots for further investigation.

With further research on the effects of different organic and inorganic contaminants on vegetation (short and long-term vegetation stress, species shifts, etc.) the application of imaging spectrometry for contaminated site detection could be extended to areas covered by vegetation and thus to humid and temperate climate regions.

With further research and development into the automated analysis of imaging spectrometry datasets for (environmental) features of interest, imaging spectrometry could also be applied toward continuous monitoring of the environment with repeated, regular imaging spectrometry data acquisition. Applications could include the detection of soil contaminations, waste deposits, general environmental damage assessment, vegetation pest infestation, and others for environmental management and law enforcement. The applicability and results could be considerably enhanced if imaging spectrometry data is fused with data of other remote sensing methods (thermal imaging, airborne laser scanning, high resolution digital aerial photography). With the automation of analysis methods, real-time (in-flight, on-board) environmental monitoring and mapping would become feasible.

Future research topics

Based on the results and the vision for future applications of imaging spectrometry, the following topics for future research are identified:

- Development of a full scale field method of imaging spectrometry data collection and analysis for the detection of organic contaminants in soils.
- Development of an automatic (programmed) detection and separation algorithm for hydrocarbons in imaging spectrometry datasets based on the band difference data interpretation method proposed.
- Investigation of the effects of organic and inorganic contaminants on vegetation (short and long-term vegetation stress, species shifts, indicator species, insensitivity of certain vegetation species to certain contaminants or concentration levels, responses of different plant species to similar contaminants, etc.).
- Fusion and combined interpretation of imaging spectrometry data with other remote sensing data, in particular airborne laser scanning data, thermal imaging data, high-resolution digital aerial photography.
- Application of self-training neural networks as a promising data interpretation tool to detect, differentiate, and identify fuel hydrocarbon contaminants in soils, synthetic hydrocarbon materials and natural hydrocarbon-bearing materials.
- Investigation of spectra of fuel hydrocarbon contaminants spectra, synthetic hydrocarbon materials, and natural hydrocarbon-bearing materials in the 3 μm – 5 μm wavelength region (thermal infrared I), where hydrocarbons typically exhibit their fundamental vibrations, which allow for better identification and analysis. Imaging spectrometry in this wavelength region is already applied to identify and map silicate minerals that do not exhibit absorption features in the 0.4 μm to 2.5 μm wavelength region despite generally low irradiance in this region (thermal emission rather than reflectance of incident solar radiation).

References

Remark: Only the cited references are listed in the subsequent list of references. A comprehensive bibliography and database of publications on the subject of imaging spectrometry and its environmental applications can be found on the enclosed CD-ROM (lit_hyperspec.mdb, Microsoft Access database) or can be obtained from the author on request. The abbreviations used here are similar to those used in the database. Therefore, some indices might seem to be missing in this reference list where, for example, only “Author 2003b” but not “Author 2003a” appears.

- Achal 1995 Identification of surface-laid mines by classification of compact airborne spectrographic imager (CASI) reflectance spectra. 1995. Achal SB, McFee JE, Anger CD. SPIE Proceedings 2496 324-335. Bellingham: SPIE. ISSN 0361-0748.
- Adler-Golden 1999a Detection of cirrus clouds at 1.13 μm in AVIRIS scenes over land. 1999. Adler-Golden SM, Levine RY, et al. Proceedings: JPL AVIRIS Workshop 1999. Pasadena: Jet Propulsion Laboratory.
- Alberotanza 1999b Hyperspectral aerial images. A valuable tool for submerged vegetation recognition in the Orbetello Lagoons, Italy. 1999. Alberotanza L, Brando VE, et al. International Journal of Remote Sensing 20 (3) 523-533. London: Taylor & Francis Ltd. ISSN 0143-1161.
- Andrefouet 2003a Airborne hyperspectral detection of microbial mat pigmentation in Rangiroa atoll (French Polynesia). 2003. Andrefouet S, Payri C, et al. Limnology and Oceanography 48 (1) 426-430. Waco: Amer Soc Limnology Oceanography. ISSN 0024-3590.
- Armstrong 1993 Remote sensing of submerged vegetation canopies for biomass estimation. 1993. Armstrong RA. International Journal of Remote Sensing 14 621-627. London: Taylor & Francis Ltd. ISSN 0143-1161.
- ASD 2002a Field spectrometry: Techniques and instrumentation. 2002. ASD. ASD Webpages. Boulder: Analytical Spectral Devices.
- ASD 2002b NIR analysis of concrete samples. 2002. ASD. ASD Webpages. Boulder: Analytical Spectral Devices.
- ASD 2003 Introduction to NIR technology. 2003. ASD. ASD Webpages. 10pp. Boulder: Analytical Spectral Devices.
- Ashton 1999 Multialgorithm solution for automated multispectral target detection. 1999. Ashton EA. Optical Engineering 38 (4) 717-724. Bellingham: SPIE. ISSN 0091-3286.
- Asner 2001b Canopy structure and chemistry of Hawaiian tropical forests using imaging spectroscopy. 2001. Asner GP, Vitousek PM. Proceedings: JPL AVIRIS Workshop 2001. Pasadena: Jet Propulsion Laboratory.
- Atkins 2001 The Elements of Physical Chemistry. 2001. Atkins P. Oxford: Oxford University Press. ISBN 019-879290-5.
- Atzberger 1998 Needle reflectance of healthy and diseased spruce stands. 1998. Atzberger C, Werner W. Proceedings of the 1st International EARSeL Workshop on Imaging Spectroscopy 271-283. Paris: EARSeL. ISBN 2-90-885-22-0.
- Azimi-Sadjadi 1995 Mine target detection using principal component and neural network method. 1995. Azimi-Sadjadi MR, Miao X. SPIE Proceedings 2496 675-686. Bellingham: SPIE. ISSN 0361-0748.

- Bach 1994 The use of AVIRIS data for the determination of agricultural plant development and water content. 1994. Bach H, Demircan A, Mauser W. ESA Publications. Noordwijk: European Space Agency.
- Bagheri 1998 Utility of hyperspectral data for bathymetric mapping in a turbid estuary. 1998. Bagheri S, Stein M, Dios R. *International Journal of Remote Sensing* 19 (6) 1179-1188. London: Taylor & Francis Ltd. ISSN 0143-1161.
- Ball 2003 *Physical Chemistry*. 2003. Ball DW. Pacific Grove: Thomson Brooks/Cole. ISBN 0-534-26658-4.
- Bammel 1994 Spectral reflectance response of big sagebrush to hydrocarbon-induced stress in the Bighorn basin, Wyoming. 1994. Bammel BH, Birnie RW. *Photogrammetric Engineering and Remote Sensing* 60 87-96. Bethesda: Amer Soc Photogrammetry. ISSN 0099-1112.
- Banninger 1990 Fluorescence line imager (FLI) measured red edge shifts in a metal-stressed Norway spruce and their relationships to canopy biochemical and morphological changes. 1990. Banninger C. *SPIE Proceedings - Imaging of the Terrestrial Environment* 1298 234-243. Bellingham: SPIE. ISSN 0361-0748.
- Banninger 1994 Determination of biochemical changes in conifer canopies with airborne visible/infrared imaging spectrometer (AVIRIS) data. 1994. Banninger C, Johnson LF, Peterson DL. *SPIE Proceedings* 2318 2-9. Bellingham: SPIE. ISSN 0361-0748.
- Banwell 1999 *Molekülspektroskopie: Ein Grundkurs*. 1999. Banwell CN, McCash EM. 417pp. Wien: Oldenbourg. ISBN 3-486-24507-4.
- Baumgardner 1985 Reflectance properties of soils. 1985. Baumgardner MF, Stoner ER, et al. In: *Advances of Agronomy* 38 1-44. New York: Academic Press Inc.
- Bell 1999 *Planetary geology*. 1999. Bell JF, Campbell BA, Robinson MS. In: *Manual of Remote Sensing Vol. 3: Remote Sensing for the Earth Sciences* 509-564. New York: John Wiley & Sons Inc. ISBN 0-471-29405-5.
- Ben-Dor 1996 Detection of atmospheric gases using GER 63 channel data acquired over Makhtesh Ramon, Negev, Israel. 1996. Ben-Dor E, Kruse FA. *International Journal of Remote Sensing* 17 (6) 1215-1232. London: Taylor & Francis Ltd. ISSN 0143-1161.
- Ben-Dor 1997b The reflectance spectra of organic matter in the visible near-infrared and short wave infrared region (400 - 2500 nm) during a controlled composition process. 1997. Ben-Dor E, Inbar Y, Chen Y. *Remote Sensing of Environment* 61 1-15. New York: Elsevier Science Inc. ISSN 0034-4257.
- Ben-Dor 1998a Soil reflectance. 1999. Ben-Dor E, Irons JA, Epema GF. In: *Manual of Remote Sensing Vol. 3: Remote Sensing for the Earth Sciences* 111-189. New York: John Wiley & Sons Inc. ISBN 0-471-29405-5.
- Ben-Dor 2001a Imaging spectrometry for urban applications. 2001. Ben-Dor E. In: *Imaging Spectrometry* 243-281. Dordrecht: Kluwer Academic Publ. ISBN 1-4020-0194-0.
- Ben-Dor 2003a The spectral reflectance properties of soil structural crusts in the 1.2 to 2.3- μ m spectral region. 2003. Ben-Dor E, Goldshleger N, et al. *Soil Science Society of America Journal* 67 (1) 289-299. Madison: Soil Sci Soc Amer. ISSN 0361-5995.
- Berendes 1991 Cloud base height and optical thickness retrievals using AVIRIS data. 1991. Berendes TA, Feid RE, et al. *Proceedings: JPL AVIRIS Workshop 1991*. Pasadena: Jet Propulsion Laboratory.

- BGR 2002 Dokumentation: Reserven, Ressourcen und Verfügbarkeit von Energierohstoffen 2002 (Kurzfassung). 2002. Bundesanstalt für Geowissenschaften und Rohstoffe. 43 pp. Berlin: Bundesministerium für Wirtschaft und Arbeit.
- Blackmer 1996 Nitrogen deficiency detection using reflected shortwave radiation from irrigated corn canopies. 1996. Blackmer TM, Schepers JM, et al. *Agronomy Journal* 88 (1). Madison: Amer Soc Agronomy. ISSN 0002-1962.
- Boardman 1995b Analysis, understanding, and visualization of hyperspectral data as convex sets in n space. 1995. Boardman JW. *SPIE Proceedings* 2480 14-22. Bellingham: SPIE. ISSN 0361-0748.
- Boggs 2003 Relationship between hyperspectral reflectance, soil nitrate-nitrogen, cotton leaf chlorophyll, and cotton yield: A step toward precision agriculture. 2003. Boggs JL, Tsegaye TD, et al. *Journal of Sustainable Agriculture* 22 (3) 5-16. Binghamton: Haworth Press. ISSN 1044-0046.
- Bohn 2001 Soil chemistry. 2001. Bohn HL, McNeal BL, O'Connor GA. 307pp. New York: John Wiley & Sons Inc. ISBN 0-471-36339-1.
- Boine 1999a Multispectral investigations of acid mine lakes of lignite open cast mines in Central Germany. 1999. Boine J, Kuka K, et al. *Proceedings of the IGARSS 1999 International Geoscience and Remote Sensing Symposium*. Hamburg.
- Boine 1999b Preliminary spectral investigations of lignite open cast residual lakes in Central Germany. 1999. Boine J, Olbert C, et al. "Proceedings of the 3rd German-Dutch Symposium Environmental Assessment and Monitoring". ISBN 3-86010-562-0.
- Borregaard 2000 Crop-weed discrimination by line imaging spectroscopy. 2000. Borregard T, Nielsen H, et al. *Journal of Agricultural Engineering Research* 75 (4) 389-400. New York: Academic Press Inc. ISSN 0021-8634.
- Brunold 1996 Stress bei Pflanzen. 1996. Stuttgart: UTB für Wissenschaft. ISBN 3-8252-8125-6.
- Buchanan 1992 NIR analysis of petrochemicals. 1992. Buchanan B. In: *Handbook of Near Infrared Analysis* 643-653. New York: Marcel Dekker. ISBN 0-8247-8657-2.
- Burns 1992 *Handbook of Near-Infrared Analysis*. 1992. New York: Marcel Dekker, Inc. ISBN 0-8247-8657-2.
- Carling 1992 Introducing neural networks. 1992. Carling A. 338pp. Wilmslow: Sigma Press. ISBN 1-85958-174-6.
- Carter 1994 Ratios of leaf reflectances in narrow waveband as indicators of plant stress. 1994. Carter GA. *International Journal of Remote Sensing* 15 697-703. London: Taylor & Francis Ltd. ISSN 0143-1161.
- Cassady 2001 Airborne hyperspectral imagery for the detection of agricultural crop stress. 2001. Cassady PE, Perry EM, et al. *SPIE Proceedings* 4151 197-204. Bellingham: SPIE. ISSN 0361-0748.
- Cermelli 1992 On line near infrared analysis applications in petrochemistry. 1992. Cermelli I, Descales B, et al. In: *Near Infrared Spectroscopy - Bridging the Gap between Data Analysis and NIR Applications* 395-400. New York: Ellis Horwood. ISBN 0-13-617416-7.
- Chabrillat 2001 Field and imaging spectrometry for identification and mapping of expansive soils. 2001. Chabrillat S, Goetz AFH, et al. In: *Imaging Spectrometry* 87-109. Dordrecht: Kluwer Academic Publ. ISBN 1-4020-0194-0.

- Chabrilat 2002 Use of hyperspectral images in the identification and mapping of expansive clay soils and the role of spatial resolution. 2002. Chabrilat S, Goetz AFH, et al. *Remote Sensing of Environment* 82 (2-3) 431-445. New York: Elsevier Science Inc. ISSN 0034-4257.
- Chang 2003b Hyperspectral Imaging: Techniques for the spectral detection and classification. 2003. Chang CI. Dordrecht: Kluwer Academic Publ. ISBN 0-306-47483-2.
- Chao 2001 Chicken heart disease characterization by multi-spectral imaging. 2001. Chao K, Chen YR, et al. *Applied Engineering in Agriculture*. 17 (1) 99-106. St Joseph: Amer Soc Agricultural Engineering. ISSN 0883-8542.
- Chao 2002 Use of hyper- and multispectral imaging for detection of chicken skin tumors. 2002. Chao K, Mehl PM, Chen YR. *Applied Engineering in Agriculture*. 18 (1) 113-119. St Joseph: Amer Soc Agricultural Engineering. ISSN 0883-8542.
- Chen 2001 Investigation of imaging spectroscopy for discriminating urban land covers and surface materials. 2001. Chen J, Hepner GF. *Proceedings: JPL AVIRIS Workshop 2001*. Pasadena: Jet Propulsion Laboratory.
- Christensen 2003 Miniature thermal emission spectrometer for the Mars exploration rovers. 2003. Christensen PR, Mehall GL, et al. *Journal of Geophysical Research - Planets* 108 (E12) 8064-8064. Washington: Amer Geophysical Union. ISSN 0148-0227.
- Christensen 2004 Modelling nitrogen and phosphorus content at early growth stages in spring barley using hyperspectral line scanning. 2004. Christensen LK, Bennedsen BS, et al. *Biosystems Engineering* 88 (1) 19-24. San Diego: Academic Press Inc. ISSN 1537-5110.
- Clark 1995b Initial vegetation species and senescence/stress indicator mapping in the San Luis Valley, Colorado, using imaging spectrometer data. 1995. Clark RN, King TVV, et al. *Proceedings JPL AVIRIS Workshop 1995*. Pasadena: Jet Propulsion Laboratory.
- Clark 1998b Mineral mapping with imaging spectroscopy: The Ray Mine, AZ. 1998. Clark RN, Vance S, Green RO. *Proceedings: JPL AVIRIS Workshop 1998*. Pasadena: Jet Propulsion Laboratory.
- Clark 2000 Spectral discrimination of coral mortality states following a severe bleaching event. 2000. Clark CD, Mumby PJ, et al. *International Journal of Remote Sensing* 21 (11) 2321-2327. London: Taylor & Francis Ltd. ISSN 0143-1161.
- Clark 2003b Imaging spectroscopy: Earth and planetary remote sensing with the USGS Tetracorder and expert systems. 2003. Clark RN, Swayze GA, et al. *Journal of Geophysical Research - Planets* 108 (E12) 5131. Washington: Amer Geophysical Union. ISSN 0148-0227.
- Clevers 1999 The use of imaging spectrometry for agricultural applications. 1999. Clevers JGPW. *ISPRS Journal of Photogrammetry and Remote Sensing* 54 (5-6) 299-304. Amsterdam: Elsevier Science BV. ISSN 0924-2716.
- Clevers 2001 Imaging spectrometry for agricultural applications. 2001. Clevers JGPW, Jongschaap R. In: *Imaging Spectrometry* 157-199. Dordrecht: Kluwer Academic Publ. ISBN 1-4020-0194-0.
- Cloutis 1989 Spectral reflectance properties of hydrocarbons: remote-sensing implications. 1989. Cloutis EA. *Science* 245 165-168. Washington: American Association for the Advancement of Science. ISSN 0193-4511.
- Cloutis 1994 Spectral reflectance properties of carbon-bearing materials. 1994. Cloutis EA, Gaffey MJ, Moslow TF. *ICARUS* 107 (2) 276. New York: Academic Press Inc. ISSN 0019-1035.

- Cloutis 1995 Characterization of minerals in oil sands by reflectance spectroscopy. 1995. Cloutis EA, Gaffey MJ, Moslow TF. Fuel 74 (6) 874. Guildford: Butterworth-Heinemann. ISSN 0016-2361.
- Cudahy 2000 Remote hyperspectral mapping and monitoring of acid rock drainage, Brukunga, South Australia. 2000. Cudahy T, Reinhäkel G, et al. Proceedings of the 2nd EARSeL Workshop on Imaging Spectroscopy. Paris: EARSeL.
- Curran 1994 Imaging Spectrometry. 1994. Curran PJ. Progress in Physical Geography 18 (2) 247-266. London: Edward Arnold Publ Ltd. ISSN 0309-1333.
- Curran 2000 Imaging spectrometry for ecological applications. 2000. Curran PJ. Proceedings of the 2nd EARSeL Workshop on Imaging Spectroscopy. Paris: EARSeL.
- Curtiss 1991 Changes in forest canopy reflectance associated with chronic exposure to high concentrations of soil trace metals. 1991. Curtiss B, Maecher AG. Proceedings of the 8th Thematic Conference on Geologic Remote Sensing 337-347. Denver: U. S. Geological Survey.
- Cwick 1995 Multispectral video data for detecting biogeochemical conditions at an Alabama oil field site. 1995. Cwick GJ, Bishop MP, et al. Geocarto International 10 59-66. Hongkong: Geocarto International Centre. ISSN 1010-6049.
- De Oliveira 1996 Detection of hydrocarbon seepage in the San Francisco basin, Brazil, through Landsat TM, soil geochemistry and airborne/field spectrometry data integration. 1996. de Oliveira WJ, Crosta AP. Proceedings of the 11th Thematic Conference and Workshop on Applied Geological Remote Sensing Vol. I 155-165. Las Vegas.
- Dehaan 2002 Field-derived spectra of salinized soils and vegetation as indicators of irrigation-induced soil salination. 2002. Dehaan RL, Taylor GR. Remote Sensing of Environment 80 (3) 406-417. New York: Elsevier Science Inc. ISSN 0034-4257.
- Dehaan 2003 Image-derived spectral endmembers as indicators of salinisation. 2003. Dehaan R, Taylor GR. International Journal of Remote Sensing 24 (4) 775-794. London: Taylor & Francis Ltd. ISSN 0143-1161.
- Dekker 2001 Imaging spectrometry of water. 2001. Dekker AG, Brando VE, et al. In: Imaging Spectrometry 307-359. Dordrecht: Kluwer Academic Publ. ISBN 1-4020-0194-0.
- DePersia 1995 Phenomenology considerations for hyperspectral mine detection. 1995. Depersia AT, Bowman AP, et al. SPIE Proceedings 2496 159-167. Bellingham: SPIE. ISSN 0361-0748.
- Dierssen 2003 Ocean color remote sensing of seagrass and bathymetry in the Bahamas Banks by high-resolution airborne imagery. 2003. Dierssen HM, Zimmermann RC, et al. Limnology and Oceanography 48 (1) 444-455. Waco: Amer Soc Limnology Oceanography. ISSN 0024-3590.
- Drollette 2000b Forensics professionals dying for hyperspectral imaging. 2000. Drollette D. Photonics Spectra 34 (5) 61-61. Pittsfield: Laurin Publ Co Inc. ISSN 0731-1230.
- EIA 2004a Annual Energy Review 2003. 2004. Energy Information Administration. Document DOE/EIA-0384(2003) 428. Washington: US Department of Energy.
- EIA 2004b Recent Energy Statistics. 2004. Energy Information Administration. 1. Washington: US Department of Energy.

- Ellis 2001 Exploring onshore oil seeps with hyperspectral imaging. 2001. Ellis JM, Davis HH, Zamudio JA. *Oil and Gas Journal* 99 (37) 49-58. Tulsa: Pennwell Publ Co. ISSN 0030-1388.
- Elvidge 1990a Visible and near infrared reflectance characteristics of dry plant materials. 1990. Elvidge CD. *International Journal of Remote Sensing* 11 1775-1795. London: Taylor & Francis Ltd. ISSN 0143-1161.
- Farone 1993 Changes in nontarget wetland vegetation following a large-scale fluridone application. 1993. Farone SM, McNabb TM. *Journal of Aquatic Plant Management* 31 185-189. Clermont: Aquatic Plant Management Soc. ISSN 0146-6623.
- Farrand 1995 Mineralogic variations in fluvial sediments contaminated by mine tailings as determined from AVIRIS data, Coeur d'Aldene River, Idaho. 1995. Farrand WH, Harsanyi JC. *Proceedings: JPL AVIRIS Workshop 1995*. Pasadena: Jet Propulsion Laboratory.
- Farrand 1997a Identification and mapping of ferric oxide and oxyhydroxide minerals in imaging spectrometer data of Summitville, Colorado, USA and the surrounding San Juan Mountains. 1997. Farrand WH. *International Journal of Remote Sensing* 18 (7) 1543-1552. London: Taylor & Francis Ltd. ISSN 0143-1161.
- Farrand 1997b Mapping the distribution of mine tailings in the Coeur d'Alene River valley, Idaho, through the use of a constrained energy minimization technique. 1997. Farrand WH, Harsanyi JC. *Remote Sensing of Environment* 59 64-76. New York: Elsevier Science Inc. ISSN 0034-4257.
- Fenstermaker 1994 Identification of fluvially redistributed mill tailings using high spectral resolution aircraft data. 1994. Fenstermaker LK, Miller RJ. *Photogrammetric Engineering and Remote Sensing* 60 989-995. Bethesda: Amer Soc Photogrammetry. ISSN 0099-1112.
- Feyaerts 1999 Hyperspectral image sensor for weed-selective spraying. 1999. Feyaerts F, Pollet P, et al. *SPIE Proceedings* 3897 193-203. Bellingham: SPIE. ISSN 0361-0748.
- Finston 2000 Oil-impacted soils detected with hyperspectral imagery. 2000. Finston L. *Journal of Petroleum Technology* 52 (12) 20. Richardson: Soc Petroleum Eng. ISSN 0149-2136.
- Flanders 1997 Hyperspectral imaging & oil spill monitoring: With IR/UV imaging power. 1997. Flanders D, Sorenson B, Shen C. *Advanced Imaging* 12 (4) 55-62. New York: PTN Publishing Co. ISSN 1042-0711.
- Folkard 1998 How far can imaging spectroscopy go in identifying the cause of vegetation stress around landfill sites. 1998. Folkard AM. *Proceedings of the 1st International EARSeL Workshop on Imaging Spectroscopy* 447-453. Paris: EARSeL. ISSN 2-90-885-22-0.
- Fourty 1996 Leaf optical properties with explicit description of its biochemical composition: Direct and inverse problems. 1996. Fourty T, Baret F, et al. *Remote Sensing of Environment* 56 104-117. New York: Elsevier Science Inc. ISSN 0034-4257.
- Fraser 1998 Hyperspectral remote sensing of turbidity and chlorophyll a among Nebraska sand hills lakes. 1998. Fraser RN. *International Journal of Remote Sensing* 19 (8) 1579-1589. London: Taylor & Francis Ltd. ISSN 0143-1161.
- Gallagher 2003b Estimation of trace vapor concentration-pathlength in plumes for remote sensing applications from hyperspectral images. 2003. Gallagher NB, Wise BM, Sheen DM. *Analytica Chimica Acta* 490 (1-2) 139-152. Amsterdam: Elsevier Science BV. ISSN 0003-2670.

- Gallagher 2003c Estimation of trace vapor concentration pathlength in plumes for remote sensing applications from hyperspectral images. 2003. Gallagher NB, Sheen DM, et al. SPIE Proceedings 5093 184-194. Bellingham: SPIE. ISSN 0361-0748.
- Gat 1999b Application of low altitude AVIRIS imagery of agricultural fields in San Joaquin Valley, CA, to precision farming. 1999. Gat N, Erives H, et al. Proceedings: JPL AVIRIS Workshop 1999. Pasadena: Jet Propulsion Laboratory.
- Gat 2000 Estimating sugar beet yield using AVIRIS-derived indices. 2000. Gat N, Erives H, et al. Proceedings: JPL AVIRIS Workshop 2000. Pasadena: Jet Propulsion Laboratory.
- Gauglitz 2004a Handbook of Spectroscopy - Volume 1. 2004. 599pp. Weinheim: Wiley-VCH. ISBN 3-527-29782-0.
- Goel 2003a Potential of airborne hyperspectral remote sensing to detect nitrogen deficiency and weed infestation in corn. 2003. Goel PK, Prasher SO, et al. Computers and Electronics in Agriculture 38 (2) 99-124. Oxford: Elsevier Science Ltd. ISSN 0168-1699.
- Goel 2003b Hyperspectral image classification to detect weed infestations and nitrogen status in corn. 2003. Goel PK, Prasher SO, et al. Transactions of the ASAE 46 (2) 539-550. St Joseph: Amer Soc Agricultural Engineers. ISSN 0001-2351.
- Goetz 1985 Imaging spectrometry for Earth remote sensing. 1985. Goetz AFH, Vane G, et al. Science 228 (4704) 1147-1153. Washington: American Association for the Advancement of Science. ISSN 0193-4511.
- Goetz 1992a Principles of narrow band spectrometry in the visible and the IR: Instruments and data analysis. 1992. Goetz AFH. In: Imaging Spectroscopy: Fundamentals and Prospective Applications. Dordrecht: Kluwer Academic Publ. . ISBN: 0-7923-1535-9.
- Goetz 1992b Imaging spectrometry for Earth remote sensing. 1992. Goetz AFH. In: Imaging Spectroscopy: Fundamental s and Prospective Applications. 1-20. Dordrecht: Kluwer Academic Publ. ISBN: 0-7923-1535-9.
- Goetz 1996a Hyperspectral imaging of the Earth: Remote analytical chemistry in an uncontrolled environment. 1996. Goetz AFH, Curtiss B. Field Analytical Chemistry and Technology 1 (2) 67-76. Chichester: John Wiley & Sons Ltd. ISSN 1086-900X.
- Goetz 1997 Atmospheric corrections: On deriving surface reflectance from hyperspectral imagers. 1997. Goetz AFH, Boardman JW, et al. SPIE Proceedings 3118 14-22. Bellingham: SPIE. ISSN 0361-0748.
- Goetz 2000a Short Course Hyperspectral Imaging & Data Analysis. 2000. Goetz AFH, Boardman JW, et al. Boulder: University of Colorado, Center for the Study of Earth from Space.
- Goodacre 1998 Rapid identification of urinary tract infection using hyperspectral whole-organism fingerprinting and artificial neural networks. 1998. Goodacre R, Timmins EM, et al. Microbiology - UK 144 1157-1170. Reading: Soc General Microbiology. ISSN 1350-0872.
- Goodenough 2003 Processing Hyperion and ALI for forest classification. 2003. Goodenough DG, Dyk A, et al. IEEE Transactions on Geoscience and Remote Sensing 41 (6) 1321-1331. New York: IEEE. ISSN 0196-2892.

- Green 1993g Estimation of aerosol optical depth, pressure elevation, water vapor, and calculation of apparent surface reflectance from radiance measured by AVIRIS. 1993. Green RO, Conel JE, Roberts DA. SPIE Proceedings - Imaging of the Terrestrial Environment 1937 2-11. Bellingham: SPIE. ISSN 0361-0748.
- Griffin 2000a Characterization and delineation of plumes, clouds and fires in hyperspectral images. 2000. Griffin MK, Hsu SM, et al. SPIE Proceedings 4049 274-283. Bellingham: SPIE. ISSN 0361-0748.
- Günzler 2002 IR Spectroscopy - an introduction. 2002. Günzler H, Gremlich HU. Weinheim: VCH. ISBN 3-527-28896-1.
- Haboudane 2004 Hyperspectral vegetation indices and novel algorithms for predicting green LAI of crop canopies: Modeling and validation in the context of precision agriculture. 2004. Haboudane D, Miller JR, et al. Remote Sensing of Environment 90 (3) 337-352. New York: Elsevier Science Inc. ISSN 0034-4257.
- Hamilton 1992 Multiple dataset water-quality analyses in the vicinity of an ocean wastewater plume. 1992. Hamilton MK, Davis CO, et al. Proceedings: JPL AVIRIS Workshop 1992. Pasadena: Jet Propulsion Laboratory.
- Harrison 2003 Earth-observing hyperspectral imaging systems: a 2003 survey. 2003. Harrison JF, Roper WE, Gomez RB. SPIE Proceedings 5097 222-232. Bellingham: SPIE. ISSN 0361-0748.
- Hauff 1999a Hyperspectral evaluation of mine waste and abandoned mine lands. 1999. Hauff PL, Lindsay N, et al. Summaries of the Eighth JPL Airborne Earth Science Workshop JPL Publ 99-17 229-238. Pasadena: Jet Propulsion Laboratory.
- Hauff 1999b Hyperspectral evaluation of mine waste and abandoned mine lands, NASA and EPA sponsored projects in Idaho. 1999. Hauff PL, Peters D, et al. Proceedings: JPL AVIRIS Workshop 1999. Pasadena: Jet Propulsion Laboratory.
- Hauff 2000 Hyperspectral investigations of mine waste and abandoned mine lands - the Dragon calibration site case study. 2000. Hauff PL, Peters DC, et al. Proceedings: JPL AVIRIS Workshop 2000. Pasadena: Jet Propulsion Laboratory.
- Heinberg 2003 The Party's Over. 2003. Heinberg R. 288pp. Gabrioli Island: New Society Publishers. ISBN 0865714827.
- Henry 2004 Remote sensing to detect herbicide drift on crops. 2004. Henry WB, Reddy KR, et al. Weed Technology 18 (2) 358-368. Lawrence: Weed Sci Soc Amer. ISSN 0890-037X.
- Hesse 1991 Spektroskopische Methoden in der organischen Chemie. 1991. Hesse M, Meier H, Zeeh B. 364pp. Stuttgart: Georg Thieme Verlag. ISBN 3-13-576105-3.
- Hildrum 1992 Near infra-red spectroscopy. 1992. Chichester: Ellis Horwood. ISBN 0-13-617416-7.
- Hinnrichs 1999 Remote sensing for gas plume monitoring using state-of-the-art infrared hyperspectral imaging. 1999. Hinnrichs M. SPIE Proceedings 3534 370-381. Bellingham: SPIE. ISSN 0361-0748.
- Hochberg 2003 Capabilities of remote sensors to classify coral, algae, and sand as pure and mixed spectra. 2003. Hochberg EJ, Atkinson MJ. Remote Sensing of Environment 85 (2) 174-189. New York: Elsevier Science Inc. ISSN 0034-4257.
- Holden 1999 Hyperspectral identification of coral reef features. 1999. Holden H, LeDrew E. International Journal of Remote Sensing 20 (13) 2545-2563. London: Taylor & Francis Ltd. ISSN 0143-1161.

- Holyer 1996 Coastal bathymetry from hyperspectral data. 1996. Holyer RL, Sandidge J. Proceedings: JPL AVIRIS Workshop 1996. Pasadena: Jet Propulsion Laboratory.
- Hook 1990 Mineralogic mapping using Airborne Visible/Infrared Imaging Spectrometer (AVIRIS) shortwave infrared (SWIR) data acquired over Cuprite, Nevada. 1990. Hook SJ, Rast M. Proceedings: JPL AVIRIS Workshop 1990. Pasadena: Jet Propulsion Laboratory.
- Hoque 1992 Spectral blue shift of red edge monitors damage class of beech trees. 1992. Hoque E, Hutzler PJS. Remote Sensing of Environment 39 81-84. New York: Elsevier Science Inc. ISSN 0034-4257.
- Hörig 2001 HyMap hyperspectral remote sensing to detect hydrocarbons. 2001. Hörig B, Kühn F, et al. International Journal of Remote Sensing 22 (8) 1413-1422. London: Taylor & Francis Ltd. ISSN 0143-1161.
- Horler 1980 Effects of heavy metals on the absorbance and reflectance spectra of plants. 1980. Horler DNH, Barber J, Barringer AR. International Journal of Remote Sensing 1 121-136. London: Taylor & Francis Ltd. ISSN 0143-1161.
- Howard 1971 Spectral reflectance properties of Pinus ponderosa in relation to copper-content of the soil - Malachite Mine, Jefferson Country, Colorado. 1971. Howard JA, Watson RD, Hessin TD. Proceedings of 7th International Symposium on Remote Sensing of Environment 1 285-297. Ann Arbor.
- Howari 2000 Spectral properties of selected dominant salt crusts. 2000. Howari F, Goodell P, et al. Proceedings of the 2nd EARSeL Workshop on Imaging Spectroscopy. Paris: EARSeL.
- Hu 2004 Retrieval of crop chlorophyll content and leaf area index from decompressed hyperspectral data: the effects of data compression. 2004. Hu B, Quan SE, et al. Remote Sensing of Environment 92 (2) 139-152. New York: Elsevier Science Inc. ISSN 0034-4257.
- Hunt 1980 Electromagnetic radiation: The communication link in remote sensing. 1980. Hunt GR. In: Remote Sensing in Geology 702pp. New York: John Wiley & Sons Inc.
- IEA 2004a IEA Monthly Oil Market Report (10 November 2004). 2004. International Energy Agency. 6pp. Paris: International Energy Agency.
- IEA 2004b Monthly Oil Survey: September 2004. 2004. International Energy Agency. 33 pp. Paris: International Energy Agency.
- Ifarraguerri 1999a Chemical agent detection and quantification with imaging spectrometry. 1999. Ifarraguerri AI. SPIE Proceedings 3753 46-50. Bellingham: SPIE. ISSN 0361-0748.
- Ingleby 2000 Reflectance models for predicting organic carbon in Saskatchewan soils. 2000. Ingleby HR, Crowe TG. Canadian Agricultural Engineering 42 (2) 57-63. Ottawa: Canadian Soc Agricultural Engineering. ISBN 0045-432X.
- Irons 1989 Soil reflectance. 1989. Irons JR, Weismiller RA, Petersen GW. In: Theory and Applications of Optical Remote Sensing 66-106. New York: John Wiley & Sons Inc. ISBN 0-471-62895-6.
- Jackson 1986 Remote sensing of biotic and abiotic plant stress. 1986. Jackson RD. Annual Review of Phytopathology 24 265-287. Palo Alto: Annual Reviews. ISSN 0066-4286.
- Jacobson 1999 Big oil comes back to Baku. 1999. Jacobson M. Natural History 3/99 54-73.
- Jensen 2000 Remote sensing of the environment. 2000. Jensen JR. Upper Saddle River: Prentice-Hall. ISBN 0-13-289733-1.

- Jiang 1998 Characteristics of the silt particles and reflection spectrum of the yellow-water at the mouth of the Yello River. 1998. Jiang B, Qi H, Hu Q. SPIE Proceedings 3502 251-253. Bellingham: SPIE. ISSN 0361-0748.
- Kailey 1996 Use of hyperspectral imagery for broad-area detection of small targets. 1996. Kailey WF, Illing LR. SPIE Proceedings 2819 15-23. Bellingham: SPIE. ISSN 0361-0748.
- Kailey 2000 Detection of isolated manmade objects using hyperspectral imagery. 1994. Kailey WF, Bennett M. Special Publication - Royal Society of Chemistry 254 132-141. London: Royal Society of Chemistry. ISSN 0260-6291.
- Kallio 2001 Retrieval of water quality from airborne imaging spectrometry of various lake types in different seasons. 2001. Kallio K, Kutser T, et al. Science of the Total Environment 268 (1-3) 59-77. Amsterdam: Elsevier Science BV. ISSN 0048-9697.
- Kallio 2003 Feasibility of airborne imaging spectrometry for lake monitoring - a case study of spatial chlorophyll alpha distribution in two meso-eutrophic lakes. 2003. Kallio K, Koponen S, Pulliainen J. International Journal of Remote Sensing 24 (19) 3771-3790. London: Taylor & Francis Ltd. ISSN 0143-1161.
- Kappus 1998 Bathymetry from fusion of airborne hyperspectral and laser data. 1998. Kappus ME, Davis CO, Rhea WJ. SPIE Proceedings 3438 40-51. Bellingham: SPIE. ISSN 0361-0748.
- Kaufmann 1998 Airborne and ground spectroscopic analysis of overburden dumps. 1998. Kaufmann H, Müller A, et al. Proceedings of the 1st International EARSeL Workshop on Imaging Spectroscopy 417-424. Paris: EARSeL. ISBN 2-90-885-22-0.
- Keller 2001b Imaging spectroscopy of lake water quality parameters. 2001. Keller PA. Remote Sensing Series 36 161. Zürich: Universität Zürich. ISBN 3-03703-002-X.
- Kemper 2000 A multiple endmember unmixing approach for mapping heavy metal contamination after the Donana mining accident (Sevilla, Spain). 2000. Kemper T, Garcia Haro J, et al. Proceedings of the 2nd EARSeL Workshop on Imaging Spectroscopy. Paris: EARSeL.
- Kenton 1999 Detection of land mines with hyperspectral data. 1999. Kenton AC, Schwartz CR, et al. SPIE Proceedings 3710 917-928. Bellingham: SPIE. ISSN 0361-0748.
- Keshava 2002b Spectral unmixing. 2002. Keshava N, Mustard JF. IEEE Signal Processing Magazine 19 (1) 44-57. New York: IEEE. ISSN 1053-5888.
- Kim 2002b Multispectral detection of fecal contamination on apples based on hyperspectral imagery: Part II. Application of hyperspectral fluorescence imaging. 2002. Kim MS, Lefcourt AM, et al. Transactions of the ASAE 45 (6) 2039-2047. St Joseph: Amer Soc Agricultural Engineers. ISSN 0001-2351.
- King 1989 Reflectance spectroscopy (0.2 to 20 μm) as an analytical method for the detection of organics. 1989. King TVV, Clark RN. Proceedings First International Symposium: Field Screening Methods for Hazardous Waste Site Investigation 485-488. EPA.

- King 2000b Applications of imaging spectroscopy data: A case study at Summitville, Colorado. 2000. King TVV, Clark RN, Swayze GA. In: Remote Sensing for Site Characterization 165-185. Berlin: Springer Verlag. ISBN 3-540-63469-X.
- Klusman 1992 The potential use of biogeochemistry in the detection of petroleum microseepage. 1992. Klusman RW, Saeed MA, Abu-Ali M. AAPG Bulletin 76 851-863. Tulsa: American Association of Petroleum Geologists. ISSN 0149-1423.
- Knap 2000 Discriminating between water and ice clouds using near-infrared AVIRIS measurements. 2000. Knap WH, Stammes P, Koelemeijer BA. Proceedings: JPL AVIRIS Workshop 2000. Pasadena: Jet Propulsion Laboratory.
- Kneubühler 2000 Assessment of crop vitality through analysis of combined field and laboratory measurements of biophysical and biochemical parameters. 2000. Kneubühler M, Naef C, Itten KI. Proceedings of the 2nd EARSeL Workshop on Imaging Spectroscopy. Paris: EARSeL.
- Kneubühler 2001 Spectroradiometry as a tool for phenological characterization of agricultural crop stands. 2001. Kneubühler M. DGPF Publikation 10 379-388. Konstanz: Deutsche Gesellschaft für Photogrammetrie und Fernerkundung. ISSN 0942-2870.
- Köhl 2001 Erfassung von Waldökosystemen durch Hyperspektraldaten. 2001. Köhl M, Lautner M. Photogrammetrie - Fernerkundung - Geoinformation 2 107-117. Stuttgart: Schweizerbart'sche Verlagsbuchhandlung. ISSN 1432-8364.
- Kooistra 2000 Possibilities of imaging spectroscopy for the classification of contaminated areas in river floodplains. 2000. Kooistra L, Wehrens R, et al. Proceedings of the 2nd EARSeL Workshop on Imaging Spectroscopy. Paris: EARSeL.
- Kooistra 2003 Exploring field vegetation reflectance as an indicator of soil contamination in river floodplains. 2004. Kooistra L, Salas EAL, et al. Environmental Pollution 127 (2) 281-290. Oxford: Elsevier Science Ltd. ISSN 0013-9327.
- Krüger 1998 Laboratory and airborne reflectance spectroscopic analyses of lignite overburden dumps. 1998. Krüger G, Erzinger J, Kaufmann H. Journal of Geochemical Exploration 64 (1-3) 47-65. Amsterdam: Elsevier Science BV. ISSN 0375-6742.
- Kruse 1988c Preliminary analysis of Airborne Visible/Infrared Imaging Spectrometer (AVIRIS) for mineralogic mapping at sites in Nevada and Colorado. 1988. Kruse FA, Taranik DL, Kierein-Young KS. Proceedings: JPL AVIRIS Workshop 1988. Pasadena: Jet Propulsion Laboratory.
- Kruse 1992b Expert-based mineral mapping using AVIRIS. 1992. Kruse FA, Lefkoff AB, Dietz JB. Proceedings: JPL AVIRIS Workshop 1992. Pasadena: Jet Propulsion Laboratory.
- Kruse 1996a Identification and mapping of minerals in drill core using hyperspectral image analysis of infrared reflectance spectra. 1996. Kruse FA. International Journal of Remote Sensing 17 (9) 1623-1632. London: Taylor & Francis Ltd. ISSN 0143-1161.
- Kruse 1996b Mineral mapping for environmental hazards assessment using AVIRIS data, Leadville, Colorado, USA. 1996. Kruse FA. Proceedings of the 11th Thematic Conference and Workshop on Applied Geological Remote Sensing Vol. II 526-533. Las Vegas.
- Kruse 2000a The AIG/HyVista 1999 USA HyMap Group Shoot: Overview and analysis examples. 2000. Kruse FA, Boardman JW, et al. Proceedings of the IEEE IGARSS 2000 13723-1375. New York: IEEE. ISBN 0-7803-6259-0.

- Kühn 2004 Hydrocarbon Index - an algorithm for hyperspectral detection of hydrocarbons. 2004. Kuhn F, Oppermann K, Horig B. *International Journal of Remote Sensing* 25 (12) 2467-2473. Oxford: Taylor & Francis Ltd. ISSN 0143-1161.
- Kulcke 2003 On-line classification of synthetic polymers using near infrared spectral imaging. 2003. Kulcke A, Gurschler C, et al. *Journal of Near Infrared Spectroscopy* 11 (1) 71-81. Chichester: NIR Publications. ISSN 0967-0335.
- Kumar 2001a Imaging spectrometry and vegetation science. 2001. Kumar L, Schmidt K, et al. In: *Imaging Spectrometry* 111-155. Dordrecht: Kluwer Academic Publ. ISBN 1-4020-0194-0.
- Kuntze 1994 *Bodenkunde*. 1998. Kuntze H, Roeschmann G, Schwerdtfeger G. 424pp. Stuttgart: Eugen Ulmer. ISBN 3-8252-8076-4.
- Kuo 1990 Cloud identification and optical thickness retrieval using AVIRIS data. 1990. Kuo KS, Welch RM, et al. *Proceedings: JPL AVIRIS Workshop 1990*. Pasadena: Jet Propulsion Laboratory.
- Laan 2000 Ozone monitoring with the OMI instrument. 2000. Laan E, de Vries J, et al. *SPIE Proceedings* 4132 334-343. Bellingham: SPIE. ISSN 0361-0748.
- Landgrebe 2002 Hyperspectral image data analysis. 2002. Landgrebe DA. *IEEE Signal Processing Magazine* 19 (1) 17-28. New York: IEEE. ISSN 1053-5888.
- Lane 1999 Remote sensing of fugitive emissions in the burning of a napalm mixture with a hyperspectral infrared imaging spectrometer. 1999. Lane GM. *Abstracts of Papers of the American Chemical Society* 218: 136-ENVR Part 1. Washington: Amer Chemical Soc. ISSN 0065-7727.
- Lareau 2002 Tactical airborne reconnaissance goes dual-band and beyond. 2002. Lareau AG. *Photonics Spectra* July 64-68. Pittsfield: Laurin Publ Co Inc. ISSN 0731-1230.
- Lass 2002 Detecting spotted knapweed (*Centaurea maculosa*) with hyperspectral remote sensing technology. 2002. Lass LW, Thill DC, et al. *Weed Technology* 16 (2) 426-432. Lawrence: Weed Sci Soc Amer. ISSN 0890-037X.
- Lauten 1992 Physiological and spectral analysis of the effects of sodium chloride on *Syringa vulgaris*. 1992. Lauten GN, Rock BN. *Proceedings of the IGARSS'92 Symposium* 1 236-238. Houston.
- Lawrence 2003c A hyperspectral imaging system for identification of faecal and ingesta contamination on poultry carcasses. 2003. Lawrence KC, Windham WR, et al. *Journal of Near Infrared Spectroscopy* 11 (4) 269-281. Chichester: NIR Publications. ISSN 0967-0335.
- Lee 1999 Hyperspectral remote sensing for shallow waters. II. Deriving bottom depths and water properties by optimization. 1999. Lee ZP, Carder KL, et al. *Applied Optics* 38 (18) 3831-3843. Washington: Optical Soc Amer. ISSN 0003-6935.
- Lee 2004c Absorption spectrum of phytoplankton pigments derived from hyperspectral remote-sensing reflectance. 2004. Lee ZP, Carder KL. *Remote Sensing of Environment* 89 (3) 361-368. New York: Elsevier Science Inc. ISSN 0034-4257.
- Lehmann 1990 Evaluation of imaging spectrometer data (GER) for the spectral analysis of an old vegetation covered waste deposit. 1990. Lehmann F, Rothfuß H, Richter R. *Proceedings of the IGARSS'90 Symposium* 1613-1616.
- Lehmann 1991 Imaging spectroscopy data used for geological and environmental analysis in Europe. 1991. Lehmann F, Rothfuss H, Werner K. *Proceedings: JPL AVIRIS Workshop 1991*. Pasadena: Jet Propulsion Laboratory.

- Lelong 1998 Hyperspectral imaging and stress mapping in agriculture: A case study on wheat in Beauce (France). 1998. Lelong CCD, Pinet PC, Poilve H. *Remote Sensing of Environment* 66 (2) 179-191. New York: Elsevier Science Inc. ISSN 0034-4257.
- Leone 1999 Evaluation of MIVIS hyperspectral data for mapping soil degradation in an upland ecosystem of Southern Italy. 1999. Leone AP, Sommer S. *Geocarto International* 14 (1) 35-43. Honkong: Geocarto International Centre. ISSN 1010-6048.
- Leone 2000 Multivariate analysis of laboratory spectra for the assessment of soil development and soil degradation in the southern Apennines (Italy). 2000. Leone AP, Sommer S. *Remote Sensing of Environment* 72 (3) 346-359. New York: Elsevier Science Inc. ISSN 0034-4257.
- Lerner 1999b Plant responses to environmental stresses. 1999. Basel: Marcel Dekker. ISBN 0-8247-0044-9.
- Levesque 1997c Site characterization of mine tailings at the INCO Copper Cliff tailings impoundment area using casi imagery. 1997. Levesque J, Singhroy V, et al. Preprint.
- Levesque 2000 Preliminary results on the investigation of hyperspectral remote sensing for the identification of uranium mine tailings. 2000. Levesque J, Neville RA, Stanz K. Preprint.
- Lillesand 1999 Remote sensing and image interpretation. 1999. Lillesand TM, Kiefer RW. New York: John Wiley & Sons Inc. ISBN 0-471-25515-7.
- Livo 1998 Environmental study of the Bonanza Mining district, Colorado, using AVIRIS, aircraft, satellite and terrain data. 1998. Livo KE, Watson K, et al. *Proceedings: JPL AVIRIS Workshop 1998*. Pasadena: Jet Propulsion Laboratory.
- Lobell 2003 Hyperion studies of crop stress in Mexico. 2003. Lobell DB, Asner GP. *Proceedings: JPL AVIRIS Workshop 2003*. Pasadena: Jet Propulsion Laboratory.
- Lu 2003 Detection of bruises on apples using near-infrared hyperspectral imaging. 2003. Lu R. *Transactions of the ASAE* 47 (2) 523-530. St Joseph: Amer Soc Agricultural Engineers. ISSN 0001-2351.
- Ma 1998 Study on biogeochemical effects and remote sensing characteristics of gold deposit. 1998. Ma Y, Xu R. *SPIE Proceedings* 3502 112-122. Bellingham: SPIE. ISSN 0361-0748.
- Malkoff 2000 Hyperspectral imaging applied to forensic medicine. 2000. Malkoff DB, Oliver WR. *SPIE Proceedings* 3920 108-117. Bellingham: SPIE. ISSN 0361-0748.
- Manolakis 2002a Detection algorithms for hyperspectral imaging applications. 2002. Manolakis DG, Shaw G. *IEEE Signal Processing Magazine* 19 (1) 29-43. New York: IEEE. ISSN 1053-5888.
- Marino 2000 Environmental applications of airborne hyperspectral remote sensing: asbestos concrete sheeting identification and mapping. 2000. Marino CM, Panigada C, et al. *Proceedings of the 14th International Conference on Applied Geologic Remote Sensing* 607-610. Las Vegas.
- Marion 2004 Measuring trace gases in plumes from hyperspectral remotely sensed data. 2004. Marion R, Michel W, Faye C. *IEEE Transactions on Geoscience and Remote Sensing* 42 (4) 854-864. Piscataway: IEEE. ISSN 0196-2892.
- Mars 2003 Mapping mine wastes and analyzing areas affected by selenium-rich water runoff in southeast Idaho using AVIRIS imagery and digital elevation data. 2003. Mars JC, Crowley JK. *Remote Sensing of Environment* 84 (3) 422-436. New York: Elsevier Science Inc. ISSN 0034-4257.

- Martin 1993 Measurements of canopy chemistry with 1992 AVIRIS data at Blackhawk Island and Harvard Forest. 1993. Martin ME, Aber JD. Proceedings: JPL AVIRIS Workshop 1993. Pasadena: Jet Propulsion Laboratory.
- Martin 1996 Determining forest species composition using high spectral resolution remote sensing data. 1996. Martin ME, Newman SD, et al. Proceedings: JPL AVIRIS Workshop 1996. Pasadena: Jet Propulsion Laboratory.
- Martini 2000 Geological and geobotanical studies of Long Valley Caldera, CA, USA utilizing new 5m hyperspectral imagery. 2000. Martini BA, Silber EA, et al. Proceedings of the IEEE IGARSS 2000 1376-1378. New York: IEEE. ISBN 0-7803-6259-0.
- McCubbin 1999 Mapping environmental contaminants at Ray Mine, AZ. 1999. McCubbin IB, Lang H. Proceedings: JPL AVIRIS Workshop 1999. Pasadena: Jet Propulsion Laboratory.
- McGregor 1998 Target detection using HSI systems: an update of TRW results. 1998. McGregor RD, Nguyen MH, et al. SPIE Proceedings 3438 52-65. Bellingham: SPIE. ISSN 0361-0748.
- McMorrow 2004 Hyperspectral indices for characterizing upland peat composition. 2004. McMorrow JM, Cutler MEJ, et al. International Journal of Remote Sensing 25 (2) 313-325. London: Taylor & Francis Ltd. ISSN 0143-1161.
- Melack 1992 Seasonal and statistical variations in phytoplanktonic chlorophyll in eutrophic Mono Lake, California, measured with the Airborne Visible and Infrared Imaging Spectrometer (AVIRIS). 1992. Melack JM, Gastil M. Proceedings: JPL AVIRIS Workshop 1992. Pasadena: Jet Propulsion Laboratory.
- Melack 2001 Airborne remote sensing of chlorophyll distributions in Mono Lake, California. 2001. Melack JM, Gastil M. Hydrobiologia 466 (1-3) 31-38. Dordrecht: Kluwer Academic Publ. ISSN 0018-8158.
- Messinger 2004 Gaseous plume detection in hyperspectral images: a comparison of methods. 2004. Messinger DW. SPIE Proceedings 5425 592-603. Bellingham: SPIE. ISSN 0361-0748.
- Metternicht 2003 Remote sensing of soil salinity: potentials and constraints. 2003. Metternicht GI, Zinck JA. Remote Sensing of Environment 85 (1) 1-20. New York: Elsevier Science Inc. ISSN 0034-4257.
- Miller 2001 Soils in our environment. 2001. Miller RW, Gardiner DT. 642pp. Upper Saddle River: Prentice Hall. ISSN 0-13-020036-0.
- Miller 2004 Plume sensing direction considerations. 2004. Miller DP, Jellison GP. SPIE Proceedings 5425 256-265. Bellingham: SPIE. ISSN 0361-0748.
- Mir-Babayev 2002 Azerbaijan's oil History: A chronology leading up to the Soviet era. 2002. Mir-Babayev MY. Azerbaijan International 10 (2). Baku.
- Mishev 1986 Spectral Characteristics of Natural Formations. 1986. Mishev D. Sofia: Publishing House of the Bulgarian Academy of Sciences. ISSN without.
- MLUR 1998 Verteilung der Altlastverdachtsflächen - Altlasten im Land Brandenburg nach Verursachergruppen (Stand 11/1998). 1998. Potsdam: Ministerium für ländliche Entwicklung, Umwelt und Raumordnung Brandenburg.
- Mortimer 1987 Chemie. 1987. Mortimer CE. 660pp. Stuttgart: Thieme. ISBN 3-13-484305-6.
- Mueksch 1998 Möglichkeiten und Grenzen zur Bestimmung der Wasserqualität aus trophieanzeigenden phytoplanktonischen Pigmentkonzentrationen mittels nicht-abbildender Flugzeug-Hyperspektral-Daten. 1998. Mueksch MC. Photogrammetrie - Fernerkundung - Geoinformation 5 295-302. Stuttgart: Schweizerbart'sche Verlagsbuchhandlung. ISSN 1432-8364.

- Müller 1996 The potential of imaging spectrometry (DAIS 7915) for the monitoring of recultivation activities in mining areas. 1996. Müller A, Lehmann F, Rothfuß H. Proceedings of the 11th Thematic Conference and Workshop on Applied Geologic Remote Sensing Vol. II 350-357. Las Vegas.
- Mumby 2004 Remote sensing of coral reefs and their physical environment. 2003. Mumby PJ, Skirving W, et al. Marine Pollution Bulletin 48 (2-4) 219-228. Kidlington: Pergamon-Elsevier Science Ltd. ISSN 0025-326X.
- Murray 1992 Making light work: advances in near infrared spectroscopy. 1992. Weinheim: VCH. ISSN 3-527-28498-2.
- Nagler 2000 Plant litter and soil reflectance. 2000. Nagler PL, Daughthy CST, Goward SN. Remote Sensing of Environment 71 (2) 207-215. New York: Elsevier Science Inc. ISBN 0034-4257.
- Narimanov 1995 Oil history, potential converge in Azerbaijan. 1995. Narimanov AA, Palaz I. Oil & Gas Journal 1995 32-39. Tusla: PennWell Publications.
- Nischan 2000 Active hyperspectral imaging. 2000. Nischan ML, Newbury AB, et al. SPIE Proceedings 4132 107-117. Bellingham: SPIE. ISSN 0361-0748.
- NN 2002c NASA test satellite collects war data provides before-and-after hyperspectral imagery of bombing targets. 2001. NN. Aviation Week & Space Technology 156 (3) 30. New York: McGraw-Hill Data Services. ISSN 0005-2175.
- Notarnicola 2004 Southern Italy illegal dumps detection based on spectral analysis of remotely sensed data and land-cover maps. 2004. Notarnicola C, Angiulli M, Giasi CI. SPIE Proceedings 5239 483-494. Bellingham: SPIE. ISSN 0361-0748.
- Nyquist 2001a Interpreting infrared, Raman, and nuclear magnetic resonance spectra. Variables in data interpretation of infrared and Raman spectra. Vol. 1. 2001. Nyquist RA. San Diego: Academic Publishers. ISBN 0-12-523355-8.
- Nyquist 2001b Interpreting infrared, Raman, and nuclear magnetic resonance spectra. Factors affecting molecular vibrations and chemical shifts of spectra. Vol. 2. 2001. Nyquist RA. San Diego: Academic Publishers. ISBN 0-12-523470-8.
- Olbert 1999 Spectral characteristics of lignite open cast mining systems: A preliminary status. 1999. Olbert C, Fischer J, et al. Proceedings of the 21st Canadian Symposium on Remote Sensing. Ottawa.
- Olbert 2000 Bestimmung räumlicher Verteilungsmuster von Wasserinhaltsstoffen in ausgewählten Berliner und Brandenburger Gewässern mit Methoden der Fernerkundung. 2000. Olbert C. PhD-Thesis 176 pp. Berlin: Freie Universität Berlin.
- Oliver 2004 Deriving in situ phytoplankton absorption for bio-optical productivity models in turbid water. 2004. Oliver MJ, Schofield O, et al. Journal of Geophysical Research - Oceans 109 (C7) C07S11. Washington: Amer Geophysical Union. ISSN 0148-0227.
- Olsen 1997 Target detection in a forest environment using spectral imagery. 1997. Olsen RC, Bergman S, Resmini RG. SPIE Proceedings 3118 46-56. Bellingham: SPIE. ISSN 0361-0748.
- Ong 2002 Deriving quantitative monitoring data related to acid drainage using multi-temporal hyperspectral data. 2002. Ong C, Cudahy TJ. Proceedings: JPL AVIRIS Workshop 2002. Pasadena: Jet Propulsion Laboratory.
- Ong 2003 Deriving quantitative dust measurements related to iron ore handling from airborne hyperspectral data. 2003. Ong CCH, Cudahy TJ, et al. Transactions of the Institution of Mining and Metallurgy Section A - Mining Technology 112 158-163. Leeds: Maney Publishing. ISSN 0371-7844.

- OPEC 2004 OPEC Annual Statistical Bulletin 2003. 2004. Tayyeb MA, Linton D, et al. 148. Vienna: OPEC.
- Oppelt 2000 Derivation of nitrogen status of different crop types with the Airborne Imaging Spectrometer AVIS - first results. 2000. Oppelt N, Mauser W. Proceedings of the 2nd EARSeL Workshop on Imaging Spectroscopy. Paris: EARSeL.
- Otto 1995 Analytische Chemie. 1995. Otto M. Weinheim: VCH. ISBN 3-527-28691-8.
- Papadakis 2003 A novel spectral microscope system: Application in quantitative pathology. 2003. Papadakis AN, Stathopoulos E, et al. IEEE Transactions on Biomedical Engineering 50 (2) 207-217. New York: IEEE. ISSN 0018-9294.
- Park 2003 Hyperspectral imaging for detection fecal and ingesta contaminants on poultry carcasses. 2003. Park B, Lawrence KC, et al. Transactions of the ASAE 45 (6) 2017-2026. St Joseph: Amer Soc Agricultural Engineers. ISSN 0001-2351.
- Pavlin 1996 Spectroradiometric remote sensing for military applications. 1996. Pavlin GB. SPIE Proceedings 2821 2. Bellingham: SPIE. ISSN 0361-0748.
- Peirs 2003 Starch index determination of apple fruit by means of a hyperspectral near infrared reflectance imaging system. 2004. Peirs A, Scheerlinck N, et al. Journal of Near Infrared Spectroscopy 11 (5) 379-389. Chichester: NIR Publications. ISSN 0967-0335.
- Penn 2002b Band ratios as a reconnaissance tool for hyperspectral data. 2002. Penn BS. Proceedings: JPL AVIRIS Workshop 2002. Pasadena: Jet Propulsion Laboratory.
- Penn 2003 Methods for detecting anomalies in AVIRIS imagery. 2003. Penn BS. Proceedings: JPL AVIRIS Workshop 2003. Pasadena: Jet Propulsion Laboratory.
- Polder 2002 Spectral image analysis for measuring ripeness of tomatoes. 2002. Polder G, vand der Heijden GWAM, Young IT. Transactions of the ASAE 45 (4) 1155-1161. St Joseph: Amer Soc Agricultural Engineers. ISSN 0001-2351.
- Press 1974 Remote sensing to detect the toxic effects of metals on vegetation for mineral exploration. 1974. Press NP. Proceedings of the 9th International Symposium on Remote Sensing of the Environment 3 2027-2038. Ann Arbor.
- Puschell 2000 Hyperspectral imagers for current and future missions. 2000. Puschell JJ. SPIE Proceedings 4041 121-132. Bellingham: SPIE. ISSN 0361-0748.
- Qiu 1998 Monitoring post fire succession in the Santa Monica Mountains using hyperspectral imagery. 1998. Qiu H, Roberts DA, Luna M. SPIE Proceedings 3502 201-207. Bellingham: SPIE. ISSN 0361-0748.
- Reinhäckel 1998b Quantitative analysis of lignite dumps in central Germany using thermal infrared spectrometry (7.5-13 μm). 1998. Reinhäckel G, Müller A. Proceedings of the 1st International EARSeL Workshop on Imaging Spectroscopy 349-356. Paris: EARSeL. ISSN 2-90-885-22-0.
- Ren 2002 Efficient anomaly detection and discrimination for hyperspectral imagery. 2002. Ren H, Du Q, Jensen JO. SPIE Proceedings 4725 234-241. Bellingham: SPIE. ISSN 0361-0748.
- Richards 1999 Remote sensing digital image analysis. 1999. Richards JA, Jia X. Berlin: Springer Verlag. ISBN 3-540-64860-7.
- Richardson 1999 Identification and classification of mixed phytoplankton assemblages using AVIRIS image-derived spectra. 1999. Richardson LL, Kruse FA. Proceedings: JPL AVIRIS Workshop 1999. Pasadena: Jet Propulsion Laboratory.

- Richardson 2000 Use of AVIRIS spectral data to discriminate mixed phytoplankton communities, seagrass beds, and benthic algal mats in Florida Bay, USA. 2000. Richardson LL, Kruse FA. Proceedings: JPL AVIRIS Workshop 2000. Pasadena: Jet Propulsion Laboratory.
- Roberts 1999a Shallow water bathymetry using integrated airborne multi-spectral remote sensing. 1999. Roberts ACB, Anderson JM. International Journal of Remote Sensing 20 (3) 497-510. London: Taylor & Francis Ltd. ISSN 0143-1161.
- Rock 1990 Spectral characterization of forest damage occurring on Whiteface Mountain, NY: studies with the fluorescence line imager and ground-based spectrometers. 1990. Rock BN, Miller JR, et al. SPIE Proceedings - Imaging of the Terrestrial Environment 1298 190-201. Bellingham: SPIE. ISSN 0361-0748.
- Rogers 1995 Neural networks for automatic target detection. 1995. Rogers SK, Colombi JM, et al. Neural Networks 8 (7-8) 1153-1184. Oxford: Pergamon-Elsevier Science Ltd. ISSN 0893-6080.
- Römpp 1995 Römpp Chemielexikon. 1995. 5314pp. Stuttgart: Thieme. ISSN 3.13.102759-2.
- Rössner 1998 Application of hyperspectral DAIS data for differentiation of urban surfaces in the city of Dresden, Germany. 1998. Rössner S, Segl K, et al. 1st EARSeL Symposium on Imaging Spectroscopy 463-472. Paris: EARSeL. ISBN 2-90-885-22-0.
- Rössner 2000 Comparison of automated methods for identification of urban surfaces using airborne hyperspectral data of reflective and thermal wavelength ranges. 2000. Rössner S, Segl K, Heiden U. Proceedings of the 2nd EARSeL Workshop on Imaging Spectroscopy. EARSeL.
- Rössner 2001 Automated differentiation of urban surfaces based on airborne hyperspectral imagery. 2001. Rössner S, Segl K, et al. IEEE Transactions on Geoscience and Remote Sensing 39 (7) 1525-1532. New York: IEEE. ISSN 0196-2892.
- Rothfuß 1994 Verarbeitung und Einsatz Abbildender Spektrometerdaten (GER) mit unterstützenden Bodenmessungen zur Erkundung einer landwirtschaftlich genutzten Altlastfläche. 1994. Rothfuß H. Düsseldorf: VDI Verlag. ISSN 3-18-313215-X.
- Rothmann 1999 Spectral imaging of histological and cytological specimens. 1999. Rothmann C, Malik Z. SPIE Proceedings 3605 282-287. Bellingham: SPIE. ISSN 0361-0748.
- RSI 2001 ENVI User's Guide. 2001. Research Systems, Inc. 948pp. Boulder: Research Systems, Inc.
- Sabins 1999 Remote sensing for mineral exploration. 1999. Sabins FF. Ore Geology Review 14 (3-4) 157-183. Amsterdam: Elsevier Science BV. ISSN 0169-1368.
- Sabol 1996 Monitoring forest regrowth using a multi-platform time series. 1996. Sabol DE, Smith MO, et al. Proceedings: JPL AVIRIS Workshop 1996. Pasadena: Jet Propulsion Laboratory.
- Salem 2002 Hyperspectral image analysis for oil spill detection. 2002. Salem F, Kafatos M, et al. Proceedings: JPL AVIRIS Workshop 2002. Pasadena: Jet Propulsion Laboratory.
- Sanchez 2003 Detection and monitoring of oil spills using hyperspectral imagery. 2003. Sanchez G, Roper WE, Gomez RB. SPIE Proceedings 5097 233-240. Bellingham: SPIE. ISSN 0361-0748.
- Sandidge 1998 Coastal bathymetry from hyperspectral observations of water radiance. 1998. Sandidge JC, Holyer RJ. Remote Sensing of Environment 65 (3) 341-352. New York: Elsevier Science Inc. ISSN 0034-4257.

- Saunders 1999 Model for hydrocarbon microseepage and related near-surface alterations. 1999. Saunders DF, Burson KR, Thompson CK. AAPG Bulletin 83 170-185. Tulsa: American Association of Petroleum Geologists. ISSN 0149-1423.
- Schachtschabel 1998 Lehrbuch der Bodenkunde. 1998. Schachtschabel P, Blume HP, et al. 494pp. Stuttgart: Enke Verlag. ISBN 3-432-84774-2.
- Schott 1997 Prediction of observed image spectra using synthetic image generation models. 1997. Schott JR, Kuo DS, et al. SPIE Proceedings 3118 81-93. Bellingham: SPIE. ISSN 0361-0748.
- Schuerger 2003 Comparison of two hyperspectral imaging and two laser-induced fluorescence instruments for the detection of zinc stress and chlorophyll concentration in bahia grass (*Paspalum notatum* Flugge). 2003. Schuerger AC, Capelle GA, et al. Remote Sensing of Environment 84 (4) 572-588. New York: Elsevier Science Inc. ISSN 0034-4257.
- Schumacher 1996 Hydrocarbon-induced alteration of soils and sediments. 1996. Schumacher D. AAPG Memoir 66 71-89. Tulsa: American Association of Petroleum Geologists. ISSN 0149-1423.
- Segl 2000 Differentiation of urban surfaces based on hyperspectral image data and a multi-technique approach. 2000. Segl K, Roessner S, Heiden U. Proceedings of the IEEE IGARSS 2000 1600-1602. New York: IEEE. ISBN 0-7803-6359-0.
- Shafique 2002 Coupling hyperspectral remote sensing with field spectrometer to monitor inland water quality parameters. 2002. Shafique NA, Fulk F, et al. Proceedings: JPL AVIRIS Workshop 2002. Pasadena: Jet Propulsion Laboratory.
- Shah 2003 Cutaneous wound analysis using hyperspectral imaging. 2003. Shah SA, Bachrach N, et al. Biotechniques 34 (2) 410+. Natick: Eaton Publishing Co. ISSN 0736-6205.
- Shang 1999a Investigating casi responses to different levels of tailing oxidation: Inco Copper Cliff tailings area, Northern Ontario, Canada. 1999. Shang J, Levesque J, et al. Preprint.
- Shang 1999b Preliminary investigation of acid mine drainage detection using casi data, Copper Cliff, Ontario, Canada. 1999. Shang J, Levesque J, et al. Preprint.
- Sharp 2002 Noise-constrained hyperspectral data compression. 2002. Sharp MH. Optical Engineering 41 (9) 2098-2101. Bellingham: SPIE. ISSN 0091-3286.
- Shaw 2002a Signal processing for hyperspectral image exploitation. 2002. Shaw G, Manolakis D. IEEE Signal Processing Magazine 19 (1) 12-16. New York: IEEE. ISSN 1053-5888.
- Singhroy 2000b Reflectance spectra of the boreal forest over mineralized sites. 2000. Singhroy V, Saint-Jean R, Levesque J. Proceedings of the IEEE IGARSS 2000 1379-1381. New York: IEEE. ISBN 0-7803-6359-0.
- Smith 1999a Hyperspectral mine detection phenomenology program. 1999. Smith AM, Kenton AC, et al. SPIE Proceedings 3710 819-829. Bellingham: SPIE. ISSN 0361-0748.
- Smith 2003b Weed-crop discrimination using remote sensing: a detached leaf experiment. 2003. Smith AM, Blackshaw RE. Weed Technology 17 (4) 811-820. Lawrence: Weed Sci Soc Amer. ISSN 0890-037X.
- Sowa 2002 Spectroscopic assessment of cutaneous hemodynamics in the presence of high epidermal melanin concentration. 2002. Sowa MG, Matas A, et al. Clinica Chimica Acta 317 (1-2) 203-212. Amsterdam: Elsevier Science BV. ISSN 0009-8981.
- Sponagel 1994 Bodenkundliche Kartieranleitung. 1994. Sponagel H, et al. 392pp. Stuttgart: Schweizerbart. ISSN 3-510-95804-7.

- Spyra 2001-2004 Project reports on the investigation and remediation of a komplex kerosene spill at the Schwarze Pumpe industrial facility, Brandenburg, Germany. 2001-2004. Spyra W, Winkelmann K. Project Reports. Cottbus: Chair of Chemical Engineering and Hazardous Wastes.
- Spyra 2001a Altlastenerkundung und -Bewertung. Ehemaliges Glaswerk Haidemühl. 2001. Spyra W, Winkelmann K. Project Report 75 pp. Cottbus: Chair of Chemical Engineering and Hazardous Wastes.
- Spyra 2001b Erkundung einer Verdachtsfläche für Altablagerungen in der Ortschaft Groß Pinnow, Land Brandenburg. 2001. Spyra W, Winkelmann K. Project Report 92 pp. Cottbus: Chair of Chemical Engineering and Hazardous Wastes.
- Spyra 2002 Description of a crude oil spill into marshland near Abadan in southern Iran. 2002. Spyra W. Internal Report. Cottbus: Chair of Chemical Engineering and Hazardous Wastes.
- Spyra 2003 NATO Advanced Research Workshop. Risk assessment, technology and treatment options for the conversion of abandoned liquid missile propellants (fuels and oxidizers) in Azerbaijan. 2003. Spyra W, Winkelmann K. Project Report 45 pp. Cottbus: Chair of Chemical Engineering and Hazardous Wastes.
- Spyra 2004 Bewertung von Kampfstofffunden, Gefährdungskartierung und Erfassung von Verdachtsflächen für Vergrabungen für den ehemaligen Truppenübungsplatz Döberitz. 2004. Spyra W, Winkelmann K, Garbotz C. Project Report 214 pp. Cottbus: Chair of Chemical Engineering and Hazardous Wastes.
- SRU 2004 Umweltgutachten 2004 des Rates von Sachverständigen für Umweltfragen. 2004. Koch HJ, Dohmann M, Eikmann T. Berlin: Bundesanzeiger Verlag. ISSN 0722-8333.
- Staenz 1998a The use of hyperspectral data for precision farming. 1998. Staenz K, Deguise JC, et al. International Archives of Photogrammetry and Remote Sensing 32 (7) 38-42. International Society for Photogrammetry and Remote Sensing. ISSN 0256-1840.
- Stark 1992 Information content in near infrared hydrocarbon spectra. 1992. Stark E. In: Making Light Work: Advances in Near Infrared Spectroscopy 81-91. Weinheim: VCH. ISBN 3-527-28498-2.
- Stein 2002b Anomaly detection from hyperspectral imagery. 2002. Stein DWJ, Beaven SG, et al. IEEE Signal Processing Magazine 19 (1) 58-69. New York: IEEE. ISSN 1053-5888.
- Stoner 1981 Characteristic variations in reflectance of surface soils. 1981. Stoner ER, Baumgardner MF. Soil Science Society of America Journal 45 1161-1165. Madison: Soil Sci Soc Amer. ISSN 0361-5995.
- Strachan 2002 Impact of nitrogen and environmental conditions on corn as detected by hyperspectral reflectance. 2002. Strachan IB, Pattey E, Boisvert JB. Remote Sensing of Environment 80 (2) 213-224. New York: Elsevier Science Inc. ISSN 0034-4257.
- Swayze 1996 Mapping acid-generating minerals at the California Gulch Superfund site in Leadville, Colorado, using imaging spectroscopy. 1996. Swayze GA, Clark RN, et al. Proceedings: JPL AVIRIS Workshop 1996. Pasadena: Jet Propulsion Laboratory.
- Swayze 1998a Using imaging spectroscopy to cost-effectively locate acid-generating minerals at mine sites: An example from the California Gulch Superfund site in Leadville, Colorado. 1998. Swayze GA, Clark RN, et al. Proceedings: JPL AVIRIS Workshop 1998. Pasadena: Jet Propulsion Laboratory.

- Swayze 1999 High resolution mineralogical mapping of Cuprite, Nevada. 1999. Swayze GA. Proceedings: JPL AVIRIS Workshop 1999. Pasadena: Jet Propulsion Laboratory.
- Swayze 2000 Using imaging spectroscopy to map acidic mine waste. 2000. Swayze GA, Smith KS, et al. Environmental Science & Technology 34 (1) 47-54. Washington: Amer Chemical Soc. ISSN 0013-936X.
- Taylor 2000 Hyperspectral remote sensing promotes - Early problem detection in facility & pipeline monitoring. 2000. Taylor AW. Pipeline & Gas Journal 227 (10) 32+. Houston: Oildom Publishing Co Texas Inc. ISSN 0032-0188.
- Tester 1998 Phytoplankton blooms and remote sensing: What is the potential for early warning?. 1998. Tester PA, Stumpf RP. Journal of Shellfish Research 17 (5) 1469-1471. Southampton: Natl Shellfisheries Assoc. ISSN 0730-8000.
- Thieme 1993 Verdachtsstandorte von Rüstungsaltslasten in Deutschland. Bd. 1 - 5. 1993. Thieme J, Heinrichsdorf F, et al. Berlin: Umweltbundesamt.
- Thomas 2002 Infrared detection and analysis of vapor plumes using an airborne sensor. 2002. Thomas MJ, Lewis PE, et al. SPIE Proceedings 4725 47-64. Bellingham: SPIE. ISSN 0361-0748.
- Tsurui 1999 Hyperspectral imaging in pathology samples. 1999. Tsurui H, Lerner JM, et al. SPIE Proceedings 3605 273-281. Bellingham: SPIE. ISSN 0361-0748.
- Tsuta 2004 Development and application of a multi-band image scanner visualization of sugar distribution of melons. 2004. Tsuta M, Ichinose S, et al. Journal of the Japanese Society for Food Science and Technology 51 (5) 247-253. Ibaraki-Ken: Japan Soc Food Sci Technol. ISSN 1341-027X.
- Udelhoven 1998 A neural network approach for the identification of the organic carbon content of soils in a degraded semiarid ecosystem (Guadalentin, SE Spain) based on hyperspectral data from the DAIS-7915 sensor. 1998. Udelhoven T, Hill J, et al. Proceedings of the 1st International EARSeL Workshop on Imaging Spectroscopy 437-444. Paris: EARSeL. ISSN 2-90-885-22-0.
- Udelhoven 2000 The acquisition of spectral reflectance measurements under field and laboratory conditions as support for hyperspectral application in precision farming. 2000. Udelhoven T, Jarmer T, et al. Proceedings of the 2nd EARSeL Workshop on Imaging Spectroscopy. Paris: EARSeL.
- UNWPP 2003 World Population Prospects. The 2002 Revision. Highlights. 2003. Document ESA/P/WP. 180 36. New York: United Nations.
- US EPA 2004a Cleaning up leaks from underground storage tanks. 2004. US EPA. Document EPA 510-F-04-003 4. Washington: US Environmental Protection Agency.
- US EPA 2004b Cleaning up the Nation's waste sites: Markets and technology trends. 2004. US EPA. Document EPA 542-R-04-015 338. Washington: US Environmental Protection Agency.
- Ustin 2004 Using imaging spectroscopy to study ecosystem processes and properties. 2004. Ustin SL, Roberts DA, et al. Bioscience 54 (6) 523-534. Washington: Amer Inst. Biological Sci. ISSN 0006-3568.
- van de Ven 2000 Analysis of the relationships between geologic substrate and vegetation in the White and Inyo Mountains, eastern California. 2000. van de Ven C, Ernst WG, et al. Proceedings JPL AVIRIS Workshop 2000. Pasadena: Jet Propulsion Laboratory.
- van der Meer 1999b Imaging spectrometry for geological remote sensing. 1999. van der Meer F. Geologie en Mijnbouw 77 137-151. Dordrecht: Kluwer Academic Publ. ISSN 0016-7746.

- van der Meer 2000d Hyperspectral hydrocarbon microseepage detection and monitoring: potentials and limitations. 2000. van der Meer F, van Dijk P, et al. Proceedings of the 2nd EARSeL Workshop on Imaging Spectroscopy. Paris: EARSeL.
- van der Meer 2001b Imaging spectrometry: Basic analytical techniques. 2001. van der Meer F, de Jong SM, Bakker W. In: Imaging Spectrometry 17-61. Dordrecht: Kluwer Academic Publ. ISBN 1-4020-0194-0.
- van der Meer 2001c Imaging spectrometry and geological applications. 2001. van der Meer F, Yang H, Lang H. In: Imaging Spectrometry 201-218. Dordrecht: Kluwer Academic Publ. ISBN 1-4020-0194-0.
- van der Meer 2001d Imaging spectrometry and petroleum geology. 2001. van der Meer F, Yang H, et al. In: Imaging Spectrometry 219-241. Dordrecht: Kluwer Academic Publ. ISBN 1-4020-0194-0.
- van der Meer 2001e Imaging spectrometry: Basic principles and prospective applications. 2001. van der Meer FD, de Jong SM. Dordrecht: Kluwer Academic Publ. ISBN: 1-4020-0194-0.
- van der Meer 2002a Remote sensing and petroleum seepage: A review and case study. 2002. van der Meer F, van Dijk P, et al. Terra Nova 14 (1) 1-17. Oxford: Blackwell Science Ltd. ISSN 0954-4879.
- Vane 1988a Terrestrial Imaging Spectroscopy. 1988. Vane G, Goetz AFH. Remote Sensing of Environment 24 1-29. New York: Elsevier Science Inc. ISSN 0034-4257.
- Vogler 1995 Angewandte Verfahren und Ergebnisse bei der Wiedernutzbarmachung von Kippenböden im Bereich von Braunkohlentagebauen im Bereich Leipzig. 1995. Vogler E, Vogler F. Z. Geol. Wiss. 23 (1/2) 233-248.
- Wall 2001 Hyperspectral recce piques USAF interest. 2001. Wall R. Aviation Week & Space Technology 154 (4) 55-56. New York: McGraw Hill Inc. ISSN 0005-2175.
- Wang 1998b Lithological discrimination using hyperspectral remote sensing. 1998. Wang Q, Guo X, Wang R. SPIE Proceedings 3502 87-93. Bellingham: SPIE. ISSN 0361-0748.
- Watts 1997 Hazardous Wastes: Sources, Pathway, Receptors. 1997. Watts RJ. 764. New York: John Wiley & Sons Inc. ISBN 0-471-00238-0.
- Wennberg 1999 In vivo detection of basal cell carcinoma using imaging spectroscopy. 1999. Wennberg AM, Gudmundson F, et al. Acta Dermato-Venerologica 79 (1) 54-61. Oslo: Scandinavian University Press. ISSN 1318-4458.
- Whiting 1999 Use of low-altitude AVIRIS data for identifying salt-affected soil surfaces in western Fresno County, California. 1999. Whiting ML, Ustin SL. Proceedings: JPL AVIRIS Workshop 1999. Pasadena: Jet Propulsion Laboratory.
- Whiting 2001 Correlating AVIRIS imagery to field sampling and spectrometer measurements for organic and inorganic soil carbon. 2001. Whiting ML, Ustin SL. Proceedings: JPL AVIRIS Workshop 2001. Pasadena: Jet Propulsion Laboratory.
- Whiting 2003 Estimating surface soil moisture in simulated AVIRIS spectra. 2003. Whiting ML, Li L, Ustin SL. Proceedings: JPL AVIRIS Workshop 2003. Pasadena: Jet Propulsion Laboratory.
- Williams 2002b Preliminary investigation of submerged aquatic vegetation mapping using hyperspectral remote sensing. 2002. Williams DJ, Rybicki NB, et al. Environmental Monitoring and Assessment 81 (1-3) 383-392. Dordrecht: Kluwer Academic Publ. ISSN 0167-6369.

- Wilson 2004 Classification of contamination in salt marsh plants using hyperspectral reflectance. 2004. Wilson MD, Ustin SL, Rocke DM. IEEE Transactions on Geoscience and Remote Sensing 42 (5) 1088-1095. Piscataway: IEEE. ISSN 0196-2892.
- Winkelmann 2001a Investigation and remediation of a complex kerosene spill. 2002. Spyra W, Winkelmann K. Proceedings: Depotech 2002 85-92. Essen: Verlag Glückauf GmbH. ISBN 3-7739-5979-6.
- Winkelmann 2001b Description of a uncontrolled waste deposit and a diesel filling station contamination in the Rio Unare Basin, Venezuela. 2001. Winkelmann K. Internal Report. Cottbus: Chair of Chemical Engineering and Hazardous Wastes.
- Winkelmann 2001c Description of the situation at the Ordchonikidse manganese metallurgical plant industrial waste dump, Ukraine. 2001. Winkelmann K. Internal Report. Cottbus: Chair of Chemical Engineering and Hazardous Wastes.
- Winkelmann 2001d Thermalaufnahmen zur Erkundung ehemaliger Truppenübungsplätze. 2001. Winkelmann K, Spyra W. Photogrammetrie Fernerkundung Geoinformation. 2001 417-426. Stuttgart: Schweizerbart. ISSN 1432-8364.
- Winkelmann 2003a Description of the situation at onshore oilfield in the Baku region and the Absheron Peninsula, Azerbaijan. 2003. Winkelmann K. Internal Report. Cottbus: Chair of Chemical Engineering and Hazardous Wastes.
- Winkelmann 2004 Location of liquid missile propellant depots in Azerbaijan, recent storage situation, and risk assessment. 2004. Winkelmann K. NATO Science Series: The Conversion of Liquid Rocket Fuels 162 53-72. Dordrecht: Kluwer Academic Publishers. ISBN 1402023804.
- Wittig 1998 Braunkohlen- und Sanierungsplanung im Land Brandenburg. 1998. Wittig H. In: Braunkohlentagebau und Rekultivierung 475-486. Berlin: Springer. ISBN 3-540-60092-2.
- Workman 1996 A brief review of near infrared in petroleum product analysis. 1996. Workman J. Journal of Near Infrared Spectroscopy 4 69-74. Chichester: NIR Publications. ISSN 0967-0335.
- Wu 1996 Best season for exploration of metal mineral under forests using imaging spectrometer. 1996. Wu J, Yang X, et al. SPIE Proceedings 2819 337-344. Bellingham: SPIE. ISSN 0361-0748.
- Xiang 1998 Crop type with hyperspectral technique. 1998. Xiang Y, Liu W, et al. SPIE Proceedings 3502 124-128. Bellingham: SPIE. ISSN 0361-0748.
- Yang 1999b Geochemistry and field spectrometry for detection hydrocarbon microseepage. 1999. Yang H, Zhang J, et al. Terra Nova 10 231-235. Oxford: Blackwell Science Ltd. ISSN 0954-4879.
- Yang 1999c Spectral characteristics of wheat associated with hydrocarbon microseepage. 1999. Yang H, Zhang J, et al. International Journal of Remote Sensing 20 807-813. London: Taylor & Francis Ltd. ISSN 0143-1161.
- Yang 2000b Imaging spectrometry data correlated to hydrocarbon microseepage. 2000. Yang H, Zhang J, et al. International Journal of Remote Sensing 21 (1) 197-202. London: Taylor & Francis Ltd. ISSN 0143-1161.
- Yost 1971 The reflectance spectral of mineralized trees. 1971. Yost E, Wenderoth S. Proceedings of 7th International Symposium on Remote Sensing of Environment. Ann Arbor.

- Zarco-Tejada 2001b Leaf and canopy pigment content estimation through RT model inversion for deciduous and coniferous forest canopies using hyperspectral data and red edge optical indices. 2001. Zarco-Tejada PJ, Miller JR, et al. Proceedings: JPL AVIRIS Workshop 2001. Pasadena: Jet Propulsion Laboratory.
- Zeinalov 2000 Importance of remote-sensing data in structural geologic analysis of oil- and gas-bearing regions of Azerbaijan. 2000. Zeinalov GA. Natural Resources Research 9 (4) 307-313. International Association for Mathematical Geography. ISSN 1520-7439.
- Zhang 1998a Study on the classification of hyperspectral data in urban area. 1998. Zhang B, Liu J, et al. SPIE Proceedings 3502 169-172. Bellingham: SPIE. ISSN 0361-0748.
- Zhou 2003 Physico-chemical properties and laboratory hyperspectral reflectance of coastal saline soil in Shangyu city of Zhejiang province, China. 2003. Shi Z, Huang MX, Li Y. Pedosphere 13 (3) 193-198. Beijing: Science China Press. ISSN 1002-0160.

List of Abbreviations

ANA	1-Acetylnaphthalene	NADIR	Point directly below the system it its focal point
AVIRIS	Airborne Visible/Infrared Imaging Spectrometer	NAP	Naphthalene
BRDF	Bidirectional Reflectance Distribution Function	NIR	Near Infrared
BT	Boulder till	NIST	National Institute of Standards and Technology
BTEX	Benzene, toluene, ethylbenzene, xylene	OCT	n-Octane
CCD	Charge-Coupled Device	PAN	Panchromatic
Cg	Clay granulate	PHE	Phenol
CRO	Crude oil	PPI	Pixel Purity Index
cS	Coarse sand	RGB	Red-Green-Blue
Cy	Clay	SAM	Spectral Angle Mapper
DIS	Diesel	SFF	Spectral Feature Fitting
DMP	2,4-Dimethylphenol	S/N	Signal-to-Noise Ratio
DN	Digital number	SNR	Signal-to-Noise Ratio
DNT	2,4-Dinitrotoluene	SS	Sea sand
EO-1	Earth Observing Mission 1	SWIR	Shortwave Infrared
FOV	Field of View	TCB	1,2,4-Trichlorobenzene
fS	Fine sand	TIR	Thermal Infrared
FWHM	Full width at half maximum	VIS	Visible light
HI	Hydrocarbon Index	WO	Waste oil
Hu	Humic soil	wt. %	Per cent by weight
HyMap	Hyperspectral Mapper	XYL	Xylene
IFOV	Instantaneous field of view		
KER	Kerosene		
MIR	Mid Infrared (=SWIR)		
MNF	Minimum Noise Fraction		
MODIS	Moderate resolution Digital Imaging Spectrometer		
MTMF	Mixture-tuned matched filtering		
N/A	not applicable / not available		

List of Figures

Figure 2-1	Oilfield on the Absheron peninsula in Azerbaijan (Satellite and ground imagery).	11
Figure 2-2	Industrial facility Schwarze Pumpe in a panchromatic aerial photograph from 1996.	13
Figure 2-3	Panchromatic aerial photograph of 1953 of the former military training area Döberitzer Heide.	16
Figure 2-4	Photograph of an uncontrolled wastes dump in the Rio Unare Basin, Venezuela.	17
Figure 2-5	Leaking steel storage tanks containing liquid rocket fuels and oxidizers in an open pit at the Mingecevir depot in Azerbaijan.	19
Figure 2-6	Red complexes in the soil indicating leakages of samine at the Mingecevir depot.	19
Figure 2-7	Leaking oxidizer tank at the Mingecevir depot.	19
Figure 2-8	Heavy crude oil leaked from a pipeline near Abadan, Iran.	20
Figure 2-9	Photograph of an illegal waste burial site in northern Brandenburg.	21
Figure 2-10	False-color infrared aerial photograph of the village of Groß Pinnow with the location of the illegal waste burial site.	22
Figure 2-11	Panchromatic aerial photograph of 1996 of the former Haidemühl glassworks.	24
Figure 2-12	Photograph of a small diesel filling station in the Rio Unare Basin, Venezuela.	26
Figure 2-13	Illustration of different cases of soil and groundwater contaminations exhibiting different or no surface expressions.	29
Figure 2-14	Graph of the development of crude oil production since 1960.	33
Figure 2-15	Sources and distribution pattern of typical fuel hydrocarbon contaminations of soil and groundwater.	35
Figure 3-1	Concept of imaging spectrometry.	38
Figure 3-2	Wavelength region definitions for analytical chemistry and remote sensing.	40
Figure 3-3	Wavelength definitions and analytical methods.	42
Figure 3-4	H ₂ O molecular vibrations.	45
Figure 3-5	Location and intensity of important vibrations of organic molecules and compounds in the visible through infrared regions (0.5 μm – 8 μm).	49
Figure 3-6	Structural formulas of four basic organic compounds.	50
Figure 3-7	Sample near infrared spectra of important organic compounds and functional groups.	51

Figure 3-8	Important absorption features of basic organic compounds and functional groups in the visible through near infrared wavelength regions (0.5 μm – 2.5 μm).	53
Figure 3-9	Absorption spectra of BTEX in the 0.38 μm – 2.5 μm wavelength region.	55
Figure 3-10	Example spectra of different groups of inorganics in the 0.38 μm – 2.5 μm wavelength region.	57
Figure 3-11	Important concepts, definitions and characteristics of near infrared spectra.	73
Figure 3-12	Spectral mixing concept.	74
Figure 3-13	Concept of n-dimensional spectrum (pixel) vectors and coordinate transformations for dimensionality reduction.	77
Figure 3-14	Binary encoding.	79
Figure 3-15	Continuum removal.	80
Figure 3-16	Spectral angle mapping classification concept.	81
Figure 4-1	Concept of the Hydrocarbon Index (HI).	90
Figure 5-1	Composition of sand, silt and clay.	104
Figure 5-2	Influence of texture on reflectance.	105
Figure 5-3	Typical reflectance of five major groups of soil types.	106
Figure 6-1	Measurement setup for laboratory reflectance measurements.	134
Figure 6-2	Spectra of n-octane, benzene and xylene illustrating characteristics absorption feature differences.	139
Figure 6-3	Spectra of alkanes, alkenes, and alkynes.	140
Figure 6-4	Spectral characteristics determined by functional groups.	140
Figure 6-5	Spectra of aliphatics-dominated contaminants selected for the experiments.	147
Figure 6-6	Spectra of aromatic contaminants selected for the experiments.	147
Figure 6-7	Spectra of phenol, 2,4-dimethylphenol compared to xylene.	148
Figure 6-8	Spectra of 1,2,4-trichlorobenzene and 2,4-dinitrotoluene compared to xylene.	148
Figure 6-9	Spectra of dry samples of the seven soils selected for the experiments.	150
Figure 6-10	Spectra of coarse sand dry and at different moisture levels.	153
Figure 6-11	Spectra of clay dry and at different moisture levels.	153
Figure 6-12	Absorption features of xylene at different concentrations in dry and moist sea sand.	155
Figure 6-13	Absorption features of different contaminants in dry fine sand in the 1,200 nm – 2,500 nm wavelength region.	158

Figure 6-14	Effects of soil moisture and soil type on absorption feature depths of contaminants in soils.	158
Figure 6-15	Measured and calculated spectra of 3% n-octane in dry sea sand.	164
Figure 6-16	Measured and calculated spectra of 3% xylene in moist boulder till.	165
Figure 6-17	Absorption feature depth determination and normalization.	167
Figure 6-18	Spectra of various real-life samples of soil and concrete contaminated with fuel hydrocarbons.	177
Figure 6-19	Spectra of soil samples containing high concentrations of explosives.	178
Figure 6-20	Spectra of household wastes.	180
Figure 7-1	Comparison of absorption feature characteristics of different natural and man-made hydrocarbon-bearing materials and hydrocarbon soil contaminations.	190
Figure 7-2	Hydrocarbon abundances (plastics and wood) detected in the HyMap dataset of the former military training area Döberitzer Heide	194
Figure 7-3	Hydrocarbon abundances detected in the HyMap dataset separated in two groups: aromatics and aliphatics.	195
Figure 7-4	Color aerial image of the Krampnitz village (reference image).	199
Figure 7-5	Subset (zoom) of the HyMap dataset for the Krampnitz village with aliphatic and aromatic hydrocarbon absorption features detected.	199
Figure 7-6	Comparison of aromatic and aliphatic absorption features of spectra from the HyMap dataset to laboratory spectra.	200

List of Tables

Table 2-1	Annual production of crude oil between 1960 and 2003.	33
Table 3-1	Remote sensing definitions and applications of wavelength regions between 0.18 μm and 1,000 μm wavelength.	41
Table 3-2	Overtone and combination bands of the water molecule in gaseous state.	47
Table 3-3	Important fundamental and resulting overtone vibrations of organic molecules.	48
Table 3-4	Relevant wavelength regions with respect to the identification of organic molecules in infrared and near infrared spectroscopy.	49
Table 3-5	Assessment of possibilities and restrictions with respect to the identification of organic chemicals in near infrared spectra.	52
Table 3-6	Characterization and separation of BTEX compounds in NIR spectra based on the 1.2 μm region absorption feature.	56
Table 3-7	System characteristics of important imaging spectrometry instruments.	69
Table 4-1	Overview of the applications of imaging spectrometry sorted by fields of application.	84
Table 5-1	Characteristics of important fuel hydrocarbon products.	110
Table 6-1	Chemicals and chemical products investigated with respect to their spectral characteristics in the 0.38 μm – 2.5 μm wavelength region.	120
Table 6-2	Anthropogenic hydrocarbon-bearing materials investigated to determine their uniqueness when compared to fuel hydrocarbon soil contaminations.	121
Table 6-3	Important characteristics of the soils used for the soil – moisture – contaminant experiments.	124
Table 6-4	Particle size distribution 0.04 mm – 1.0 mm of fine sand, coarse sand, boulder till, and humic soil.	125
Table 6-5	Soil moisture levels selected for the experiments for the different soil types.	127
Table 6-6	Contaminant concentration levels selected for the experiments.	128
Table 6-7	Contaminants selected for the experiments with composition, structural formula and state of aggregation in experiment conditions.	129
Table 6-8	Soil moisture level sample preparation.	131
Table 6-9	Soil quantities and contaminant quantities used to prepare soil samples of defined contaminant concentration.	132
Table 6-10	Contaminant-solvent mixtures added to dry soil to prepare defined contaminant concentration soil samples with solid contaminants.	133
Table 6-11	Characteristic differences of aromatics and aliphatics in the absorption feature wavelength regions.	138

Table 6-12	Characteristic absorption features of functional groups compared to basic organic compounds.	141
Table 6-13	Comparison of absorption features of natural and man-made hydrocarbon bearing materials and hydrocarbon compounds.	144
Table 6-14	Exact location of aliphatic and aromatic absorption features of the selected contaminants.	149
Table 6-15	Effects of crude oil contaminations of sea sand on the reflectance intensity at different moisture and contaminant concentration levels.	156
Table 6-16	Effects of diesel fuel contaminations of clay on the reflectance intensity at different moisture and contaminant concentration levels.	156
Table 6-17	Absorption feature depth (total reflectance percentage) of the 1,700 nm feature of different contaminants at different concentrations in an identical matrix (dry sea sand).	160
Table 6-18	Absorption feature depth (total reflectance percentage) of the 1,700 nm feature of n-octane in different types of dry soil.	160
Table 6-19	Absorption feature depth (total reflectance percentage) of the 1,700 nm feature crude oil at different concentrations in a soil sample at different moisture levels.	160
Table 6-20	Absorption feature depths of measured and calculated spectra for dry sea sand contaminated with 3.0 % n-octane.	162
Table 6-21	Absorption feature depths of measured and calculated spectra for moist boulder till contaminated with 3.0 % xylene.	163
Table 6-22	Relative reflectance of different soil samples at different moisture levels in the important 1,700 nm and 2,300 nm wavelength regions. The detection limit is defined as 3 % of the relative reflectance measured at the respective wavelength.	168
Table 6-23	Detection limits of crude oil in different soil type and moisture matrices defined for the 1,700 nm hydrocarbon absorption feature.	169
Table 6-24	Detection limits of crude oil in different soil type and moisture matrices defined for the 2,300 nm hydrocarbon absorption feature.	169
Table 6-25	Detection limits of diesel in different soil type and moisture matrices defined for the 1,700 nm hydrocarbon absorption feature.	170
Table 6-26	Detection limits of diesel in different soil type and moisture matrices defined for the 2,300 nm hydrocarbon absorption feature.	170